"Deterministic and Probabilistic Evaluation of Retrofit Alternatives for a Five-Story Flat-Slab RC Building"

by

Jong-Wha Bai and Mary Beth D. Hueste

Texas A&M University

Zachry Department of Civil Engineering

College Station, Texas 77843-3136

January 2007

This research was conducted at Texas A&M University and was supported by the Mid-America Earthquake Center through the Earthquake Engineering Research Centers Program of the National Science Foundation under NSF award number EEC-9701785, the Zachry Department of Civil Engineering, and the Texas Engineering Experiment Station at Texas A&M University. Any opinions, findings and conclusions or recommendations expressed in this material are those of the authors and do not necessarily reflect those of the National Science Foundation and the other sponsors.

ABSTRACT

The effectiveness of seismic retrofitting applied to enhance seismic performance was assessed for a five-story reinforced concrete (RC) flat-slab building structure in the central United States. In addition to this, an assessment of seismic fragility that relates the probability of exceeding a performance level to the earthquake intensity was conducted. The response of the structure was predicted using nonlinear static and dynamic analyses with synthetic ground motion records for the central U.S. region. In addition, two analytical approaches for nonlinear response analysis were compared.

FEMA 356 (ASCE 2000) criteria were used to evaluate the seismic performance of the case study building. Two approaches of FEMA 356 were used for seismic evaluation: global-level and member-level using three performance levels (Immediate Occupancy, Life Safety and Collapse Prevention). In addition to these limit states, punching shear drift limits were also considered to establish an upper bound drift capacity limit for collapse prevention. Based on the seismic evaluation results, three possible retrofit techniques were applied to improve the seismic performance of the structure, including addition of shear walls, addition of RC column jackets, and confinement of the column plastic hinge zones using externally bonded steel plates.

Seismic fragility relationships were developed for the existing and retrofitted structure using several performance levels. Fragility curves for the retrofitted structure were compared with those for the unretrofitted structure. For development of seismic fragility curves, FEMA global drift limits were compared with the drift limits based on the FEMA member-level criteria. In addition to this, performance levels which were based on additional quantitative limits were also considered and compared with FEMA drift limits. Finally, recommendations are made for implementing the seismic fragility analysis results into MAEviz, the damage visualization module developed by the Mid-America Earthquake Center.

ACKNOWLEDGMENTS

This research was conducted at Texas A&M University and was supported by the Mid-America Earthquake Center through the Earthquake Engineering Research Centers Program of the National Science Foundation under NSF award number EEC-9701785 and the Zachry Department of Civil Engineering at Texas A&M University. Any opinions, findings and conclusions or recommendations expressed in this material are those of the authors and do not necessarily reflect those of the National Science Foundation and the other sponsors.

TABLE OF CONTENTS

Page

Page

LIST OF FIGURES

Page

Page

Page

Page

Page

Page

Page

Page

LIST OF TABLES

Page

Page

Page

Page

1 INTRODUCTION

1.1 Background

1.1.1 General

Improved understanding of the dynamic behavior and seismic performance of structures has led to new advances in earthquake engineering in recent years. In particular, the performance-based design approach allows for selection of a specific performance objective based on various parameters, including the owner's requirements, the functional utility of the structure, the seismic risk, and the potential economic losses. However, many structures in the central United States (U.S.) were not designed for seismic resistance until the early 1990s following the 1989 Loma Prieta earthquake in San Francisco, California. The presence of the New Madrid seismic zone in the central U.S. led to increased concern for the seismic vulnerability of structures in this area. Based on damage due to past earthquakes, structures in the central U.S. built before the 1990s and not designed according to the current seismic design codes may be vulnerable due to their proximity to the New Madrid Seismic Zone. Therefore, it is important to evaluate these structures and improve the seismic resistance of systems that are found to be vulnerable. To improve the seismic performance of systems that are found to be deficient, practitioners use various seismic retrofit techniques.

1.1.2 Retrofit of Reinforced Concrete Structures

Many existing structures located in seismic regions are inadequate for lateral resistance based on current seismic design codes. In general, buildings that were constructed before the 1970s have significant deficiencies in their overall structural configuration, such as discontinuity of positive reinforcement in beams and slabs, or wide spacing of transverse reinforcement. In addition, a number of major earthquakes during recent years have demonstrated the improved seismic performance of retrofitted structures and increased the importance of mitigation to reduce seismic risk. Seismic

retrofit of existing structures is one method to mitigate the risk that potentially exists. Recently, a significant amount of research has been devoted to the study of various retrofit techniques to enhance the seismic performance of reinforced concrete (RC) structures.

1.1.3 New Madrid Seismic Zone

The New Madrid Seismic Zone (NMSZ) lies within the central Mississippi Valley, extending from northeast Arkansas, through southeast Missouri, western Tennessee, and western Kentucky to southern Illinois. In North America, one of the largest series of earthquakes is known as the New Madrid Earthquakes. The New Madrid Earthquakes consisted of three major earthquakes between 1811 and 1812, with moment magnitude (M_w) estimates of 8.1, 7.8, and 8.0, and hundreds of aftershocks that followed over a period of several years (Johnston 1996)

There are several differences between earthquakes in the NMSZ and those that occur in the western U.S. The most important difference is that the earth's crust in the Midwest region attenuates energy 25% as effectively as the earth's crust in the western U.S. As a result, earthquakes in the central U.S. affect much larger areas than earthquakes of similar magnitude in the western U.S. (Shedlock and Johnston 1994). Another significant difference is the ratio between change of ground motion and probability in the probabilistic seismic hazard curves (Leyendecker et al. 2000). Because the range of the recurrence interval for maximum magnitude earthquake is wide throughout the U.S., the United States Geological Survey (USGS) developed the probabilistic hazard maps for design purposes. Fig. 1.1 shows the normalized hazard curves for a 2% in 50 years probability for several selected cities. As shown in Fig. 1.1, the slope of the hazard curves for cities in central and eastern U.S. is relatively steep as compared with those for cities in western U.S. Therefore, the difference between the 2% in 50 years ground motion and the 10% in 50 years motion for central U.S. is typically larger than that for western U.S. This provides a greater difference between the

Maximum Considered Earthquake (MCE) ground motion (2% in 50 years motion) and the 10% in 50 years motion that has been typically used for design of structures in central U.S. cities.

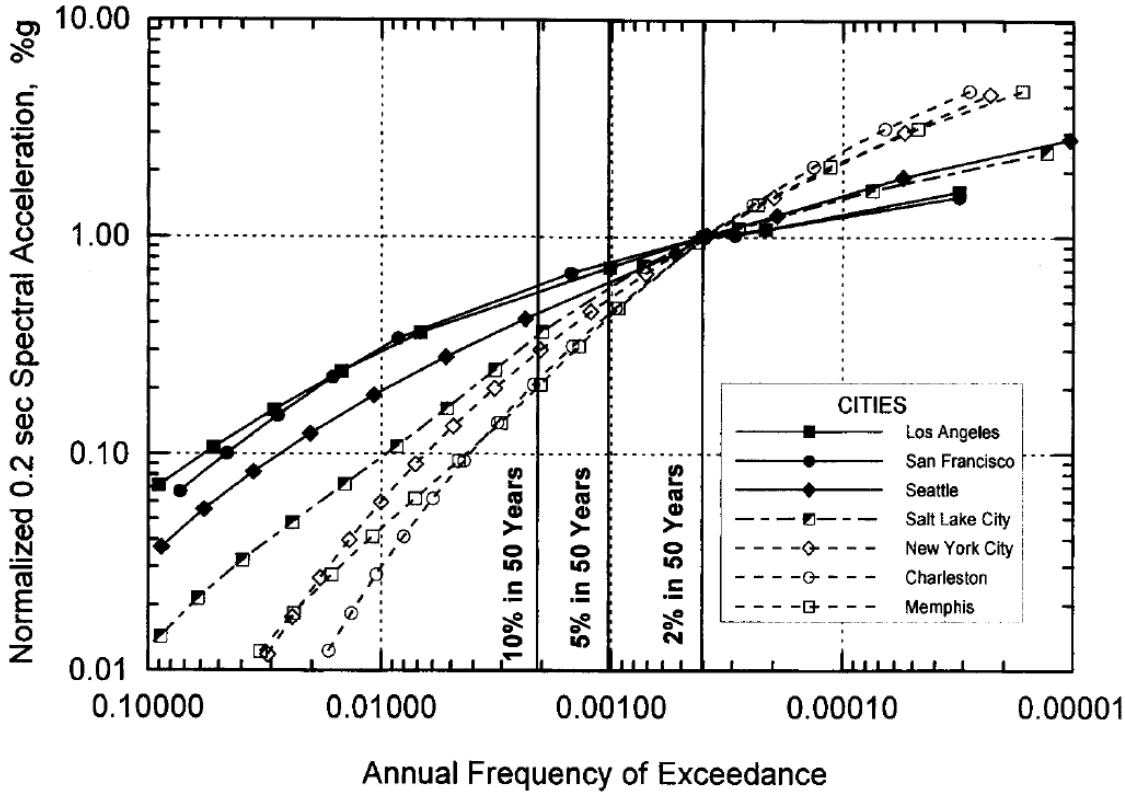

Fig. 1.1. Normalized hazard curves for selected cities (Leyendecker et al. 2000)

1.1.4 Consequence-Based Engineering

This study is part of the Mid-America Earthquake (MAE) Center project CM-4 "Structure Retrofit Strategies." The MAE Center is developing a new paradigm called Consequence-Based Engineering (CBE) to evaluate the seismic risk across regions or systems. CBE incorporates identification of uncertainty in all components of seismic risk modeling and quantifies the risk to societal systems and subsystems enabling policy-makers and decision-makers to ultimately develop risk reduction strategies and implement mitigation actions. The core research thrust areas are Damage Synthesis, Hazard Definition, and Consequence Minimization. This project is included in the

Consequence Minimization thrust area. More information about the CBE paradigm is provided by Abrams et al. (2002).

1.2 Scope and Purpose

The objectives of this study are to evaluate the seismic vulnerability of a typical 1980s RC building in the central U.S. and to determine the improvement in the seismic performance for various seismic retrofit techniques. Fragility curves were developed to reflect the alteration of response characteristics due to the application of selected intervention techniques to the case study structure. By developing fragility curves that link measures of earthquake intensity to the probability of exceeding specific performance levels for the existing and retrofitted structure, the improvement in seismic performance was evaluated. To compute global structural parameters, such as stiffness, strength and deformation capacity; nonlinear static (push-over) analysis and nonlinear dynamic (time history) analysis was conducted for the RC structure. The results of the push-over analysis were compared with nonlinear time-history analysis to evaluate how closely the push-over analysis estimates the dynamic, nonlinear response of the structure. Two sources of synthetic ground motion data were used (Wen and Wu 2000 and Rix and Fernandez-Leon 2004).

1.3 Methodology

The particular tasks that were performed to achieve the main objectives of this research are summarized below.

Task 1: Identification of Case Study Structure

Lightly reinforced RC building structures were selected as the structural system of interest for this study. The selected case study building is a five-story RC flat slab structure that is not specially detailed for ductile behavior. Low to moderate rise flat-

slab buildings were found to be of particular interest because they are common in the central U.S. and because there is a concern for potential damage to this type of structure during an earthquake of moderate intensity. After the type of structural system and overall dimensions were defined, the structure was designed according to the load requirements in the 1980s building code used in this region.

Task 2: Analytical Studies for Unretrofitted Case Study Building

Push-over and nonlinear dynamic analyses were performed using two different structural analysis programs to investigate the case study building. For the push-over analysis, the distribution of lateral loads over the building height included the typical first mode and rectangular (uniform) load patterns. All push-over analysis results were compared to nonlinear time history analysis results to determine how well the push-over analysis represents the dynamic response of the structure at the system level. Ground motions for the cities of St. Louis, Missouri and Memphis, Tennessee were used in this analysis. Because no recorded strong motion data from New Madrid Seismic Zone earthquakes are available, synthetic ground motions were used.

Task 3: Evaluation of Unretrofitted Case Study Building

Based on the analytical results, seismic evaluations were conducted using FEMA 356 performance criteria. FEMA 356 suggests two approaches for seismic evaluation: global-level and member-level using three performance levels (Immediate Occupancy, Life Safety and Collapse Prevention). For global-level evaluation, the maximum interstory drifts for each floor level were determined based on nonlinear dynamic analysis results. The member-level evaluation of FEMA 356 using plastic rotation limits was also performed to determine more detailed information for structural behavior and seismic performance. The case study building was evaluated to determine if the expected seismic response was acceptable for different performance levels. Nonlinear time-history analysis was performed using sets of synthetic ground motion records

corresponding to both two percent and ten percent probabilities of exceedance in 50 years for St. Louis, Missouri and Memphis, Tennessee.

Task 4: Review and Selection of Relevant Intervention Techniques

The fourth task involved review of relevant seismic retrofit techniques for RC structures, especially flat-slab RC buildings. The goal of this task was to gather information in the literature for the most effective seismic intervention techniques that primarily modify the stiffness, strength or deformation capacity of a structure. Several different intervention techniques were selected and evaluated for the case study structure.

Task 5: Development of Fragility Curves

Fragility curves were developed using FEMA 356 global- and member-level performance criteria for the existing and retrofitted structures. In addition to this, performance levels based on additional quantitative limits were derived and corresponding fragility curves were developed.

Task 6: Implementation into MAEviz

Recommendations were made for implementing the seismic fragility analysis results into MAEviz, the damage visualization module developed by the MAE Center.

1.4 Outline

This report is organized as follows. The introduction in Section 1 presents a brief background, scope, purpose and methodology for this study. Section 2 summarizes previous related research that was useful as guidance for this study. Section 3 describes the case study building. In Section 4, the ground motion data and analytical modeling procedures are discussed. Section 5 presents results from the nonlinear static and dynamic analyses for the unretrofitted case study building. In addition, the seismic evaluation and the fragility analysis performed for the existing building are summarized.

Section 6 presents retrofit techniques, analytical results and fragility curves of the retrofitted case study building. In Section 7, additional seismic fragility analysis results and recommendations for implementation into MAEviz are summarized. Finally, Section 8 summarizes the results of the study, and presents conclusions and recommendations based on this research.

2 LITERATURE REVIEW

2.1 Introduction

This section provides the background of performance-based design, structural analysis, seismic vulnerability evaluation and seismic retrofit techniques for RC buildings. The topics included are general information and a review of previous research related to the above areas.

2.2 Performance-Based Design

Performance-based provides a different approach for establishing design objectives and desired performance levels as compared to conventional code-based design. ATC-40 (ATC 1996) and FEMA 273 (FEMA 1997a) provided guidelines for the evaluation and performance-based seismic retrofitting of existing buildings, while the Vision 2000 report (SEAOC 1995) applied this concept to new construction. According to Vision 2000, a performance objective is defined as "an expression of the desired performance level for each earthquake design level." Multiple performance objectives that meet the diverse needs of owners can be considered within this performance-based design approach.

Performance-based earthquake engineering consists of all the required procedures including site selection, development of conceptual, preliminary and final structural designs, evaluation, and construction (Krawinkler 1999). The major procedure includes selection of performance objectives, conceptual design, design evaluation and modification, and socio-economic evaluation. As the performance-based design paradigm become more accepted for new structures, seismic retrofitting and rehabilitation methods have been affected by this concept. Consequently, retrofitting procedures can be selected and applied so that the performance objective of the retrofit

depends upon the importance of the structure and the desired structural performance during a seismic event with a particular recurrence interval.

2.3 Structural Analysis

2.3.1 General

FEMA 356 (ASCE 2000) outlines four different analysis procedures for a performance-based evaluation of a structure: the linear static procedure, the linear dynamic procedure, the nonlinear static procedure (push-over analysis), and the nonlinear dynamic procedure. In this study, push-over analysis and nonlinear dynamic analysis were conducted to estimate the nonlinear response characteristics of a case study structure.

2.3.2 Linear Procedures

The linear analysis procedures provided in FEMA 356 consist of linear static and linear dynamic analysis. When the linear static or dynamic procedures are used for seismic evaluation, the design seismic forces, the distribution of applied loads over the height of the buildings, and the corresponding displacements are determined using a linear elastic analysis. It is difficult to obtain accurate results for structures that undergo nonlinear response through linear procedures. Therefore, linear procedures may not be used for irregular structures unless the earthquake demands on the building comply with the demand capacity ratio (DCR) provided in the FEMA 356 guidelines.

2.3.3 Nonlinear Procedures

Nonlinear procedures consist of nonlinear static and nonlinear dynamic analyses. A nonlinear static analysis, also known as a push-over analysis, consists of laterally pushing the structure in one direction with a certain lateral force or displacement distribution until a specified drift is attained. Because linear procedures have limitations and nonlinear dynamic procedures are more time consuming, nonlinear static analysis is

commonly used by many engineers. This procedure has gained popularity in recent years as a relatively simple way to evaluate the design of a structure and predict the sequence of damage in the inelastic range of behavior. Both ATC-40 (ATC 1996) and FEMA 273 (FEMA 1997a) adopted an approach for performance evaluation based on nonlinear static analysis.

The nonlinear dynamic procedure (nonlinear time history analysis) provides an estimate of the dynamic response of the structure when subjected to certain ground motion demands. However, because the results computed by the nonlinear dynamic procedure can be highly sensitive to characteristics of individual ground motions, the analysis should be carried out with more than one ground motion record. This is also true for the linear dynamic analysis. FEMA 356 provides guidelines regarding the required number of ground motions that should be used for dynamic analysis.

Lew and Kunnath (2002) investigated the effectiveness of nonlinear static analysis in predicting the inelastic behavior of four case study structures: a six-story steel moment frame building, a thirteen-story steel moment-resisting frame building, a seven-story RC moment frame building and a twenty-story RC moment frame building. According to Lew and Kunnath (2002), the maximum displacement profiles predicted by both nonlinear static and dynamic procedures were similar. However, nonlinear static analysis did not give a good estimate of the interstory drift values compared to nonlinear dynamic analysis. In this study, interstory drifts were generally underestimated at upper levels and overestimated at lower levels.

2.4 Seismic Vulnerability Evaluation

2.4.1 FEMA 356 (ASCE 2000)

2.4.1.1 General

The *Prestandard and Commentary for the Seismic Rehabilitation of Buildings* – FEMA 356 (ASCE 2000) is used to evaluate the expected seismic performance of existing structures using performance levels that are defined qualitatively. The provisions and commentary of this standard are primarily based on FEMA 273 (FEMA 1997a) and FEMA 274 (FEMA 1997b). FEMA 356 covers general information and methodology for seismic rehabilitation of existing building structures. This document begins by introducing rehabilitation objectives according to seismic performance level and discussing the general seismic rehabilitation process. The document also describes general requirements, such as as-built information, and provides an overview of rehabilitation strategies. Finally, the details of the four possible analysis procedures and the methodology for member-level evaluation according to each structural type are explained.

2.4.1.2 Rehabilitation Objectives

The rehabilitation objectives must be selected by the engineer, in consultation with the building owner or code official, prior to evaluation of the existing building and selection of a retrofit, if needed. FEMA 356 presents many possible rehabilitation objectives that combine different target building performance levels with associated earthquake hazard levels, as shown in Table 2.1. FEMA 356 defines performance levels related to the structural system as follows.

(1) Immediate Occupancy (IO) – The post-earthquake damage state that remains safe to occupy, essentially retains the pre-earthquake design strength and stiffness of the structure.

(2) Life Safety (LS) – The post-earthquake damage state that includes damage to structural components but retains a margin against onset of partial or total collapse.

(3) Collapse Prevention (CP) – The post-earthquake damage state that includes damage to structural components such that the structure continues to support gravity loads but retains no margin against collapse.

Table 2.1. FEMA 356 rehabilitation objectives (adapted from ASCE 2000)

		Target building performance levels			
		Operational performance level (1-A)	Immediate occupancy performance level (1-B)	Life safety performance level (1-C)	Collapse prevention performance level (1-D)
Earthquake hazard level	50% / 50 years	a	b	c	d
	20% / 50 years	e	f	g	h
	BSE - 1 10% / 50 years	i	j	k	l
	BSE - 2 2% / 50 years	m	n	o	p

Notes:

1. Each cell in the above matrix represents a discrete Rehabilitation Objective.
2. The Rehabilitation Objectives in the matrix above may be used to represent the three specific Rehabilitation Objectives defined in Section 1.4.1, 1.4.2, and 1.4.3 of FEMA 356, as follows:

   k+p = Basic Safety Objective (BSO)
   k+p+any of a, e, i, b, j, or n = Enhanced Objectives
   o alone or n alone or m alone = Enhanced Objectives
   k alone or p alone = Limited Objective
   c, g, d, h, l = Limited Objective

2.4.1.3 Global-Level Approach

FEMA 356 defines a wide range of structural performance requirements for the specific limit state. Limits are given for many types of structures including concrete frames, steel moment frames, braced steel frames, concrete walls, unreinforced masonry infill walls, unreinforced masonry walls, reinforced masonry walls, wood stud walls, precast concrete connections and foundations. Global-level drift limits for concrete frames and concrete walls associated with three performance levels are provided in Table 2.2.

Table 2.2. Structural performance levels and damage – vertical elements (adapted from ASCE 2000)

Elements	Type	Structural performance levels		
		Collapse prevention S-5	Life safety S-3	Immediate occupancy S-1
Concrete frames	Primary	Extensive cracking and hinge formation in ductile elements. Limited cracking and/or splice failure in some nonductile columns. Severe damage in short columns.	Extensive damage to beams. Spalling of cover and shear cracking (<1/8" width) for ductile columns. Minor spalling in nonductile columns. Joint cracks <1/8" wide.	Minor hairline cracking. Limited yielding possible at a few locations. No crushing (strains below 0.003).
	Secondary	Extensive spalling in columns (limited shortening) and beams. Severe joint damage. Some reinforcing buckled.	Extensive cracking and hinge formation in ductile elements. Limited cracking and/or splice failure in some nonductile columns. Severe damage in short columns.	Minor spalling in a few places in ductile columns and beams. Flexural cracking in beams and columns. Shear cracking in joints <1/16" width.
	Drift	4% transient or permanent	2% transient; 1% permanent	1% transient; negligible permanent
Concrete walls	Primary	Major flexural and shear cracks and voids. Extensive crushing and buckling of reinforcement. Failure around openings. Severe boundary element damage. Coupling beams shattered and virtually disintegrated.	Some boundary element stress, including limited buckling of reinforcement. Some sliding at joints. Damage around openings. Some crushing and flexural cracking. Coupling beams: extensive shear and flexural cracks; some crushing, but concrete generally remains in place.	Minor hairline cracking of walls, <1/16" wide. Coupling beams experience cracking <1/8" width.
	Secondary	Panels shattered and virtually disintegrated.	Major flexural and shear cracks. Sliding at joints. Extensive crushing. Failure around openings. Severe boundary element damage. Coupling beams shattered and virtually disintegrated.	Minor hairline cracking of walls. Some evidence of sliding at construc-tion joints. Coupling beams experience cracks <1/8" width. Minor spalling.
	Drift	2% transient or permanent	1% transient; 0.5% permanent	0.5% transient; negligible permanent

2.4.1.4 Member-Level Approach

FEMA 356 classifies the structural types by materials, such as steel, concrete, masonry, wood and light metal framing. For each structural type, FEMA 356 describes

the procedure for evaluating seismic performance based on member-level limits. For instance, in Chapter 6, the seismic evaluation of concrete structures includes member-level limits for concrete moment frames, precast concrete frames, concrete frames with infills, concrete shear walls, precast concrete shear walls, concrete-braced frames, cast-in-place concrete diaphragms, precast concrete diaphragms and concrete foundation elements.

Several categories of concrete moment frames are addressed by FEMA 356, including RC beam-column moment frames, prestressed concrete beam-column moment frames, and slab-column moment frames. For concrete moment frames, the plastic rotation of each member is used as a parameter to assess inelastic behavior. Plastic rotation is defined as the amount of rotation beyond the yield rotation of the member. FEMA 356 provides the maximum permissible plastic rotation corresponding to each performance level. Tables 2.3 to 2.8 show the modeling parameters and numerical acceptance criteria for RC beams, RC columns, RC beam-column joints, two-way slabs and slab-column connections, members controlled by flexure, and members controlled by shear, respectively.

Table 2.3. FEMA 356 modeling parameters and numerical acceptance criteria for nonlinear procedures - RC beams (adapted from ASCE 2000)

Conditions			Modeling parameters[3]			Acceptance criteria[3]				
			Plastic rotation angle, radians		Residual strength ratio	Plastic rotation angle, radians				
						Performance level				
							Component type			
							Primary		Secondary	
			a	b	c	IO	LS	CP	LS	CP
i. Beams controlled by flexure[1]										
$\frac{\rho-\rho'}{\rho_{bal}}$	Transverse Reinforce-ment[2]	$\frac{V}{b_w d\sqrt{f'_c}}$								
≤ 0.0	C	≤ 3	0.025	0.05	0.2	0.01	0.02	0.025	0.02	0.05
≤ 0.0	C	≥ 6	0.02	0.04	0.2	0.005	0.01	0.02	0.02	0.04
≥ 0.5	C	≤ 3	0.02	0.03	0.2	0.005	0.01	0.02	0.02	0.03
≥ 0.5	C	≥ 6	0.015	0.02	0.2	0.005	0.005	0.015	0.015	0.02
≤ 0.0	NC	≤ 3	0.02	0.03	0.2	0.005	0.01	0.02	0.02	0.03
≤ 0.0	NC	≥ 6	0.01	0.015	0.2	0.0015	0.005	0.01	0.01	0.015
≥ 0.5	NC	≤ 3	0.01	0.015	0.2	0.005	0.01	0.01	0.01	0.015
≥ 0.5	NC	≥ 6	0.005	0.01	0.2	0.0015	0.005	0.005	0.005	0.01
ii. Beams controlled by shear[1]										
Stirrup spacing ≤ d/2			0.003	0.02	0.2	0.0015	0.002	0.003	0.1	0.02
Stirrup spacing ≥ d/2			0.003	0.01	0.2	0.0015	0.002	0.003	0.005	0.01
iii. Beams controlled by inadequate development or splicing along the span[1]										
Stirrup spacing ≤ d/2			0.003	0.02	0	0.0015	0.002	0.003	0.1	0.02
Stirrup spacing ≥ d/2			0.003	0.01	0	0.0015	0.002	0.003	0.005	0.01
iv. Beams controlled by inadequate embedment into beam-column joint[1]										
			0.015	0.03	0.2	0.01	0.01	0.015	0.02	0.03

Notes:

1. When more than one of the conditions i, ii, iii, and iv occurs for a given component, use the minimum appropriate numerical value from the table.
2. "C" and "NC" are abbreviations for conforming and nonconforming transverse reinforcement. A component is conforming if, within the flexural plastic hinge region, hoops are spaced at ≤ d/3, and if, for components of moderate and high ductility demand, the strength provided by the hoops (V_s) is at least three-fourths of the design shear. Otherwise, the component is considered nonconforming.
3. Linear interpolation between values listed in the table shall be permitted.

Table 2.4. FEMA 356 modeling parameters and numerical acceptance criteria for nonlinear procedures - RC columns (adapted from ASCE 2000)

Conditions			Modeling parameters[4]			Acceptance criteria[4]				
			Plastic rotation angle, radians		Residual strength ratio	Plastic rotation angle, radians				
						Performance level				
							Component type			
							Primary		Secondary	
			a	b	c	IO	LS	CP	LS	CP
i. Columns controlled by flexure[1]										
$\frac{P}{A_g f'_c}$	Transverse Reinforce-ment[2]	$\frac{V}{b_w d\sqrt{f'_c}}$								
≤ 0.1	C	≤ 3	0.02	0.03	0.2	0.005	0.015	0.02	0.02	0.03
≤ 0.1	C	≥ 6	0.016	0.024	0.2	0.005	0.012	0.016	0.016	0.024
≥ 0.4	C	≤ 3	0.015	0.025	0.2	0.003	0.012	0.015	0.018	0.025
≥ 0.4	C	≥ 6	0.012	0.02	0.2	0.003	0.01	0.012	0.013	0.02
≤ 0.1	NC	≤ 3	0.006	0.015	0.2	0.005	0.005	0.006	0.01	0.015
≤ 0.1	NC	≥ 6	0.005	0.012	0.2	0.005	0.004	0.005	0.008	0.012
≥ 0.4	NC	≤ 3	0.003	0.01	0.2	0.002	0.002	0.003	0.006	0.01
≥ 0.4	NC	≥ 6	0.002	0.008	0.2	0.002	0.002	0.002	0.005	0.008
ii. Columns controlled by shear[1, 3]										
All cases[5]			-	-	-	-	-	-	0.003	0.004
iii. Columns controlled by inadequate development or splicing along the clear height[1, 3]										
Hoop spacing ≤ d/2			0.01	0.02	0.4	0.005	0.005	0.01	0.01	0.02
Hoop spacing ≥ d/2			0	0.01	0.2	0	0	0	0.005	0.01
iv. Columns with axial loads exceeding $0.70P_o$[1, 3]										
Conforming hoops over the entire length			0.015	0.025	0.02	0	0.005	0.01	0.01	0.02
All other cases			0	0	0	0	0	0	0	0

Notes:

1. When more than one of the conditions i, ii, iii, and iv occurs for a given component, use the minimum appropriate numerical value from the table.
2. "C" and "NC" are abbreviations for conforming and nonconforming transverse reinforcement. A component is conforming if, within the flexural plastic hinge region, hoops are spaced at ≤ d/3, and if, for components of moderate and high ductility demand, the strength provided by the hoops (V_s) is at least three-fourths of the design shear. Otherwise, the component is considered nonconforming.
3. To qualify, columns must have transverse reinforcement consisting of hoops. Otherwise, actions shall be treated as force-controlled.
4. Linear interpolation between values listed in the table shall be permitted.
5. For columns controlled by shear, see Section 6.5.2.4.2 for acceptance criteria.

Table 2.5. FEMA 356 modeling parameters and numerical acceptance criteria for nonlinear procedures - RC beam-column joints (adapted from ASCE 2000)

Conditions			Modeling parameters[4]			Acceptance criteria[4]				
			Plastic rotation angle, radians		Residual strength ratio	Plastic rotation angle, radians				
						Performance level				
							Component type			
							Primary		Secondary	
			a	b	c	IO	LS	CP	LS	CP
i. Interior joints[2, 3]										
$\frac{P}{A_g f'_c}$	Transverse Reinforcement	$\frac{V}{V_n}$ [3]								
≤ 0.1	C	≤ 1.2	0.015	0.03	0.2	0	0	0	0.02	0.03
≤ 0.1	C	≥ 1.5	0.015	0.03	0.2	0	0	0	0.015	0.02
≥ 0.4	C	≤ 1.2	0.015	0.025	0.2	0	0	0	0.015	0.025
≥ 0.4	C	≥ 1.5	0.015	0.02	0.2	0	0	0	0.015	0.02
≤ 0.1	NC	≤ 1.2	0.005	0.02	0.2	0	0	0	0.015	0.02
≤ 0.1	NC	≥ 1.5	0.005	0.015	0.2	0	0	0	0.01	0.015
≥ 0.4	NC	≤ 1.2	0.005	0.015	0.2	0	0	0	0.01	0.015
≥ 0.4	NC	≥ 1.5	0.005	0.015	0.2	0	0	0	0.01	0.015
ii. Other joints[2, 3]										
$\frac{P}{A_g f'_c}$	Transverse Reinforce-ment[1]	$\frac{V}{V_n}$								
≤ 0.1	C	≤ 1.2	0.01	0.02	0.2	0	0	0	0.015	0.02
≤ 0.1	C	≥ 1.5	0.01	0.015	0.2	0	0	0	0.01	0.015
≥ 0.4	C	≤ 1.2	0.01	0.02	0.2	0	0	0	0.015	0.02
≥ 0.4	C	≥ 1.5	0.01	0.015	0.2	0	0	0	0.01	0.015
≤ 0.1	NC	≤ 1.2	0.005	0.01	0.2	0	0	0	0.0075	0.01
≤ 0.1	NC	≥ 1.5	0.005	0.01	0.2	0	0	0	0.0075	0.01
≥ 0.4	NC	≤ 1.2	0	0	-	0	0	0	0.005	0.0075
≥ 0.4	NC	≥ 1.5	0	0	-	0	0	0	0.005	0.0075

Notes:

1. "C" and "NC" are abbreviations for conforming and nonconforming transverse reinforcement. A joint is conforming if hoops are spaced at ≤ $h_c/3$ within the joint. Otherwise, the component is considered nonconforming.
2. P is the design axial force on the column above the joint and A_g is the gross cross-sectional area of the joint.
3. V is the design shear force and V_n is the shear strength for the joint. The design shear force and shear strength shall be calculated according to Section 6.5.2.3.
4. Linear interpolation between values listed in the table shall be permitted.

Table 2.6. FEMA 356 modeling parameters and numerical acceptance criteria for nonlinear procedures – two-way slabs and slab-column connections (adapted from ASCE 2000)

Conditions		Modeling parameters[4]			Acceptance criteria[4]				
		Plastic rotation angle, radians		Residual strength ratio	Plastic rotation angle, radians				
					Performance level				
						Component type			
						Primary		Secondary	
		a	b	c	IO	LS	CP	LS	CP
i. Slabs controlled by flexure, and slab-column connections[1]									
$\frac{V_g}{V_o}$ [2]	Continuity Reinforce-ment[3]								
≤ 0.2	Yes	0.02	0.05	0.2	0.01	0.015	0.02	0.03	0.05
≥ 0.4	Yes	0	0.04	0.2	0	0	0	0.03	0.04
≤ 0.2	No	0.02	0.02	-	0.01	0.015	0.02	0.015	0.02
≥ 0.4	No	0	0	-	0	0	0	0	0
ii. Slabs controlled by inadequate development or splicing along the span[1]									
		0	0.02	0	0	0	0	0.01	0.02
iii. Slabs controlled by inadequate embedment into slab-column joint[1]									
		0.015	0.03	0.2	0.01	0.01	0.015	0.02	0.03

Notes:

1. When more than one of the conditions i, ii, iii, and iv occurs for a given component, use the minimum appropriate numerical value from the table.
2. V_g = the gravity shear acting on the slab critical section as defined by ACI 318; V_o = the direct punching shear strength as defined by ACI 318
3. Under the heading "Continuity Reinforcement," use "Yes" where at least one of the main bottom bars in each direction is effectively continuous through the column cage. Where the slab is post-tensioned, use "Yes" where at least one of the post-tensioning tendons in each direction passes through the column cage. Otherwise, use "No."
4. Linear interpolation between values listed in the table shall be permitted.

Table 2.7. FEMA 356 modeling parameters and numerical acceptance criteria for nonlinear procedures – member controlled by flexure (adapted from ASCE 2000)

Conditions			Modeling Parameters			Acceptance Criteria				
			Plastic Rotation Angle, radians		Residual Strength Ratio	Plastic Rotation Angle, radians				
						Performance Level				
							Component Type			
							Primary		Secondary[4]	
			a	b	c	IO	LS	CP	LS	CP
i. Shear walls and wall segments										
$\frac{(A_s - A_s')f_y + P}{t_w l_w f_c'}$	$\frac{Shear}{t_w l_w \sqrt{f_c'}}$	Confined Boundary[1]								
≤ 0.1	≤ 3	Yes	0.015	0.02	0.75	0.005	0.01	0.015	0.015	0.02
≤ 0.1	≥ 6	Yes	0.01	0.015	0.4	0.004	0.008	0.01	0.01	0.015
≥ 0.25	≤ 3	Yes	0.009	0.012	0.6	0.003	0.006	0.009	0.009	0.012
≥ 0.25	≥ 6	Yes	0.005	0.01	0.3	0.0015	0.003	0.005	0.005	0.01
≤ 0.1	≤ 3	No	0.008	0.015	0.6	0.002	0.004	0.008	0.008	0.015
≤ 0.1	≥ 6	No	0.006	0.01	0.3	0.002	0.004	0.006	0.006	0.01
≥ 0.25	≤ 3	No	0.003	0.005	0.25	0.001	0.002	0.003	0.003	0.005
≥ 0.25	≥ 6	No	0.002	0.004	0.2	0.001	0.001	0.002	0.002	0.004
ii. Columns supporting discontinuous shear walls										
Transverse reinforcement[2]										
Conforming			0.01	0.015	0.2	0.003	0.007	0.01	n.a.	n.a.
Nonconforming			0	0.01	0.2	0	0	0	n.a.	n.a.
iii. Shear wall coupling beams										
Longitudinal reinforcement and transverse reinforcement[3]	$\frac{Shear}{t_w l_w \sqrt{f_c'}}$									
Conventional longitudinal reinforcement with conforming transverse reinforcement	≤ 3		0.025	0.05	0.75	0.01	0.02	0.025	0.025	0.05
	≥ 6		0.02	0.04	0.5	0.005	0.01	0.02	0.02	0.04
Conventional longitudinal reinforcement with nonconforming transverse reinforcement	≤ 3		0.02	0.035	0.5	0.006	0.012	0.02	0.02	0.035
	≥ 6		0.01	0.025	0.25	0.005	0.008	0.01	0.01	0.025
Diagonal reinforcement	n.a.		0.03	0.05	0.8	0.006	0.018	0.03	0.03	0.05

Notes:

1. Requirements for a confined boundary are the same as those given in ACI 318.
2. Requirements for conforming transverse reinforcement in columns are: (a) hoops over the entire length of the column at a spacing ≤ d/2, and (b) strength of hoops V_s ≥ required shear strength of column.
3. Conventional longitudinal reinforcement consists of top and bottom steel parallel to the longitudinal axis of the coupling beam. Conforming transverse reinforcement consists of: (a) closed stirrups over the entire length of the coupling beam at a spacing ≤ d/3, and (b) strength of closed stirrups V_s ≥ 3/4 of required shear strength of the coupling beam.
4. For secondary coupling beams spanning < 8'-0", with bottom reinforcement continuous into the supporting walls, secondary values shall be permitted to be doubled.

Table 2.8. FEMA 356 modeling parameters and numerical acceptance criteria for nonlinear procedures – member controlled by shear (adapted from ASCE 2000)

Conditions		Modeling Parameters			Acceptance Criteria				
		Total Drift Ratio (%), or Chord Rotation, radians[1]		Residual Strength Ratio	Acceptable Total Drift (%), or Chord Rotation, radians[1]				
					Performance Level				
						Component Type			
						Primary		Secondary	
		a	b	c	IO	LS	CP	LS	CP
i. Shear walls and wall segments									
All shear walls and wall segments[2]		0.75	2.0	0.40	0.40	0.60	0.75	0.75	1.5
ii. Shear wall coupling beams[4]									
Longitudinal reinforcement and transverse reinforcement[3]	$\frac{Shear}{t_w l_w \sqrt{f_c'}}$								
Conventional longitudinal reinforcement with conforming transverse reinforcement	≤ 3	0.002	0.030	0.60	0.006	0.015	0.020	0.020	0.030
	≥ 6	0.016	0.024	0.30	0.005	0.012	0.016	0.016	0.024
Conventional longitudinal reinforcement with nonconforming transverse reinforcement	≤ 3	0.012	0.025	0.40	0.006	0.008	0.010	0.010	0.020
	≥ 6	0.008	0.014	0.20	0.004	0.006	0.007	0.007	0.012

Notes:

1. For shear walls and wall segments, use drift; for coupling beams, use chord rotation; refer to Figures 6-3 and 6-4.
2. For shear walls and wall segments where inelastic behavior is governed by shear, the axial load on the member must be $\leq 0.15A_g f'_c$; otherwise, the member must be treated as a force-controlled component.
3. Conventional longitudinal reinforcement consists of top and bottom steel parallel to the longitudinal axis of the coupling beam. Conforming transverse reinforcement consists of: (a) closed stirrups over the entire length of the coupling beam at a spacing ≤ d/3, and (b) strength of closed stirrups $V_s \geq 3/4$ of required shear strength of the coupling beam.
4. For secondary coupling beams spanning < 8'-0", with bottom reinforcement continuous into the supporting walls, secondary values shall be permitted to be doubled.

2.4.2 Fragility Curves

Many research studies related to development of fragility curves have been conducted including Cornell et al. (2002), Gardoni et al. (2002), and Wen et al. (2003). Cornell et al. (2002) developed a probabilistic framework for seismic design and assessment of steel moment frame building structures for the SAC Federal Emergency Management Agency (FEMA) guidelines. Demand and capacity were expressed in terms of the maximum interstory drift ratio with a nonlinear dynamic relationship. The probability assessment framework was developed with the assumption of distribution on parameters in a closed form. In addition, probabilistic models for structural demand and capacity were used to include uncertainties.

Gardoni et al. (2002; 2003) developed multivariate probabilistic capacity and demand models for RC bridges that account for the prevailing aleatory and epistemic uncertainties. A Bayesian approach was used to account for different types and sources of information including lower and upper bound data. The fragility of structural components and systems were estimated. Point and predictive fragilities were revealed as well as confidence intervals that reflect the influence of the epistemic uncertainties.

According to Wen et al. (2003), a fragility curve is defined as "the probability of entering a specified limit state conditioned on the occurrence of a specific hazard, among the spectrum of hazards." Wen et al. (2003) defines a vulnerability function as "the probability of incurring losses equal to (or greater than) a specified monetary unit, conditioned on the occurrence of an earthquake with a specified intensity."

The vulnerability of a structure is determined by a probabilistic relation between the predicted limit state and some measure of the earthquake demand, such as spectral acceleration (S_a), peak ground acceleration (PGA) probability of recurrence, or a specified ground motion magnitude. Therefore, the evaluation of the seismic

vulnerability of a building requires knowledge of the dynamic response of the structure and potential for damage under a certain seismic demand.

Limit state probability, $P_t[LS]$, is defined as the conditional probability of a set of given limit states of a system being reached at a given location over a given period of time (0, t), calculated as follows (Wen et al. 2003).

$$P_t[LS] = \Sigma\, P[LS|D=d]\, P[D=d] \tag{2.1}$$

where:

$P_t[LS]$	=	Probability of a given limit state (LS) for a system being reached over a given period of time (0,t).
D	=	Spectrum of uncertain hazards.
d	=	Control of interface variable, such as occurrence of a specific hazard intensity.
P[LS|D=d]	=	*fragility* = Conditional limit state probability, given that D=d, and the summation is taken over all values of D.
P[D=d]	=	Defines the hazard in terms of a probabilistic density function (or cumulative distribution function, P[D>d]).

2.4.3 Additional Literature

Many research studies related to seismic evaluation have been conducted. In particular, after developing the performance-based design concept, the methodology of seismic evaluation for existing buildings that are inadequate based on current seismic design codes was developed. Recently, research related to seismic vulnerability and the methodology of developing fragility curves has been actively conducted.

Hassan and Sozen (1997) described the seismic vulnerability of low-rise buildings with and without masonry infilled walls damaged by the 1992 Erzincan earthquake in Turkey. In addition, Gulkan and Sozen (1999) proposed a method to select buildings with higher seismic vulnerability based on wall and column indices relating the effective cross-sectional area to the total area of each member.

Shinozuka et al. (2000a) developed empirical fragility curves for the Hanshin Expressway Public Corporations' (HEPC's) bridges for the 1995 Kobe earthquake. In addition, analytical fragility curves were obtained for bridges in Memphis, Tennessee and these fragility curves were estimated by statistical procedures. In addition, Shinozuka et al. (2000b) applied nonlinear static procedures to develop fragility curves for bridges in Memphis. Synthetic ground motion generated by Hwang and Huo (1996) were used in this study. A fragility curve developed using the capacity spectrum method (CSM), which is a simplified approach, was compared with a fragility curve developed using nonlinear dynamic analysis. The fragility curve developed using the CSM showed good agreement for the region of minor damage, but the comparison was not as good for the region of major damage where nonlinear effects control structural systems.

Dumova-Jovanoska (2000) developed fragility curves for two RC structures (6-story and 16-story frame structures) in Skopje, Macedonia using 240 synthetic ground motion data for this region. The fragility curves were developed using discrete damage states from the damage index defined by Park et al. (1985).

Shama et al. (2002) investigated seismic vulnerability analysis for bridges supported by steel pile bents. They developed fragility curves for the original and retrofitted bridge probabilistically based on the uncertainties in demand and capacity. This curve showed that the retrofitting was effective for this bridge type.

Reinhorn et al. (2002) introduced a method for developing global seismic fragility of a RC structure with shear walls by a simplified approach in which fragility is evaluated from the spectral capacity curve and the seismic demand spectrum. The performance limit states which were investigated by Hwang and Huo (1994) were used to evaluate the seismic fragility of the structure. The investigation showed that the inelastic response was influenced by structural parameters such as yield strength,

damping ratio and post-yielding stiffness ratio. In addition, they investigated the fragility of structure and structural parameters including strength, stiffness and damping.

2.5 Seismic Retrofit Techniques for RC Structures

2.5.1 General

Generally, there are two ways to enhance the seismic capacity of existing structures. The first approach is based on strength and stiffness, which involves global modifications to the structural system (see Fig. 2.1). Common global modifications include the addition of structural walls, steel braces, or base isolators. The second approach is based on deformation capacity (see Fig. 2.2). In this approach, the ductility of components with inadequate capacities is increased to satisfy their specific limit states. The member-level retrofit includes methods such as the addition of concrete, steel, or fiber reinforced polymer (FRP) jackets to columns for confinement.

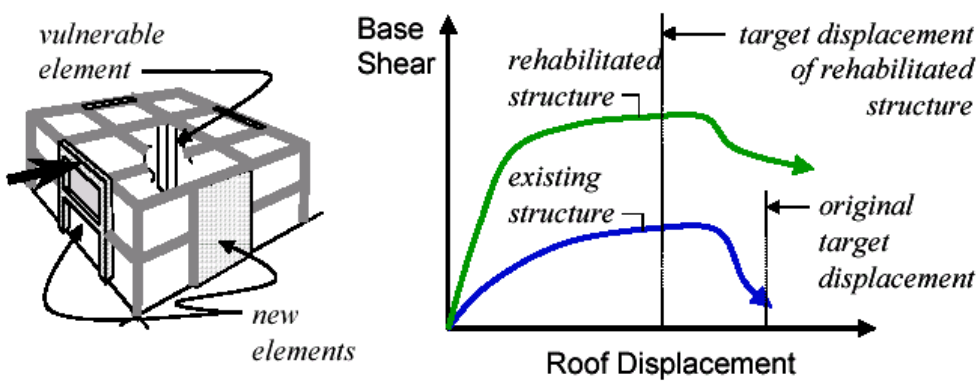

Fig. 2.1. Global modification of the structural system (Moehle 2000)

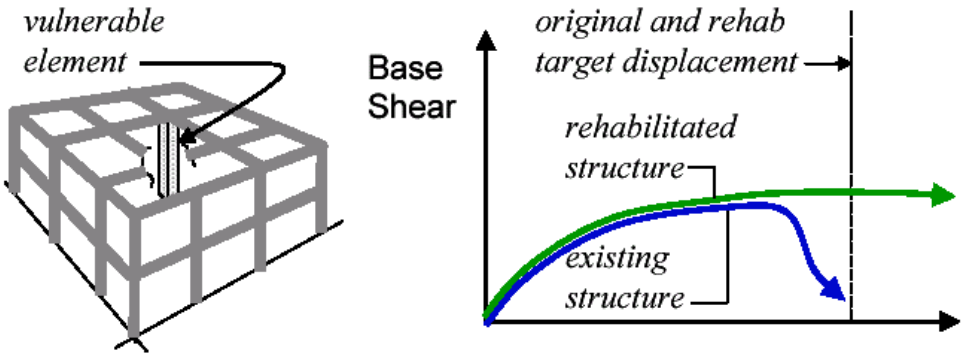

Fig. 2.2. Local modification of structural components (Moehle 2000)

There are many seismic retrofit techniques available, depending upon the various types and conditions of structures. Therefore, the selection of the type of intervention is a complex process, and is governed by technical as well as financial and sociological considerations. The following are some factors affecting the choice of various intervention techniques (Thermou and Elnashai 2002).

- Cost versus importance of the structure
- Available workmanship
- Duration of work/disruption of use
- Fulfillment of the performance goals of the owner
- Functionally and aesthetically compatible and complementary to the existing building
- Reversibility of the intervention
- Level of quality control
- Political and/or historical significance
- Compatibility with the existing structural system
- Irregularity of stiffness, strength and ductility
- Adequacy of local stiffness, strength and ductility
- Controlled damage to non-structural components
- Sufficient capacity of foundation system
- Repair materials and technology available

2.5.2 Structure-Level Retrofit

Structure-level retrofits are commonly used to enhance the lateral resistance of existing structures. Such retrofits for RC buildings include steel braces, post-tensioned cables, infill walls, shear walls, masonry infills, dampers, and base isolators. The methods described below are commonly used when implementing a structure-level retrofit technique.

2.5.2.1 Addition of RC Structural Walls

Adding structural walls is one of the most common structure-level retrofitting methods to strengthen existing structures. This approach is effective for controlling global lateral drifts and for reducing damage in frame members. Approaches include stiffening an existing shear wall or infilling one of the bays in the frame structure. In order to reduce time and cost, shotcrete or precast panels can be used.

Many research studies have been conducted for structural walls, and findings corresponding to detailed interventions have been reported (Altin et al. 1992, Pincheira and Jirsa 1995, Lombard et al. 2000, Inukai and Kaminosono 2000). The research shows that with the infilling process, details play an important role in the response of panels and the overall structure. The infilling process tends to stiffen the structure, which can lead to an increase in the lateral forces. The overturning effects and base shear are concentrated at the stiffer infill locations. Therefore, strengthening of the foundation is typically required at these locations.

Jirsa and Kreger (1989) tested one-story infill walls using four specimens. In their experiment, they used three one-bay, single-story, non-ductile RC frames that were designed to represent 1950s construction techniques. These included wide spacing in the column shear reinforcement and compression splices that were inadequate to develop the required tensile yield strength. In their experiment, the first three walls varied in their opening locations. Longitudinal reinforcement was added adjacent to the existing

columns to improve the continuity of the steel in the fourth specimen. The first three experiments had brittles failures due to the deficient column lap splices, even though the infill strengthened the frame. The fourth specimen enhanced both the strength and ductility of the frame (see Fig. 2.3).

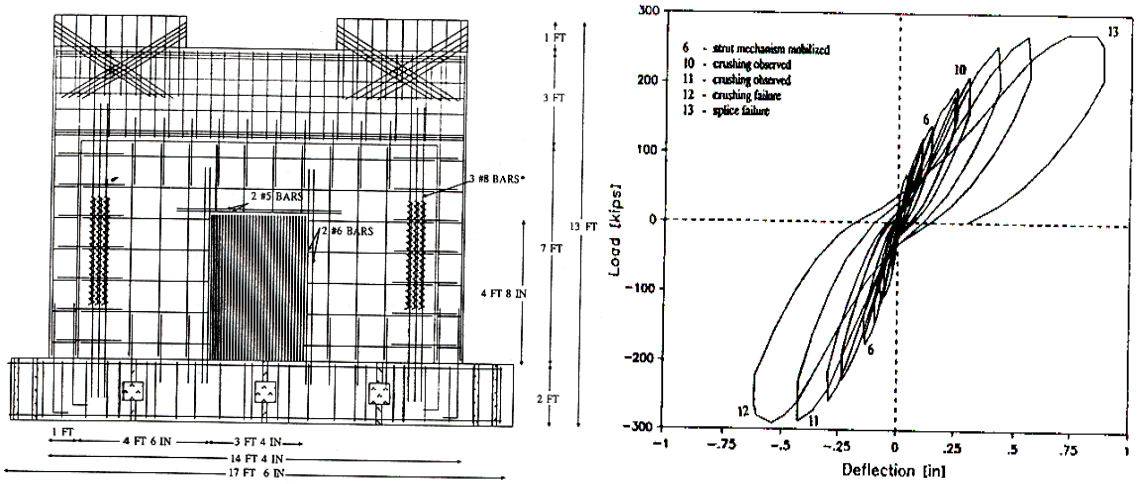

Fig. 2.3. Infill wall and load-deflection history of the specimen (Jirsa and Kreger 1989)

2.5.2.2 Use of Steel Bracing

The addition of steel bracing can be effective for the global strengthening and stiffening of existing buildings. Concentric or eccentric bracing schemes can be used in selected bays of an RC frame to increase the lateral resistance of the structure. The advantage of this method is that an intervention of the foundation may not be required because steel bracings are usually installed between existing members. Increased loading on the existing foundation is possible at the bracing locations and so the foundation must still be evaluated. In addition, the connection between the existing concrete frame and the bracing elements should be carefully treated because the connection is vulnerable during earthquakes.

Several researchers have investigated the application of steel bracing to upgrade RC structures (Badoux and Jirsa 1990, Bush et al. 1991, Teran-Gilmore et al. 1995).

Furthermore, post-tensioned steel bracing was studied by Miranda and Bertero (1990) to upgrade the response of low-rise school buildings in Mexico.

Pincheira and Jirsa (1995) conducted an analytical study for three-, seven-, and twelve-story RC frames using the computer program DRAIN-2D (Kannan and Powell 1973). They applied several retrofit techniques including post-tensioned bracing, structural steel bracing systems (X-bracing), and infill wall as rehabilitation schemes for low- and medium-rise RC frames. Nonlinear static and dynamic analyses were performed and five earthquake records on firm and soft soils were used for dynamic analysis. The bracing systems and infill walls were added only to the perimeter frames. Fig. 2.4 shows the comparison of base shear coefficient and drift for original and retrofitted twelve-story RC frame.

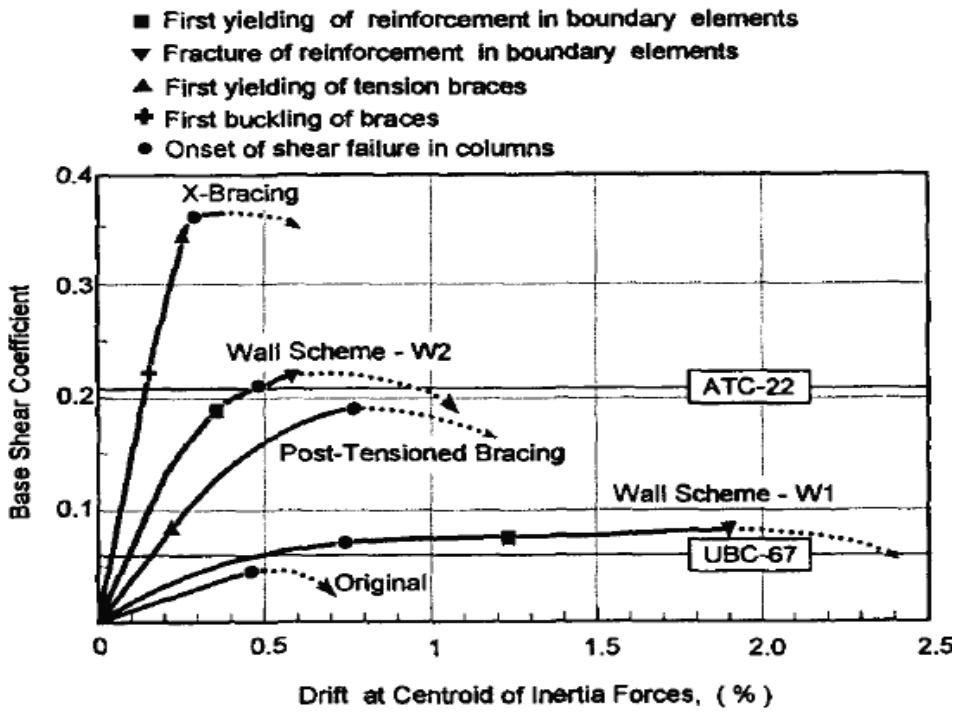

Fig. 2.4. Comparison of base shear coefficient and drift relationships for original and retrofitted 12-story building (Pincheira and Jirsa 1995)

Goel and Masri (1996) tested a weak slab-column building structure using a one-third scale, two-bay, two-story RC slab-column frame specimen. They tested two different phases of the steel bracing on both the exterior and interior bays, respectively, and compared them with the original RC frame. Fig. 2.5 shows the layout of the braced frame specimen. Fig 2.6 compares the hysteretic loops for the unretrofitted and retrofitted frame, showing the increase in strength, stiffness and energy dissipation due to retrofit. This observation was true for both retrofitted specimens. In particular, the results after applying the concrete-filled braces showed that the frame behaved in a very ductile manner through all fifteen cycles, with no failures.

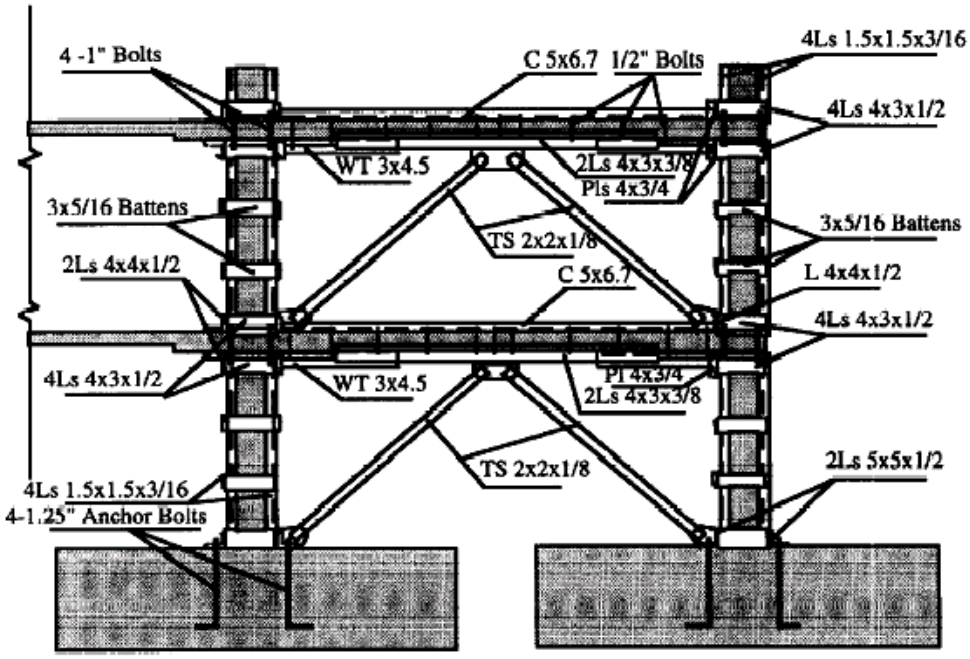

Fig. 2.5. Layout of the braced frame (Goel and Masri 1996)

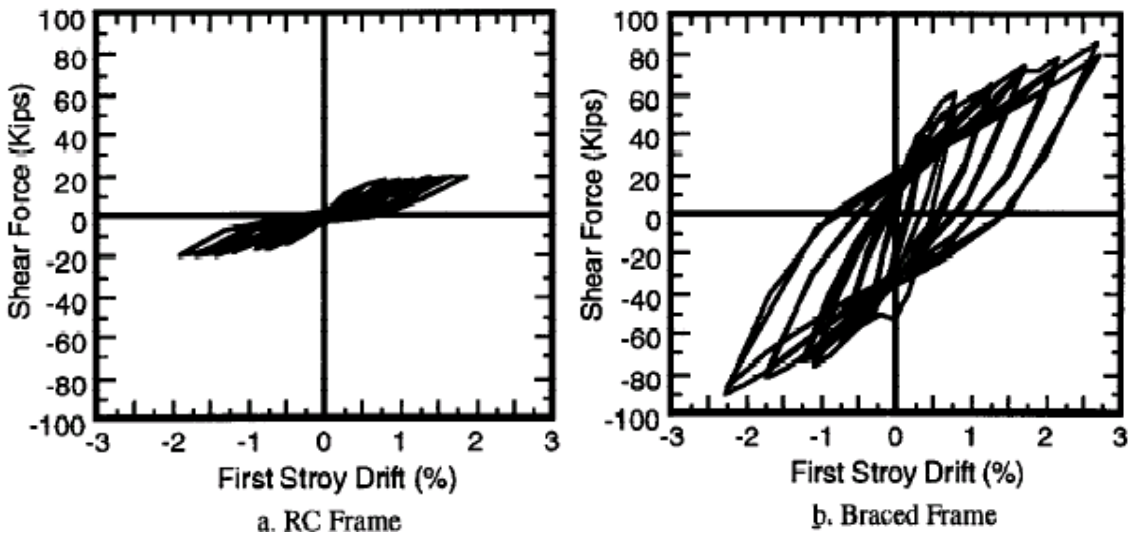

Fig. 2.6. Hysteretic loops of the RC and braced frames (Goel and Masri 1996)

2.5.2.3 Seismic Isolation

Recently, many researchers have studied seismic isolation as a possible retrofit method (Gates et al. 1990, Kawamura et al. 2000, Tena-Colunga et al. 1997, Constantinou et al. 1992). The objective of this type of retrofit is to isolate the structure from the ground motion during earthquake events. The bearings are installed between the superstructure and its foundations. Because most bearings have excellent energy dissipation characteristics, this technique is most effective for relatively stiff low-rise buildings with heavy loads.

2.5.2.4 Supplemental Energy Dissipation

The most commonly used approaches to add energy dissipation to a structure include installing frictional, hysteretic, viscoelastic, or magnetorheological (MR) dampers as components of the braced frames. A number of researchers have studied supplemental energy dissipation methods (Pekcan et al. 1995, Kunisue et al. 2000, Fu 1996, Munshi 1998, Yang et al. 2002). However, while lateral displacements are reduced through the use of supplemental energy dissipation, the forces in the structure can increase if they are not designed properly (ASCE 2000).

2.5.3 Member-Level Retrofit

In selected situations, member-level retrofit can provide a more cost-effective strategy than structure-level retrofit because only those components needed to enhance the seismic performance of the existing structure are selected and upgraded. The member-level retrofit approaches include the addition of concrete, steel, or fiber reinforced polymer (FRP) jackets for use in confining RC columns and joints. In particular, in flat-slab structures, punching shear failures are likely to occur if the slab is not designed for the combined effects of lateral and gravity loads. Therefore, local retrofits could be performed on slab-column connections. Recently, research related to member-level retrofits in the U.S. has actively investigated columns, beam-column joints, and slab-column joints (Harries et al. 1998, Luo and Durrani 1994, Farhey et al. 1993, Martinez et al. 1994).

2.5.3.1 Column Jacketing

Column retrofitting is often critical to the seismic performance of a structure. To prevent a story mechanism during an earthquake, columns should never be the weak link in the building structure. The response of a column in a building structure is controlled by its combined axial load, flexure, and shear. Therefore, column jacketing may be used to increase strength so that columns are not damaged (Bracci et al. 1995).

Recently, research has emphasized the applications of composite materials. In particular, carbon fiber reinforced polymer composite (FRPC) material may be used for jackets when retrofitting columns. Because these jackets sufficiently confine the columns, column failure through the formation of a plastic hinge zone can be prevented (see Fig. 2.7).

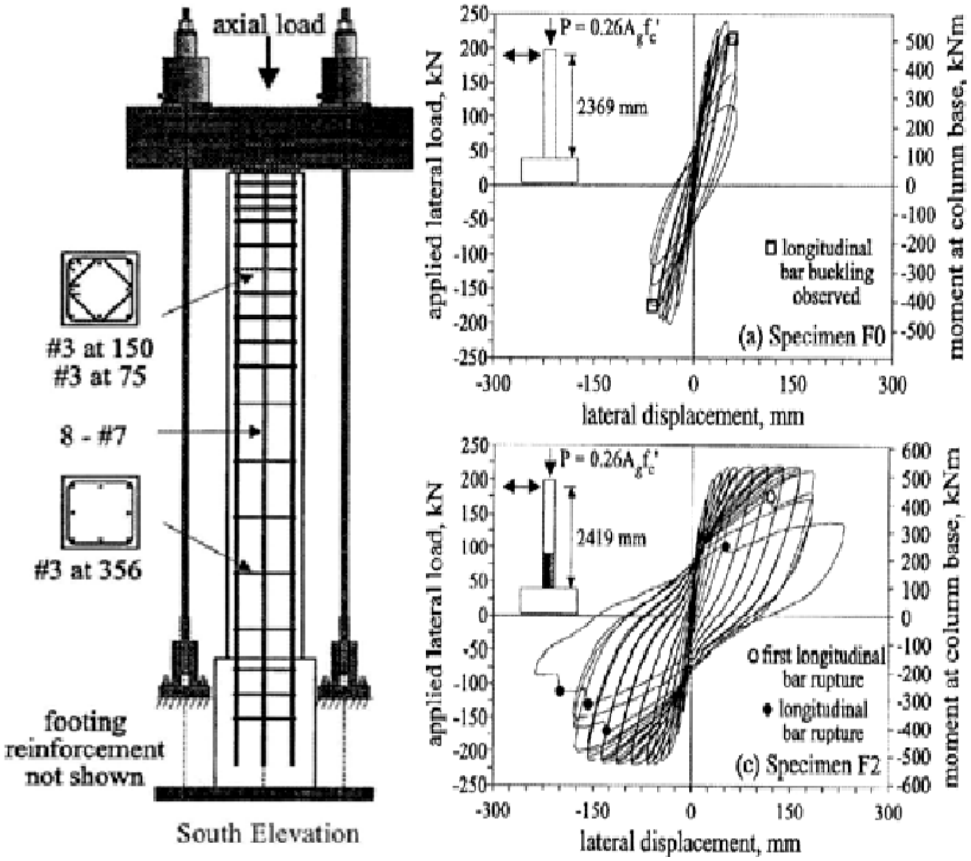

Fig. 2.7. Column retrofitting by carbon FRPC (Harries et al. 1998)

2.5.3.2 Slab-Column Connection Retrofits

In slab-column connections, punching shear failure due to the transfer of unbalanced moments is the most critical type of structural damage. The retrofitting of slab-column connections is beneficial for the prevention of punching shear failures and much research into retrofitting slab-column connections has been conducted (Luo and Durrani 1994, Farhey et al. 1993, Martinez et al. 1994) reported that adding concrete capitals or steel plates on both sides of the slab can prevent punching shear failures. Both solutions showed improvement in strength along the perimeter. The details of this method are shown in Fig 2.8.

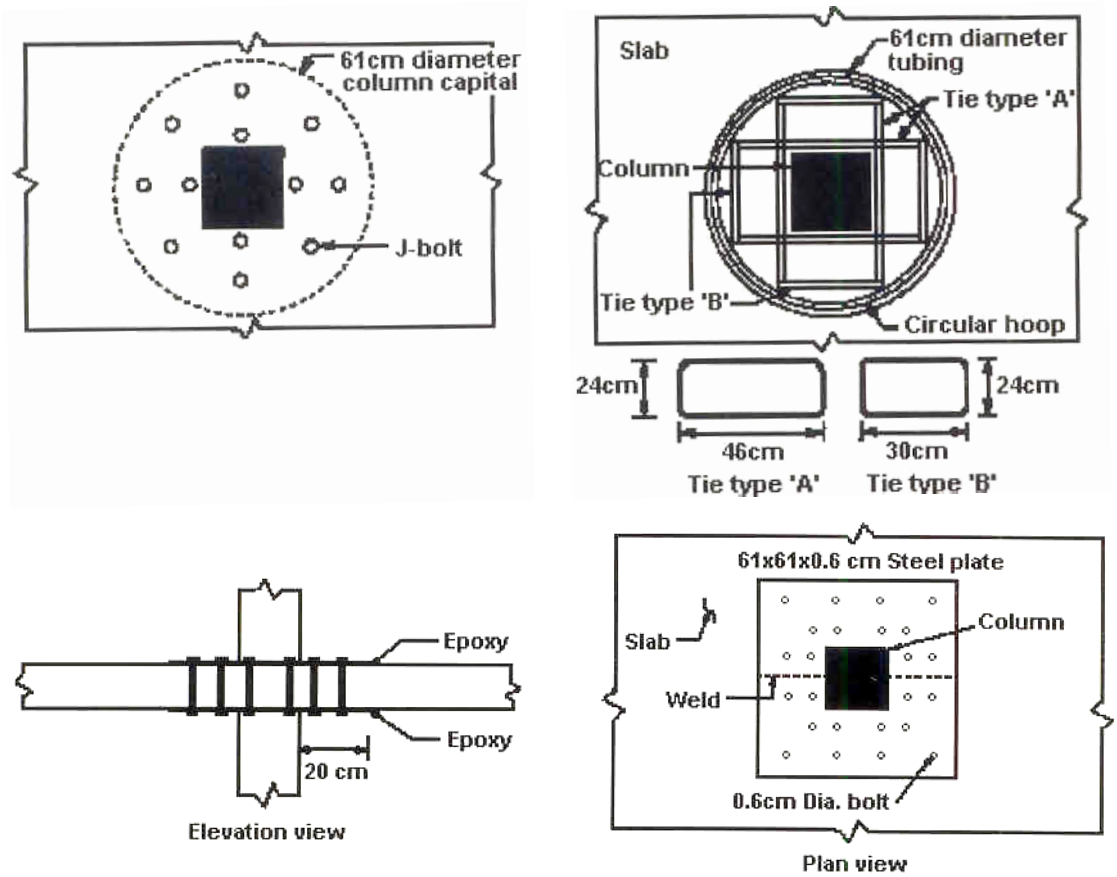

Fig. 2.8. Retrofit of slab-column connections (Martinez et al. 1994)

2.5.4 Selective Techniques

Elnashai and Pinho (1998) suggest classification of retrofitting techniques by their impact on structural response characteristics. This approach can be economical because only the necessary structural characteristics are modified. The experimental program was conducted by Elnashai and Salama (1992) at Imperial College. This theory was tested by individually increasing the three design response parameters: stiffness, strength and ductility. Concrete walls were used for the experimental program, and the experimental data were compared with computer analysis results. The influence of selective intervention techniques on the global behavior was determined. Fig 2.9 shows the elevation and cross-section of the specimen.

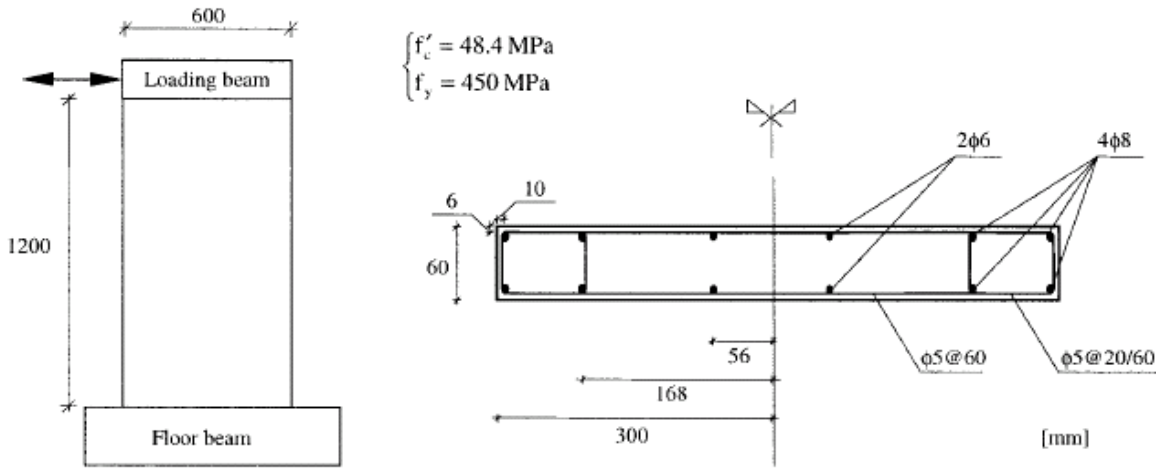

Fig. 2.9. Elevation and cross-section of the specimen (Elnashai and Pinho 1998)

For the stiffness-only scenario, external bonded steel plates were used to increase stiffness while minimizing any change in strength and ductility. In this approach, the height, width and thickness of the plate were important parameters to control the level of increase in the stiffness. To get the best results, the plates were placed as near to the edges of the specimens as possible. External unbonded reinforcement bars or external unbonded steel plates were used to increase strength only. Finally, for the ductility-only scenario, U-shaped external confinement steel plates were used. This was most effective when the plates were close together and the total height of the plates was maximized. The details of the test specimens are shown in Figs. 2.10 to 2.12.

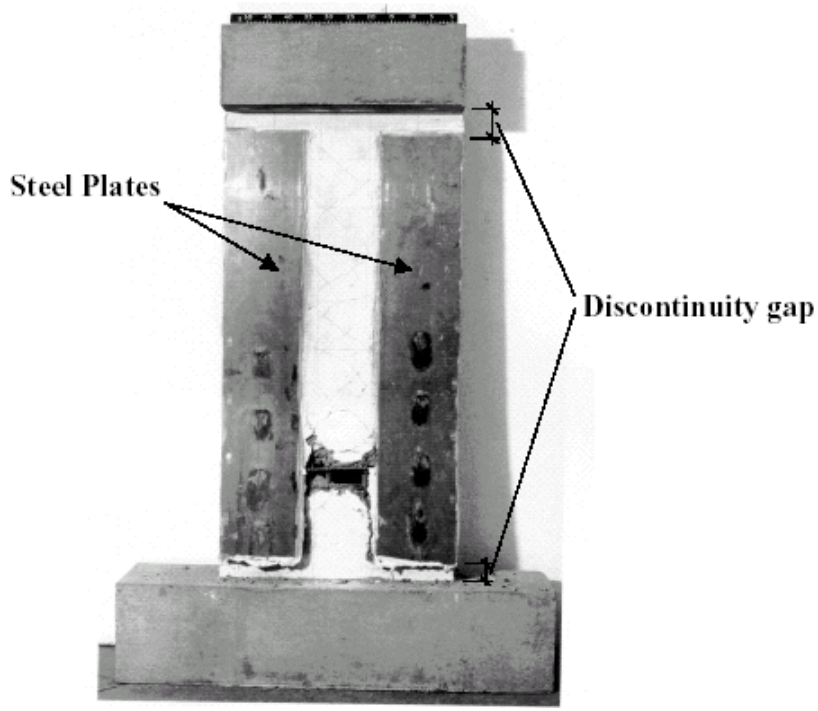

Fig. 2.10. Stiffness-only intervention test specimen (Elnashai and Salama 1992)

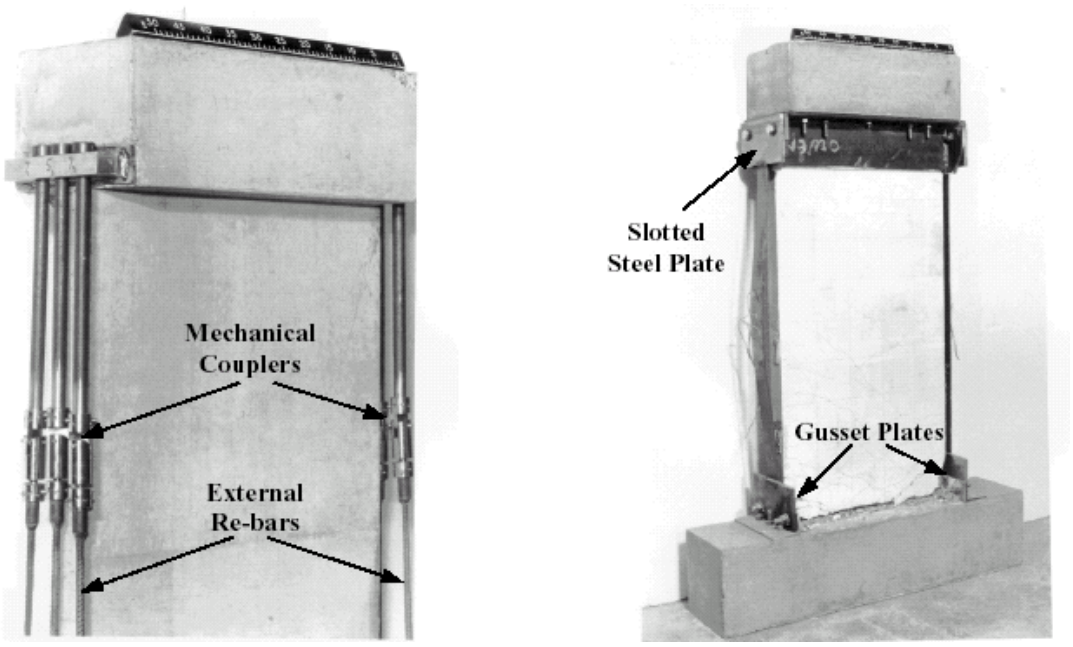

(a) External Unbonded Reinforcement Bars (b) External Unbonded Steel Plates

Fig. 2.11. Strength-only intervention test specimens (Elnashai and Salama 1992)

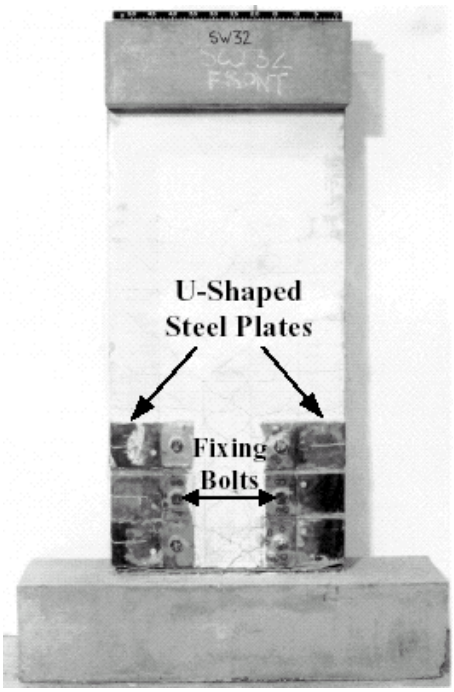

Fig. 2.12. Ductility-only intervention test specimen (Elnashai and Salama 1992)

3 CASE STUDY BUILDING

3.1 Introduction

Lightly reinforced RC building structures were selected as the structural system of interest for this study. The case study building is a five-story RC flat-slab structure with a perimeter frame that is based on a building layout developed by Hart (2000). The building is a frame system that is not detailed for ductile behavior and is designed based on codes used in the central U.S. in the mid-1980s. Hart (2000) surveyed several practicing engineers to determine typical structural systems used for office buildings in the central U.S. Low to moderate rise flat-slab buildings were found to be of particular interest because they are very common in the central U.S. and because there is a concern for potential damage to this type of structure during an earthquake of moderate intensity.

3.2 Building Description

The case study building is a five story RC flat-slab building with an overall height of 20.4 m (67 ft.) and a perimeter moment resisting frame. The first story is 4.58 m (15 ft.) high and the height of each of the remaining four stories is 3.97 m (13 ft.). The building is essentially rectangular in shape and is 42.7 m (140 ft.) long by 34.2 m (112 ft.) wide. The bay size is 8.54 m (28 ft.) by 8.54 m (28 ft.). Figs. 3.1 and 3.2 show the plan and elevation views of the case study building.

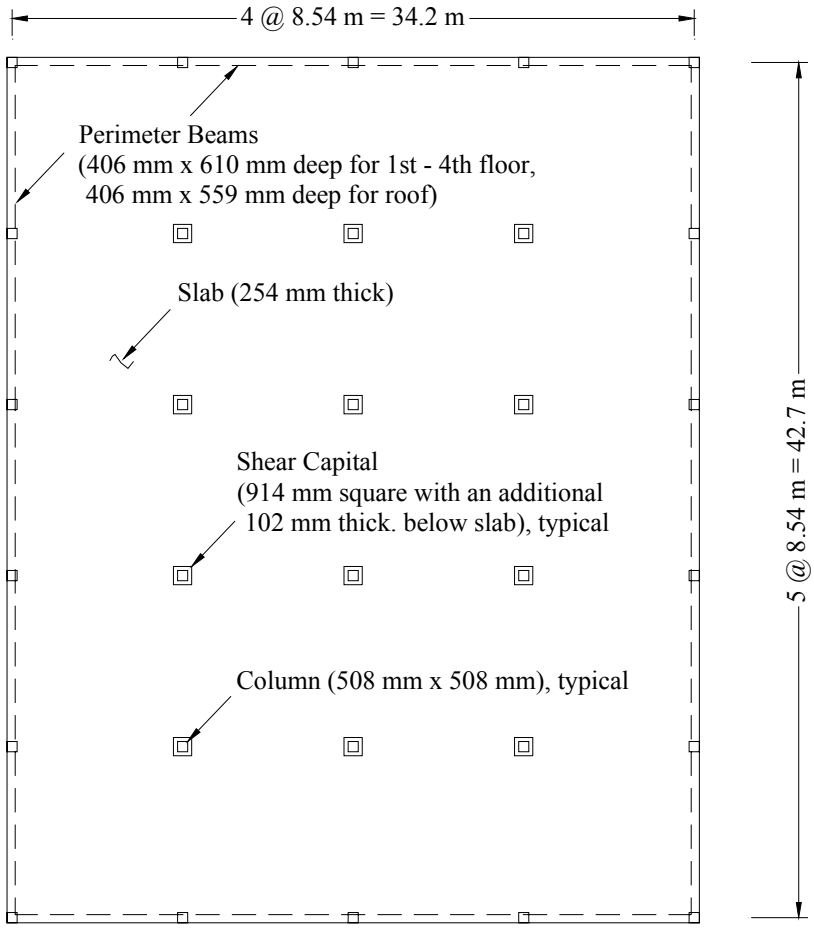

Fig. 3.1. Plan view of case study building

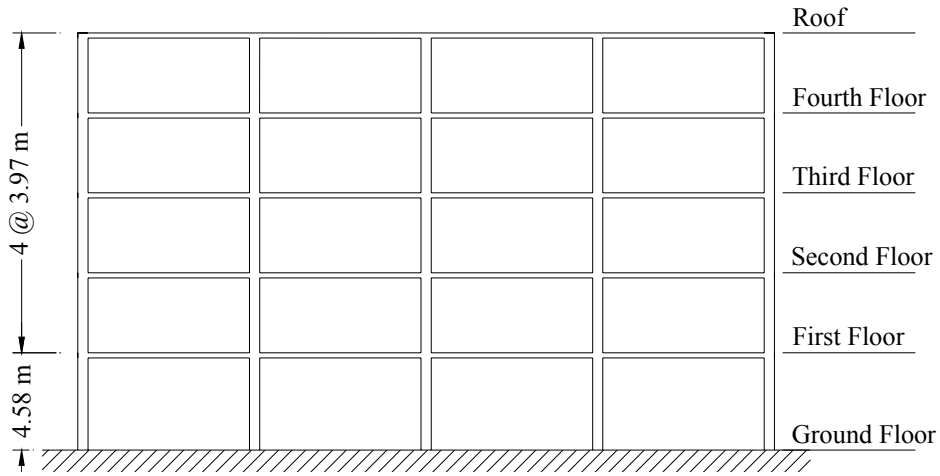

Fig. 3.2. Elevation view of case study building

3.3 Building Design

3.3.1 Design Codes

The case study building was designed according to the load requirements in the ninth edition of the *Building Officials and Code Administrators (BOCA) Basic/National Code* (BOCA 1984). This building was designed to be representative of those constructed in St. Louis, Missouri and Memphis, Tennessee in the mid-1980s. According to 1984 *BOCA* code, St. Louis, Missouri and Memphis, Tennessee have the same design wind loads and seismic zone factor (Zone 1). The design of structural components was carried out according to the provisions of the *American Concrete Institute (ACI) Building Code Requirements for Reinforced Concrete, ACI 318-83* (ACI Comm. 318 1983).

3.3.2 Loading

All design loads were determined according to Chapter 9 of the 1984 *BOCA* code. Dead loads included the self-weight of the structure, the partition load and the cladding load. The self-weight of reinforced concrete was assumed to be 23.6 kN/m^3 (150 pcf) and a partition loading of 958 N/m^2 (20 psf) was considered. For the exterior frames, a cladding loading of 719 N/m^2 (15 psf) was applied to each perimeter beam as a uniform load based on the vertical tributary area. The design live load for this office building is 2400 N/m^2 (50 psf) on each floor. The roof live load was calculated as the larger value of the roof loads and snow loads. The roof load for interior frame members is 575 N/m^2 (12 psf), which is for structural members with tributary area larger than 55.7 m^2 (600 ft.^{2}). The roof load for exterior frame members is 766 N/m^2 (16 psf), which is for buildings with tributary area between 18.6 m^2 (200 ft.^{2}) and 55.7 m^2 (600 ft.^{2}). The snow load for this structure is 814 N/m^2 (17 psf). The wind load was applied as a uniform load distributed vertically on the windward and leeward sides of the building and horizontally on the building's roof. Fig. 3.3 and Table 3.1 describe the wind load applied to the case study building.

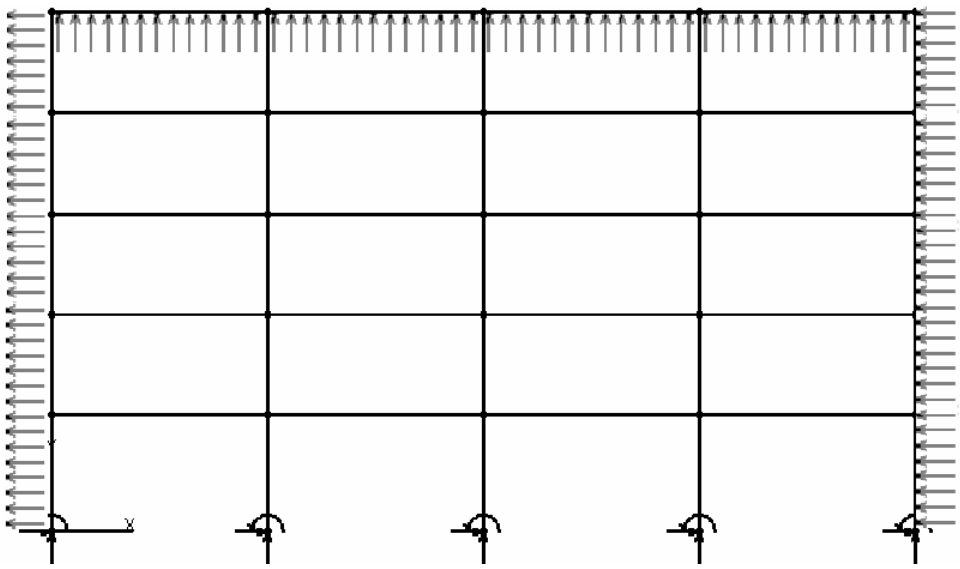

Fig. 3.3. Load pattern for wind load

Table 3.1. Wind load

Load type	WL_E (kN/m)	WL_I (kN/m)
Windward Wall	1.96	3.93
Leeward Wall	1.23	2.45
Roof	2.45	4.91

Notes:
WL_E = Wind load for exterior frame
WL_I = Wind load for interior frame
1 kN/m = 0.0685 kips/ft.

The 1984 *BOCA* specifies the total design seismic base shear as follows.

$$V = ZKCW \tag{3.1}$$

where:

Z = Seismic zone factor = 0.25 for Zone 1 in Figure 916 of 1984 *BOCA*
K = Horizontal force factor for buildings = 1.0
C = Coefficient based on fundamental period of building = $0.05 \div \sqrt[3]{T}$ = 0.063

T = Fundamental period of vibration of the building or structure in seconds in the direction under consideration, estimated as $0.10N$ = 0.5 s

W = Weight of structure = 55,100 kN (includes self-weight, cladding and partition load)

Based on the above equation, the base shear of this case study building is 868 kN (195 kips). This is 1.6 percent of the building's seismic weight, W. The design seismic loads at each level are calculated using the following expression.

$$F_x = \frac{(V - F_t) w_x h_x}{\sum w_i h_i} \tag{3.2}$$

where:

F_x = Lateral force applied to level x

V = Design seismic base shear, as calculated using Eq. 3.1

F_t = That portion of V considered concentrated at the top of the structure at level n, not exceeding $0.15V$ and may be considered as 0 for values of h_n / D_s of 3 or less, where h_n =20.4 m and D_s =42.7 m

w_x, w_i = Weight of a given floor level x or i measured from the base

h_x, h_i = Height of a given floor level x or i measured from the base

The factored load combinations of *ACI 318-83,* listed in Eqs. 3.3 through 3.7, were used to compute the factored design forces. Fig. 3.4 shows the four live load patterns for the frame in the short direction.

(i) $U = 1.4D + 1.7L$ (3.3)

(ii) $U = 0.75\ (1.4D + 1.7L + 1.7W)$ (3.4)

(iii) $U = 0.9D \pm 1.3W$ (3.5)

(iv) $U = 0.75\ (1.4D + 1.7L \pm 1.7\ (1.1E))$ (3.6)

(v) $U = 0.9D \pm 1.3\ (1.1E)$ (3.7)

where:

D = Dead load
L = Live load
W = Wind load
E = Earthquake load

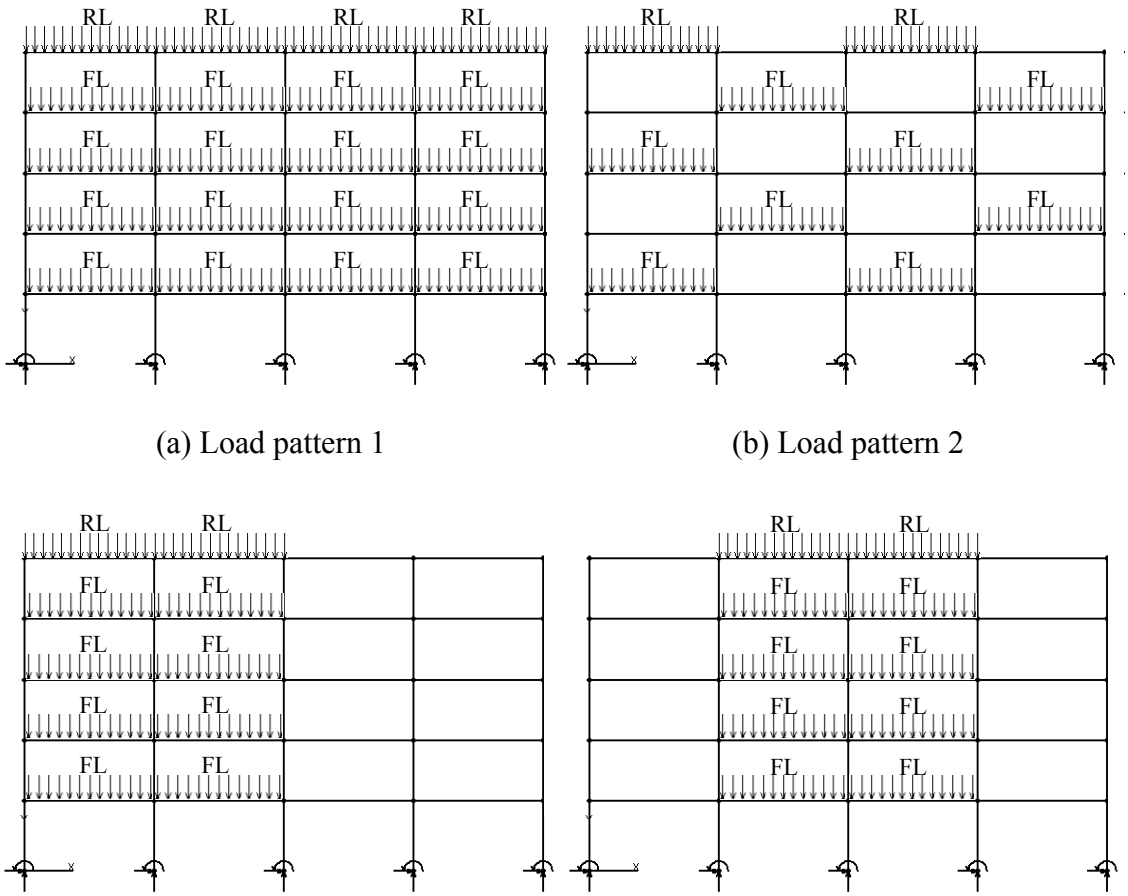

(a) Load pattern 1 (b) Load pattern 2

(c) Load pattern 3 (d) Load patterns 4

RL = Roof live load, FL = Floor live load

Fig. 3.4. Live load patterns

A structural analysis of the building was conducted using Visual Analysis 3.5 (IES 1998). Because the case study building has a symmetrical configuration and no irregularities, half of the building as a two-dimensional analytical model, was analyzed.

The perimeter beams and columns were designed based on the results of structural analysis using the above factored load combinations. The perimeter frames were designed to resist the full design lateral loads, including wind and seismic loads, based on design practices that were common and generally accepted during the 1980s. Based on the analytical results, the perimeter beams and columns were mostly controlled by load combinations including earthquake loads.

3.3.3 Structural Member Details

Normal weight concrete having a specified compressive strength of 27.6 MPa (4000 psi) was used for the design of the beams, slabs and columns. Grade 60 reinforcement was used for the longitudinal and transverse reinforcement in all major structural members. The perimeter beams are 406 mm (16 in.) wide by 610 mm (24 in.) deep for the first through the fourth floors, and the roof perimeter beams are 406 mm (16 in.) wide by 559 mm (22 in.) deep. The two-way slab is 254 mm (10 in.) thick. The minimum thickness of the slab was calculated using the following equations from *ACI 318-83*:

$$h = \frac{l_n(800 + 0.005 f_y)}{36,000 + 5000\beta\left[\alpha_m - 0.5(1-\beta_s)\left(1+\frac{1}{\beta}\right)\right]} \tag{3.8}$$

but not less than

$$h = \frac{l_n(800 + 0.005 f_y)}{36,000 + 5000\beta(1+\beta_s)} \tag{3.9}$$

and need not be more than

$$h = \frac{l_n(800 + 0.005 f_y)}{36,000} \tag{3.10}$$

where:

h = Overall thickness of two-way slab member, in.
l_n = Length of clear span in long direction of two-way construction, measured face-to-face of supports in slabs without beams and face-to-face of beams or other supports in other cases
f_y = Specified yield strength of nonprestressed reinforcement, psi
α_m = Average value of α for all beams on edges of a panel
β = Ratio of clear spans in long to short direction of two-way slabs
β_s = Ratio of length of continuous edges to total perimeter of a slab panel

The slabs were designed for gravity loads using the direct design method for two-way slab design, which is described in Chapter 11 of *ACI 318-83*. Shear capitals that are 914 mm (36 in.) square and provide an additional 102 mm (4 in.) of thickness below the slab are used at all interior slab-column connections, except at the roof level. The shear capitals were needed because the two-way shear strength at the slab-column connections was not adequate for gravity loads when only a 254 mm (10 in.) thick slab is used. The columns are 508 mm (20 in.) square. The transverse reinforcement in the beam and column members was selected to meet the minimum requirements in Chapter 7of *ACI 318-83*. According to *ACI 318-83*, the maximum permissible spacing of the transverse reinforcement for the perimeter beams and columns are 279 mm (11 in.) and 457 mm (18 in.), respectively. For the beam members, 254 mm (10 in.) spacing was selected. Tables 3.2 to 3.5 summarize the reinforcement in the perimeter beams, slabs for the specific floor levels and columns, respectively.

Table 3.2. Reinforcement in perimeter beams

Floor level	Beam width (mm)	Beam depth (mm)	Number of reinforcing bars		Bar size (US)	Stirrups (US)
1st – 2nd	406	610	Top	7	#8	#4 @ 254 mm c/c
			Bottom	3		
3rd	406	610	Top	6	#8	#4 @ 254 mm c/c
			Bottom	3		
4th	406	610	Top	5	#8	#4 @ 254 mm c/c
			Bottom	3		
Roof	406	559	Top	5	#8	#4 @ 254 mm c/c
			Bottom	3		

Note: 1 in. = 25.4 mm

Table 3.3. Reinforcement in slabs (1st – 4th floor level)

Frame	Span	Strip		Reinforcement (US)
Edge	End	Column	Exterior negative	#5 @ 432 mm
			Positive	
			Interior negative	
		Middle	Exterior negative	#5 @ 432 mm
			Positive	
			Interior negative	#5 @ 406 mm
	Interior	Column	Positive	#5 @ 432 mm
			Interior negative	
		Middle	Positive	#5 @ 432 mm
			Interior negative	
Interior	End	Column	Exterior negative	#5 @ 254 mm
			Positive	#5 @ 229 mm
			Interior negative	#5 @ 127 mm
		Middle	Exterior negative	#5 @ 432 mm
			Positive	#5 @ 356 mm
			Interior negative	#5 @ 406 mm
	Interior	Column	Positive	#5 @ 330 mm
			Interior negative	#5 @ 127 mm
		Middle	Positive	#5 @ 432 mm
			Interior negative	

Note: 1 in. = 25.4 mm

Table 3.4. Reinforcement in slabs (roof level)

Frame	Span	Strip		Reinforcement (US)
Edge	End	Column	Exterior negative	#5 @ 318 mm
			Positive	
			Interior negative	
		Middle	Exterior negative	#5 @ 406 mm
			Positive	
			Interior negative	
	Interior	Column	Positive	#5 @ 318 mm
			Interior negative	
		Middle	Positive	#5 @ 406 mm
			Interior negative	
Interior	End	Column	Exterior negative	#5 @ 305 mm
			Positive	#5 @ 229 mm
			Interior negative	#5 @ 152 mm
		Middle	Exterior negative	#5 @ 368 mm
			Positive	
			Interior negative	
	Interior	Column	Positive	#5 @ 368 mm
			Interior negative	#5 @ 165 mm
		Middle	Positive	#5 @ 368 mm
			Interior negative	

Note: 1 in. = 25.4 mm

Table 3.5. Reinforcement in columns

Column location	Story	Column width (mm)	Number of reinforcing bars	Bar size (US)	Tie bar size (US)
Exterior	1st – 5th	508	8	#9	#3 @ 457 mm c/c
Interior	1st	508	16	#9	#3 @ 457 mm c/c
Interior	2nd - 5th	508	8	#9	#3 @ 457 mm c/c

Note: 1 in. = 25.4 mm

Typical details for the columns and perimeter beams are shown in Figs. 3.5 and 3.6. The ties for the columns have 90 degree hooks. Figs. 3.7 and 3.8 show details for the slab reinforcement and Fig. 3.9 show details for the beam reinforcement.

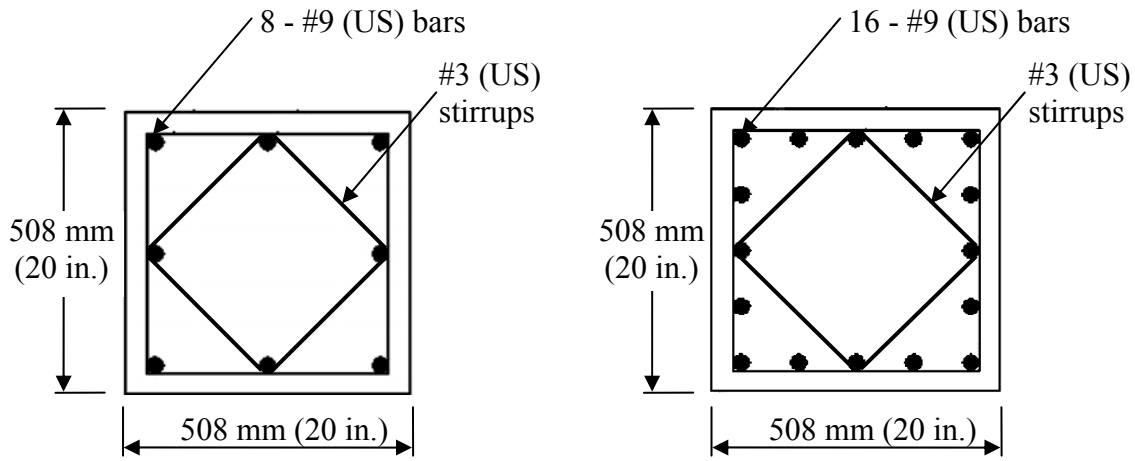

(a) 1st ~ 5th Story for External Frame
2nd ~ 5th Story for Interior Frame

(b) 1st Story for Interior Frame

Fig. 3.5. Typical column cross sections

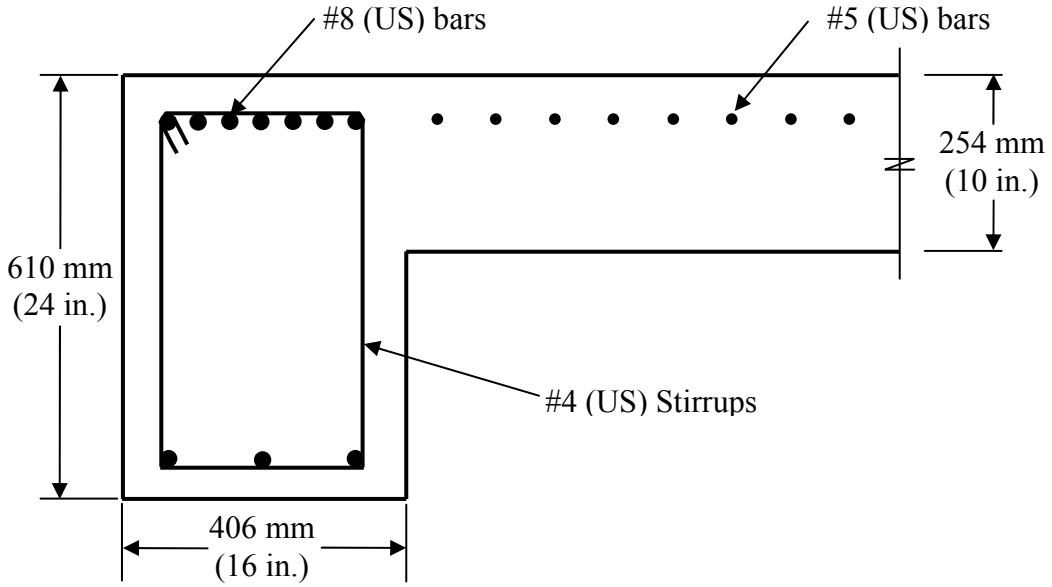

Fig. 3.6. Typical first floor beam cross section

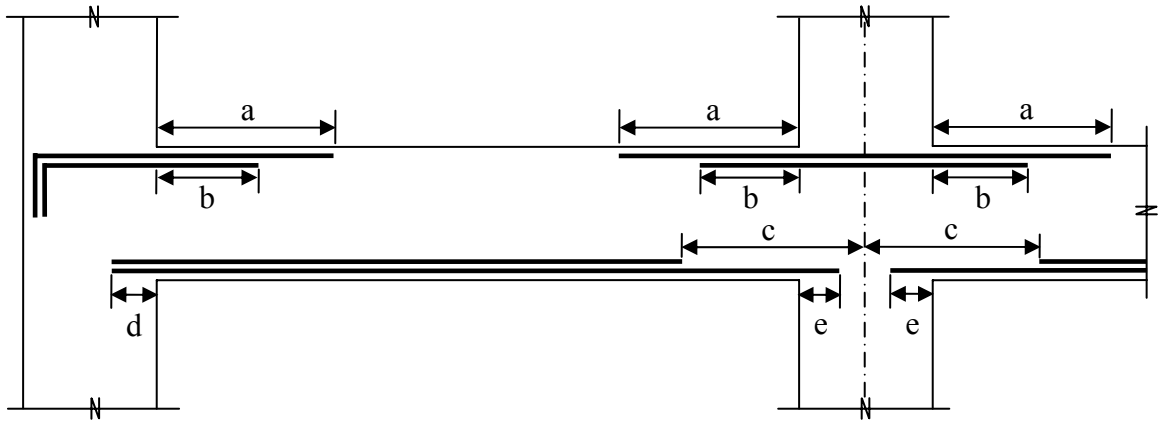

a: 241 cm (95 in.) - 50% of negative moment reinforcement
b: 163 cm (64 in.) - 50% of negative moment reinforcement
c: 107 cm (42 in.) - 50% of positive moment reinforcement
d: 15.2 cm (6 in.) - positive moment reinforcement embedded at exterior support
e: 17.8 cm (7 in.) - 50% of positive moment reinforcement embedded at interior support

Fig. 3.7. Details of slab reinforcement for column strip of case study building

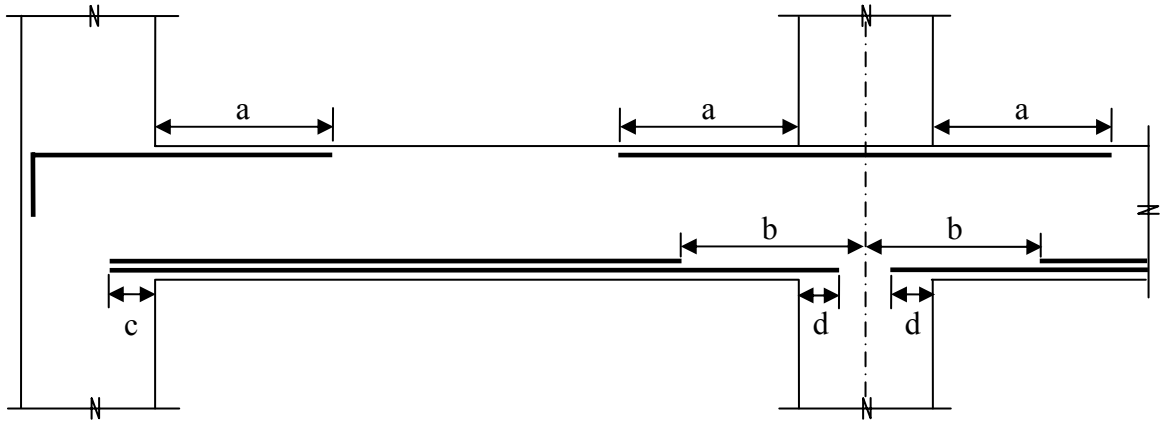

a: 178 cm (70 in.) - 100% of negative moment reinforcement
b: 127 cm (50 in.) - 50% of positive moment reinforcement
c: 15.2 cm (6 in.) - positive moment reinforcement embedded at exterior support
d: 17.8 cm (7 in.) - 50% of positive moment reinforcement embedded at interior support

Fig. 3.8. Details of slab reinforcement for middle strip of case study building

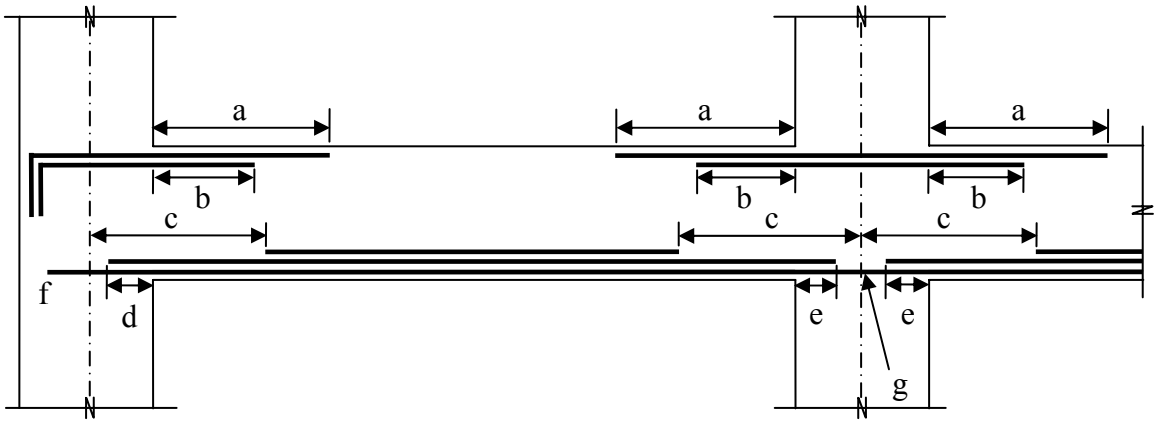

a: 345 cm (136 in.) - 1 bar of negative moment reinforcement at 1st and 2nd floors
b: 178 cm (70 in.) - 4 bars of negative moment reinforcement at 1st and 2nd floors
208 cm (82 in.) - 4 bars of negative moment reinforcement at 3rd floor
178 cm (70 in.) - 3 bars of negative moment reinforcement at 4th floor and roof
c: 127 cm (50 in.) - 1 bar of positive moment reinforcement at 1st - 4th floors
224 cm (88 in.) - 1 bar of positive moment reinforcement at roof
d: 15.2 cm (6 in.) - positive moment reinforcement except 2 bars that are fully-developed at exterior support
e: 17.8 cm (7 in.) - positive moment reinforcement except 2 bars that are continuous at interior support
f: 2 bars of positive moment reinforcement fully-developed at exterior support
g: 2 bars of positive moment reinforcement continuous at interior support

Fig. 3.9. Details of beam reinforcement for case study building

4 MODELING OF CASE STUDY BUILDING

4.1 Introduction

This section presents the modeling procedures for the case study building. In this study, two different approaches for modeling and analyzing the case study building were evaluated and compared: a fiber model and a macromodel. The ZEUS-NL program (Elnashai et al. 2002) was selected for the fiber model and DRAIN-2DM program (Kanann and Powell 1973, Powell 1973, Al-Haddad and Wight 1986, Tang and Goel 1988, Raffaelle and Wight 1992, Soubra et al. 1992, Hueste and Wight 1997a) was used for the macromodel. The synthetic ground motion data developed by Wen and Wu (2000) for St. Louis, Missouri and Memphis, Tennessee were used for the dynamic analysis and fragility curve development. In addition, new synthetic ground motion data developed by Rix and Fernandez-Leon (2004) for Memphis, Tennessee were used for the development of additional fragility curves. The following sections describe the analytical models, modeling assumptions and synthetic ground motions.

4.2 Description of Nonlinear Analysis Tools

4.2.1 General

In this study, the ZEUS-NL and DRAIN-2DM programs were used for the nonlinear structural analysis. The fundamental equation of motion used to determine the dynamic response for the structural models is given in Eq. 4.1.

$$[M]\{a\} + [C]\{v\} + [K]\{u\} = -[M]\,a_g \tag{4.1}$$

where:

[M] = Mass matrix
{a} = Acceleration vector

[C] = Viscous damping matrix
{v} = Velocity vector
[K] = Structural stiffness matrix
{u} = Displacement vector
a_g = Ground acceleration

Both programs use the Newmark integration method to solve the equation of motion for each time step. An integration factor of 0.5, corresponding to an average acceleration during the time step, was selected for this study. The programs have significant differences in the formulation of the structural elements, as described below. The time step of 0.005 second for DRAIN-2DM was used for nonlinear time history analysis. However, to reduce computation time, a time step of 0.01 second was used for the ZEUS-NL analysis with ground motions developed by Wen and Wu (2000). This is the same as the time step for the ground motion records. For ground motions developed by Rix and Fernandez-Leon (2004), a time step of 0.005 second was used for the ZEUS-NL analysis. This also corresponds to the time step for the ground motion records.

4.2.2 ZEUS-NL Program

4.2.2.1 General

ZEUS-NL is a finite element structural analysis program developed for nonlinear dynamic, conventional and adaptive push-over, and eigenvalue analysis. The program can be used to model two-dimensional and three-dimensional steel, RC and composite structures, taking into account the effects of geometric nonlinearities and material inelasticity. The program uses the fiber element approach to model these nonlinearities. Fiber models are widely used because of their suitability for describing the interaction between the flexural behavior and the axial force. Fig. 4.1 presents a decomposition of a rectangular RC section. As shown below, the response of elements is computed by assembling the responses of individual fibers that consist of many individual areas of monitoring points where the constitutive relationships are applied. Each fiber is classified by the appropriate material stress-strain relationship.

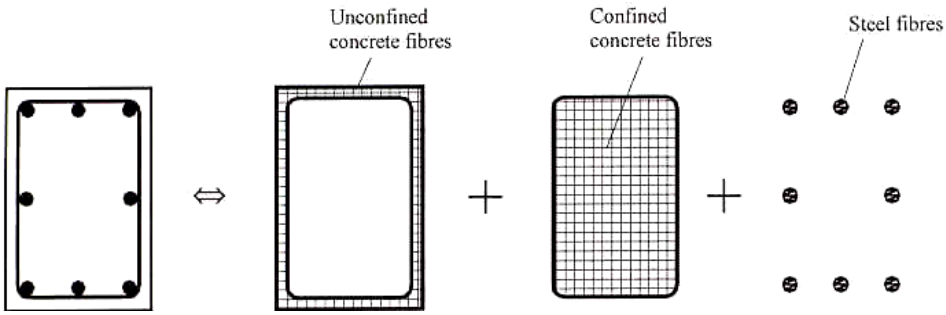

Fig. 4.1. Decomposition of a rectangular RC section (Elnashai et al. 2000)

4.2.2.2 Element and Cross Section Types

There are six element types in ZEUS-NL, as shown in Table 4.1. The Cubic element is used to model structural elements. The Cubic element is an elasto-plastic three-dimensional (3D) beam-column element used for detailed inelastic modeling. To compute the element forces, the stress-strain relationship of monitoring areas is computed by numerical integration at the two Gauss points. For instance, 100 monitoring points may be used for an rss (rectangular solid section) section, which is a single-material section, but more complicated sections such as an rcts (RC T-section) section, may require 200 monitoring points. Several elements are available to include mass and damping (Lmass, Dmass, Ddamp and Rdamp). The joint element is used for modeling supports and joints. Fourteen cross-section types are available in the ZEUS-NL program (see Table 4.2). The cross-section types include single-material sections, RC sections and composite sections.

Table 4.1. Element types in ZEUS-NL

Type	Description
Cubic	Cubic elasto-plastic 3D beam-column element
Joint	3D joint element with uncoupled axial, shear and moment actions
Lmass	Lumped mass element
Dmass	Cubic distributed mass element
Ddamp	Dashpot viscous damping element
Rdamp	Rayleigh damping element

Table 4.2. Cross-section types in ZEUS-NL

Type	Description
rss	Rectangular solid section
css	Circular solid section
chs	Circular hollow section
sits	Symmetric I- or T-section
alcs	Asymmetric L- or C-section
pecs	Partially encased composite I-section
fecs	Fully encased composite I-section
rcrs	RC rectangular section
rccs	RC circular section
rcts	RC T-section
rcfws	RC flexural wall section
rchrs	RC hollow rectangular section
rchcs	RC hollow circular section
rcjrs	RC jacket rectangular section

4.2.2.3 Material Models

There are four material models in the ZEUS-NL program. Stl1 is a bilinear elasto-plastic model with kinematic strain-hardening. This material model is used for steel and includes definition of Young's modulus, the yield strength and a strain-hardening parameter. Con1 is the simplified model for uniaxial modeling of concrete where the initial stiffness, compressive strength, degradation stiffness and residual strength are defined. Con2 is applied for uniaxial modeling of concrete assuming constant confinement with a confinement factor. Con3 is a uniaxial variable confinement concrete model. Descriptions of each material model are shown in Table 4.2. Fig. 4.2 shows typical stress-strain curves for each material model, respectively.

Table 4.3. Material models in ZEUS-NL

Type	Description
Stl1	Bilinear elasto-plastic model with kinematic strain-hardening
Con1	Trilinear concrete model
Con2	Uniaxial constant confinement concrete model
Con3	Uniaxial variable confinement concrete model

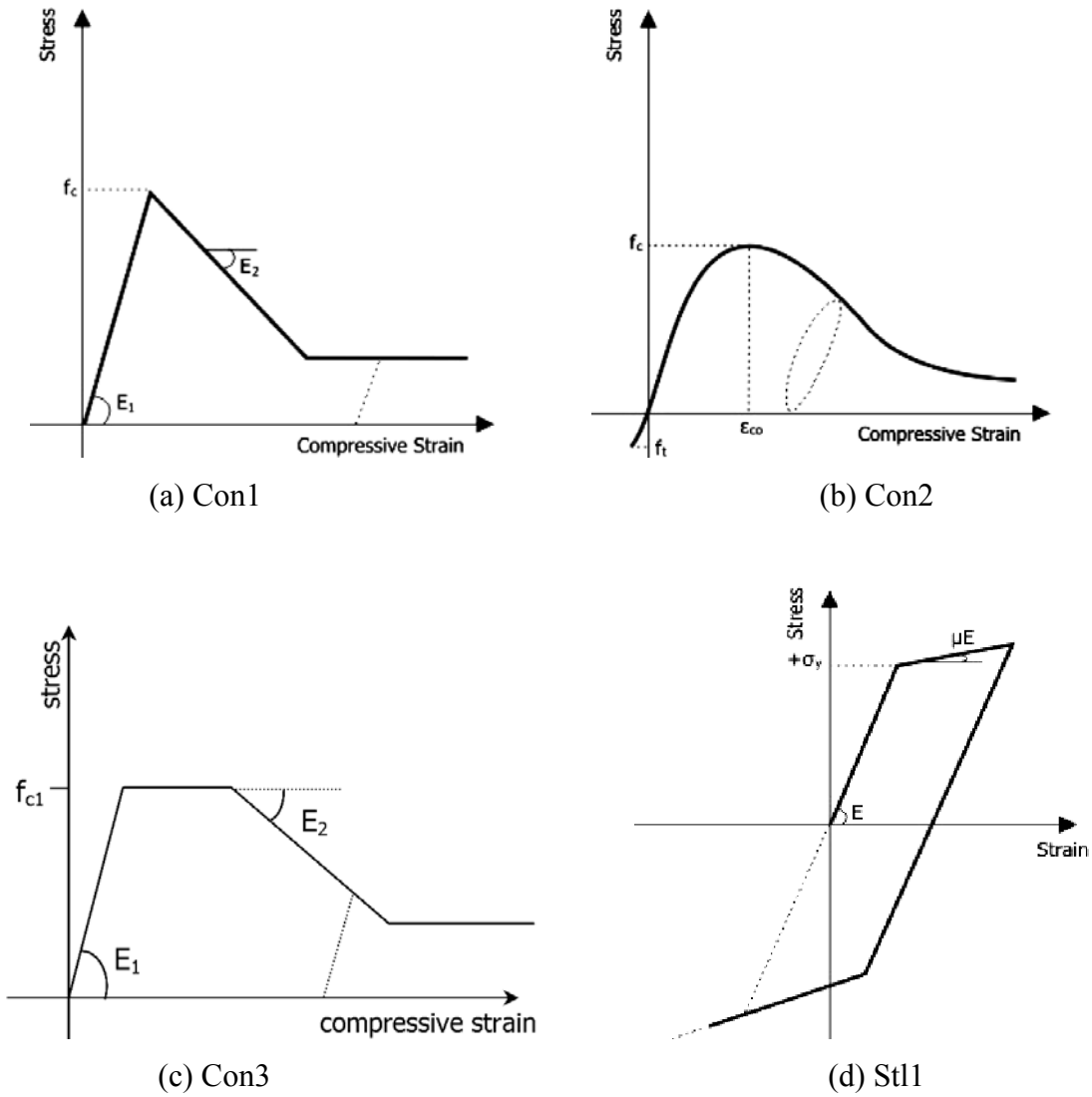

(a) Con1 (b) Con2

(c) Con3 (d) Stl1

Fig. 4.2. Material models for ZEUS-NL analysis (Elnashai et al. 2002)

4.2.3 DRAIN-2DM Program

4.2.3.1 General

The original program DRAIN-2D was developed at the University of California, Berkeley (Kanaan and Powell 1973, Powell 1973). This program is capable of modeling the behavior of structures in the elastic and inelastic ranges for static and dynamic analysis. In this study, a modified version of the program called DRAIN-2DM, which

was developed at the University of Michigan, was used. DRAIN-2DM performs nonlinear analysis of frame structure with the capability of predicting punching shear behavior of RC slab members (Al-Haddad and Wight 1986, Tang and Goel 1988, Raffaelle and Wight 1992, Soubra et al. 1992, Hueste and Wight 1997a).

4.2.3.2 Element and Cross Section Types

Table 4.4 shows ten element types available in DRAIN-2DM. In most cases for RC structures, the beam-column element, RC beam element and RC slab element are used for structural analysis.

Table 4.4. Element types in DRAIN-2DM

Type	Description
Element 1	Truss element
Element 2	Beam-column element
Element 3	Infill panel element
Element 4	Semi-rigid connection element
Element 5	Beam element
Element 6	Shear link element
Element 8	RC beam element
Element 9	Buckling element
Element 10	End moment-buckling element
Element 11	RC slab element

The beam-column element (Element 2) has both flexural and axial stiffness. Yielding may occur only in concentrated plastic hinges at the element ends. A plastic hinge is formed within the elasto-plastic element when the combination of axial force and moment falls outside the axial load versus moment interaction envelope, which describes yield conditions for the member cross-section. Strain hardening is assumed such that the element consists of elastic and elasto-plastic components in parallel, as describes by the moment versus rotation relationship shown in Fig. 4.3.

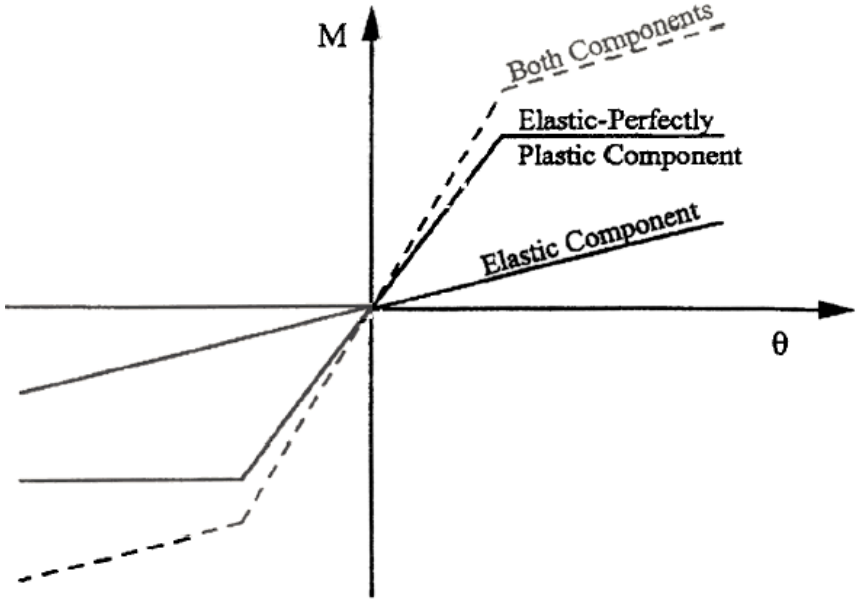

Fig. 4.3. Bilinear moment-rotation relationship for beam-column element (Element 2) (Soubra et al. 1992)

Element 8 is a RC beam element that yields under flexure only. This element consists of an elastic line element and two nonlinear flexural springs. The nonlinear behavior is concentrated in the springs, which can be located at some distance from the column face. The hysteretic model for this element includes the effects of stiffness degradation, strength deterioration and pinching (see Fig. 4.4).

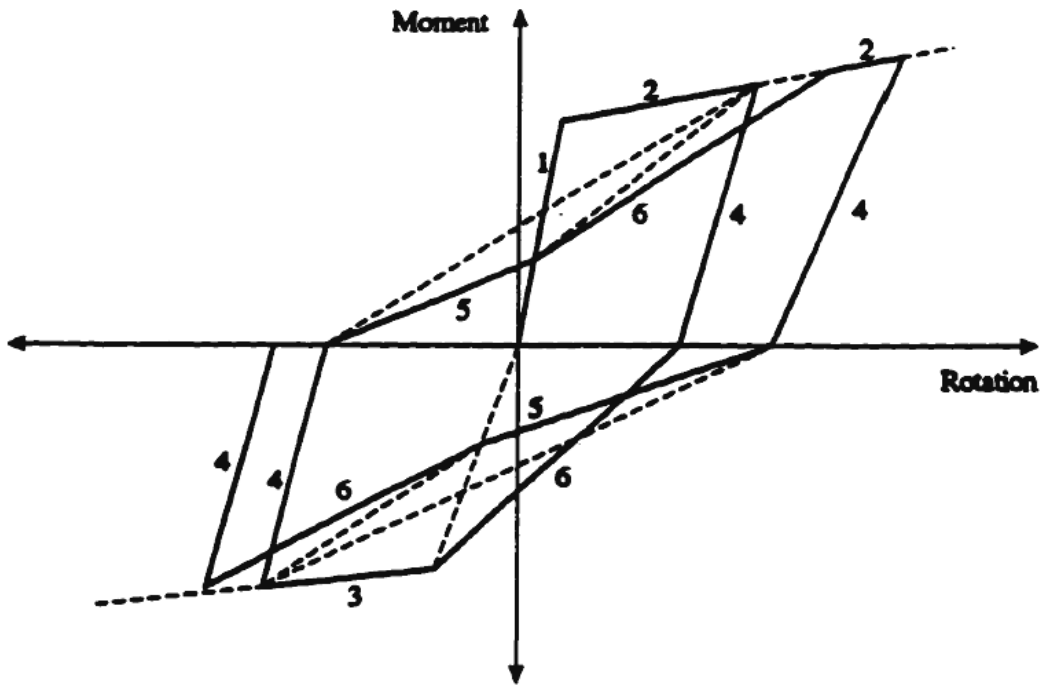

Fig. 4.4. Generalized model for the hysteretic behavior of the RC beam element (Element 8) (Raffaelle and Wight 1992)

Element 11 is a RC slab element that allows inelastic rotation at the member ends and also includes a punching shear failure prediction. This element behaves exactly like the RC beam element (Element 8) until a punching shear failure is predicted. The punching shear model, developed by Hueste and Wight (1999), monitors the member-end rotations for each time step. In order to detect the punching shear failure in Element 11, the gravity shear ratio (V_g/V_o) and critical rotation (θ_{cr}) are defined by the user. The gravity shear ratio is the ratio of the shear at a slab-column joint due to gravity loads and the shear strength of the critical section around the column, described in Chapter 11 of ACI 318-02. Fig. 4.5 shows the response model used for Element 11 when punching shear is predicted. The response prior to the prediction of punching shear is the same as that for Element 8, shown in Fig. 4.4.

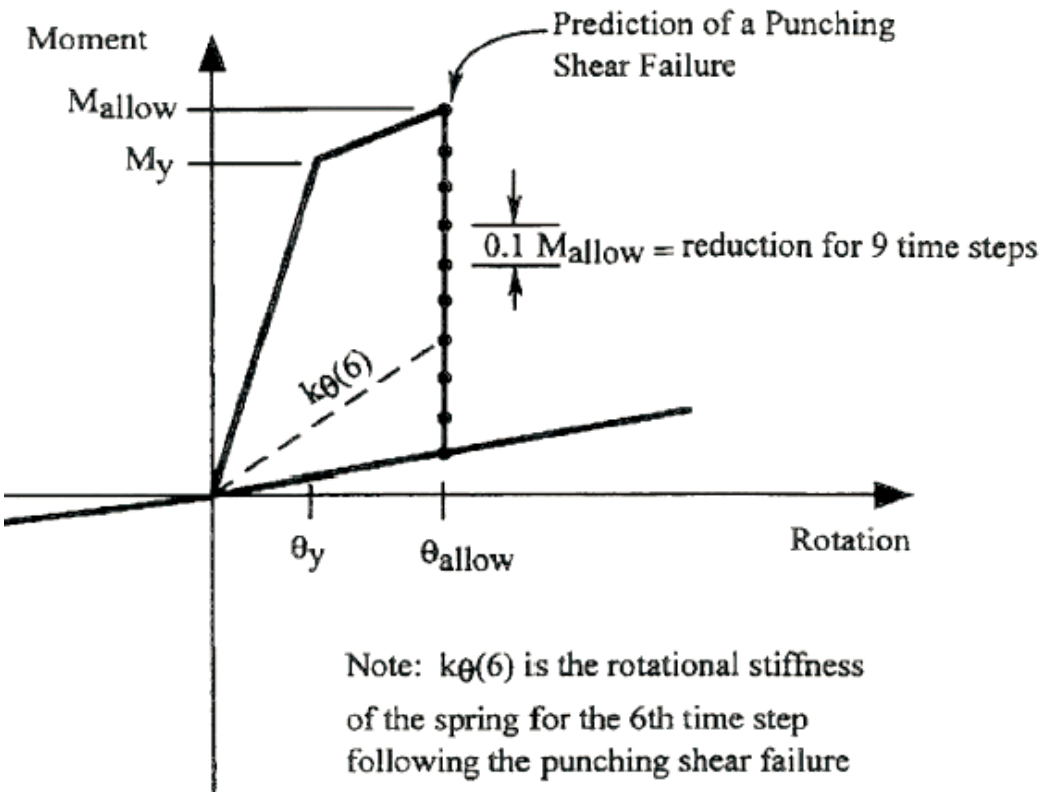

Fig. 4.5. Hysteretic response model used for the RC slab element (Element 11) (Hueste and Wight 1999)

4.3 Description of Analytical Models for Case Study Building

4.3.1 ZEUS-NL Model

4.3.1.1 Model Geometry

The building has a symmetrical configuration and so only half of the building was analyzed. Because there are no irregularities, a two-dimensional analytical model of the case study building is adequate to simulate the structural behavior under lateral forces. One exterior and two interior frames were linked at each floor level using rigid elements with no moment transfer between frames (see Fig. 4.6).

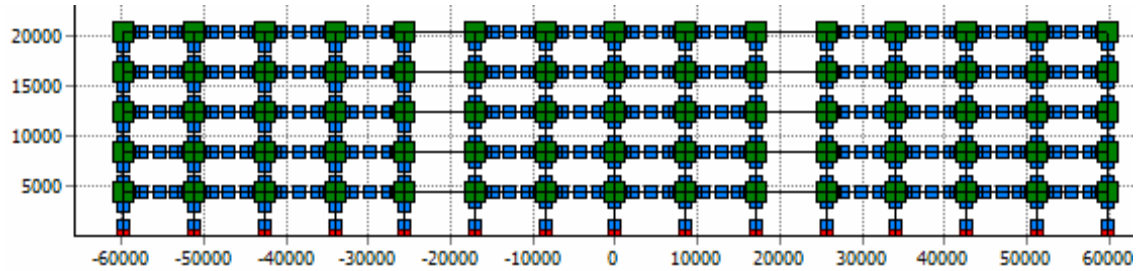

Fig. 4.6. Model of case study building used in ZEUS-NL analysis (units in mm)

In this study, rigid-end zones at the beam-column and slab-column joints were used. This assumption is often used for structural analysis of reinforced concrete structures (Hueste and Wight 1997b). In addition, this assumption is used for the DRAIN-2DM model. As shown in Fig. 4.7, rigid elements were placed at every beam-column and slab-column joint. This prevents plastic hinges from forming inside the joints and moves the inelastic behavior outside the joint region where it is expected to occur.

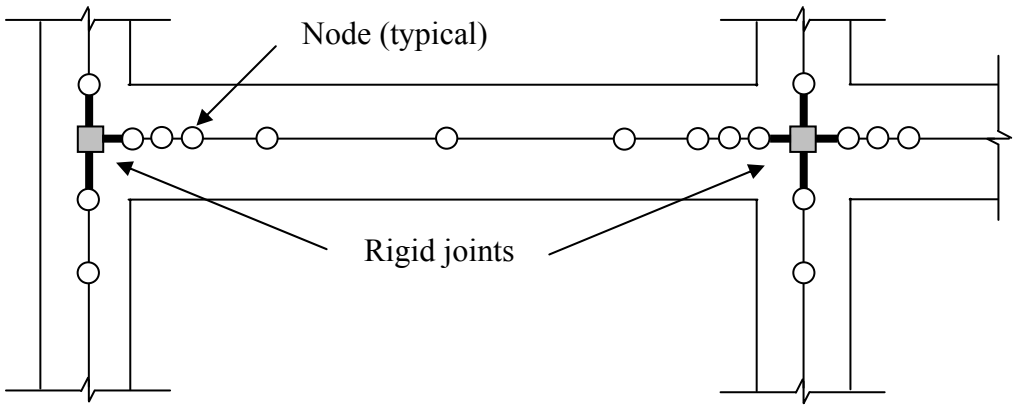

Fig. 4.7. Definition of rigid joints

The effective width of beam and slab members is also an important issue for two-dimensional modeling. Because the ZEUS-NL program calculates and updates various section properties at every time-step during analysis, it is not necessary to define cracked section properties. The uncracked section properties were defined based on the recommendations by Hueste and Wight (1997a). To define the stiffness of the spandrel

beam members, an effective width of 1120 mm was used based on the effective flange width defined in Section 8.10.3 of *ACI 318-02* (ACI Comm. 318 2002). Tables 4.5 and 4.6 present the parameters used to model the exterior and interior frame members, respectively.

Table 4.5. Parameters for exterior frame

Parameter	Description	Expression	Value, mm (in.)
Effective beam width for stiffness	I_g	$b_w + 1/12\ l_2$	1120 (44)
	A_g		
Effective beam width for strength	Compression zone for positive bending [ACI 318, Sec. 8.10.3]	$b_w + 1/12\ l_2$	1120 (44)
	Compression zone for negative bending	b_w	406 (16)
	Tension zone for negative bending	$b_w + 1/4\ l_2$	2540 (100)

Notes:
I_g = Gross moment of inertia
A_g = Gross area
l_2 = Length of slab span in transverse direction (center-to-center of supports)
b_w = Width of beam section projecting below the slab
h_w = Distance beam projects below the slab

Table 4.6. Parameters for interior frame

Parameter	Description	Value
Slab-Beam Effective Width	Strength	Full Width, l_2
	Stiffness	$1/2\ l_2$

Notes:
l_2 = Length of slab span in transverse direction (center-to-center of supports)

To obtain more precise results from the analysis, all the beam and slab members were divided into ten-sub elements. To apply the gravity loads using point loads, three nodes were defined at the quarter points, dividing the beams and slabs into four sub elements. For modeling of the rigid zone within the joints, a node was added at each column face. In order to reflect the cut-off of reinforcement, a node was added at 914

mm (3 ft.) from each column face. In addition to this, the closest members from each column face were divided by two sub elements so that the location of Gauss points is close enough to calculate the forces more accurately. Columns were divided into five-sub elements using a similar approach where more refinement is used at the element ends. Fig. 4.8 shows the overall node geometry for a typical frame and Fig. 4.9 shows the details of the boxed area in Fig. 4.8. For the nonlinear dynamic analysis, masses were lumped at the beam-column and slab-column joints.

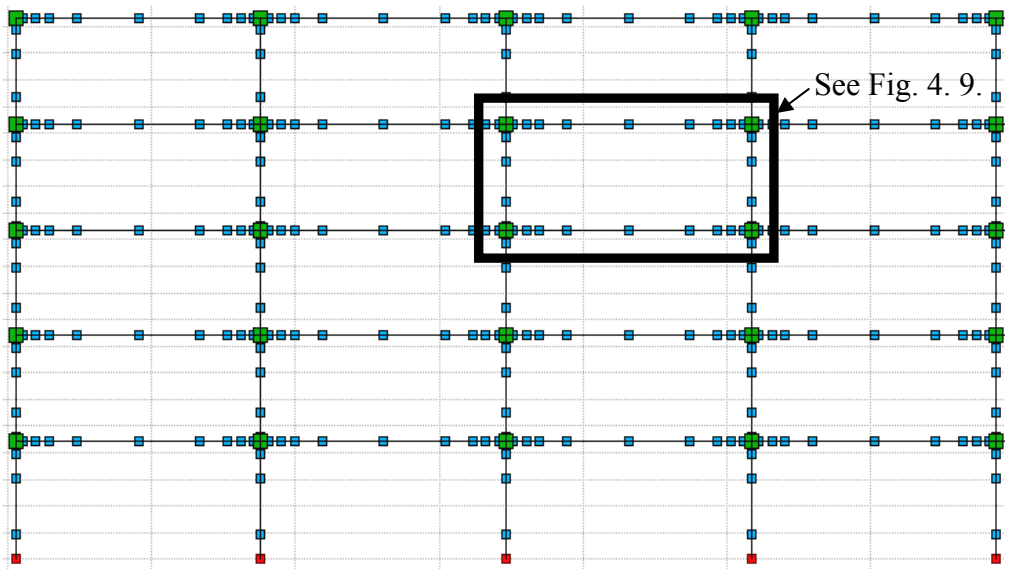

Fig. 4.8. Modeling of case study building in ZEUS-NL – typical frame geometry

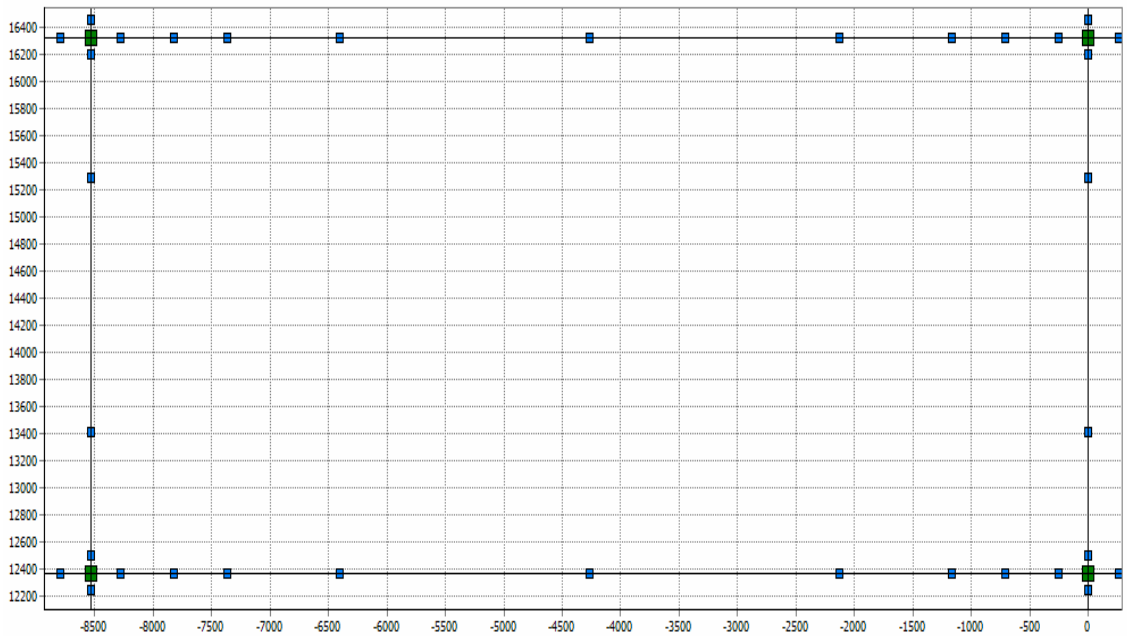

Fig. 4.9. Details of typical modeling of frame members from Fig. 4.8. (units in mm)

4.3.1.2 Material Models

Two material models were used in the ZEUS-NL model of the case study building. The bilinear elasto-plastic model with kinematic strain-hardening model (stl1) was used for the reinforcement and rigid connections, and the uniaxial constant confinement concrete model (conc2) was used for the concrete.

Three parameters are required for the stl1 model: Young's modulus (E), yield strength (σ_y) and a strain-hardening parameter (μ). For the conc2 model, four parameters are required: compressive strength (f'_c), tensile strength (f_t), maximum strain (ε_{co}) corresponding to f'_c, and a confinement factor (k). Table 4.7 shows the values for the parameters used in this study. For the rigid connections, the values of the Young's modulus and yield strength were chosen to be very large to prevent yielding. The parameter k is discussed below.

Table 4.7. Values for material modeling parameters in ZEUS-NL

Material type	Parameter	Values
stl1 (Steel)	E	200,000 N/mm^2 (29,000 ksi)
	σ_y	413 N/mm^2 (60,000 psi)
	μ	0.02
stl1 (Rigid connection)	E	6,890,000 N/mm^2 (1,000,000 ksi)
	σ_y	34,500 N/mm^2 (5,000,000 psi)
	μ	0.02
conc2 (Concrete for columns)	f'_c	27.6 N/mm^2 (4000 psi)
	f_t	2.76 N/mm^2 (400 psi)
	ε_{co}	0.002
	k	1.02
conc2 (Concrete for beams and slabs)	f'_c	27.6 N/mm^2 (4000 psi)
	f_t	2.76 N/mm^2 (400 psi)
	ε_{co}	0.002
	k	1.0

Note: See Fig. 4.3 for graphical description of variables.

Based on the material stress-strain relationships, moment-curvature analysis is conducted to predict the ductility and expected member behavior under varying loads. The confinement factor (k) for a rectangular concrete section with axial compression forces is based on the model of Mander et al. (1988) and is calculated as follows:

$$k = \frac{f'_{cc}}{f'_{co}} \tag{4.2}$$

where f'_{cc} is the confined concrete compressive strength and f'_{co} is the unconfined concrete compressive strength. These are calculated using the following equations.

$$f'_{cc} = f'_{co}\left(-1.254 + 2.254\sqrt{1 + \frac{7.94 f'_l}{f'_{co}}} - 2\frac{f'_l}{f'_{co}}\right) \tag{4.3}$$

$$f'_l = k_e \rho f_{yh} \tag{4.4}$$

$$k_e = \frac{A_e}{A_{cc}} \tag{4.5}$$

$$A_e = \left(b_c d_c - \sum_{i=1}^{n} \frac{(w_i')^2}{6} \right) \left(1 - \frac{s'}{2b_c} \right) \left(1 - \frac{s'}{2d_c} \right) \tag{4.6}$$

$$A_{cc} = A_c (1 - \rho_{cc}) \tag{4.7}$$

where:

f'_l = Effective lateral confining stresses
k_e = Confinement effectiveness coefficient
f_{yh} = Yield strength of transverse reinforcement
A_e = Area of effectively confined core concrete
A_{cc} = Area of core within center lines of perimeter spiral or hoops excluding area of longitudinal steel
A_c = Area of core of section within center lines of perimeter spiral
b_c = Concrete core dimension to center line of perimeter hoop in x-direction
d_c = Concrete core dimension to center line of perimeter hoop in y-direction
w_i' = i^{th} clear transverse spacing between adjacent longitudinal bars
s' = Clear spacing between spiral or hoop bars
ρ_{cc} = Ratio of area of longitudinal steel to area of core of section

For this model, the nominal values for the steel yield strength and concrete compressive strength were used. The minimum value of k is 1.0, which indicates an unconfined section. In this case, for the columns, where the transverse reinforcement is placed at every 457 mm (18 in.), the confinement factor is only 1.02 based on the above calculation.

4.3.1.3 Element and Cross-Section Types

For column, beam, slab and rigid elements, a cubic elasto-plastic three-dimensional element (cubic) was used. The lumped mass element (Lmass) was used to define the lumped masses at the joints for the dynamic and eigenvalue analysis. For the rigid joints, a three-dimensional joint element with uncoupled axial, shear and moment actions (joint) was used. The force-displacement characteristics for the axial forces, shear forces, and moments in the joint elements were determined by the joint curves that describe joint action, such as an elastic or elasto-plastic behavior.

For the cross-sections in the ZEUS-NL analysis, the RC rectangular section (rcrs) was selected to model the column members and the RC T-section (rcts) was selected to model the beam and slab members in the frame. Because there is no typical section for slab member, the rcts section was used with a negligible flange width and length. The input parameters for rcrs are section height, stirrup height, section width and stirrup width. The rcts section requires eight dimensional parameters: slab thickness, beam height, confined height in slab, confined height in beam, slab effective width, beam width, confined width in slab and confined width in beam. Fig. 4.10 shows cross sections used in the case study building analysis and Table 4.8 shows the values used in this analysis.

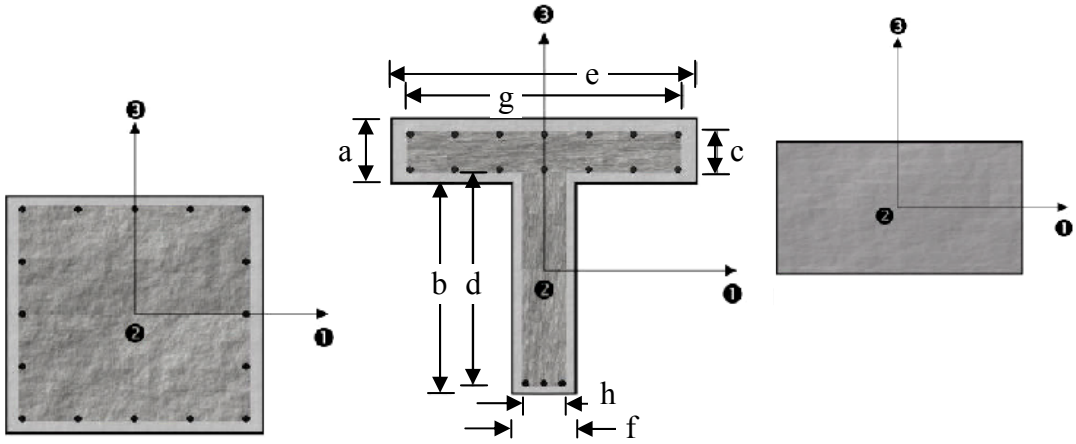

(a) rcrs (RC rectangular) (b) rcts (RC T-section) (c) rss (Rectangular solid)

Fig. 4.10. Sections for the case study building analysis (Elnashai et al. 2002)

In addition, the reinforcement for the short member in beam and slab elements which is located near the joints, were reduced to reflect bar cutoffs and discontinuous bottom bars that had reduced embedment lengths. The available tensile force was calculated based on the proportional relationship of embedment length and development length of the bottom bars, using the following equations (Aycardi et al. 1994).

$$F_t = \frac{l_{embedment}}{l_{development}} A_s f_y \tag{4.8}$$

where:

F_t = Tensile force that can be developed by reinforcement with reduced embedment length

$l_{embedment}$ = Embedment length of a reinforcing bar

$l_{development}$ = Development length of a reinforcing bar (from *ACI 318-02*)

A_s = Area of steel reinforcement

The reduced reinforcement area, *As(red)*, for bars that are not fully developed was then found using the following relationship.

$$As(red) = \frac{F_t}{f_y} \tag{4.9}$$

This reduced reinforcement area was then modeled in ZEUS-NL. The reduction factor, which is the ratio between embedment length and development length in Eq. 4.8, was 0.295. In addition, a 0.5 reduction factor was used for the element located between the elements containing this reduced area and the full area of reinforcement.

Table 4.8. Values for section modeling parameters in ZEUS-NL

Section type	Dimensional parameter	Values, mm (in.)
Column	Section height and width	508 (20)
	Stirrup height and width	384 (15.1)
Beam (Ground floor - 4th floor)	a. Slab thickness	254 (10)
	b. Beam web height	356 (14)
	c. Confined height in slab	178 (7)
	d. Confined height in beam web	356 (14)
	e. Slab effective width	1120 (44)
	f. Beam web width	406 (16)
	g. Confined width in slab	1090 (43)
	h. Confined width in beam web	330 (13)
Beam (Roof level)	a. Slab thickness	254 (10)
	b. Beam web height	305 (12)
	c. Confined height in slab	178 (7)
	d. Confined height in beam web	305 (12)
	e. Slab effective width	1120 (44)
	f. Beam web width	406 (16)
	g. Confined width in slab	1090 (43)
	h. Confined width in beam web	330 (13)
Slab	a. Slab thickness	254 (10)
	b. Beam web height	0.01*
	c. Confined height in slab	216 (8.5)
	d. Confined height in beam web	0.01*
	e. Slab effective width	4270 (168)
	f. Beam web width	4270 (168)
	g. Confined width in slab	4230 (167)
	h. Confined width in beam web	4230 (167)
Rigid element	Height	254 (10)
	Width	254 (10)

* To model slab members using the rcts (RC T-Section), a very small value was used for the beam web height.

4.3.1.4 Loads, Masses and Damping

The gravity loads consist of distributed loads (w) due to the weight of beams and slabs, and point loads due to the column weight. Point loads were applied to the beam-column and slab-column joints to include the column weight. Because there is no distributed load definition in the ZEUS-NL program, beams and slabs were divided into

four sub-elements and three equivalent point loads were applied to the nodes between sub elements. Equivalent point loads were calculated using the concentrated load equivalents factors in the Table 5-16 of the third edition of *LRFD* (AISC 2001). Fig. 4.12 shows the equivalent point loads applied on beams and slabs. For the nonlinear dynamic analysis, masses were lumped at beam-column or slab-column joints.

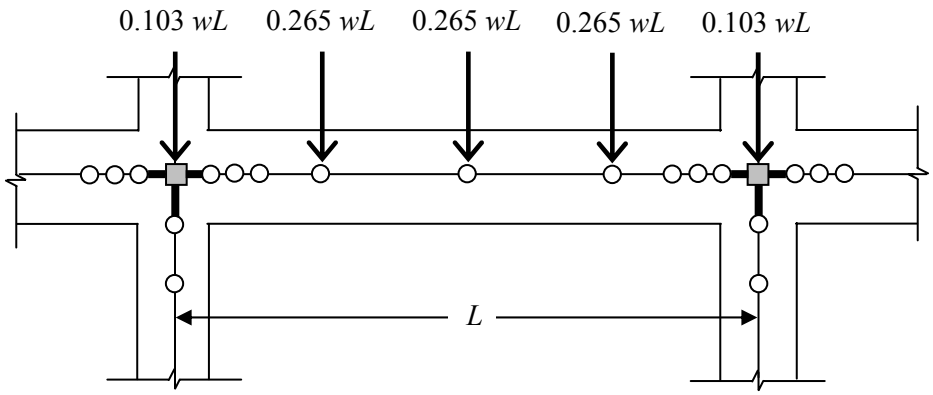

Fig. 4.11. Equivalent point loads applied on beam and slab members

4.3.2 DRAIN-2DM Model

4.3.2.1 Model Geometry and Material Models

Fig. 4.13 shows the analytical model used in the DRAIN-2DM analysis. Half of the case study building was analyzed with a two-dimensional analytical model, which is the same as the ZEUS-NL model geometry. Rigid zones within the beam-column and slab-column joints were also defined, as described by Fig. 4.14.

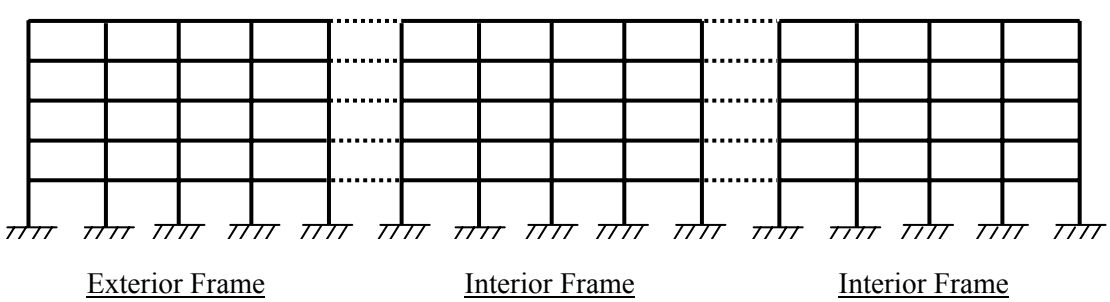

Fig. 4.12. Model of case study building used in DRAIN-2DM analysis

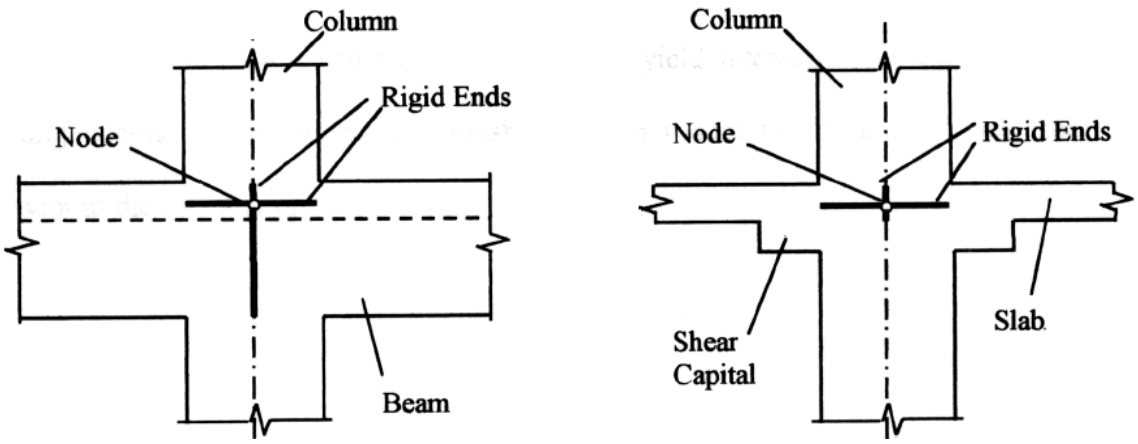

(a) Beam-column connection (b) Slab-column connection

Fig. 4.13. Rigid end zones for connections (Hueste and Wight 1997a)

All material properties, including the Young's modulus, yield strength and strain-hardening modulus for the reinforcement and the concrete compressive strength were defined as the same values used for the ZEUS-NL model.

4.3.2.2 Element and Cross-Section Types

The beam-column element (Element 2) was selected to model the column members, and the buckling element (Element 9), which carries axial load only, was used to model the rigid links. The RC beam element (Element 8) was selected to model the beam members in the exterior frame. The slab members were modeled using the RC slab element (Element 11), which allows punching shear failure prediction.

The hysteretic behavior modeled at the member ends required a pinching factor, which describe slippage of bars and crack closure within the beam-column joint. A pinching factor of 0.75 was selected for all beam and slab members, to correspond to a moderate level of pinching (Hueste and Wight 1997a). The unloading stiffness factor of 0.30 and no strength deterioration factor were used for this analysis. To define the punching shear model for Element 11, the critical rotation (θ_{cr}) was determined from a push-over analysis. The procedure to determine appropriate rotation values followed the methodology suggested by Hueste and Wight (1999). In this study, the critical rotation

was calculated as the average member-end rotation in the slab elements when the building drift reaches 1.25%.

For the initial stiffness for beam and slab members, the cracked section properties are used in the DRAIN-2DM model. For beams, the cracked moment of inertia is the gross moment of inertia multiplied by a factor of 0.35. The corresponding factors for column and slab members are 0.70 and 0.25, respectively. These factors are based on those recommended by *ACI 318-02* (ACI Comm. 318 2002). The gross moment of inertia for slab members in Table 4.9 was calculated based on full length of a slab span in transverse direction. Table 4.9 summarizes the parameters for section modeling in DRAIN-2DM.

Table 4.9. Parameters for section modeling in DRAIN-2DM

Section type	Parameter	Value
Beam	Cracked stiffness	$0.35*I_g$
	Pinching factor	0.75
	Unloading stiffness factor	0.30
	Strength deterioration factor	0
Column	Cracked stiffness	$0.70*I_g$
Slab	Cracked stiffness	$0.25*I_g$
	Pinching factor	0.75
	Unloading stiffness factor	0.30
	Strength deterioration factor	0
Floor slabs	Gravity shear ratio	0.29
	Average yield rotation	0.0151 rad.
	Average critical rotation	0.0173 rad.
	Average allowable rotation	0.0399 rad.
Roof slab	Gravity shear ratio	0.39
	Average yield rotation	0.0111 rad.
	Average critical rotation	0.00646 rad.
	Average allowable rotation	0.0128 rad.

Note: See Tables 4.5 and 4.6 for calculation of parameters.

4.3.2.3 Loads, Masses and Damping

In order to account for gravity loads, fixed end forces were applied to the beam and slab member ends. These were computed based on the results from an analysis for the applied gravity loads using the Visual Analysis program (IES 1998). For dynamic analysis, the viscous damping [C] was assumed to be proportional to the mass matrix [M] and the initial elastic stiffness [K_0], as follows:

$$[C] = \alpha_0 [M] + \beta_0 [K_0] \tag{4.10}$$

where α_0 and β_0 are the mass proportional damping factor and stiffness proportional damping factor, respectively. These proportional factors are calculated using the following equations (Raffaelle and Wight 1992). The periods of the first and second

modes were found from the eigenvalue analysis with uncracked section properties using the ZEUS-NL program. The results for this case study building were α_0 = 0.167 and β_0 = 0.0018.

$$\alpha_0 = \frac{4\pi(T_1\xi_1 - T_2\xi_2)}{T_1^2 - T_2^2} \tag{4.11}$$

$$\beta_0 = \frac{T_1T_2(T_1\xi_1 - T_2\xi_2)}{\pi(T_1^2 - T_2^2)} \tag{4.12}$$

where:

T_1 = Natural period for the 1st mode of vibration = 1.14 s
T_2 = Natural period for the 2nd mode of vibration = 0.367 s
ζ_1 = Target critical damping ratio for the 1st mode of vibration = 2%
ζ_2 = Target critical damping ratio for the 2nd mode of vibration = 2%

4.4 Synthetic Ground Motion Data

In order to predict the response of structures during an earthquake, representative ground motion data for that location should be used. However, there is not adequate recorded strong motion data to characterize the seismicity for specific locations in the Mid-America region. Therefore, synthetic ground motion records have been developed for cities in the region impacted by the New Madrid Seismic Zone (NMSZ). For this study, synthetic ground motions from two sources were used: Wen and Wu (2000) and Rix and Fernandez-Leon (2004). The ground motions are described below.

4.4.1 Ground Motions Developed by Wen and Wu (2000)

Synthetic ground motions developed by Wen and Wu (2000) for the cities of St. Louis, Missouri and Memphis, Tennessee were used in this study. These motions include suites of ten ground motion records for each of two probabilities of exceedance

levels: 2% and 10% in 50 years. In addition, the ground motions are available for both representative soil and rock sites. In this study ground motions for representative soil were selected because soil can affect the ground motion of an earthquake by amplifying the accelerations and the structural model does not include a soil model. To reduce the computational time, the ground motions were shortened for the nonlinear dynamic analysis at the time point where the energy reaches 95% of the total energy imparted by a particular ground motion record. This procedure was based on the methodology developed by Trifunac and Brady (1975). The equation to compute the total energy of a strong ground motion record is given in Eq. 4.13. Based on this relationship, Trifunac and Brady suggested the duration of the strong ground motion to be the time interval remaining between the low and high 5% cut-off of the total energy. For this study, only the high 5% cut-off of the ground motion was used to reduce the record.

$$E_{Total} = \int_0^t a^2(t)dt \tag{4.13}$$

where:

E_{Total} = Total energy of a ground motion record
$a(t)$ = Acceleration at a time, t

Figs. 4.14 and 4.15 show the response spectra for the ground motion sets at five percent damping. Details of each ground motion record including plots are provided in Appendix A.

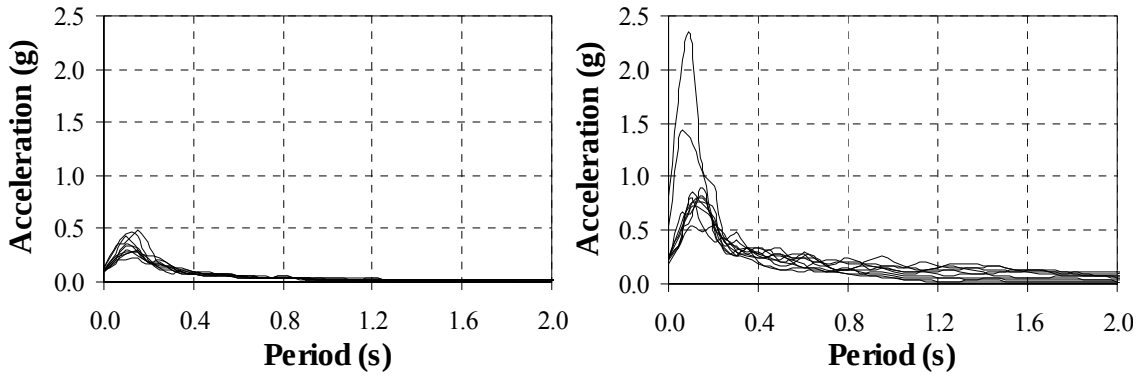

(a) 10% in 50 years (b) 2% in 50 years

Fig. 4.14. Response spectra for St. Louis ground motions (Wen and Wu 2000)

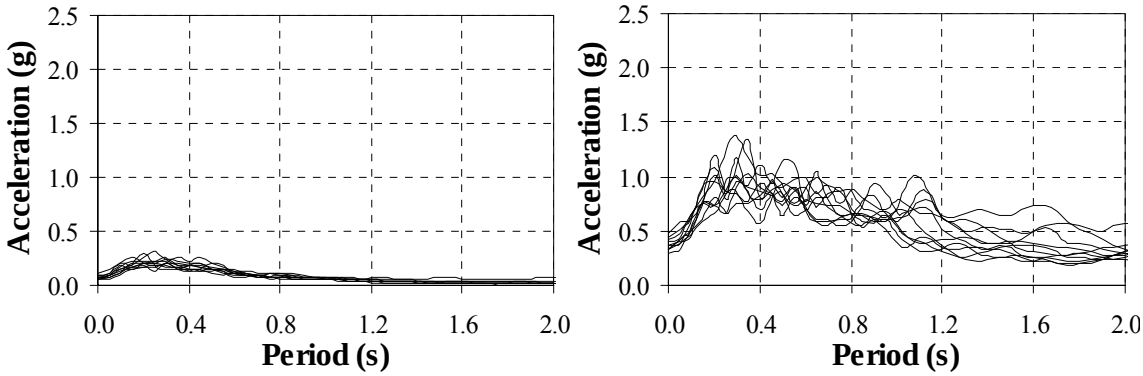

(a) 10% in 50 years (b) 2% in 50 years

Fig. 4.15. Response spectra for Memphis ground motions (Wen and Wu 2000)

4.4.2 Ground Motions Developed by Rix and Fernandez-Leon (2004)

Synthetic ground motions for Memphis, Tennessee developed by Rix and Fernandez-Leon (2004) using stochastic ground motion models were also used in this study. Two source models were considered by Rix, Atkinson and Boore (1995) and Frankel et al. (1996), to help capture the impact of modeling uncertainty. Synthetic ground motion sets were developed for three body wave magnitudes (5.5, 6.5 and 7.5) and four hypocentral distances (10, 20, 50 and 100 km). Site amplification factors developed by Drosos (2003) were adopted to reflect the effect of the deep soil column of

the Upper Mississippi Embayment. Site amplification factors were calculated using one-dimensional, equivalent linear site response analyses using random vibration theory. These synthetic ground motions differ from those developed by Wen and Wu (2000) because recent research allowed the inclusion of soil nonlinearity and uncertainties in the site response parameters.

Each scenario event for a given magnitude and distance includes twenty ground motion records. In this study, 120 ground motions for 20 km of hypocentral distance were used for the development of fragility curves for the case study structure. Because the ground motions for 10 km of hypocentral distance with magnitude of 7.5 were not available, the 20 km records were selected. The ground motions corresponding to 50 km and 100 km are relatively low in magnitude and would not provide significant additional information for characterizing structural fragility. Table 4.10 shows all the scenario events available for Memphis, Tennessee, and the sets of ground motion records used in this study are shaded.

Table 4.10. Sets of ground motion records for Memphis, Tennessee (Rix and Fernandez-Leon 2004)

	Atkinson and Boore (1995) Model			**Frankel et al. (1996) Model**		
Distance (km)	**Magnitude**			**Magnitude**		
	5.5	**6.5**	**7.5**	**5.5**	**6.5**	**7.5**
10	✓	✓	N.A.	✓	✓	N.A.
20	✓	✓	✓	✓	✓	✓
50	✓	✓	✓	✓	✓	✓
100	✓	✓	✓	✓	✓	✓

N.A. = Not Available

Table 4.11 shows the median of peak ground acceleration of each scenario earthquake for a hypocentral distance of 20 km. Fig. 4.16 shows response spectra plots

for the ground motion sets. These response spectra were calculated based on 5% critical damping. Details of each ground motion record are provided in Appendix A.

Table 4.11. Median of peak ground accelerations of each scenario earthquake (20 km hypocentral distance) (Rix and Fernandez-Leon 2004)

Atkinson and Boore (1995) Model			**Frankel et al. (1996) Model**		
Magnitude			**Magnitude**		
5.5	**6.5**	**7.5**	**5.5**	**6.5**	**7.5**
0.0481g	0.104g	0.215g	0.0717g	0.202g	0.425g

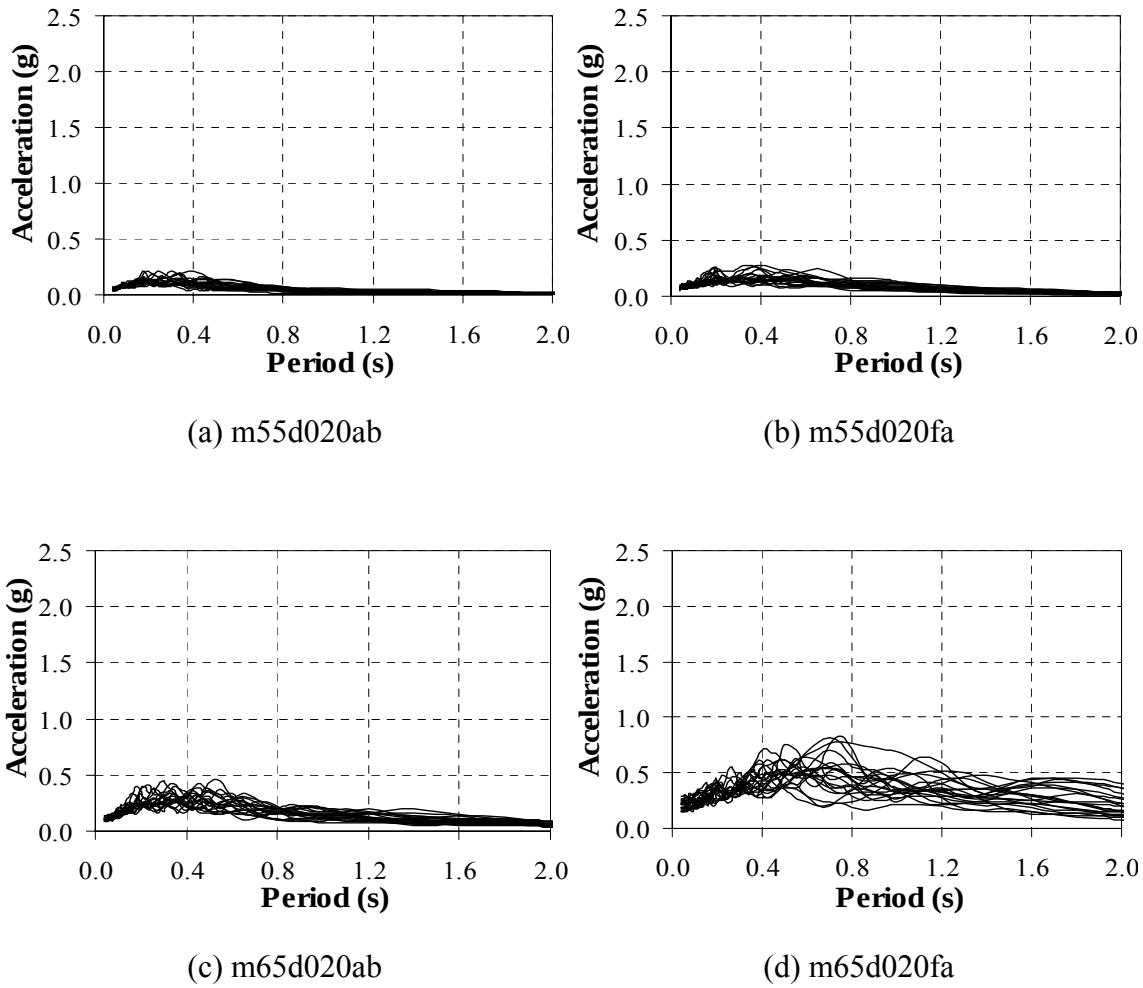

(a) m55d020ab (b) m55d020fa

(c) m65d020ab (d) m65d020fa

Fig. 4.16. Response spectra for Memphis ground motions (Rix and Fernandez-Leon 2004)

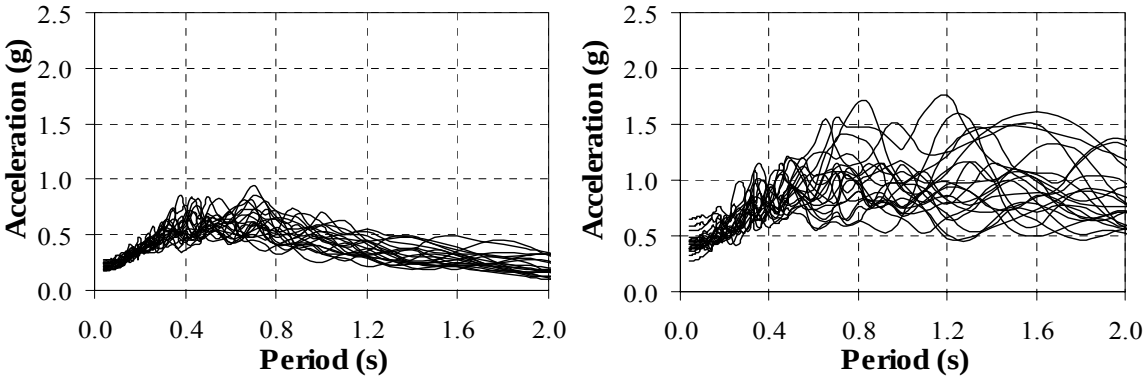

(e) m75d020ab (f) m75d020fa

Fig. 4.16. Continued

5 ANALYSIS OF UNRETROFITTED CASE STUDY BUILDING

5.1 Introduction

This section presents the analysis of the unretrofitted case study building. Two structural analysis methods, nonlinear static analysis and nonlinear dynamic analysis, were used to predict the seismic behavior of the building under lateral forces. A comparison of these analysis results is provided. In addition, results from two structural nonlinear analysis programs (ZEUS-NL and DRAIN-2DM) are compared. The ZEUS-NL program was selected for additional analytical studies to evaluate the expected seismic performance of the structure for St. Louis and Memphis synthetic ground motions. Based on the analytical results, fragility curves were developed using the FEMA 356 performance criteria and additional limit states. FEMA 356 provides global-level and member-level criteria for three performance levels for seismic evaluation. In this study, both global-level and member-level criteria were used for seismic evaluation of the unretrofitted and retrofitted case study building.

5.2 Comparison of ZEUS-NL and DRAIN-2DM

5.2.1 Nonlinear Static Analysis

Two different load patterns for conventional push-over analysis were used: uniform (rectangular) and inverted triangular cases. The inverted triangular load case is based on first mode shape from an eigenvalue analysis of the case study building (see Fig. 5.1). The results of the push-over analyses using the ZEUS-NL and DRAIN-2DM programs are shown in Fig. 5.2. In addition to this, a comparison of push-over analysis from these two programs is shown in Fig. 5.3.

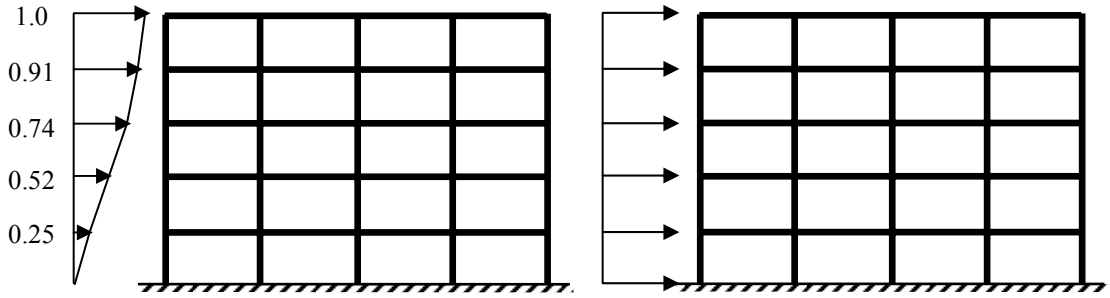

(a) Inverted triangular load pattern (b) Rectangular load pattern

Fig. 5.1. Load patterns for conventional push-over analysis

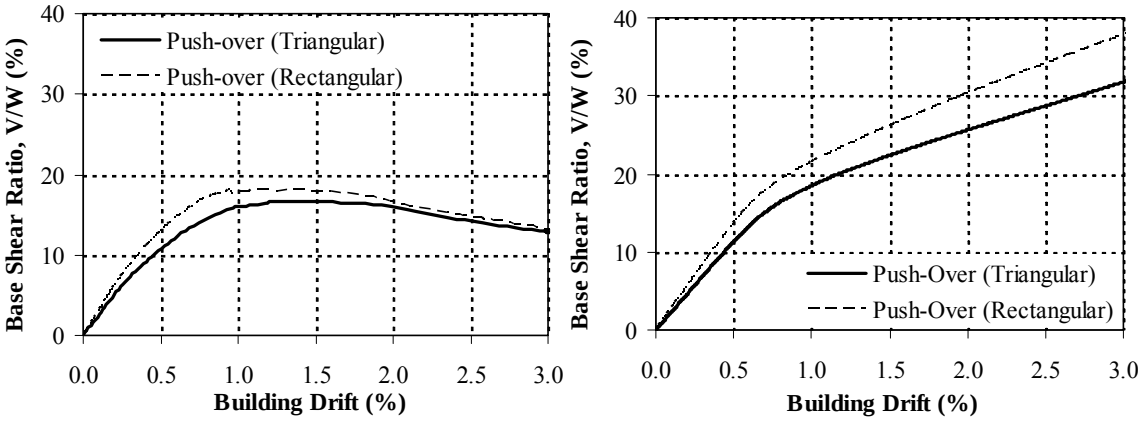

(a) ZEUS-NL (b) DRAIN-2DM

Fig. 5.2. Push-over curves

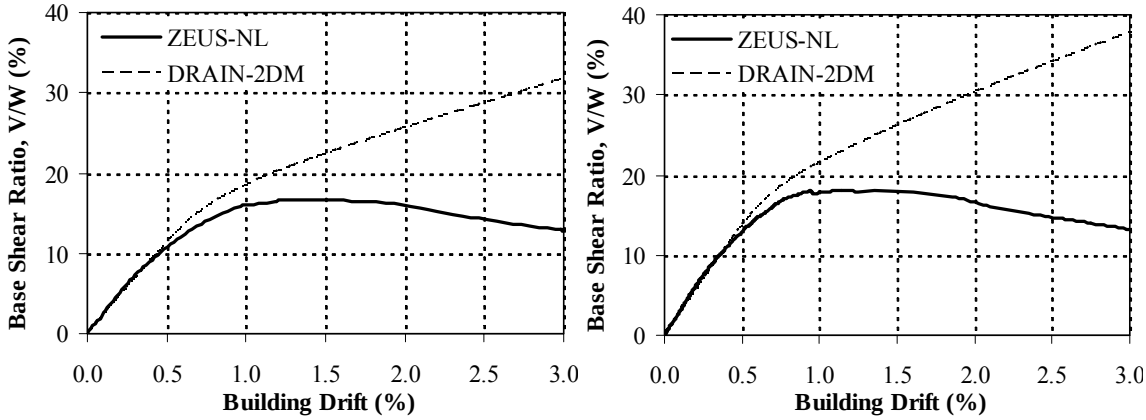

(a) Inverted triangular load pattern (b) Rectangular load pattern

Fig. 5.3. Comparison of push-over curves from ZEUS-NL and DRAIN-2DM

As shown in Fig. 5.2, the overall responses for the two load patterns have a similar shape. For both programs, however, the rectangular load case gave a slightly larger base shear ratio at a certain building drift. A comparison of the response predictions from the two programs shows some significant differences (see Fig. 5.3). From 0.0% to 0.5% building drift, the results from both programs match quite well. However, after 0.5% drift, the ZEUS-NL model had a peak value at about 1.2% building drift, while the DRAIN-2DM model had a yielding point around 0.8% building drift, but continued to take on significant load for both load patterns. Based on the above comparison, ZEUS-NL seems to more appropriately take into account P-delta effects and stiffness degradation.

The comparison of interstory drift profiles for both 1% and 2% average building drifts are shown in Fig. 5.4. At 1% building drift, both models gave a similar shape for the interstory drift profile. However, at 2% building drift, ZEUS-NL gives higher interstory drift values for the lower story levels and lower drifts for the upper story levels.

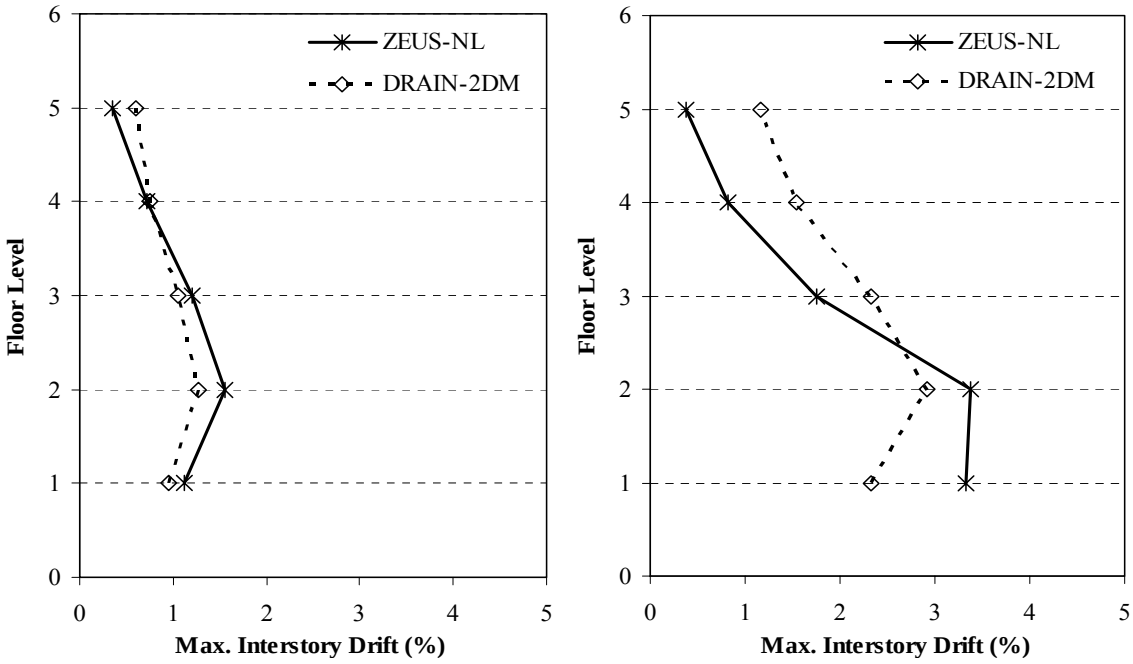

(a) 1% Building Drift (b) 2% Building Drift

Fig. 5.4. Comparison of interstory drifts for push-over analysis

5.2.2 Nonlinear Dynamic Analysis

Nonlinear dynamic analysis was performed using the ZEUS-NL and DRAIN-2DM program for twenty St. Louis ground motions (see Tables 4.9 and 4.10) to compare the predicted behavior of the case study building under dynamic loads. Modeling of seismic action was achieved by applying the ground acceleration history at the column supports. Tables 5.1 and 5.2 show the results of the nonlinear dynamic analysis for the St. Louis motions. Fig. 5.5 provides a comparison of the building drift versus time for the two models. According to Tables 5.1 and 5.2, the maximum values of building drifts are quite similar for the two models. However, as shown in Fig. 5.5, the overall response is not very close. The ground motions shown are those that gave a maximum building drift closest to the median value of the maximum building drift for each ground motion set. Because the synthetic ground motion data were developed with the lognormally distributed parameters, the median values of the maximum building drift and maximum base shear ratio were assumed to be lognormally distributed and calculated based on the natural log of these values (see Eq. 5.1).

$$Y_M = e^{average\_\ln(x_i)} \tag{5.1}$$

where:

Y_M = Median response
x_i = Response for a given ground motion record i

Table 5.1. Maximum building drift and maximum base shear ratio for St. Louis motions (10% in 50 years)

Ground motion	Max. building drift (%)		Max. base shear ratio, V/W (%)	
	ZEUS-NL	DRAIN-2DM	ZEUS-NL	DRAIN-2DM
l10_01s	0.0390	0.0387	3.20	1.27
l10_02s	0.0768	0.0763	4.33	1.52
l10_03s	0.0654	0.112	3.35	2.08
l10_04s	0.0849	0.0753	3.61	1.67
l10_05s	0.0411	0.0538	2.67	1.73
l10_06s	0.0635	0.0763	3.56	2.02
l10_07s	0.0940	0.0790	4.41	1.46
l10_08s	0.0711	0.109	3.93	2.15
l10_09s	0.0567	0.0637	4.26	1.79
l10_10s	0.0787	0.105	3.63	1.91
Median	0.0688	0.0753	3.66	1.74

Table 5.2. Maximum building drift and maximum base shear ratio for St. Louis motions (2% in 50 years)

Ground motion	Max. building drift (%)		Max. base shear ratio, V/W (%)	
	ZEUS-NL	DRAIN-2DM	ZEUS-NL	DRAIN-2DM
l02_01s	0.774	0.686	13.2	11.9
l02_02s	0.722	0.539	14.1	10.7
l02_03s	0.0714	0.107	6.63	4.88
l02_04s	0.227	0.306	8.76	7.42
l02_05s	0.725	0.644	14.3	9.61
l02_06s	0.212	0.240	8.71	5.90
l02_07s	0.502	0.488	12.1	9.78
l02_08s	0.253	0.597	8.2	9.58
l02_09s	0.720	0.498	14.2	10.5
l02_10s	0.0808	0.115	4.99	3.49
Median	0.377	0.352	9.95	7.86

The modeling assumptions for the case study building using both programs were taken to be as consistent as possible. However, the programs use different element formulations and computing procedures, and so the results are not exactly the same for the two models. However, the maximum building drift results are reasonably close to each other.

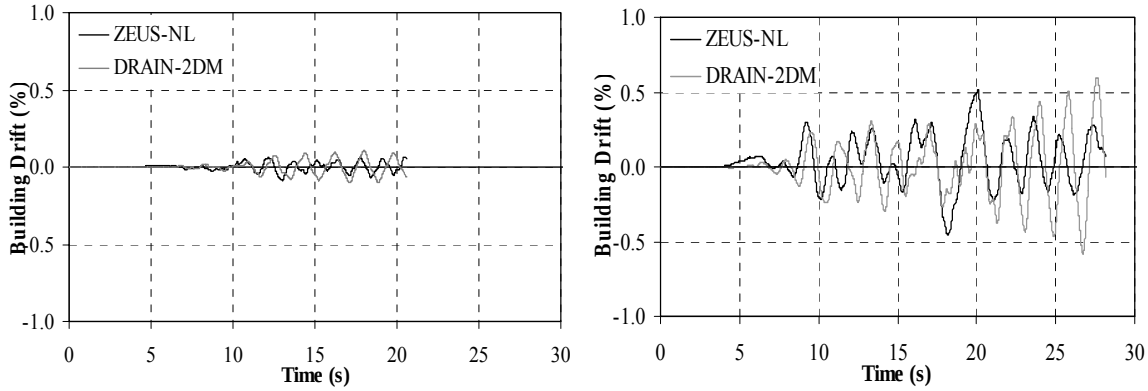

(a) l10_08s (b) l02_08s

Fig. 5.5. Comparison of building drifts for St. Louis motions

Fig. 5.6 provides a comparison of the building drift versus time for the two models using the median motion of the 2% in 50 years Memphis motions. Based on the comparison of push-over analysis results, there was a significant difference between the ZEUS-NL and DRAIN-2DM models at about 2.0% building drift. However, as shown in Fig. 5.6, the maximum building drift for the dynamic analysis are reasonably close to each other, although the response versus time varies.

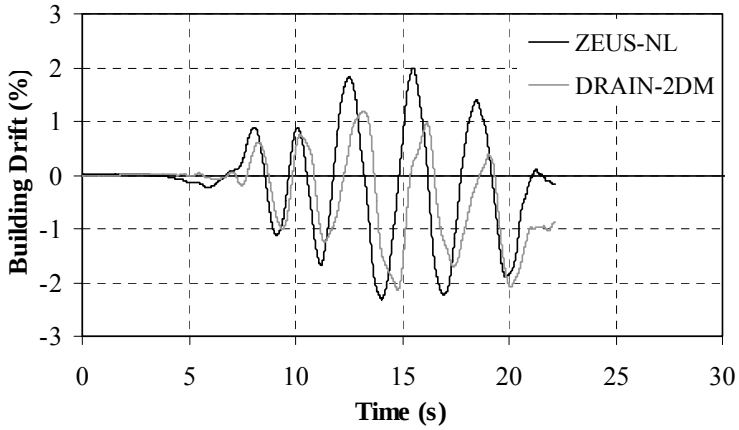

Fig. 5.6. Comparison of building drifts for Memphis motions (m02_10s)

5.3 Further Analysis Using ZEUS-NL Program

The ZEUS-NL program was selected for further analysis of the case study building based on the comparison discussed in the previous section. To compute the fundamental period of the case study building, an eigenvalue analysis was performed. To further understand the dynamic behavior of the structure, nonlinear dynamic analysis was also conducted using the Memphis motions. Finally, the results of push-over analysis and nonlinear dynamic analysis using ZEUS-NL were compared.

5.3.1 Eigenvalue Analysis

Based on an eigenvalue analysis, the fundamental period of the case study building is 1.14 seconds. It should be noted that ZEUS-NL initially models members as uncracked and so this value corresponds to the fundamental period based on uncracked section properties. Mode shapes determined by eigenvalue analysis with the ZEUS-NL program are shown in Fig. 5.7. The first four mode shapes and profiles developed from combining mode shapes on the basis of the Square-Root-of-Sum-of-Squares (SRSS) rule are shown. These mode shapes were used to determine the lateral load pattern for additional push-over analysis.

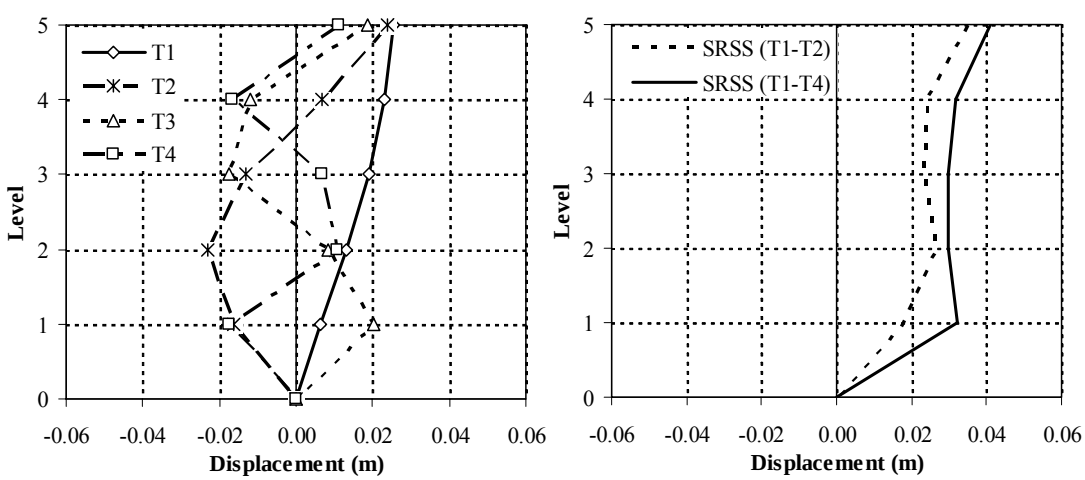

(a) First four mode shapes (b) SRSS shapes

Fig. 5.7. Mode shapes from eigenvalue analysis

Fig. 5.8 shows a comparison of the structural response from the push-over analysis with different load patterns. As shown in Fig. 5.8, the push-over results for the load patterns of SRSS are bounded between the inverted triangular and rectangular case. The triangular and rectangular load patterns were used for further comparison.

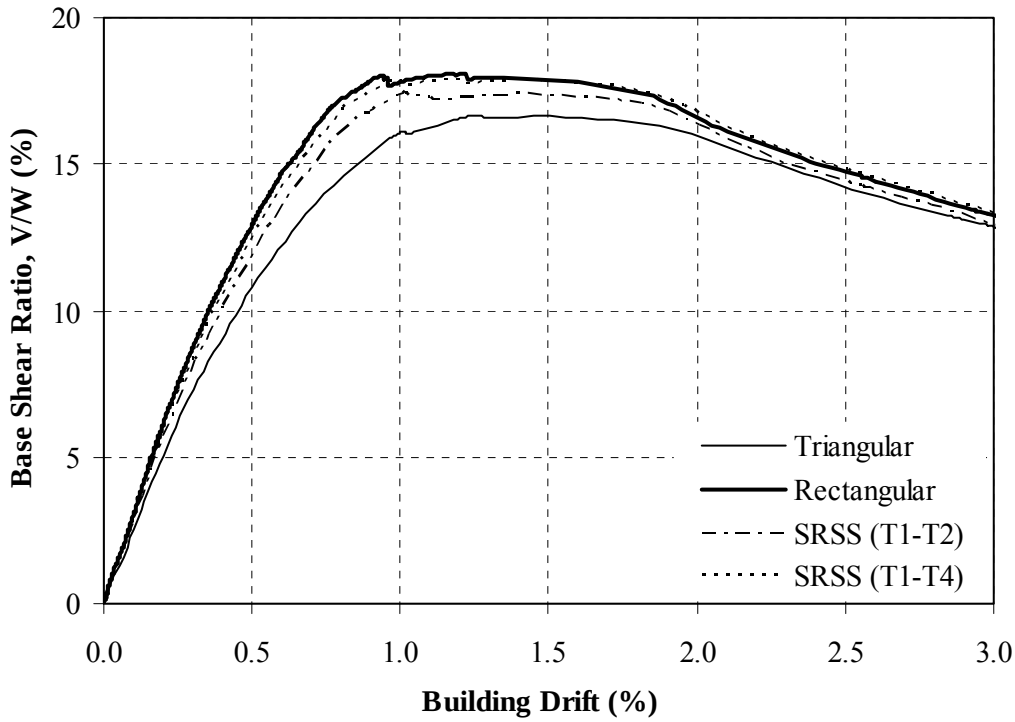

Fig. 5.8. Push-over analysis using SRSS shapes from eigenvalue analysis

5.3.2 Nonlinear Dynamic Analysis

Synthetic ground motion records from both St. Louis and Memphis were used to evaluate the dynamic behavior of the case study building. The results from the nonlinear analyses using the St. Louis motions were provided in Tables 5.1 and 5.2. The results for the twenty Memphis motions are shown in Tables 5.3 and 5.4. (The building drift time histories for the St. Louis and Memphis motions are provided in Appendix A.)

Table 5.3. Maximum building drift and maximum base shear ratio for Memphis motions (10% in 50 years, ZEUS-NL)

Ground motion	Max. building drift (%)	Max. base shear ratio, V/W (%)
m10_01s	0.142	4.54
m10_02s	0.122	5.29
m10_03s	0.164	4.97
m10_04s	0.153	4.54
m10_05s	0.129	4.99
m10_06s	0.425	7.81
m10_07s	0.134	4.65
m10_08s	0.155	5.97
m10_09s	0.0800	4.84
m10_10s	0.0950	4.21
Median	0.144	5.10

Table 5.4. Maximum building drift and maximum base shear ratio for Memphis motions (2% in 50 years, ZEUS-NL)

Ground motion	Max. building drift (%)	Max. base shear ratio, V/W (%)
m02_01s	1.99	18.4
m02_02s	2.36	19.1
m02_03s	1.94	18.8
m02_04s	1.92	18.9
m02_05s	2.64	18.5
m02_06s	2.47	18.2
m02_07s	1.99	19.6
m02_08s	2.74	17.9
m02_09s	1.88	18.7
m02_10s	2.31	18.1
Median	2.20	18.6

As shown in Tables 5.3 and 5.4, the median value of the maximum building drifts for the 10% in 50 years Memphis motions is quite small and maximum base shear ratios are less than the design shear. In addition to this, the median values of the maximum building drifts and maximum base shear ratios for the 2% in 50 years Memphis motions are significantly increased due to the larger magnitude of the ground motions.

5.3.3 Comparison of Push-Over and Dynamic Analysis

A comparison of the overall structural response from the push-over and nonlinear dynamic analyses using ZEUS-NL are shown in Fig. 5.9. As shown, the points from the dynamic analyses representing the maximum building drift and base shear for each ground motion show a reasonable match with the push-over curves. The global responses of the structure from the static and dynamic analyses show relatively similar values for lower amplitudes of motion and diverge for greater demands. In particular, the base shear ratios from the 2% in 50 years Memphis motions are slightly underestimated by the push-over analysis curve.

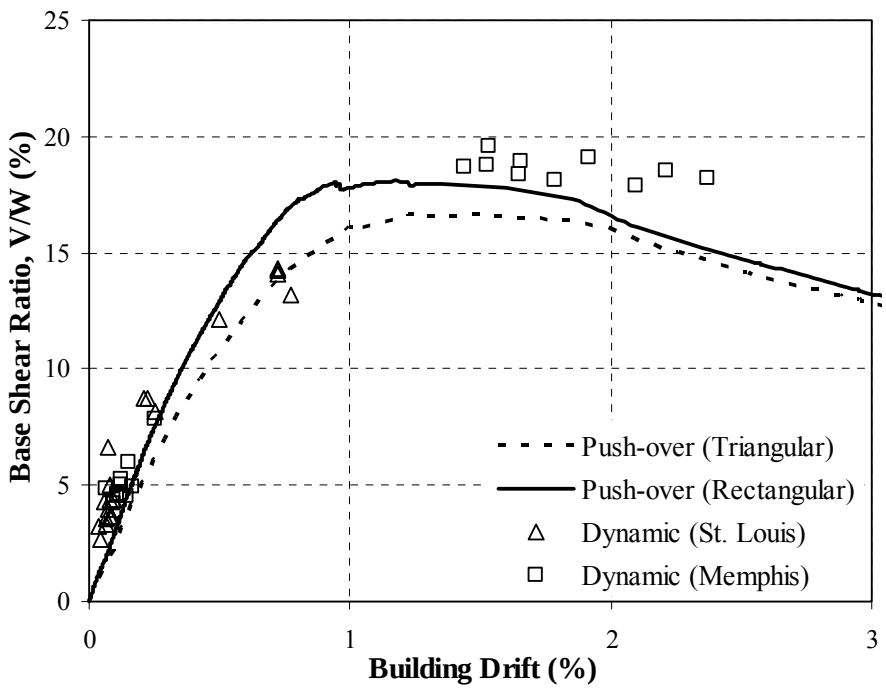

Fig. 5.9. Comparison of push-over and dynamic analysis

5.4 Seismic Evaluation for Unretrofitted Case Study Building

5.4.1 Global-Level Evaluation

The performance criteria for the global-level approach are defined by the maximum interstory drift. This approach may not be appropriate for predicting member-

level performance. However, it provides a first approximation of structural behavior under seismic demands. It is necessary to conduct a member-level evaluation to determine specific member performance.

The case study building is a RC flat slab building, which is very vulnerable to punching shear failure under significant lateral displacements during seismic loadings. For this reason, the punching shear model based on the gravity shear ratio (V_g/V_o) and interstory drift proposed by Hueste and Wight (1999) was used to establish an upper bound drift limit for the Collapse Prevention limit state. The gravity shear ratio (V_g/V_o) is the ratio of the two-way shear demand from gravity loads to the nominal two-way shear strength at the slab-column connection. It is defined as the value of the vertical gravity shear (V_g) divided by the nominal punching shear strength (V_o) for the connection without moment transfer. Fig. 5.10 shows the proposed relationship between interstory drift and the gravity shear ratio under seismic loads. As shown in Fig. 5.10, several results from the 2% in 50 years Memphis motions exceed the corresponding punching shear drift limit. Therefore, the punching shear failure may occur under the large magnitude seismic events.

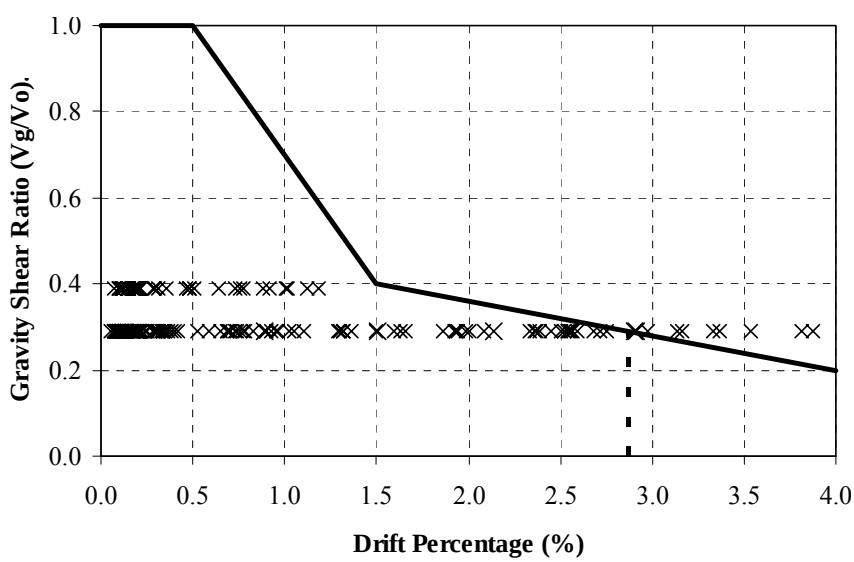

Fig. 5.10. Prediction model for punching shear and flexural punching shear failures with analytical results

For the case study building, V_g/V_o is 0.29 at the floor levels and 0.39 at the roof level. Because the maximum interstory drift occurred at the lower stories for the push-over and dynamic analyses, a gravity shear ratio of 0.29 was used to find corresponding drift limit for the prediction of punching shear failure. As shown in Fig. 5.10, the corresponding drift limit at which punching shear is predicted at the interior slab-column connections is 2.9%. Therefore, this drift limit was used for derivation of the CP fragility curve for the unretrofitted building. Table 5.5 summarizes the selected global drift limits.

Table 5.5. Selected global drift limits for concrete frame elements

Structural performance levels	Drift (%)
Immediate occupancy (IO)	1
Life safety (LS)	2
Collapse prevention (CP)	4 (2.9*)

* Drift limited to 2.9% for Collapse Prevention based on punching shear failure prediction model.

Because the analytical results from ZEUS-NL did not include a shear failure, the shear strength of the columns at the base was calculated and compared with the current requirement. According to the *ACI 318-02*, a shear strength provided by concrete members subjected to axial compression was defined using the following equation. Based on the results from nonlinear dynamic analysis, the maximum values of base shear were less than the shear capacity of columns.

$$V_c = 2\left(1+\frac{N_u}{2000A_g}\right)\sqrt{f'_c}\,b_w d \tag{5.2}$$

where:

V_c = Nominal shear strength provided by concrete, lb

A_g = Gross area of section, in.^{2}

f'_c = Specified compressive strength of concrete, psi

N_u = Factored axial load normal to cross section occurring simultaneously with V_u or T_u; to be taken as positive for compression, lb

b_w = Web width, in.

d = Distance from extreme compression fiber to centroid of longitudinal tension reinforcement

Fig. 5.11 shows the maximum interstory drift profiles for the unretrofitted case study building from the analyses using the St. Louis motions. The median value is also indicated. According to FEMA 356, the proposed Basic Safety Objective (BSO) is LS performance for the Basic Safety Earthquake 1 (BSE-1) earthquake hazard level and CP performance for the BSE-2 earthquake hazard level. BSE-1 is defined as the smaller of an event corresponding to 10% probability of exceedance in 50 years (10% in 50 years) and 2/3 of BSE-2, which is the 2% probability of exceedance in 50 years (2% in 50 years) event.

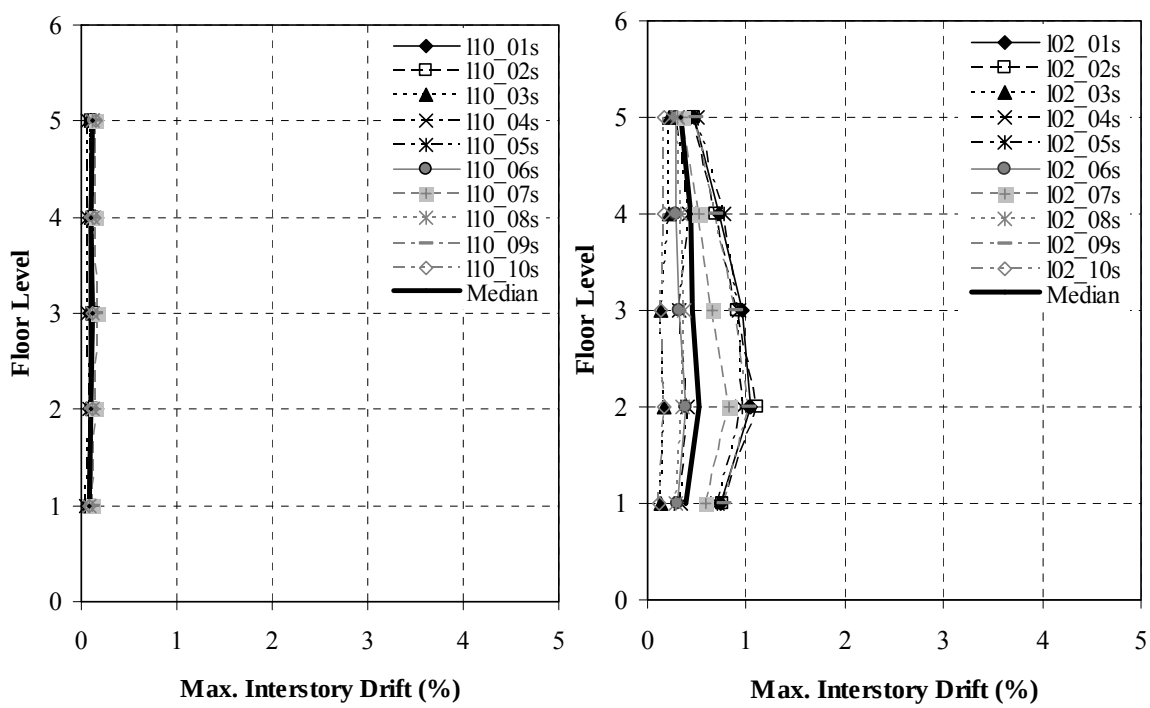

(a) 10% in 50 years (b) 2% in 50 years

Fig. 5.11. Maximum interstory drifts for St. Louis motions

As seen in Fig. 5.11, because all the maximum interstory drift values are less than 1% maximum interstory drift, the structural response is within the FEMA 356 global-level limit of 2% for LS for the 10% in 50 years motions. For the 2% in 50 years motions, the median interstory drifts are much less than the CP limit of 2.9%. Therefore, the case study building meets the BSO under St. Louis motions based on a global-level evaluation.

Fig. 5.12 shows the global-level evaluation of the case study building for the Memphis motions. Similar to the St. Louis motions, the maximum interstory drift values for 10% in 50 years motions are less than 1%. However, for the 2% in 50 years motions, the median responses of the structure at the 1st and 2nd floor lever are slightly greater than 2.9%, which is the limit for CP performance. Therefore, based on a global-level evaluation, the case study building requires retrofitting to meet the BSO for the Memphis motions.

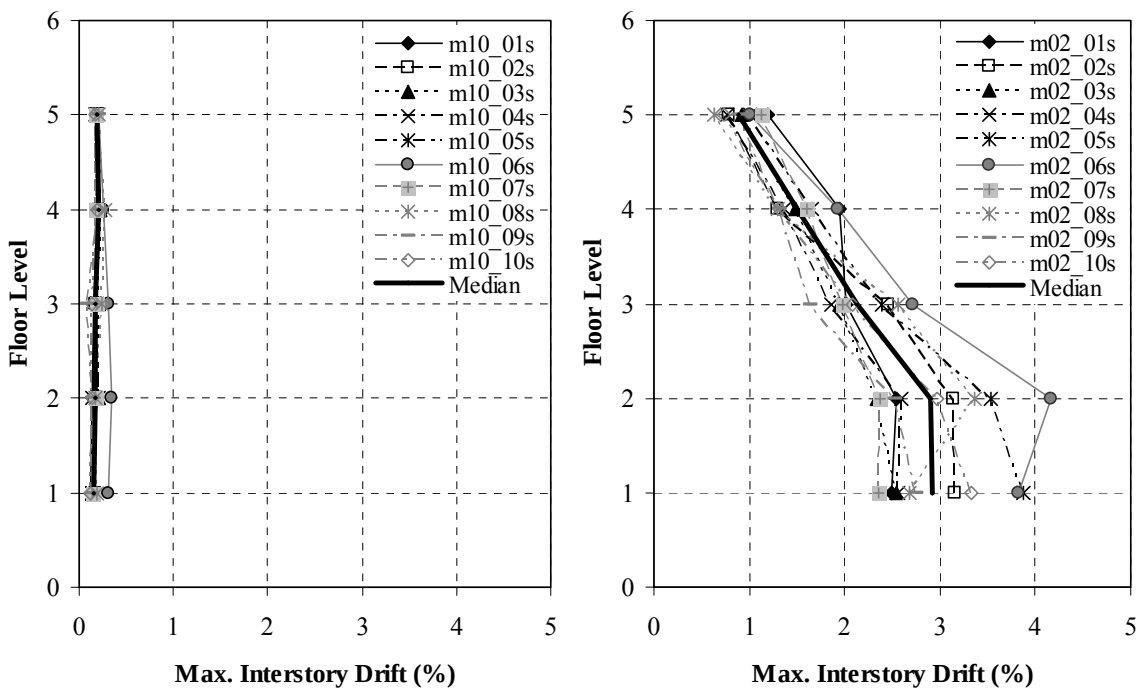

(a) 10% in 50 years (b) 2% in 50 years

Fig. 5.12. Maximum interstory drifts for Memphis motions

5.4.2 Member-Level Evaluation

The global-level evaluation provides a general assessment of the seismic performance of a structure. However, it does not identify member deficiencies and a vulnerable member, which is necessary to select appropriate member-level retrofit techniques. Therefore, in this study, the member-level evaluation of FEMA 356 was also performed to determine more detailed information for structural behavior and seismic performance. Based on this evaluation, several retrofit techniques were selected and applied to the case study structure.

Plastic rotation limits are provided by FEMA 356 for a member-level evaluation of the structural components. Plastic rotation is defined as the difference between the maximum rotation at a member end and the yield rotation for that member. Fig. 5.13 provides an example of the determination of the plastic rotation for a beam member.

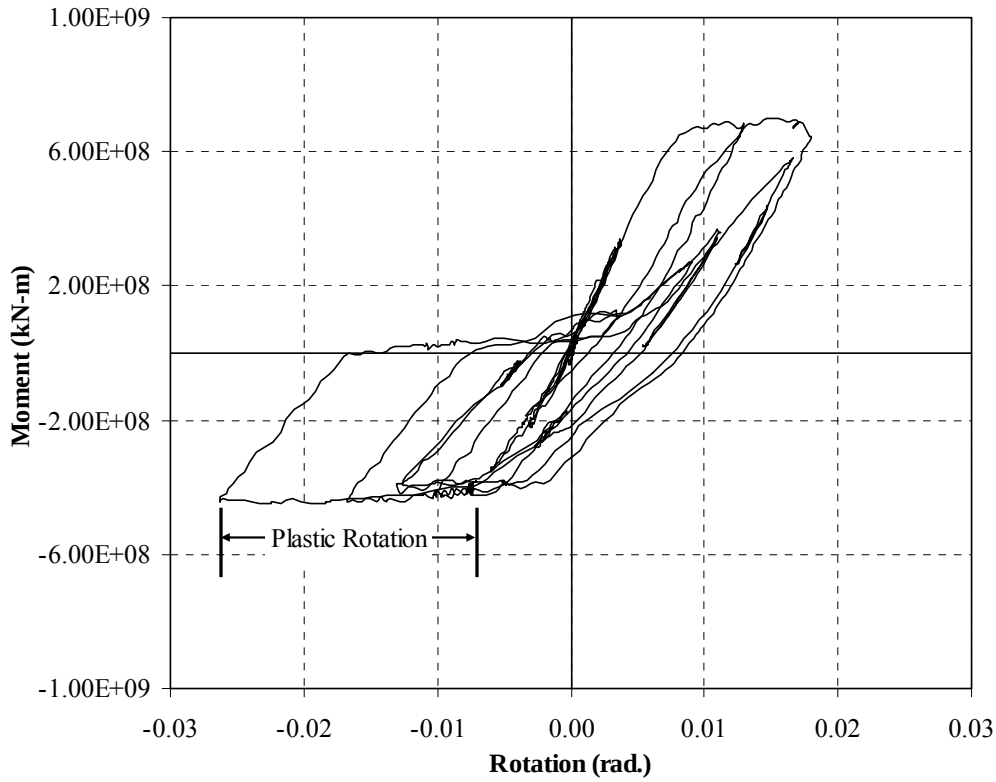

Fig. 5.13. Plastic rotation for a first floor beam member

For the member-level approach, the median ground motion for each story was selected as that which caused an interstory drift closest to the median interstory drift. This approach was used due to limitations in the post-processed data, particularly plastic rotation information. The FEMA plastic rotation limits for each member type (beams, columns, and slabs) were described in the Tables 2.3 to 2.7. Specific limits for this case study structure are given in Table 5.6. The analysis for the 10% and 2% in 50 years St. Louis motions and the 10% in 50 years Memphis motions resulted in no plastic rotations. Therefore, those events met the FEMA 356 criteria for the BSO, as was the case for the global-level evaluation.

Table 5.6. FEMA 356 plastic rotation limits for the unretrofitted case study building

Story	Performance Level	Beams	Columns	Beam-Column Joints	Slabs and Slab-Column Joints
1	IO	0.00500	0.00418	0	0.00550
	LS	0.0100	0.00418	0	0.00825
	CP	0.0100	0.00518	0	0.0110
2	IO	0.00500	0.00453	0	0.00550
	LS	0.0100	0.00453	0	0.00825
	CP	0.0100	0.00553	0	0.0110
3	IO	0.00500	0.00481	0	0.00550
	LS	0.0100	0.00481	0	0.00825
	CP	0.0153	0.00581	0	0.0110
4	IO	0.00500	0.00500	0	0.00550
	LS	0.0100	0.00500	0	0.00825
	CP	0.0161	0.00600	0	0.0110
5	IO	0.00500	0.00500	0	0.000500
	LS	0.0100	0.00500	0	0.000750
	CP	0.0157	0.00600	0	0.00100

Table 5.7 summarizes the results of the member-level evaluation for the 2% in 50 years Memphis motions. For the 2% in 50 years events, the BSO is met when the plastic rotations are within the limits for CP. However, as shown in Table 5.7, the BSO of CP is not satisfied because the CP limits for plastic rotation are exceeded in several members (noted with bold font). According to this result, the first and second floor level may experience significant damage and all the columns, except the fifth story, may be

vulnerable under the expected earthquake event. However, this does not mean that the entire system would experience a collapse.

Table 5.7. Maximum plastic rotations for 2% in 50 years Memphis motions

Story	Median Ground Motion	Beams	Columns	Slabs
1	m02_09s	**0.0179**	**0.0286**	**0.0179**
2	m02_10s	**0.0168**	**0.0222**	**0.0127**
3	m02_10s	0.0110	**0.0175**	0.00768
4	m02_03s	0.00487	**0.0112**	0
5	m02_09s	0	0.00507	0

Fig. 5.14 shows the locations of inelastic behavior in the unretrofitted structure where the plastic rotations exceed the limits for each performance level (IO, LS, and CP) under the median ground motion for the 2% in 50 years Memphis event. Locations where the rotations exceeded the FEMA 356 member-level criteria for each limit state are shown with black circles. These figures demonstrate that most columns in the external frame, along with the beams and some slab members at the 1st and 2nd floor levels are vulnerable.

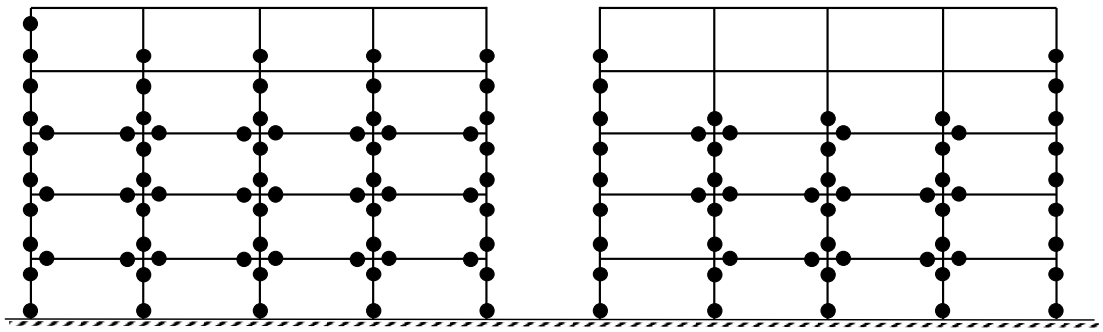

(a) IO Limit State

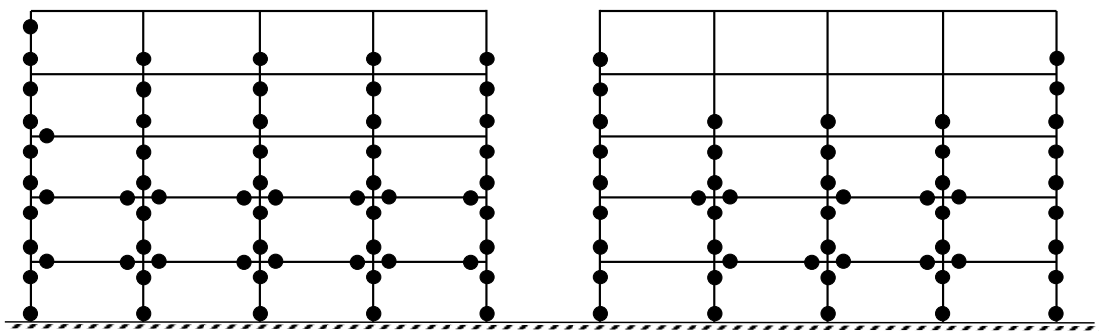

(b) LS Limit State

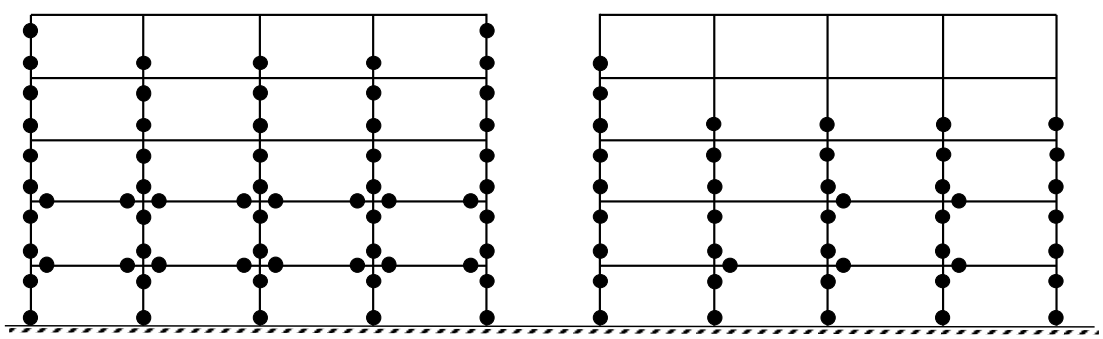

(c) CP Limit State

● = Exceedance of plastic rotation limit

Fig. 5.14. Locations in unretrofitted building where FEMA 356 plastic rotation limits are exceeded (2% in 50 years Memphis event)

5.4.3 Additional Evaluation

During strong earthquake events, RC frame buildings may undergo a story mechanism or column failure mechanism in cases where plastic hinges form at the ends of all column members in a story. Therefore, it is important to determine the column-to-beam flexural strength ratio to evaluate the structure's seismic vulnerability. The expression given in ACI 318 (ACI Comm. 318 2002) to evaluate this ratio is as follows.

$$\sum M_c \geq (6/5)\sum M_g \tag{5.3}$$

where:

$\sum M_c$ = Sum of moments at the faces of the joint corresponding to the nominal flexural strength of the columns framing into that joint. Column flexural strength shall be calculated for the factored axial force, consistent with the direction of the lateral forces considered, resulting in the lowest flexural strength

$\sum M_g$ = Sum of moments at the faces of the joint corresponding to the nominal flexural strength of the girders framing into that joint

For the unretrofitted structure, the column-to-beam strength ratio for the perimeter moment frames of the 1st floor level was 1.27, which satisfied the minimum requirement of 1.2 for special moment frame members in the current ACI 318 (ACI Comm. 318 2002). This minimum requirement is given to reduce the likelihood of yielding in columns that are part of the lateral system. The column-to-beam strength ratios for the perimeter moment frames at the upper level are 1.27 (2nd floor), 1.39 (3rd floor), 1.53 (4th floor), and 0.85 (roof level).

5.5 Fragility Curves for Unretrofitted Case Study Building

5.5.1 Methodology

In this study, the objective of the seismic fragility analysis was to assess the effectiveness of retrofit by estimating the reduction in the probability of exceeding a certain limit state, as compared to the unretrofitted structure. To develop the desired fragility curves, several parameters were needed, including structural characteristics, earthquake intensities, and uncertainties for capacity and demand. The seismic demand was determined from the twenty synthetic Memphis ground motions summarized in Tables A.3 and A.4 in Appendix A. The desired fragility curves were developed using the following equation which assumes that both capacity and demand are lognormally distributed (Wen et al. 2004). This approach is similar to the SAC FEMA framework developed by Cornell et al. (2002).

$$P(LS|S_a) = 1 - \Phi\left(\frac{\lambda_{CL} - \lambda_{D|S_a}}{\sqrt{\beta_{D|S_a}{}^2 + \beta_{CL}{}^2 + \beta_M{}^2}}\right) \tag{5.4}$$

where:

$P(LS|S_a)$ = Probability of exceeding a limit state given the spectral acceleration at the fundamental period of the building

Φ = Standard normal cumulative distribution function

λ_{CL} = ln(*median drift capacity for a particular limit state*), where drift capacity is expressed as a percentage of the story height

$\lambda_{D|S_a}$ = ln(*calculated median demand drift given the spectral acceleration*), where demand drift is determined from a fitted power law equation

$\beta_{D|S_a}$ = Uncertainty associated with the fitted power law equation used to estimate demand drift $= \sqrt{\ln(1+s^2)}$

β_{CL} = Uncertainty associated with the drift capacity criteria, taken as 0.3 for this study (Wen et al. 2004)

β_M = Uncertainty associated with analytical modeling of the structure, taken as 0.3 for this study (Wen et al. 2004)

s^2 = Square of the standard error = $\dfrac{\sum\left[\ln(Y_i)-\ln(Y_p)\right]^2}{n-2}$

Y_i and Y_p = Observed demand drift and power law predicted demand drift, respectively, given the spectral acceleration

n = Number of sample data points for demand

Wen et al. (2004) compared the fragility curves with varying modeling uncertainty from 0.2 to 0.4 and showed that the fragility results are not sensitive to this parameter. Therefore, the value for the uncertainty associated with the analytical modeling of the structure was taken as 0.3 for their study. The same value was used in this study. In addition, the value of 0.3 was also used to quantify the dispersion in the drift capacity. The 0.3 dispersion is not a specific value, but was considered reasonable for this study based on the report by Wen et al. (2004).

5.5.2 Global-Level Limits

The λ_{CL} term for the fragility analysis was calculated with the natural log of the specified drift limit in percent. For example, according to the FEMA 356 global-level drift limits for concrete frame structures, 1, 2 and 4 were used for IO, LS, and CP, respectively. In addition to this, a 2.9% drift limit for CP, based on the punching shear failure prediction model, was used in this study (see Table 5.5).

To demonstrate the methodology for derivation of the fragility curves, the unretrofitted case study building is considered. Fig. 5.15 provides the relationship between maximum interstory drift and the corresponding spectral acceleration for both the 10% in 50 years and the 2% in 50 years Memphis motions. A total of twenty points are plotted, where each data point represents the demand relationship for one ground motion record. The spectral acceleration (S_a) for a given ground motion record is the value corresponding to the fundamental period of the structure based on cracked section properties (T_1 = 1.62 s) and 5 percent damping. The drift demand value is the maximum interstory drift determined during the nonlinear time history analysis of the structure

when subject to that ground motion record. The best-fit power law equation is also provided in the graph. This equation is used to describe the demand drift when constructing the fragility curves for the unretrofitted structure. The corresponding value of s^2 for the unretrofitted case is 0.114, which gives a $\beta_{D|S_a}$ value of 0.328. The fragility curves developed using FEMA global-level performance criteria are shown in Fig. 5.16.

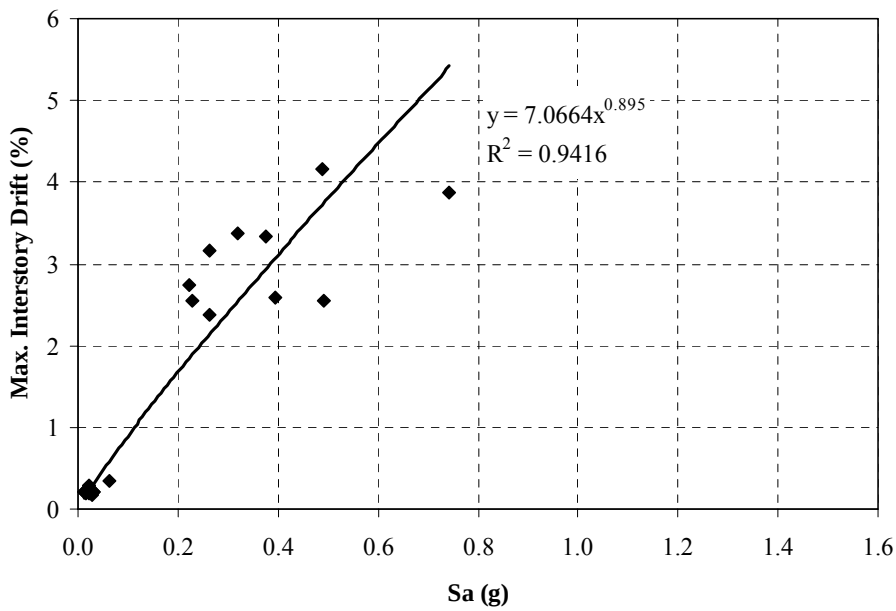

Fig. 5.15. Development of power law equation for unretrofitted structure (Memphis motions)

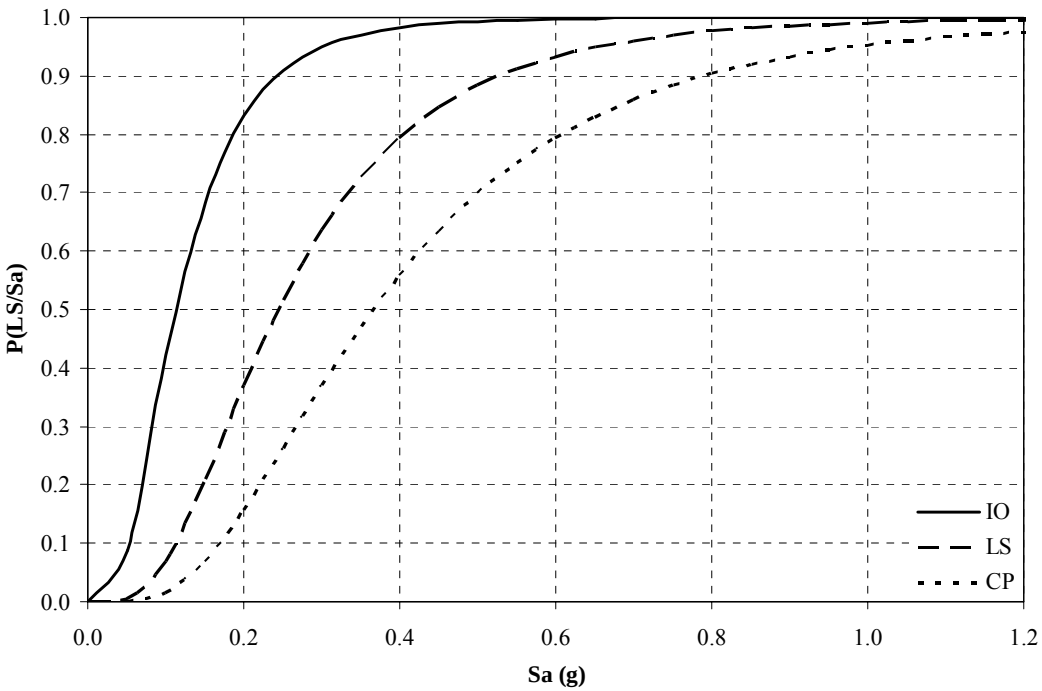

Fig. 5.16. Global-level fragility curves of the unretrofitted structure for Memphis motions

5.5.3 Member-Level Limits

To develop fragility curves based on the FEMA 356 member-level criteria, drift limits corresponding to those criteria were determined. In this study, two different analyses were used for determining the most critical interstory drift corresponding to the member-level criteria: regular push-over analysis and the method developed by Dooley and Bracci (2001). For regular push-over analysis, the inverted triangular load pattern was used. The second method, which was suggested by Dooley and Bracci (2001), was used to find critical drifts based on the development of a plastic mechanism within a story. Fig. 5.17 shows a comparison between a regular push-over analysis and a push-over analysis to evaluate the critical response of a story. As shown in Fig. 5.17, in order to determine the drift capacity of a story, the x-direction deformation of the level below is restrained to create the most critical story mechanism.

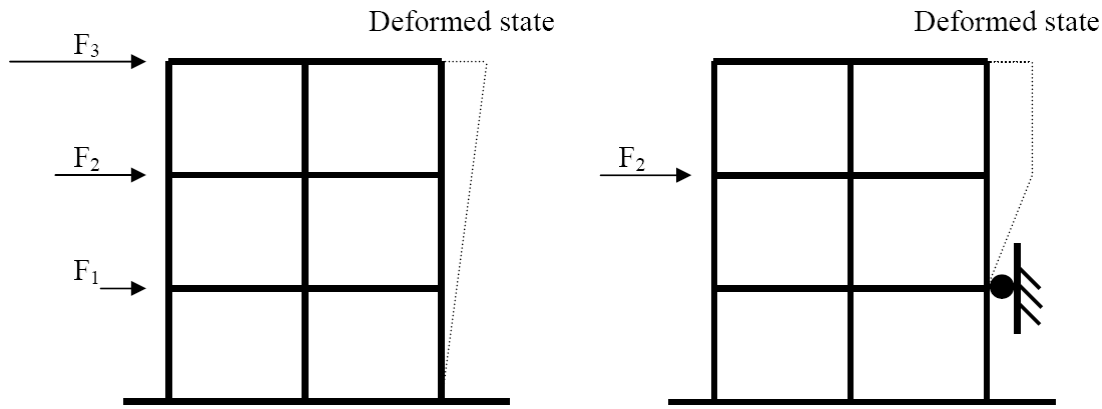

(a) Inverted triangular loading (first mode response) (b) Critical second story response

Fig. 5.17. Example loading patterns for push-over analysis (Wen et al. 2003)

First of all, the FEMA 356 member-level limit states were determined using a regular push-over analysis. Push-over analysis with the inverted triangular load pattern was performed to define the drift limit at which a member-level rotation limit is exceeded. The drift limits corresponding to the exceedance of FEMA 356 member-level criteria are provided in Table 5.8 and Fig. 5.18.

Table 5.8. Drift limits based on FEMA 356 member-level criteria

Structural performance levels	Drift (%)
Immediate occupancy	0.88
Life safety	0.88
Collapse prevention	1.07

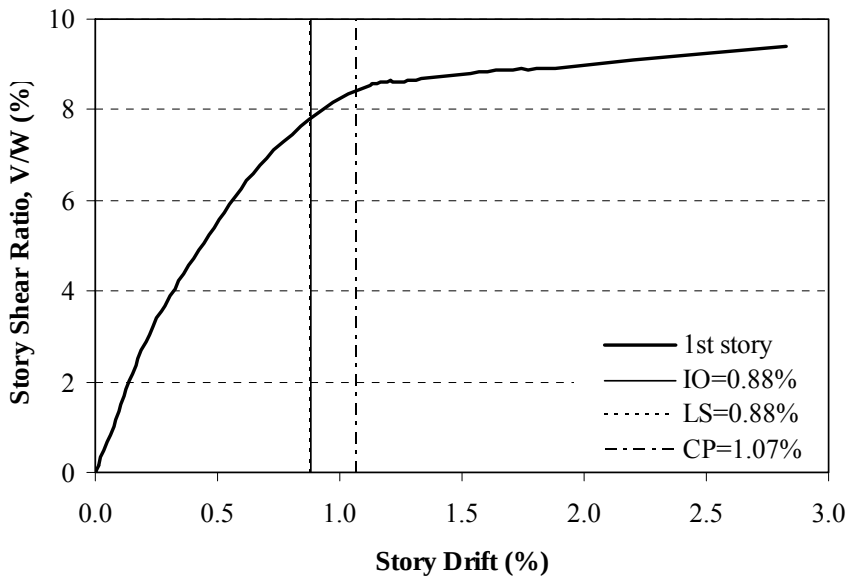

Fig. 5.18. FEMA limits based on member-level criteria with push-over curve for the 1st story

The response of the first story provided the minimum value for drift limits. As shown in Table 5.8, the drift limits between FEMA global-level and member-level criteria provided some differences. Using the member-level criteria, all the drift limits are much less than global-level drifts. In particular, the drifts for LS and CP are close each other. Since plastic rotation limits of RC column member for IO and LS limit states had the same values in this study, the corresponding drift limits for IO and LS are the same values. Fig. 5.19 shows the fragility curves using the drift limits based on the FEMA 356 member-level criteria. For comparison, the fragility curves using the global drift limits are represented on each graph with dotted lines. As shown in Fig. 5.19, the probability of exceeding each limit for the FEMA member-level criteria gave larger values than that for the FEMA global-level criteria.

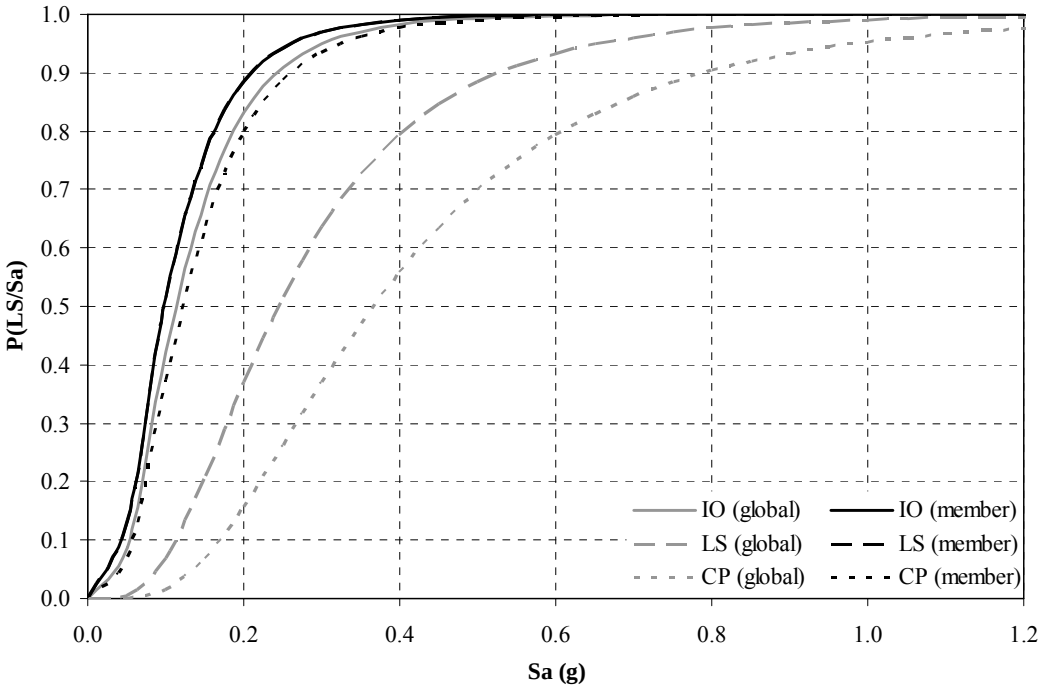

Fig. 5.19. Fragility curves for the FEMA member-level criteria from a regular push-over analysis

A second method, suggested by Dooley and Bracci (2001), was used to find more critical drifts based on the plastic mechanism of each story. Push-over analysis using a story-by-story procedure (see Fig. 5.17) was performed for each story to define the drift limits. In order to obtain more accurate results, displacements were controlled during the push-over analysis. The drift limits corresponding to the first exceedance of the FEMA member-level criteria are provided in Table 5.9 and Fig. 5.20.

Table 5.9. Drift limits based on FEMA 356 member-level criteria for the critical response

Structural performance levels	Drift (%)
Immediate occupancy	0.62
Life safety	0.62
Collapse prevention	0.69

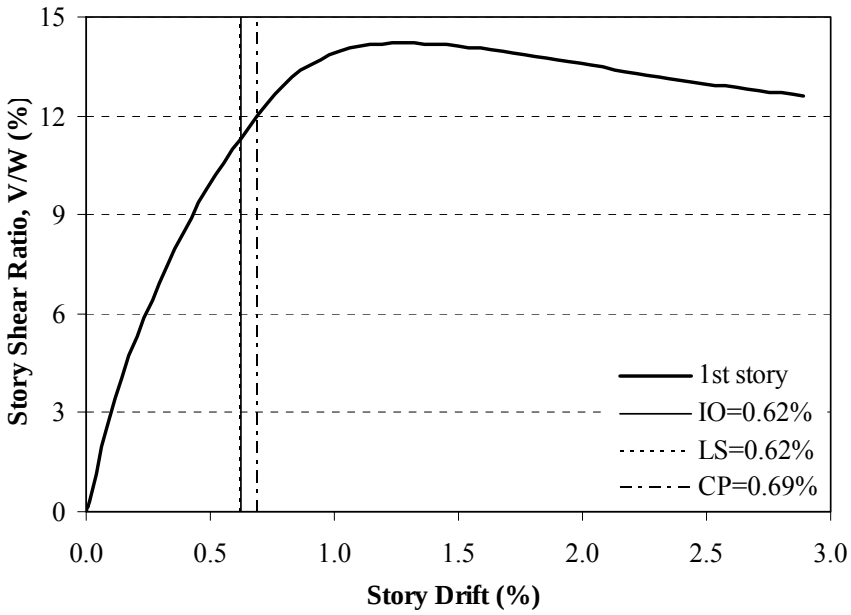

Fig. 5.20. FEMA limits based on member-level criteria with critical response push-over curve for the 1st story

In this case, the response of the 1st story also provided the minimum value for drift limits. As shown in Table 5.9, the drift limits are much less than FEMA global-level and even less than member-level criteria with a regular push-over analysis. Fig. 5.21 shows the fragility curves for the FEMA member-level criteria based on limits from the critical response push-over analysis. For comparison, the fragility curves using the FEMA 356 global-level drift limits are also represented on each graph with dotted lines.

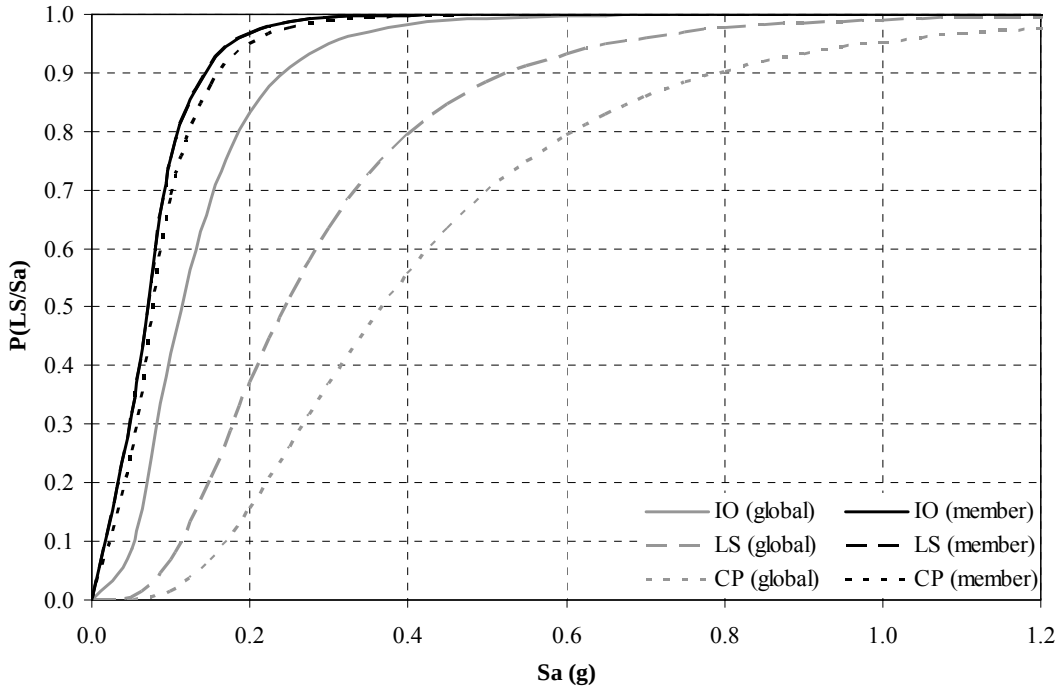

Fig. 5.21. Fragility curves for the FEMA member-level criteria from the critical response push-over analysis

5.5.4 Additional Quantitative Limits

Additional quantitative limit states were evaluated based on limits described by Wen et al. (2003), as follows.

(1) First Yield (FY) – Interstory drift at which a member of a story or a structure initiates yielding under an imposed lateral loading.

(2) Plastic Mechanism Initiation (PMI) – Interstory drift at which a story mechanism (typical of a column sidesway mechanism), an overall beam sidesway mechanism, or a hybrid mechanism initiates under an imposed lateral loading.

(3) Strength Degradation (SD) – Interstory drift at which the story strength (resistance) has degraded by more than a certain percentage of the maximum strength (about 20 percent). Note that strength degradation can occur due to

material nonlinearities in the analytical models and also due to geometric nonlinearities from P-delta effects.

First, the drift limits corresponding to the above limit states were determined using a regular push-over analysis. Push-over analysis with the inverted triangular load pattern was performed to define the drift limits. The drift limits for the quantitative limit states are provided in Table 5.10 and Fig. 5.22. In addition, Fig. 5.23 shows the locations of inelastic rotation when the PMI limit state occurred for the 1st story.

Table 5.10. Drift limits for quantitative limit states (regular push-over analysis)

Structural performance levels	Drift (%)
First yield	0.66
Plastic mechanism initiation	0.81

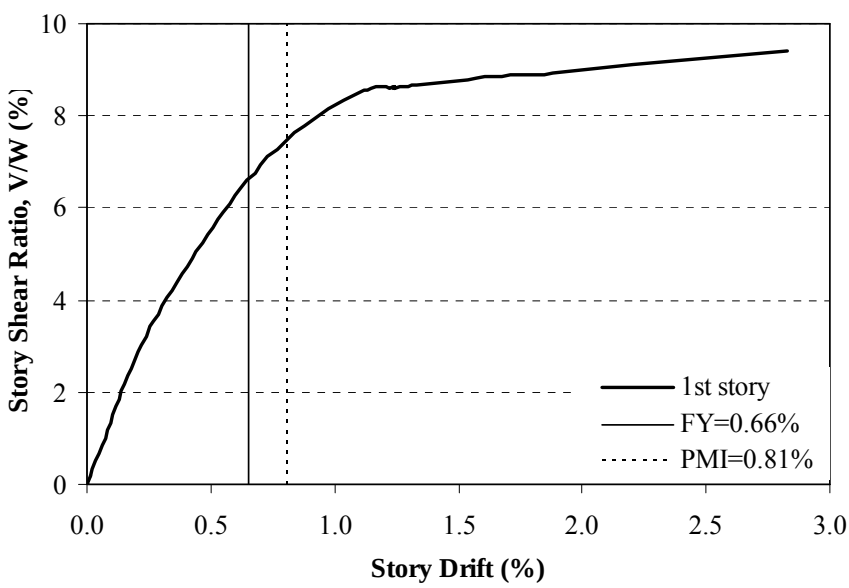

Fig. 5.22. Drift limits for quantitative limit states with push-over curve for the 1st story (regular push-over analysis)

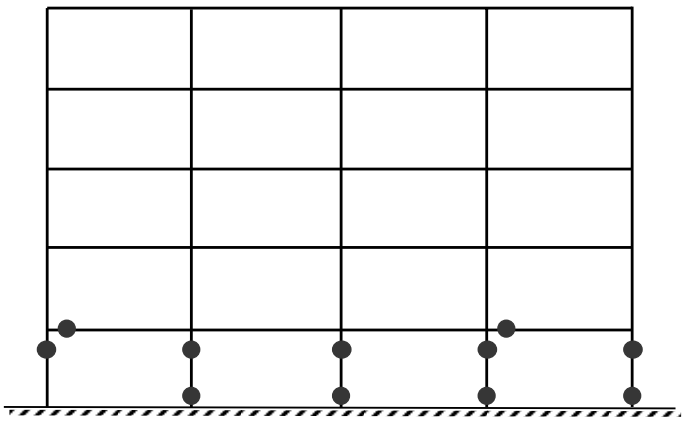

Fig. 5.23. Locations of inelastic rotation at PMI limit state based on the quantitative approach with push-over curve for the 1st story

As shown in Table 5.10, drift limits based on the quantitative limit states are even less than those found for the FEMA member-level criteria. In this case, the SD limit state was not detected because the strength did not fall to 20% of the maximum strength. Fig. 5.24 shows the fragility curves using these limit state definitions. For comparison, the fragility curves using the global drift limits are represented on each graph with dotted lines. As shown, the drift limits from the additional quantitative limits gave a much higher probability of failure than the drifts for the FEMA global-level criteria.

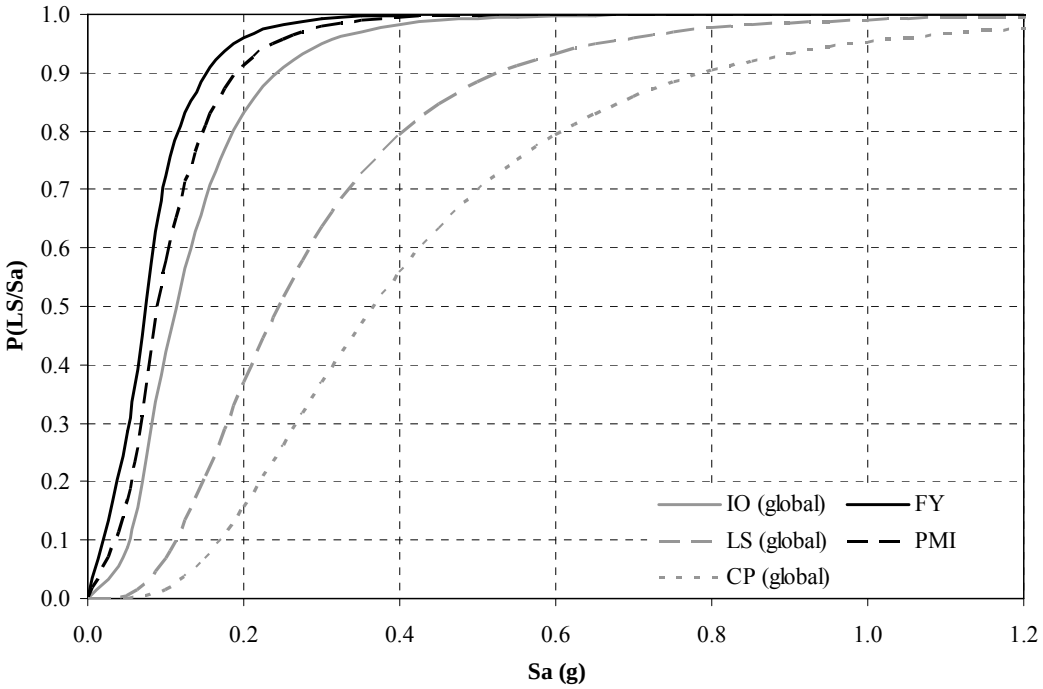

Fig. 5.24. Fragility curves based on additional quantitative limits from a regular push-over analysis

The method suggested by Dooley and Bracci (2001) was used to find more critical drifts based on the story-by-story push-over analysis. The corresponding drift limits for the quantitative limit states are provided in Table 5.11 and Fig. 5.25. In Table 5.11, the minimum drifts for each limit state are noted with bold font. In addition, Fig. 5.26 shows the locations of inelastic rotation when the PMI limit state occurred for the 1st story.

Table 5.11. Drift limits for the limit states based on the quantitative approach

	Interstory drift (%)		
	FY	PMI	SD
1st story	**0.36**	**0.66**	·
2nd story	0.51	0.86	**2.81**
3rd story	0.52	0.89	3.27
4th story	0.61	0.91	4.23
5th story	0.49	0.82	·

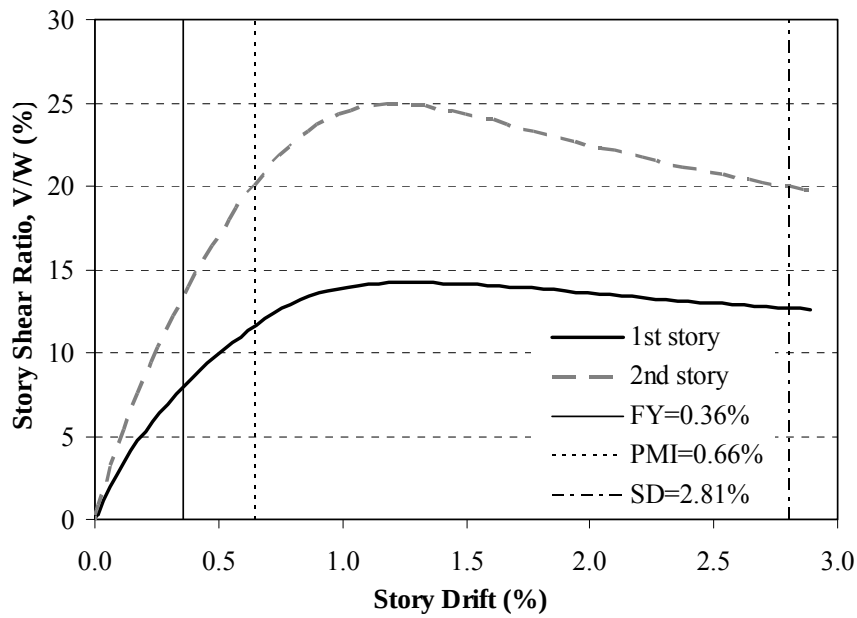

Fig. 5.25. Drift limits for the limit states based on the quantitative approach with critical response push-over curve for the 1st and 2nd stories

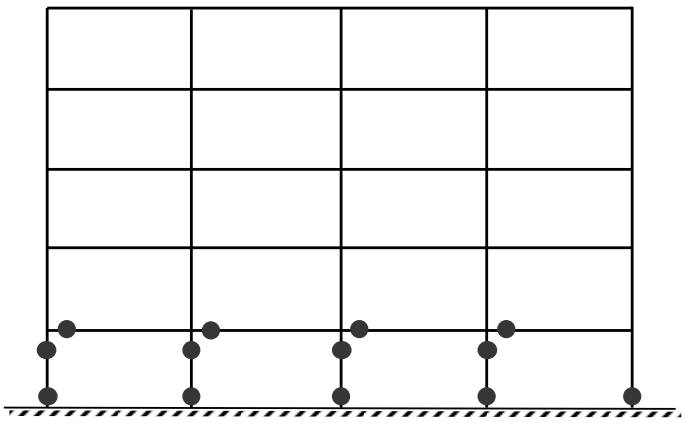

Fig. 5.26. Locations of inelastic rotation at PMI limit state based on the quantitative approach with push-over curve for the 1st story

As shown in Fig. 5.25, the minimum drifts for the FY and PMI limit states were provided by the 1st story push-over curve while SD limit state was given by the response of the 2nd story. The drift for SD limit state is similar in magnitude to the global-level drift limit assigned to CP which is associated with punching shear failure.

Fig. 5.27 shows the fragility curves with the critical response push-over analysis. For comparison, the fragility curves using the global drift limits are also represented on each graph with dotted lines.

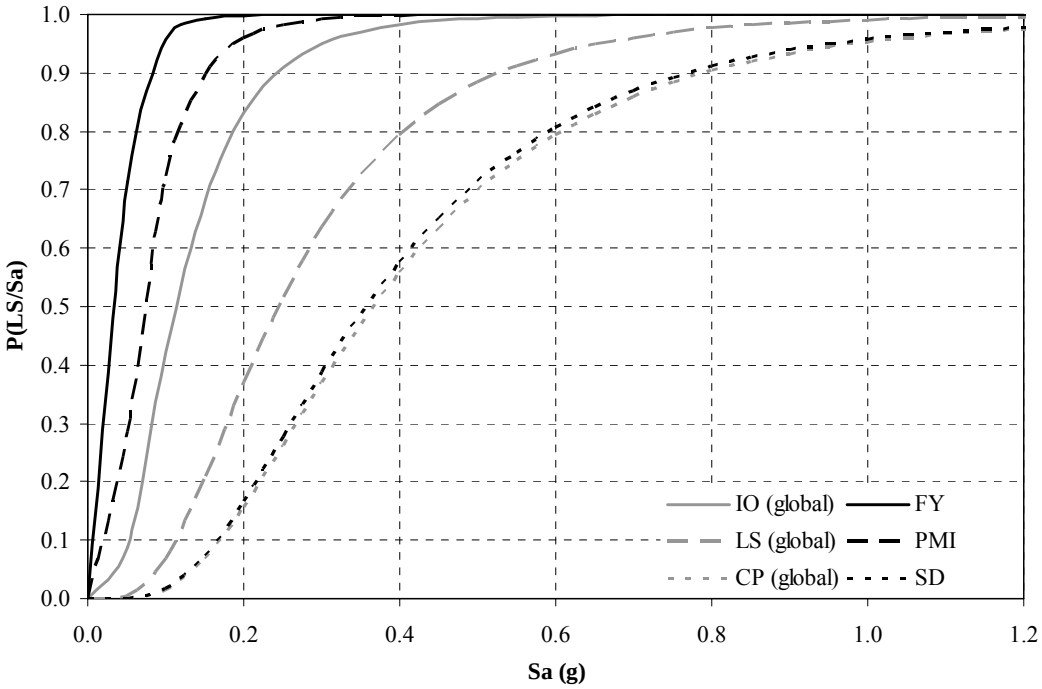

Fig. 5.27. Fragility curves based on additional quantitative limits from the critical response push-over analysis

5.6 Summary

In this section, the analysis of the unretrofitted case study building was described. Results from two structural analysis methods (nonlinear static analysis and nonlinear dynamic analysis) and two structural nonlinear analysis programs (ZEUS-NL and DRAIN-2DM) were compared. The ZEUS-NL program was selected for additional analytical studies to evaluate the expected seismic performance of the structure for St. Louis and Memphis synthetic ground motions. Based on the analytical results, fragility curves were developed using the FEMA 356 performance criteria and additional limit states. The fragility curves developed based on FEMA global-level drift limits and member-level plastic rotation limits were compared. In addition to this, additional quantitative limit states, described by Wen et al. (2003), were determined and compared to the limits based on the FEMA 356 criteria.

6 RETROFIT DESIGN AND ANALYSIS OF RETROFITTED CASE STUDY BUILDING

6.1 Introduction

This section presents the analytical results of the retrofitted case study building. Three seismic retrofit techniques were applied to enhance the seismic performance of the structure. The seismic behavior of the retrofitted structure and seismic evaluation using FEMA 356 were conducted through nonlinear analyses. In addition, the probabilistic fragility curves for the retrofitted structure were developed and compared with the original structure.

6.2 Retrofit Strategies

6.2.1 General

From the structural design point of view, the selection of the most appropriate retrofit strategy depends on the structural characteristics of the building and the inelastic behavior of each member. This implies that the most vulnerable structural characteristic and the weakest part of the structure should be considered prior to others. It is also important to consider the effects of different retrofit techniques on the seismic performance, including the dynamic response of the structure and each member.

As discussed in Section 5, the member-level evaluation for the unretrofitted structure did not satisfy the FEMA 356 BSO in several structural members for the 2% in 50 years Memphis motions. Based on this result, three retrofit schemes were selected. The application of retrofits that modified different structural response parameters was of interest in this study. Because IO performance is mainly related to stiffness, shear walls were added to the external frame to increase the lateral stiffness of the structure. To impact LS performance, the existing columns were encased with RC jackets to increase

their strength. Finally, to impact CP performance, the expected plastic hinge zones of the existing columns were confined with external steel plates to increase ductility. Table 6.1 summarizes the rehabilitation objectives and retrofit techniques corresponding to each limit state (performance level). It is noted that for the shear wall and column jacketing retrofit, both stiffness and strength increase.

Table 6.1. Rehabilitation objectives for each limit state criteria

Limit state	Rehabilitation objective	Retrofit technique
IO	Increase stiffness (& strength)	Add shear walls to external frame
LS	Increase strength (& stiffness)	Add RC column jacketing
CP	Increase ductility	Confine columns plastic hinge zones with steel plates

6.2.2 Retrofit 1: Addition of Shear Walls

The first retrofit strategy consisted of adding RC shear walls to the two center bays of the exterior frame. The addition of shear walls is a common seismic retrofit technique for RC frame structures. This technique increases both the stiffness and strength of the structure. Because lateral stiffness has the most significant change from this retrofit technique, the IO limit state was considered to select a target drift limit. For design load calculations, the *International Building Code 2003* (ICC 2003) was used. Based on *IBC 2003*, a shear wall-frame system with ordinary RC frames is not permitted for seismic design category D, which is the appropriate seismic design category for this analysis. According to Table 1617.6.2 of *IBC 2003*, the response modification coefficient, *R*, is 6 for special RC shear wall systems with intermediate moment frames, which is a system that is allowed to be considered for seismic design category D. Because the existing structure contains ordinary RC moment frames, a response modification coefficient of 5.5, which corresponds to a shear wall-frame interactive system with ordinary RC moment frames and ordinary RC shear walls, was selected for load calculations. The shear walls were then designed by *ACI 318-02* (ACI Comm. 318

2002) Chapter 21 provisions for special RC shear walls to better satisfy the requirements for seismic design category D. The shear walls are 203 mm (8 in.) thick. Two layers of #4 (US) reinforcing bars at 457 mm (18 in.) spacing were selected for the vertical and horizontal reinforcement. For special boundary elements, sixteen #10 (US) reinforcing bars were selected for flexure, and #4 (US) hoops and crossties were placed around every longitudinal bar at each end of the wall. Fig. 6.1 shows the elevation view of the external frame after adding shear walls and Fig. 6.2 shows the details of the shear wall members.

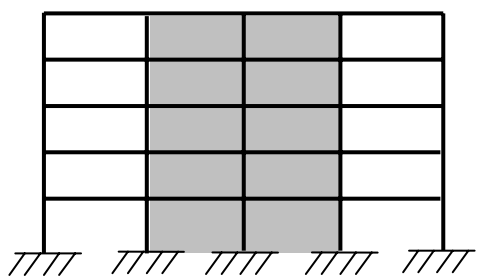

Fig. 6.1. Retrofit 1: Shear walls added to exterior frame

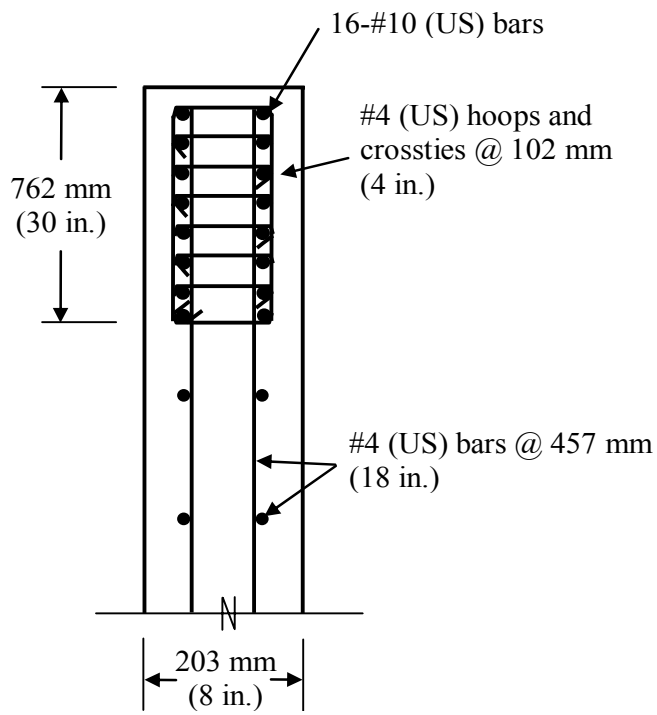

Fig. 6.2. Cross-sectional details of RC shear wall

6.2.3 Retrofit 2: Column Jacketing

Based on the FEMA 356 member-level evaluation of the unretrofitted case study building (Chapter 5), the columns had the most deficiencies in meeting the BSO of CP for the 2% in 50 years Memphis events. To strengthen these vulnerable members, the column jacketing technique was selected as the second retrofit scheme. Based on the member-level seismic evaluation, the columns that did not satisfy the FEMA 356 CP criteria were selected and retrofitted with additional reinforcement and concrete jackets. Because this is primarily a strengthening technique, it best corresponds to improving LS performance. Therefore, the size of the RC jackets and the amount of reinforcement were determined based on the 2% LS drift global-level drift limit. Fig. 6.3 shows the location of jacketed members and Fig. 6.4 shows typical details of the jacketed columns.

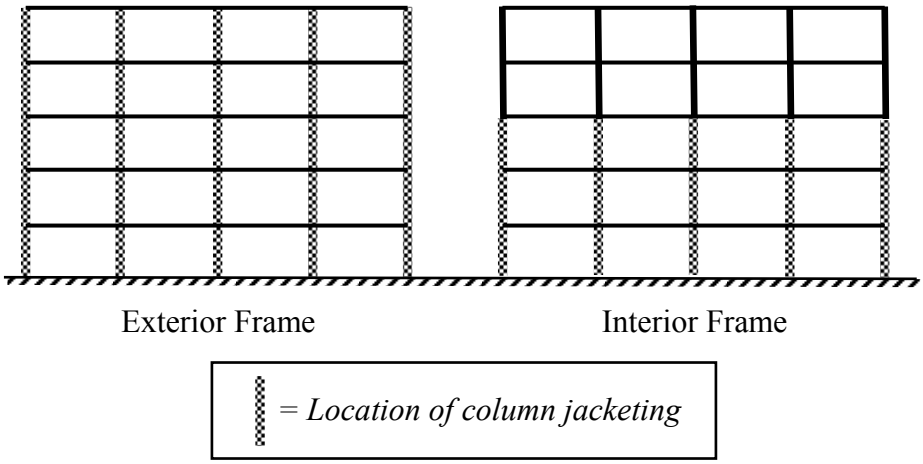

Fig. 6.3. Retrofit 2: Addition of RC column jackets

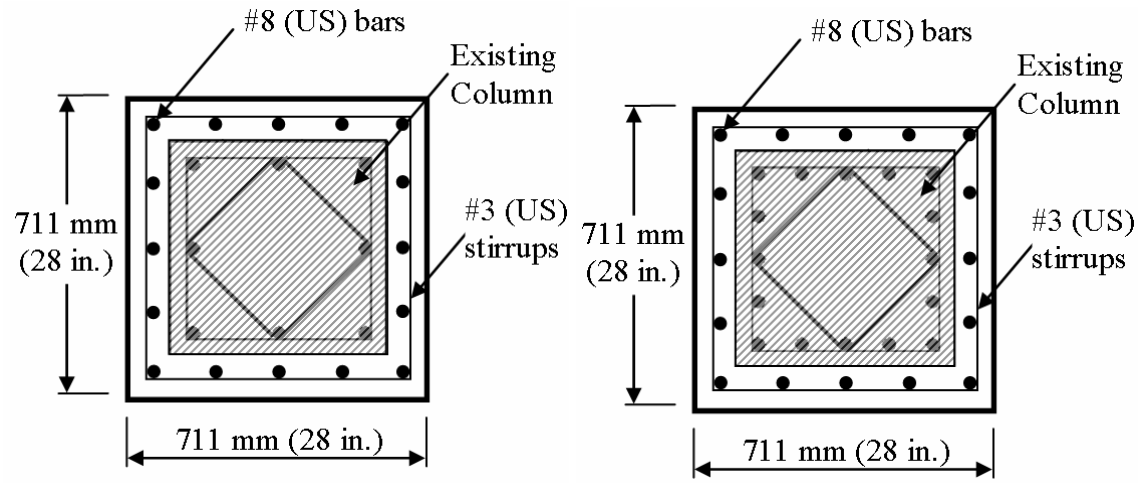

(a) 1st - 5th story for external frame
2nd - 3rd story for interior frame

(b) 1st story for interior frame

Fig. 6.4. Cross-sectional details of RC column jacket retrofit

6.2.4 Retrofit 3: Confinement of Column Plastic Hinge Zones

The third retrofit scheme was to add external steel plates to confine the expected plastic hinge zones of the columns to increase the ductility of the members. This technique was suggested by Elnashai and Pinho (1998) for the ductility-only scenario of selective retrofit techniques described in Section 2. This type of retrofit was also used for strengthening of RC bridge columns (Priestley et al. 1994). When the member ends of columns are vulnerable, failure mechanisms, such as a soft story mechanism can occur. In order to prevent this serious failure mechanism, external confinement steel plates were utilized to confine the columns. The column ends that were confined with steel plates are shown in Fig. 6.5. These correspond to the locations in the unretrofitted structure where the plastic rotations exceeded the CP limits for the 2% in 50 years Memphis motions.

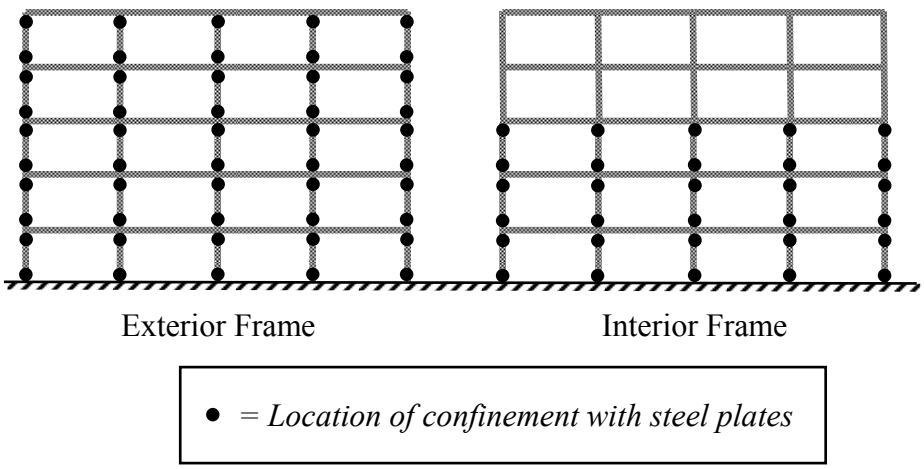

Fig. 6.5. Retrofit 3: Confinement of column plastic hinge zones

6.3 Analytical Modeling of Retrofitted Case Study Building

6.3.1 General

ZEUS-NL was also used for the structural analysis of the retrofitted structure. For the nonlinear dynamic analysis, the twenty ground motions for Memphis, Tennessee, were used (see Tables 4.11 and 4.12). To model the selected retrofit techniques, several sections and material properties developed in ZEUS-NL were utilized.

6.3.2 Retrofit 1: Addition of Shear Walls

To model the shear walls, the RC flexure wall section (rcfws) in the ZEUS-NL program library was used. Fig. 6.6 shows a cross-section of the rcfws member and Table 6.2 provides the values used for each parameter in this analysis. The fully confined region of the rcfws section (labeled as “e”) is for a boundary element of a special RC shear wall.

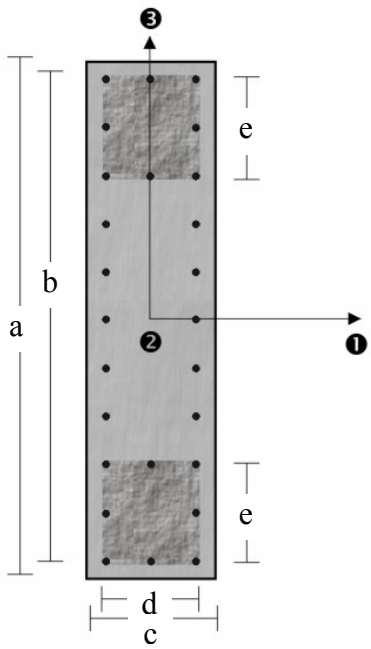

Fig. 6.6. RC flexural wall section in ZEUS-NL (Elnashai et al. 2002)

Table 6.2. Values for modeling parameters of RC flexural wall section

Dimensional parameter	Values, mm (in.)
a. Wall width	8026 (316)
b. Confined width	7950 (313)
c. Wall thickness	203 (8)
d. Confined area thickness	127 (5)
e. Height of fully confined region	762 (30)

6.3.3 Retrofit 2: Addition of RC Column Jackets

For modeling of the RC jacketed columns, RC jacket rectangular section (rcjrs) in ZEUS-NL was used. Fig. 6.7 shows a cross-section of the rcjrs member and Table 6.3 provides the values used for each parameter in this analysis.

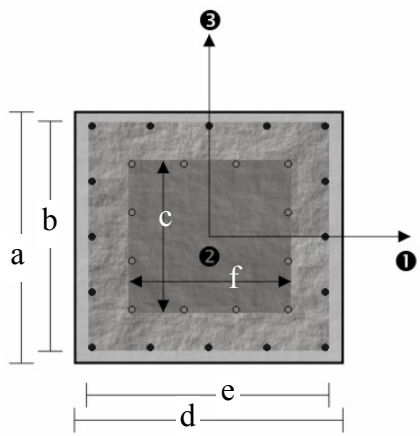

Fig. 6.7. RC jacket rectangular section in ZEUS-NL (Elnashai et al. 2002)

Table 6.3. Values for modeling parameters of RC jacket rectangular section

Dimensional parameter	Values, mm (in.)
a. Section height	711 (28.0)
b. External stirrup height	635 (25.0)
c. Internal stirrup height	384 (15.1)
d. Section width	711 (28.0)
e. External stirrup width	635 (25.0)
f. Internal stirrup width	384 (15.1)

For comparison, the column-to-beam strength ratios for the unretrofitted structure and the retrofitted structure by adding RC jackets were calculated. The current ACI 318 code requires a minimum column-to-beam ratio of 1.2 (ACI Comm. 318 2002). The column-to-beam strength ratio of the 1st floor level for the unretrofitted structure is 1.27 and that for the retrofitted structure by adding RC jackets is 3.78. According to Dooley and Bracci (2001), a minimum strength ratio of 2.0 is a more appropriate value to prevent the formation of a story mechanism under design seismic loading.

6.3.4 Retrofit 3: Confinement of Column Plastic Hinge Zones

For modeling of the third retrofit scheme, the confinement factor (k), which was discussed in Sec. 4.3.1.2, was increased for the expected plastic hinge zones of the vulnerable columns. This is intended to model the effect of physically confining the

columns with external steel plates. To find the proper value of k, the FEMA 356 requirements for ductile column detailing were used. Based on the minimum transverse reinforcement for ductile behavior, a confinement factor k of 1.3 was adopted. The external steel plates were assumed to be applied over a 910 mm (36 in.) length at the column ends indicated in Fig. 6.5. This length was selected to exceed the expected flexural plastic hinge length of 625 mm (24.6 in.) for the first story columns based on the following equation (Paulay and Priestly 1992).

$$L_p = 0.15 d_b f_y + 0.08L \tag{6.1}$$

where:

L_p = Plastic hinge length (in.)
d_b = Longitudinal bar diameter (in.)
f_y = Yield strength of reinforcement (ksi)
L = Member length (in.)

6.4 Comparison of Analytical Results between Unretrofitted and Retrofitted Case Study Building

6.4.1 Push-Over Analysis

Push-over analysis were conducted with an inverted triangular load pattern for the retrofitted case study building and compared with the original structure. The inverted triangular load pattern is based on the first mode shape from an eigenvalue analysis of each retrofitted structure. Fig. 6.8 shows the load patterns for each structure. The push-over curves, relating base shear to building drift, for each retrofitted structure are shown in Fig. 6.9. As seen in Fig. 6.9, the results from the three retrofit schemes demonstrate that each retrofit method affects the global structural response characteristics differently.

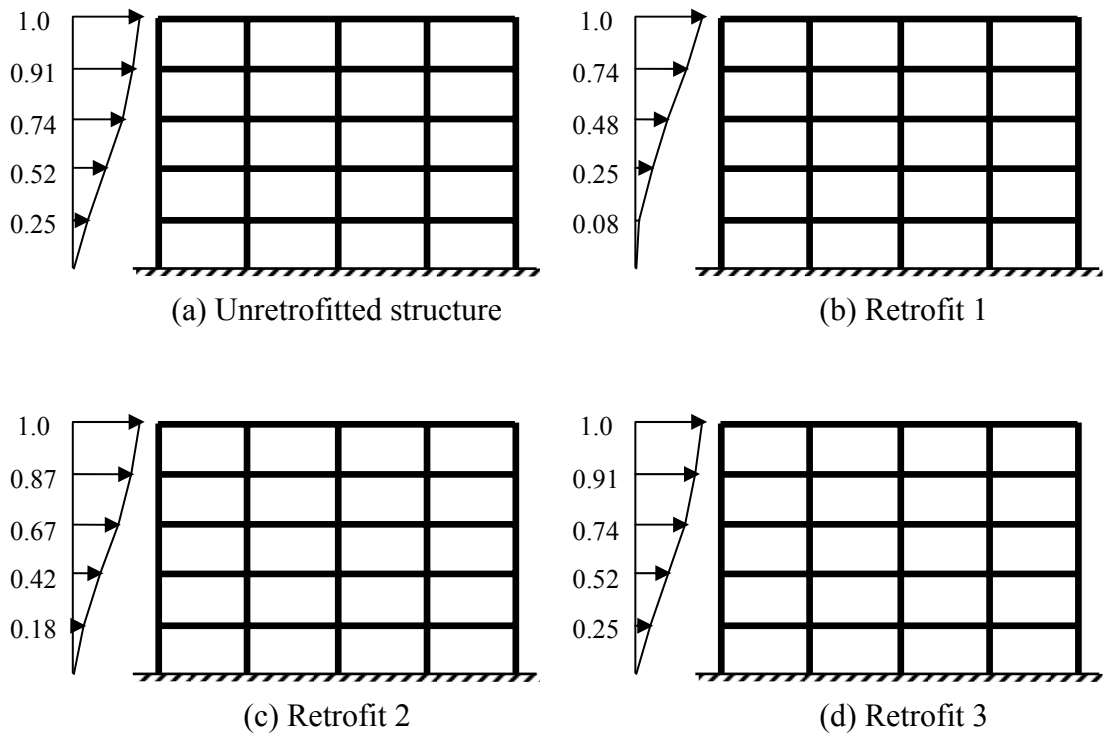

Fig. 6.8. Inverted triangle load patterns for push-over analysis

Table 6.4 summarizes the values of the weight for half of each structure as modeled. First, the retrofitted structure by adding shear walls provided much stiffer behavior than the original structure, but also increased the strength with a maximum base shear ratio of 54.8% of the seismic weight, *W*. This was a 229% increase compared to the unretrofitted building. With this retrofit technique, most of the lateral resistance of the building was provided by the shear walls of the exterior frame and strength degradation occurred slowly. However, attaining 5% building drift for the retrofitted structure when adding shear walls seems too high and it is noted that shear failure is not considered in the model. Based on the additional calculation of shear capacity for the shear wall retrofitted structure, shear failure occurred at 1.2% building drift and a base shear ratio of 48.9%. As shown in Fig. 6.9, the push-over curve after this point for the shear wall retrofitted structure is shown with a dotted line. Column jacketing provided a 59.7% increase of the maximum base shear ratio compared to the original structure. In addition, this retrofit provides more ductile behavior during the analysis, including a

gradual transformation from the linear to nonlinear range and enhancement of the deformation capacity due to the confinement of the jacketed columns. For the structure retrofitted by confining the column plastic hinge zones with external steel plates, the initial stiffness and change of strength up to the peak base shear were almost the same as for the unretrofitted structure. This retrofit did not significantly affect the strength or stiffness of the original structure. However, strength degradation occurred more slowly due to the increase of ductility in the columns.

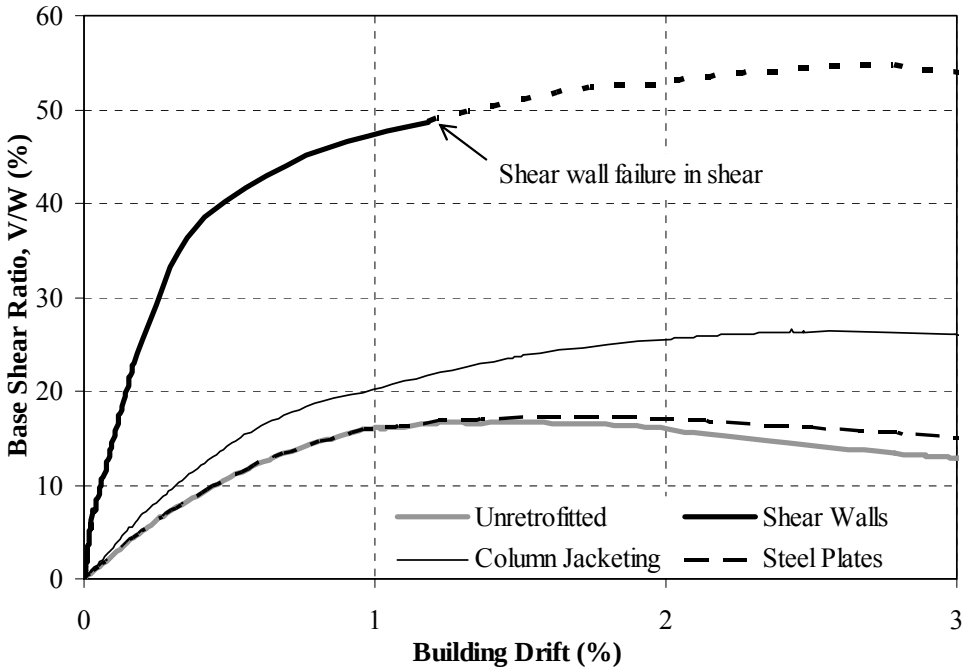

Fig. 6.9. Comparison of push-over curves from the original structure and retrofitted structures

Table 6.4. Seismic weight (*W*) for half of structure

Model	Weight (kN)
Unretrofitted structure	27,513
Retrofit 1: Addition of shear walls	29,451
Retrofit 2: Addition of RC column jackets	27,977
Retrofit 3: Confinement of column plastic hinge zones	27,513

Note: 1 kN = 4.45 kips

6.4.2 Fundamental Periods

Eigenvalue analyses were performed to find the fundamental periods of the retrofitted structure. The fundamental period of the unretrofitted structure was 1.14 seconds based on uncracked (gross section) member properties. Table 6.5 shows the fundamental periods for the unretrofitted and retrofitted structures after applying each retrofitting scheme. As seen in Table 6.5, the addition of shear walls and column jacketing reduced the value of the fundamental period. However, the retrofit using confinement with steel plates gave the same fundamental period because the stiffness and mass were not changed in this case.

Table 6.5. Fundamental periods for each retrofit scheme

Model	Uncracked T_1 (s)	Cracked T_1 (s)
Unretrofitted structure	1.14	1.62
Retrofit 1: Addition of shear walls	0.40	0.66
Retrofit 2: Addition of RC column jackets	0.93	1.38
Retrofit 3: Confinement of column plastic hinge zones	1.14	1.62

The results from the ZEUS-NL program were based on the fundamental period only reflecting load effects due to gravity loads. To better understand the dynamic behavior of the structure under lateral loadings, the fundamental period should be calculated after cracking occurs in the structural members. Therefore, an impulse load with magnitude 0.5g was applied to each structure and the resulting fundamental period was determined for the damaged structure. Fundamental periods should be considered carefully because the response of a structure is significantly affected by the spectral acceleration corresponding to the fundamental period of the structure. Fig. 6.10 shows the difference of spectral acceleration values for 2% in 50 years Memphis motions corresponding to the two different fundamental period values determined for the unretrofitted case building structure.

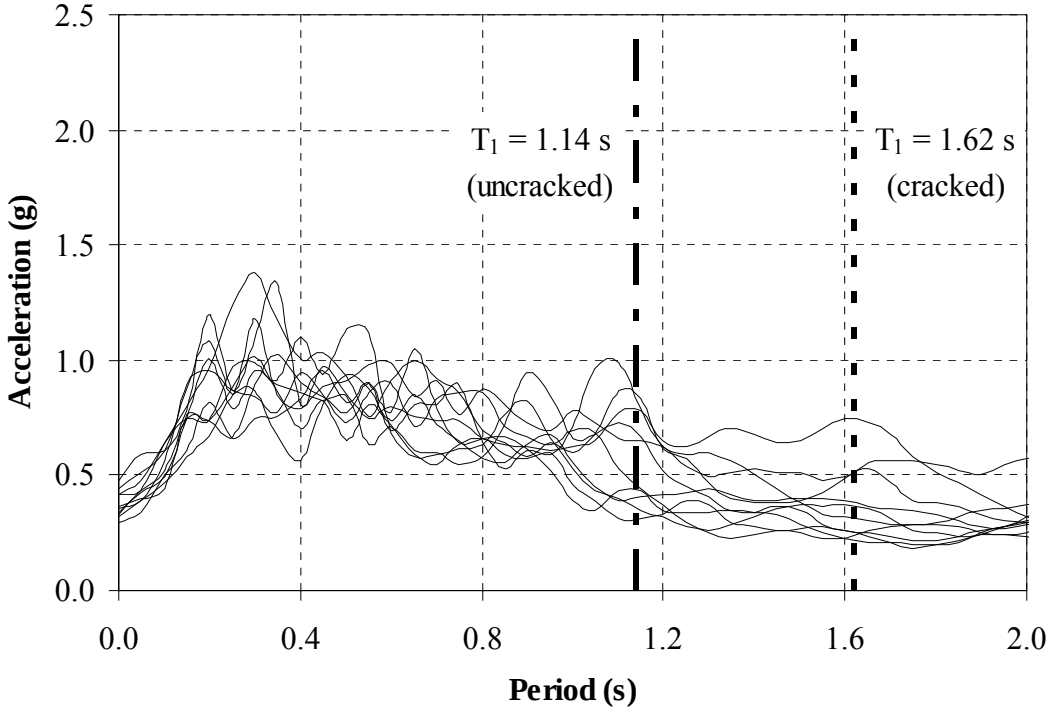

Fig. 6.10. Difference of the spectral acceleration values corresponding to fundamental periods for unretrofitted building (2% in 50 years Memphis motions)

The fundamental periods for the unretrofitted and retrofitted structures after cracking are also shown in Table 6.5. For comparison, the fundamental period computed with cracked section properties using a DRAIN-2DM model was 1.70 seconds for the unretrofitted structure. This is very close to 1.62 seconds computed using the impulse analysis in ZEUS-NL. As seen in Table 6.5, the fundamental periods based on cracked sections are larger than for the uncracked properties. This means that the structure with cracked sections is more flexible and the fundamental periods from the eigenvalue analysis overestimate the stiffness of the structure.

6.4.3 Dynamic Analysis

The dynamic behavior of the retrofitted case study building was investigated using the Memphis synthetic ground motions (Wen and Wu 2000). The results from the nonlinear analyses were compared between before and after applying retrofit techniques

to verify the effectiveness of retrofitting under the dynamic loadings. The results from the nonlinear analyses for three retrofit schemes using Memphis motions are provided in Tables 6.6 to 6.9. Fig. 6.11 provides comparisons of the building drift between the original structure and three retrofitted structures. The ground motions to represent the median demand were selected based on the median maximum building drift for the original structure. The median values of the maximum building drift were calculated based on the natural log of each value, as discussed in Section 5.

Table 6.6. Maximum building drift (%) for retrofitted structure (10% in 50 years Memphis motions)

Ground Motion	Unretrofitted	Retrofit 1	Retrofit 2	Retrofit 3
m10_01s	0.142	0.106	0.234	0.112
m10_02s	0.122	0.158	0.155	0.126
m10_03s	0.164	0.0977	0.150	0.164
m10_04s	0.153	0.189	0.144	0.146
m10_05s	0.129	0.139	0.179	0.124
m10_06s	0.425	0.139	0.333	0.255
m10_07s	0.134	0.166	0.163	0.112
m10_08s	0.155	0.185	0.116	0.152
m10_09s	0.0800	0.156	0.0994	0.0680
m10_10s	0.0950	0.144	0.0930	0.0956
Median	0.144	0.145	0.155	0.128

Table 6.7. Maximum building drift (%) for retrofitted structure (2% in 50 years Memphis motions)

Ground Motion	Unretrofitted	Retrofit 1	Retrofit 2	Retrofit 3
m02_01s	1.99	0.717	1.78	1.88
m02_02s	2.36	0.617	1.74	2.00
m02_03s	1.94	0.663	0.975	1.54
m02_04s	1.92	0.533	1.85	1.74
m02_05s	2.64	0.700	2.60	2.26
m02_06s	2.47	0.712	2.28	2.42
m02_07s	1.99	0.492	1.19	1.58
m02_08s	2.74	0.821	1.59	2.12
m02_09s	1.88	0.770	1.12	1.45
m02_10s	2.31	0.611	1.32	1.81
Median	2.20	0.656	1.57	1.86

Table 6.8. Maximum base shear ratio, V/W (%) for retrofitted structure (10% in 50 years Memphis motions)

Ground Motion	Unretrofitted	Retrofit 1	Retrofit 2	Retrofit 3
m10_01s	4.54	14.0	11.4	4.58
m10_02s	5.29	20.5	5.74	5.28
m10_03s	4.97	14.2	6.85	5.00
m10_04s	4.54	24.8	7.93	4.57
m10_05s	4.99	18.4	8.43	5.00
m10_06s	7.81	29.0	10.6	7.89
m10_07s	4.65	21.8	7.81	4.60
m10_08s	5.97	22.6	6.94	5.95
m10_09s	4.84	18.0	7.16	4.84
m10_10s	4.21	18.9	6.16	4.20
Median	5.10	19.8	7.73	5.11

Table 6.9. Maximum base shear ratio, V/W (%) for retrofitted structure (2% in 50 years Memphis motions)

Ground Motion	Unretrofitted	Retrofit 1	Retrofit 2	Retrofit 3
m02_01s	18.4	54.5	31.7	18.9
m02_02s	19.1	46.9	29.1	19.8
m02_03s	18.8	49.3	24.8	19.6
m02_04s	18.9	43.3	28.4	19.8
m02_05s	18.5	55.3	29.3	19.0
m02_06s	18.2	52.3	32.5	18.8
m02_07s	19.6	52.5	24.6	20.2
m02_08s	17.9	45.6	28.0	18.3
m02_09s	18.7	45.4	24.3	19.2
m02_10s	18.1	49.1	30.2	19.2
Median	18.6	49.3	28.2	19.3

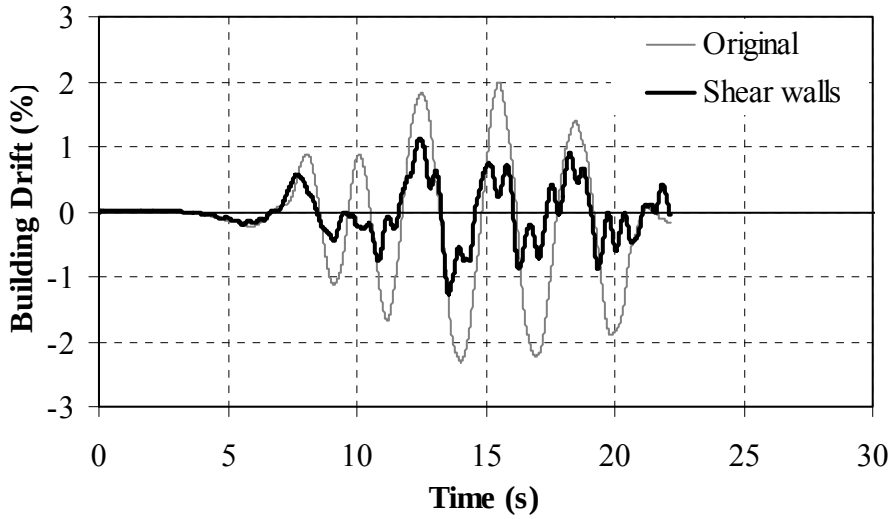

(a) Retrofit 1: Addition of shear walls

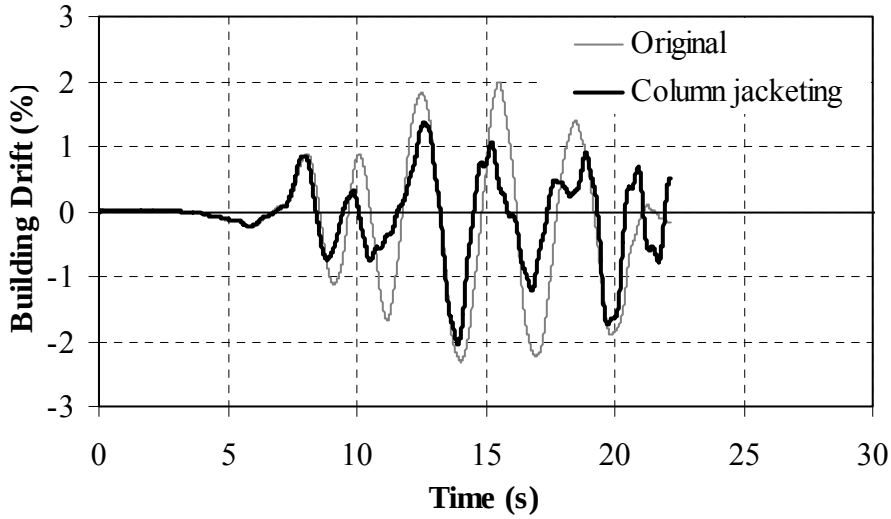

(b) Retrofit 2: Addition of RC column jackets

Fig. 6.11. Comparison of building drifts for the median motion (m02_10s) of 2% in 50 years Memphis data

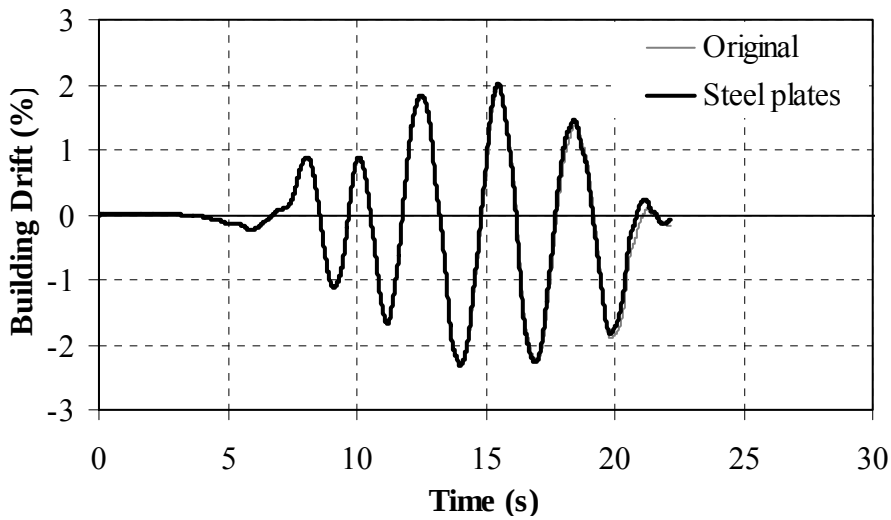

(c) Retrofit 3: Confinement of column plastic hinge zones

Fig. 6.11. Continued

6.5 Seismic Evaluation for Retrofitted Case Study Building

6.5.1 Global-Level Evaluation

For evaluating the retrofitted structure based on the FEMA 356 global-level criteria, the maximum interstory drift values were taken from the nonlinear dynamic analyses. As discussed in Section 5.4.1, the drift limit of concrete frames for CP limit state was limited to 2.9% based on the punching shear failure prediction model. In addition, the drift limit of concrete wall for CP limit state was limited to 1.2% based on structural wall failure in shear. While full collapse is not anticipated following a shear failure in the walls, this was selected as a reasonable drift limit to maintain structural integrity. The value of drift limit for LS limit state was calculated from linear interpolation between two values. Table 6.10 provides the interstory drift limits for three structural performance levels for concrete frame and concrete wall elements suggested by FEMA 356 (ASCE 2000).

Table 6.10. Selected global-level drift limits

	Drift limits (%)		
	IO	LS	CP
Concrete frame	1	2	4 (2.9[1])
Concrete wall	0.5	1 (0.85[2])	2 (1.2[2])

[1] CP limited to 2.9% versus 4% based on punching shear prediction.
[2] LS and CP limited to 0.85% and 1.2% versus 1% and 2% based on shear wall failure in shear.

The BSO was satisfied for the 10% and 2% in 50 years St. Louis motions and for the 10% in 50 years Memphis motions based on the global-level evaluation for the unretrofitted case study building. Therefore, the 2% in 50 years Memphis motions were used to evaluate the retrofitted structure. Figs. 6.12 to 6.14 show the maximum interstory drift profiles for the three retrofitted structures based on the analyses using the 2% in 50 years Memphis motions. The median values for the unretrofitted case are also indicated and compared with the median drifts of the retrofitted structures.

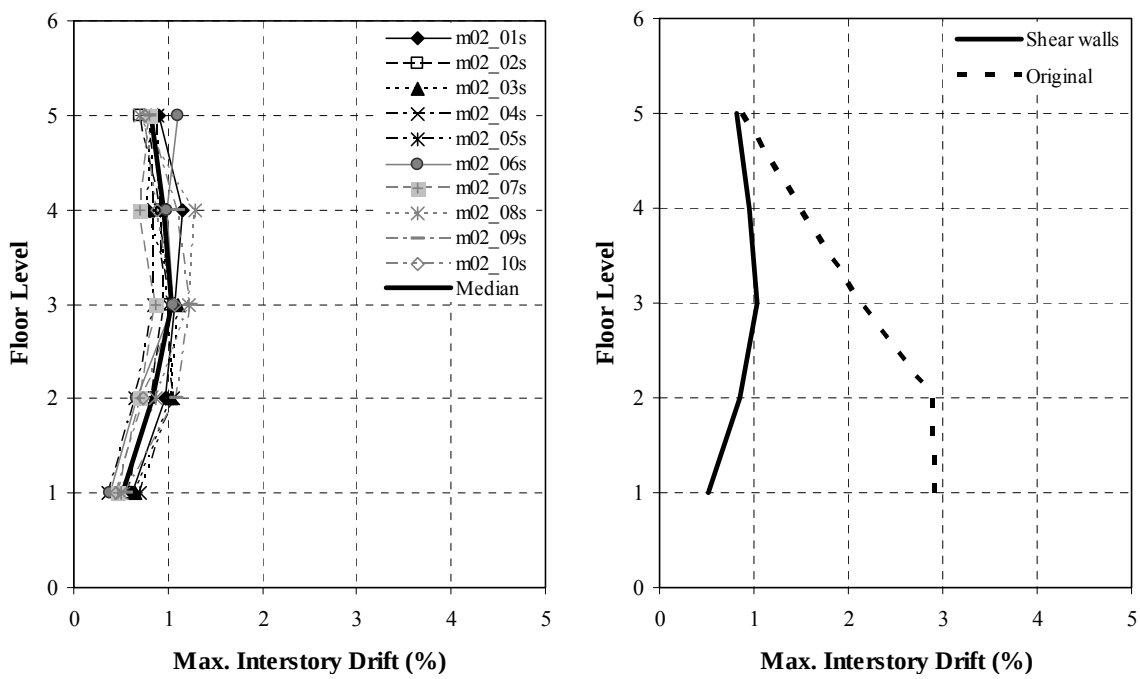

(a) Retrofitted structure (b) Comparison with unretrofitted structure

Fig. 6.12. Maximum interstory drifts for retrofitted structure with shear walls (2% in 50 years Memphis motions)

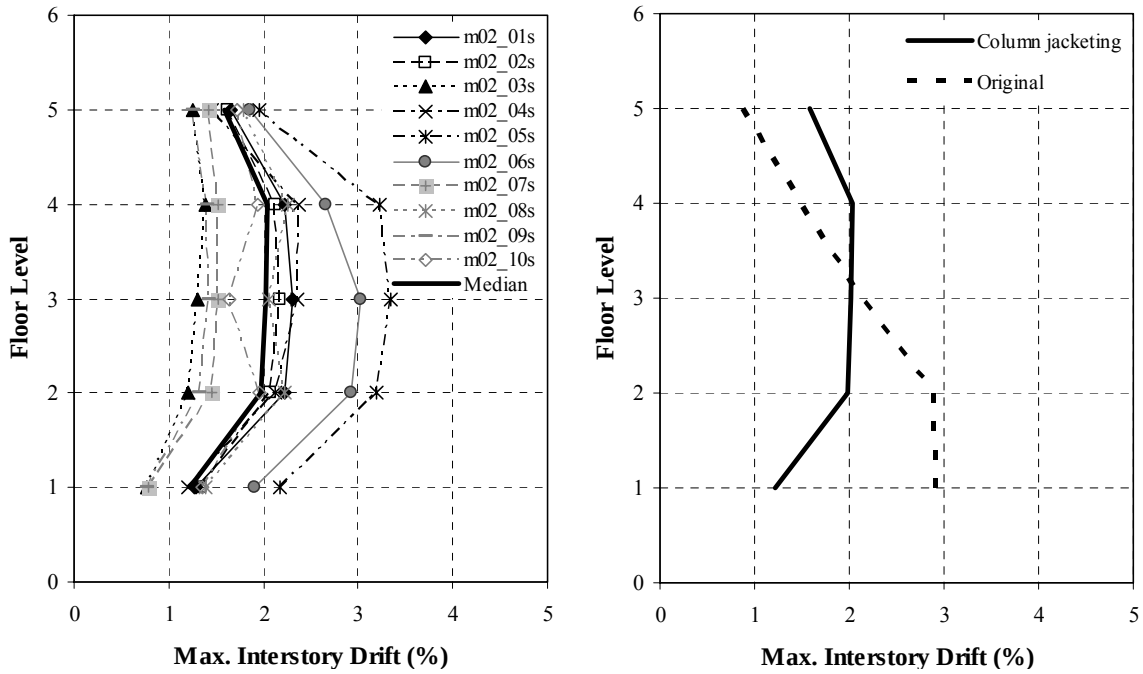

(a) Retrofitted structure (b) Comparison with unretrofitted structure

Fig. 6.13. Maximum interstory drifts for retrofitted structure with RC column jackets (2% in 50 years Memphis motions)

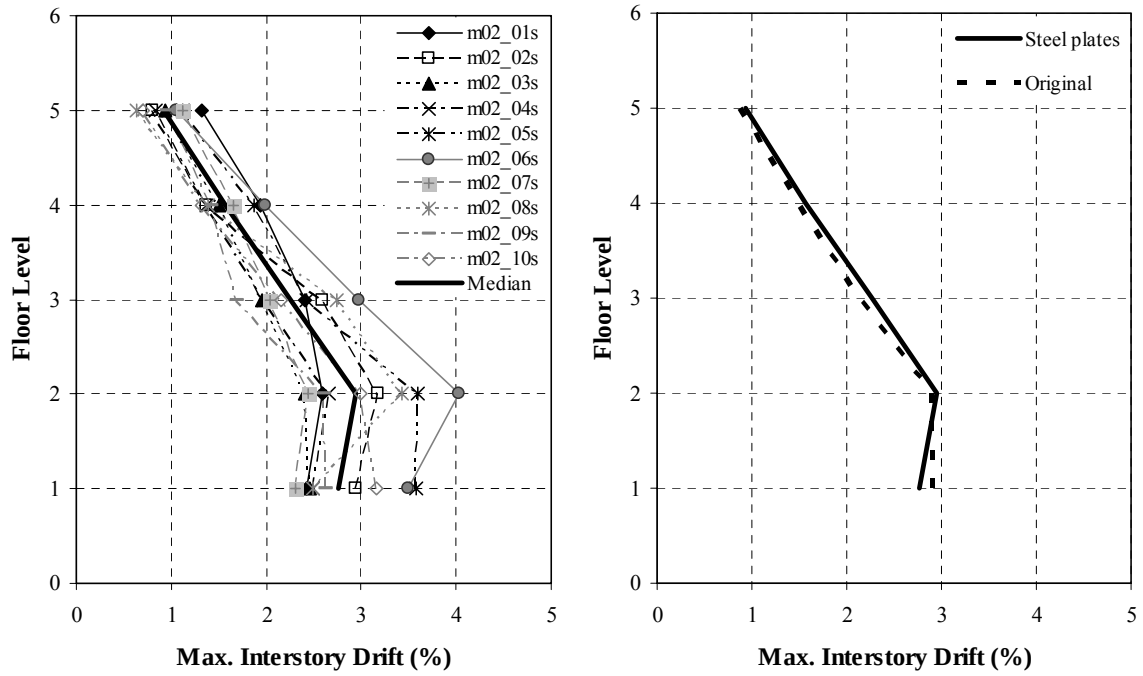

(a) Retrofitted structure (b) Comparison with unretrofitted structure

Fig. 6.14. Maximum interstory drifts for retrofitted structure with plastic hinge zone confinement (2% in 50 years)

For the shear wall retrofit, the performance of the building based on a global-level evaluation showed a significant improvement. As shown in Fig. 6.12, the drifts of the lower stories were substantially reduced. The maximum interstory drifts for the RC column jacketing retrofit shown in Fig. 6.13, were also reduced at the lower stories. However, for the fourth and fifth stories where the retrofit was not applied, the maximum interstory drifts increased slightly. Finally, for the retrofit involving confinement of the column plastic hinge zones, no major change occurred in the median drift profile. As shown in Fig. 6.14b, the overall profiles for the unretrofitted and retrofitted structures have a similar shape. Therefore, the shear wall retrofitted structure and the RC column jacketing retrofitted structure satisfied the BSO (CP performance for a 2% in 50 years event) based on the global-level evaluation. However, the retrofit by confinement of column plastic hinge zones did not satisfy the BSO based on the global-level evaluation.

6.5.2 Member-Level Evaluation

The member-level evaluation was performed for each retrofitted structure. For shear wall retrofitting, the acceptable total drift for the members controlled by shear in FEMA 356, were used (see Table 2.8). The results of the member-level evaluation for each retrofitted structure are shown in Tables 6.11 to 6.13. In these tables, the FEMA 356 criteria are listed vertically in the order of the IO, LS and CP limit states. The maximum values for the median motions are reported and values noted by bold font exceed the FEMA 356 limits for CP performance. For Retrofit 1 case, the member-level the maximum drift of shear wall member was assumed to be the same as the maximum interstory drift at the center of the structure.

Table 6.11. Member-level evaluation for Retrofit 1: Addition of shear walls (2% in 50 years Memphis motions)

Floor level	Median motion	Beams		Columns		Slabs		Shear walls	
		FEMA 356 limits (rad.)	Max. plastic rotation (rad.)	FEMA 356 limits (rad.)	Max. plastic rotation (rad.)	FEMA 356 limits (rad.)	Max. plastic rotation (rad.)	FEMA 356 limits (Acceptable total drift, %)	Max. drift (%)
1	m02_09s	0.00500	0.00184	0.00481	0.00219	0.00550	0	0.4	0.544
		0.0100		0.0147		0.00825		0.6	
		0.0100		0.0195		0.0110		0.75	
2	m02_08s	0.00500	0.00432	0.00506	0.00433	0.00550	0	0.4	**0.865**
		0.0100		0.0150		0.00825		0.6	
		0.0100		0.0200		0.0110		0.75	
3	m02_06s	0.00500	0.00421	0.00531	0.00415	0.00550	0	0.4	**1.05**
		0.0100		0.0153		0.00825		0.6	
		0.0153		0.0204		0.0110		0.75	
4	m02_06s	0.00500	0.00415	0.00522	0.00420	0.00550	0	0.4	**0.982**
		0.0100		0.0153		0.00825		0.6	
		0.0161		0.0206		0.0110		0.75	
5	m02_05s	0.00500	0.00288	0.00500	0.00185	0.000500	0	0.4	**0.890**
		0.0100		0.0150		0.000750		0.6	
		0.0157		0.0200		0.00100		0.75	

Table 6.12. Member-level evaluation for Retrofit 2: Addition of RC column jackets (2% in 50 years Memphis motions)

Floor level	Median motion	Beams		Columns		Slabs	
		FEMA 356 limits (rad.)	Max. plastic rotation (rad.)	FEMA 356 limits (rad.)	Max. plastic rotation (rad.)	FEMA 356 limits (rad.)	Max. plastic rotation (rad.)
1	m02_01s	0.00500	**0.0124**	0.00485	0.0193	0.00550	**0.0149**
		0.0100		0.0148		0.00830	
		0.0100		0.0196		0.0110	
2	m02_02s	0.00500	**0.0111**	0.00496	0.0155	0.00550	0.0102
		0.0100		0.0149		0.00830	
		0.0100		0.0199		0.0110	
3	m02_08s	0.00500	0.0102	0.005	0.0149	0.00550	0.00768
		0.0100		0.015		0.00830	
		0.0153		0.02		0.0110	
4	m02_02s	0.00500	0.0131	0.005	0.0124	0.00550	0
		0.0100		0.015		0.00830	
		0.0161		0.02		0.0110	
5	m02_02s	0.00500	0.00557	0.005	0.00729	0.000500	0
		0.0100		0.015		0.000800	
		0.0157		0.02		0.00100	

Table 6.13. Member-level evaluation for Retrofit 3: Confinement of column plastic hinge zones (2% in 50 years Memphis motions)

Floor level	Median motion	Beams		Columns		Slabs	
		FEMA 356 limits (rad.)	Max. plastic rotation (rad.)	FEMA 356 limits (rad.)	Max. plastic rotation (rad.)	FEMA 356 limits (rad.)	Max. plastic rotation (rad.)
1	m02_09s	0.00500	**0.0194**	0.00445	**0.0264**	0.00550	**0.0179**
		0.0100		0.0142		0.00830	
		0.0100		0.0186		0.0110	
2	m02_10s	0.00500	**0.0179**	0.00469	**0.0233**	0.00550	**0.0137**
		0.0100		0.0145		0.00830	
		0.0100		0.0192		0.0110	
3	m02_10s	0.00500	0.0127	0.00487	0.0182	0.00550	0.00768
		0.0100		0.0148		0.00830	
		0.0153		0.0197		0.0110	
4	m02_03s	0.00500	0.00614	0.00500	0.0113	0.00550	0
		0.0100		0.0150		0.00830	
		0.0161		0.0200		0.0110	
5	m02_03s	0.00500	0	0.00500	0.00468	0.000500	0
		0.0100		0.0150		0.000800	
		0.0157		0.0200		0.00100	

For all the retrofit schemes, member-level evaluations did not completely meet the suggested FEMA BSO of CP for the 2% in 50 years event. However, the evaluation shows that the retrofits improve the seismic performance. Retrofitting resulted in a reduction of plastic rotations, or increase of member capacity. For instance, the plastic rotations for Retrofit 3 are very similar to the unretrofitted structure. However, the columns at the third and fourth stories are within the FEMA limit due to an increase in column ductility. Consequently, the overall seismic performance was enhanced.

Fig. 6.15 shows the locations of inelastic behavior in the unretrofitted structure and retrofitted structure where the plastic rotations exceed the limits for CP performance level under the median ground motion for the 2% in 50 years Memphis event. Locations where the rotations exceeded the FEMA 356 member-level criteria for each limit state are shown with black circles. Although the retrofits did not meet the FEMA 356 criteria for all members, these figures demonstrate the relative improvement after applying each retrofit technique. The figure for Retrofit 1 is not shown because the maximum plastic rotations did not exceed the CP limits based on the FEMA 356 member-level criteria. However, it should be noted that for Retrofit 1 the maximum interstory drifts, except those for the first story, exceeded the acceptable total drift limits for the CP limit state based on the FEMA 356 member-level criteria.

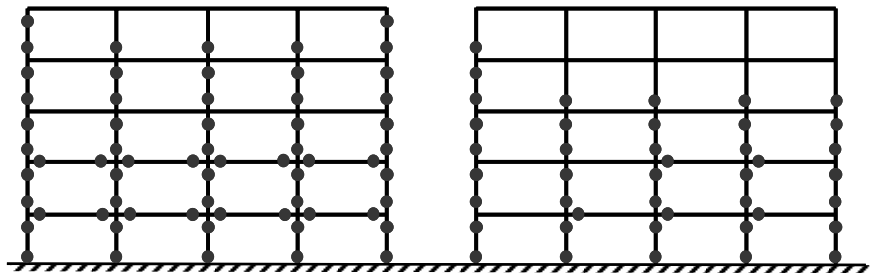

(a) Unretrofitted structure

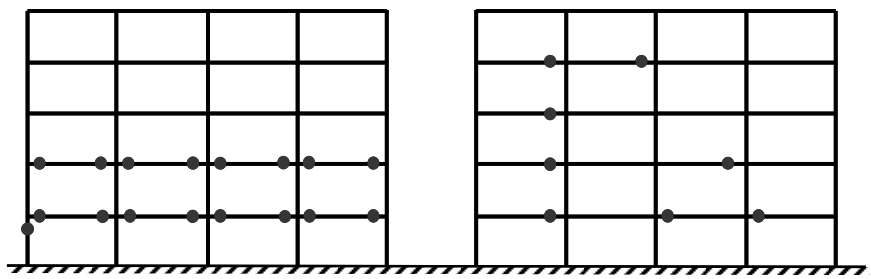

(b) Retrofit 2: Addition of RC column jackets

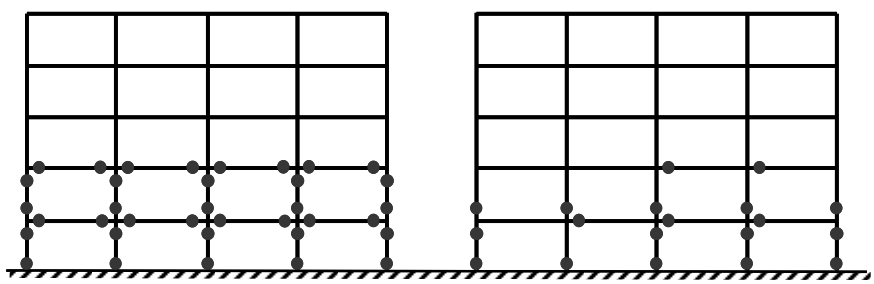

(c) Retrofit 3: Confinement of column plastic hinge zones

● = Exceedance of plastic rotation limit

Fig. 6.15. Locations in unretrofitted and retrofitted building where CP plastic rotation limits are exceeded (2% in 50 years Memphis event)

6.6 Fragility Curves for Retrofitted Case Study Building

6.6.1 Global-Level Limits

To compare the enhancement of seismic performance of the structure, probabilistic fragility curves were also developed for the retrofitted structures and

compared to those for the unretrofitted structure. As discussed in Section 5, spectral acceleration values from each ground motion record were used to develop the relationship between demand and structural response (drift), and fragility curves were developed using Eq. 5.1. Fig. 6.16 shows the fitted power law equations for each retrofitted structure reflecting the maximum interstory drift and spectral acceleration for the twenty synthetic Memphis motions. The spectral acceleration (S_a) for a given ground motion record is the value corresponding to the fundamental period of a particular structure based on cracked section properties and 5 percent damping.

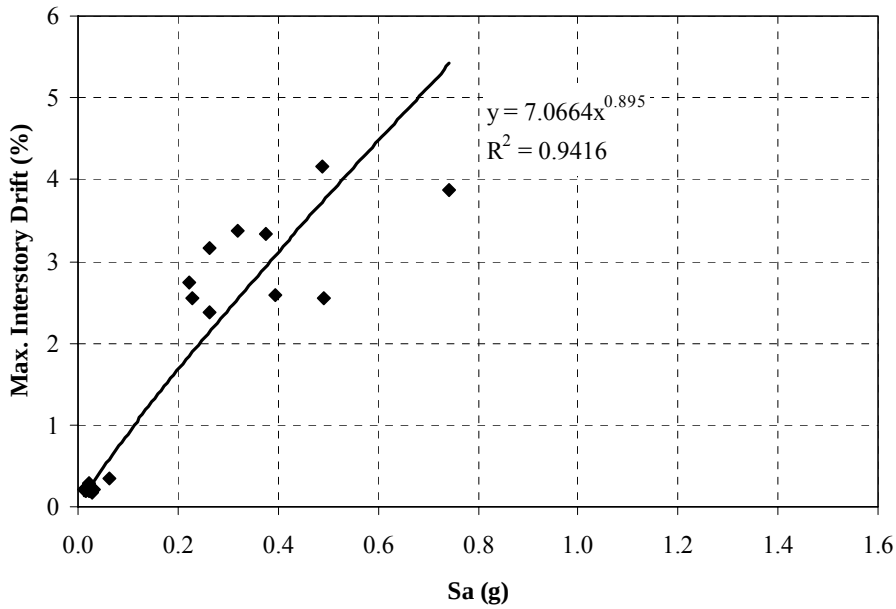

(a) Unretrofitted structure

Fig. 6.16. Development of power law equation for demand drift

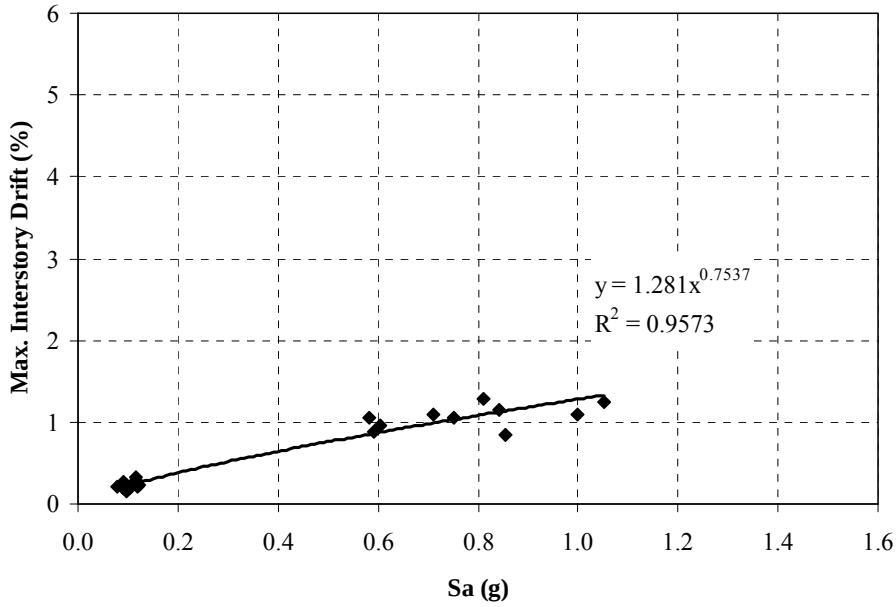

(b) Retrofit 1: Addition of shear walls

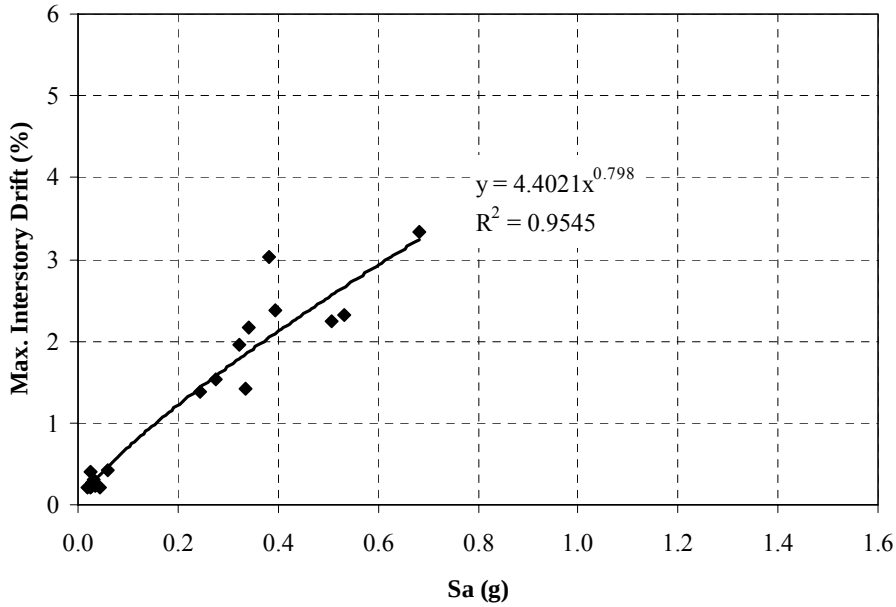

(c) Retrofit 2: Addition of RC column jackets

Fig. 6.16. Continued

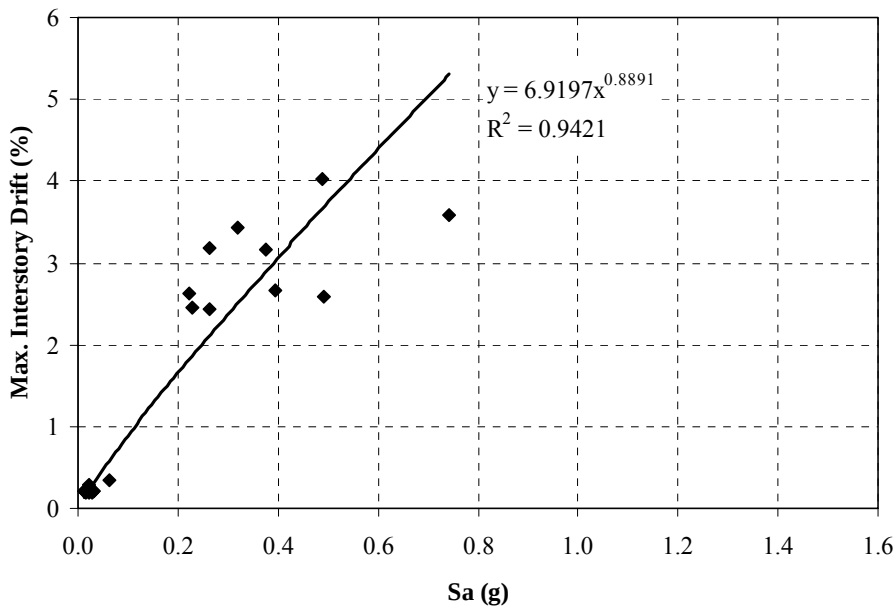

(d) Retrofit 3: Confinement of column plastic hinge zones

Fig. 6.16. Continued

Table 6.14 provides the parameters for Eq. 5.4 used in developing the global-level fragility curves for the retrofitted structures

Table 6.14. Parameters for developing the global-level fragility curves for retrofit

Model	Parameter	Value
Retrofit 1: Addition of shear walls	s^2	0.0294
	$\beta_{D\|S_a}$	0.170
	β_{CL}	0.3
	β_M	0.3
Retrofit 2: Addition of RC column jackets	s^2	0.0574
	$\beta_{D\|S_a}$	0.236
	β_{CL}	0.3
	β_M	0.3
Retrofit 3: Confinement of column plastic hinge zones	s^2	0.111
	$\beta_{D\|S_a}$	0.325
	β_{CL}	0.3
	β_M	0.3

The fragility curves developed for the three retrofitted structures are provided in Fig. 6.17. For comparison, the fragility curves for the unretrofitted structure are represented on each graph with gray lines. Based on the global drift limits of FEMA 356, the IO, LS and CP performance levels are defined differently for concrete wall elements; with drift limits of 0.5, 1 and 2 percent, respectively. However, as discussed in Section 6.5.1, shear wall failure in shear was included as an upper bound for the CP limit state of shear wall retrofitted structure. Therefore, adjusted drift limits of 0.5, 0.85 and 1.2 percent were used for the IO, LS and CP limit state, respectively, to define drift capacity for the shear wall retrofit fragility curves.

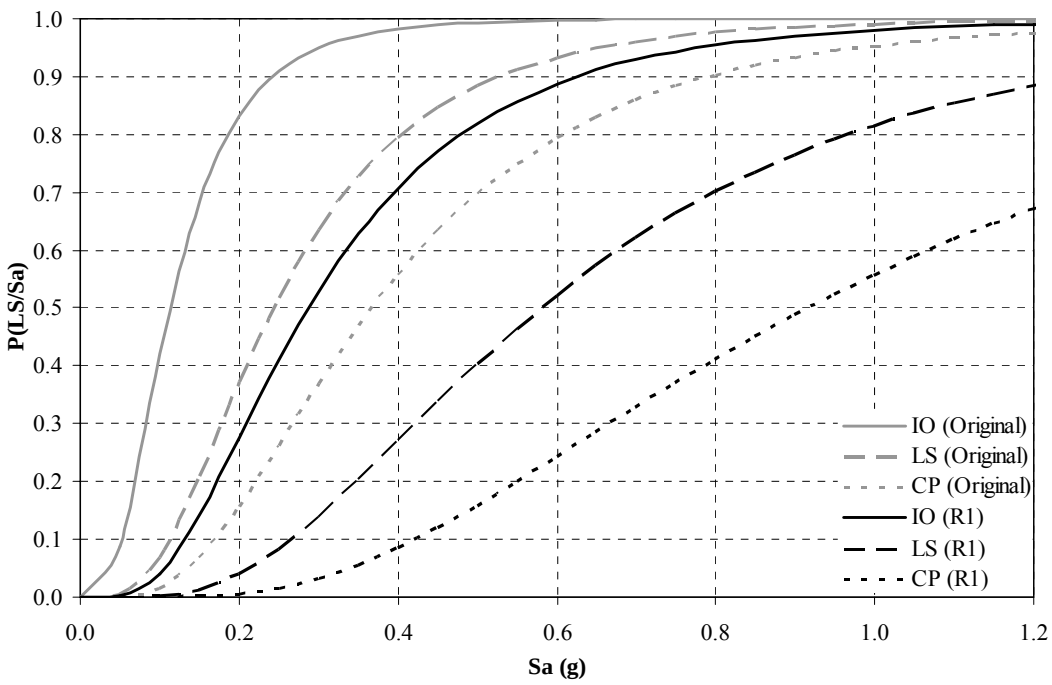

(a) Retrofit 1: Addition of shear walls

Fig. 6.17. Global-level fragility curves for the retrofitted structure

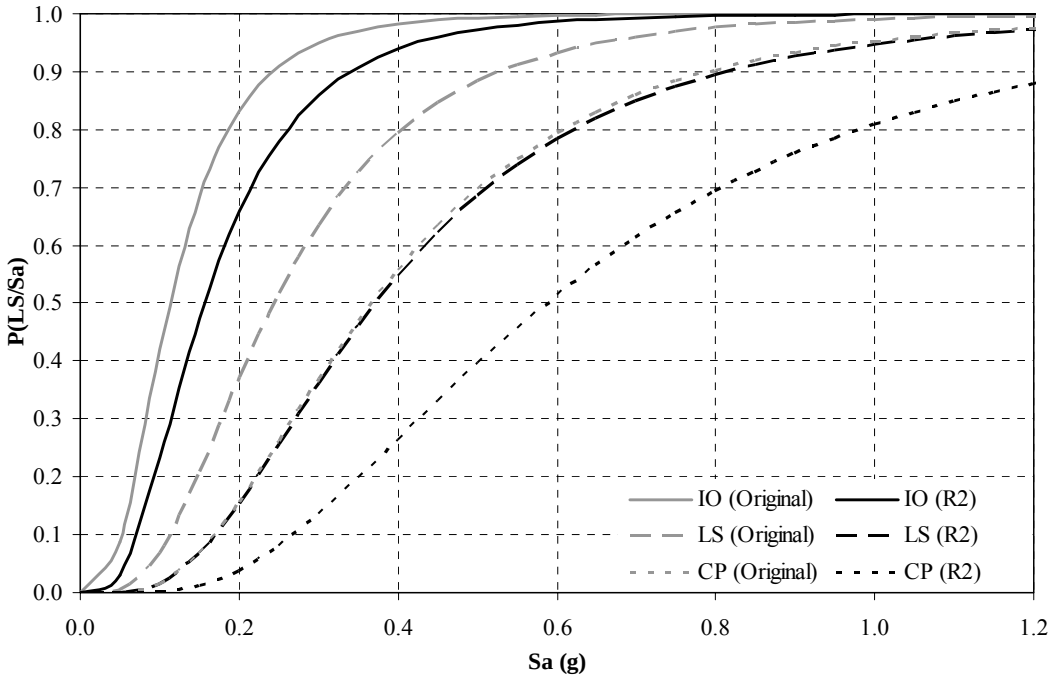

(b) Retrofit 2: Addition of RC column jackets

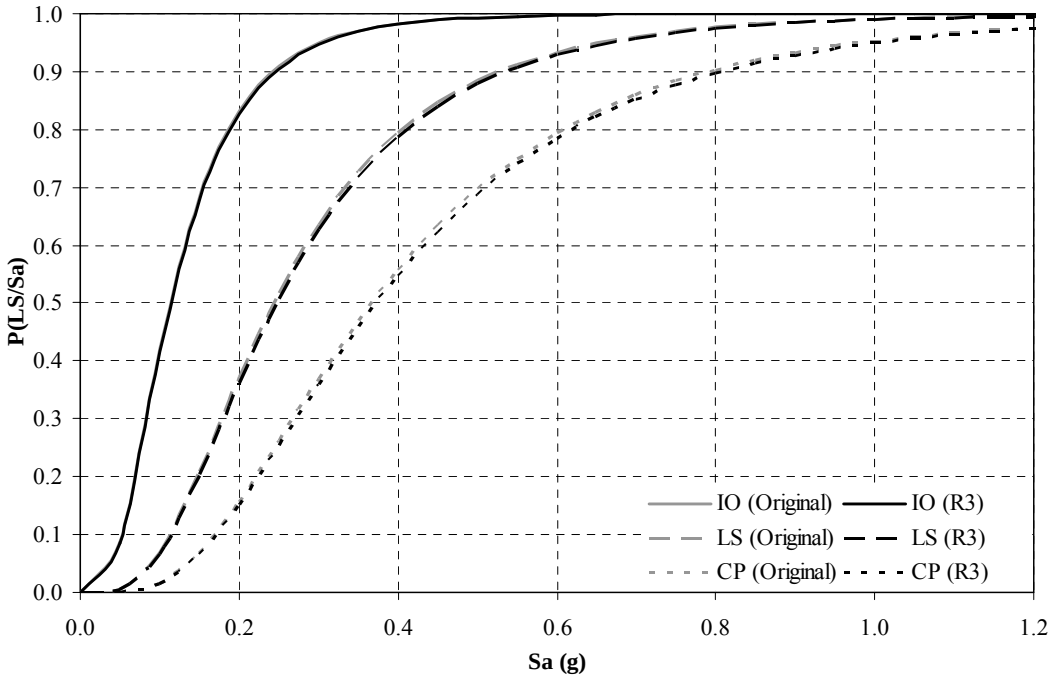

(c) Retrofit 3: Confinement of column plastic hinge zones

Fig. 6.17. Continued

As shown in Figs. 6.17a and 6.17b, the addition of shear walls and RC column jackets were effective in decreasing the probability of exceeding each limit state. However, for the case of confining the plastic hinge zones (Retrofit 3), the fragility curves for each limit state are the same as those for the unretrofitted structure. This is because there is no distinction in the global-level capacity drift limits suggested in FEMA 356 and used for the unretrofitted and Retrofit 3 structures. In addition, the demand drifts are nearly the same because the added confinement of Retrofit 3 does not modify the global structural response. Fig. 6.18 shows the fragility curves for each limit state. As shown in Fig. 6.18, the probabilities of exceeding each limit state for the addition of shear walls and RC column jackets were reduced while those for the confinement of column plastic hinge zones were the same as for the unretrofitted structure.

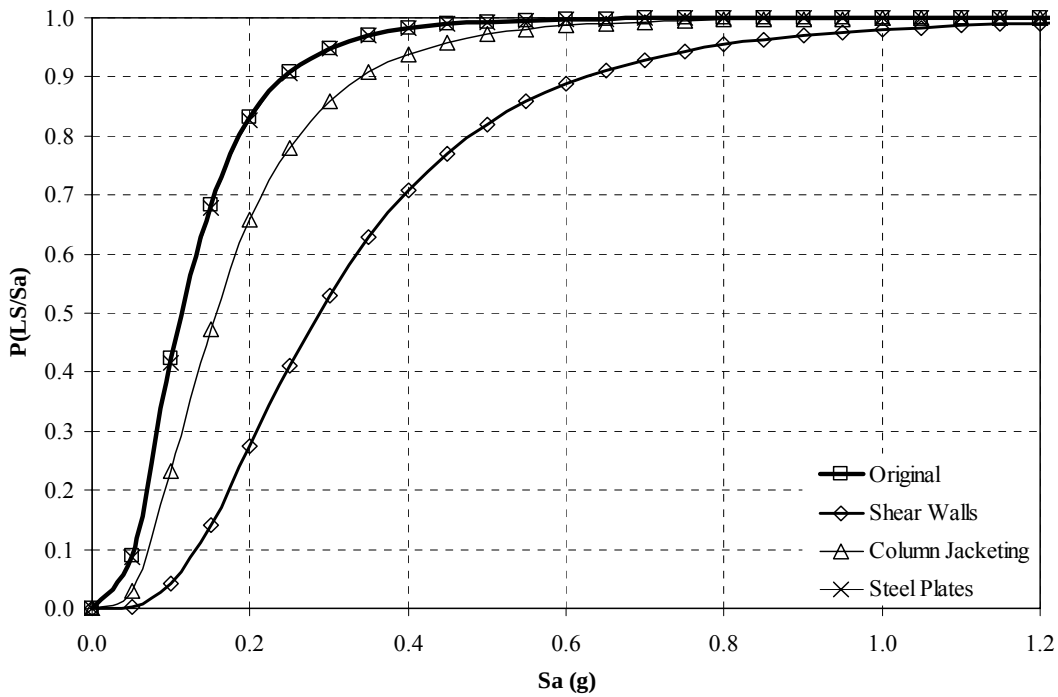

(a) IO Limit State

Fig. 6.18. Comparisons of global-level fragility curves for each limit state

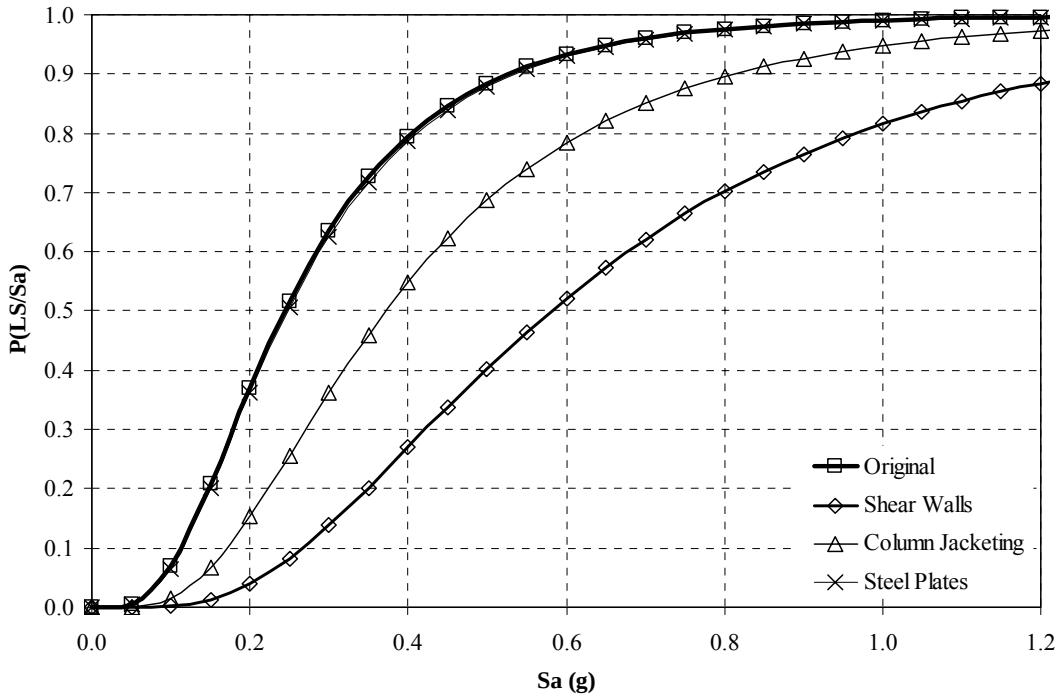

(b) LS Limit State

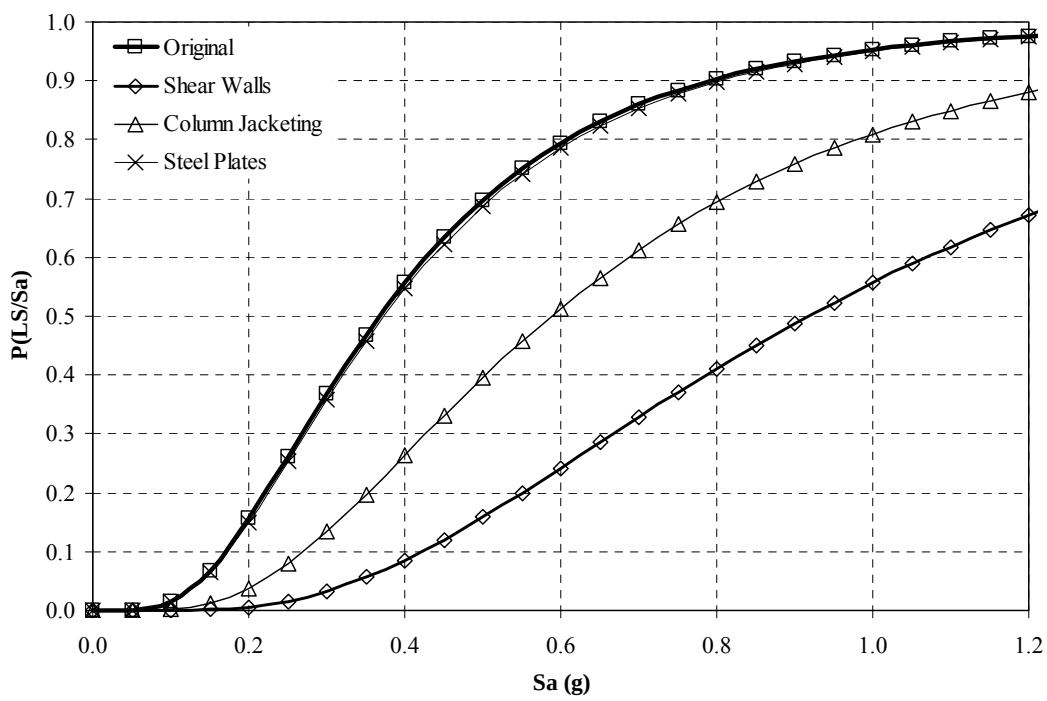

(c) CP Limit State

Fig. 6.18. Continued

It should be noted that the spectral acceleration of concern can vary when the structure is retrofitted and so a direct comparison for a specific spectral acceleration may not be appropriate. For comparison, the fragility curves for the CP limit state are provided using peak ground acceleration (PGA) on the horizontal axis in Fig. 6.19. The same ground motions were used to develop the fragility curves based on PGA. As shown in Fig. 6.19, the probabilities of exceeding CP limit state for the RC column jackets were reduced while those for the confinement of column plastic hinge zones were the same as for the unretrofitted structure. For the addition of shear walls, the probabilities of exceeding CP limit state were reduced for the peak ground acceleration values above 0.25g.

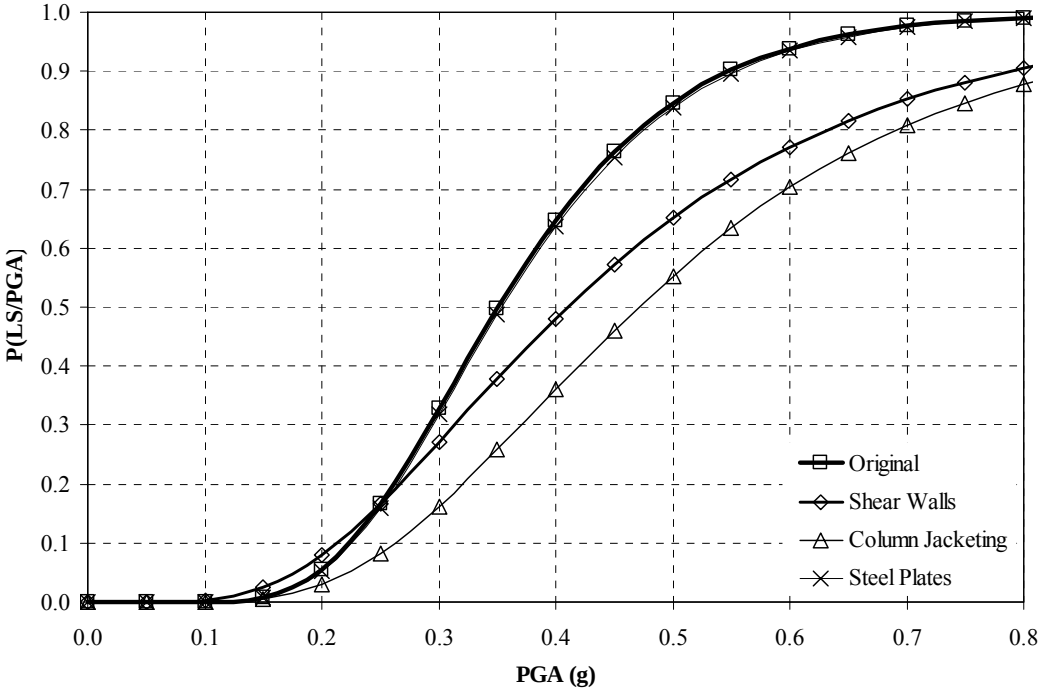

Fig. 6.19. Comparisons of global-level fragility curves for CP limit state using PGA

6.6.2 Member-Level Limits

As discussed in Section 5, member-level fragility curves were developed based on drift capacities determined from a regular push-over analysis with an inverted triangular load pattern and a critical response push-over analysis.

First, drift limits corresponding to member-level limits for each the retrofitted structure were determined using a regular push-over analysis. The inverted triangular load pattern was used for these analyses (see Fig. 6.8). The push-over analysis method to determine the critical response, suggested by Dooley and Bracci (2001), was also performed for the retrofitted structures. The drift limits corresponding to the first occurrence of the FEMA 356 member-level limits are summarized in Table 6.15. The FEMA 356 global limits along with adjusted values used in this study are provided for comparison. For the shear wall retrofitted structure, the interstory drift limits corresponding to the plastic rotation limits were greater than the acceptable total drifts from the FEMA 356 member-level criteria for shear wall members in Table 2.8. Therefore, drift limit values of 0.4, 0.6 and 0.75 percent were used for the IO, LS and CP, respectively.

Table 6.15. Interstory drift (%) limits based on FEMA 356 member-level criteria

Structure	FEMA 356 Global			Regular push-over			Critical response push-over		
	IO	LS	CP	IO	LS	CP	IO	LS	CP
Unretrofitted	1	2	2.9[1]	0.88	0.88	1.07	0.62	0.62	0.69
Retrofit 1	0.5	0.85[2]	1.2[2]	0.4[3]	0.6[3]	0.75[3]	0.4[3]	0.6[3]	0.75[3]
Retrofit 2	1	2	2.9[1]	0.96	1.29	1.29	0.88	1.37	1.37
Retrofit 3	1	2	2.9[1]	1.07	1.74	1.89	0.83	1.46	1.81

[1] Drift limits for CP limited to 2.9% versus 4% based on punching shear prediction.
[2] Drift limits for LS and CP limited to 0.85% and 1.2% versus 1% and 2% based on shear wall failure in shear.
[3] Drift limits governed by the FEMA 356 member-level criteria for shear wall members in Table 2.8.

As shown in Table 6.15, the drift limit of IO limit state using a regular push-over for Retrofit 3 is larger than the FEMA 356 global drift limits for the IO limit state. However, the drift limit of IO limit state for Retrofit 1 and 2, and the drift limits of LS and CP limit states for all retrofit cases are less than the FEMA global drift limits. Figs. 6.20 to 6.22 show the fragility curves based on these criteria for each retrofitted structure. For comparison, the fragility curves using the global drift limits are represented on each graph with gray lines.

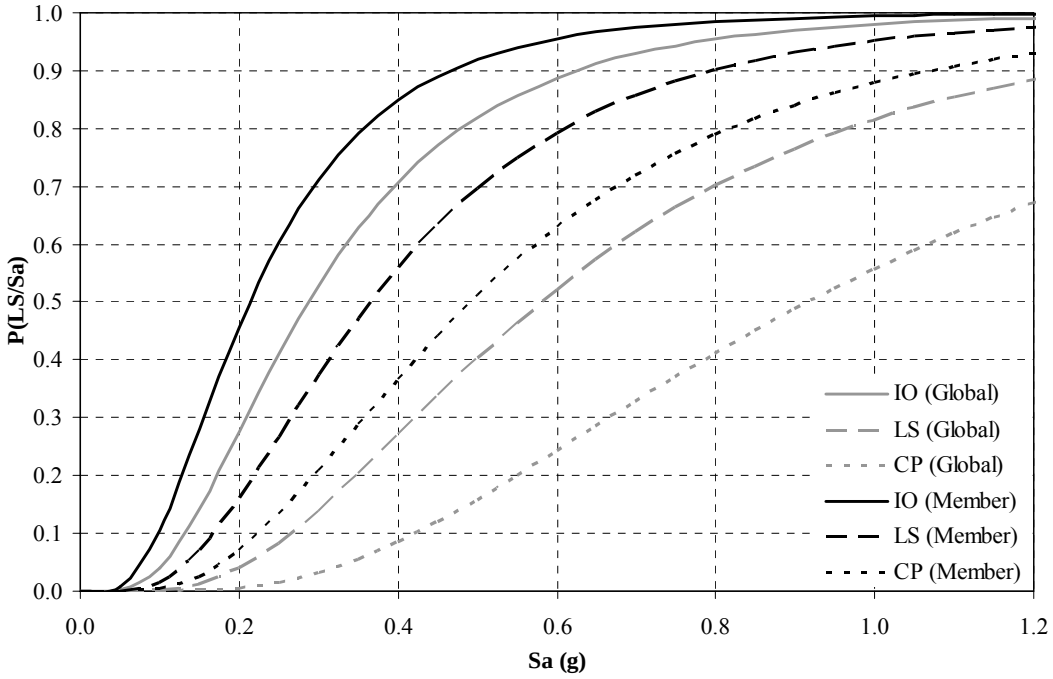

(a) Regular push-over analysis

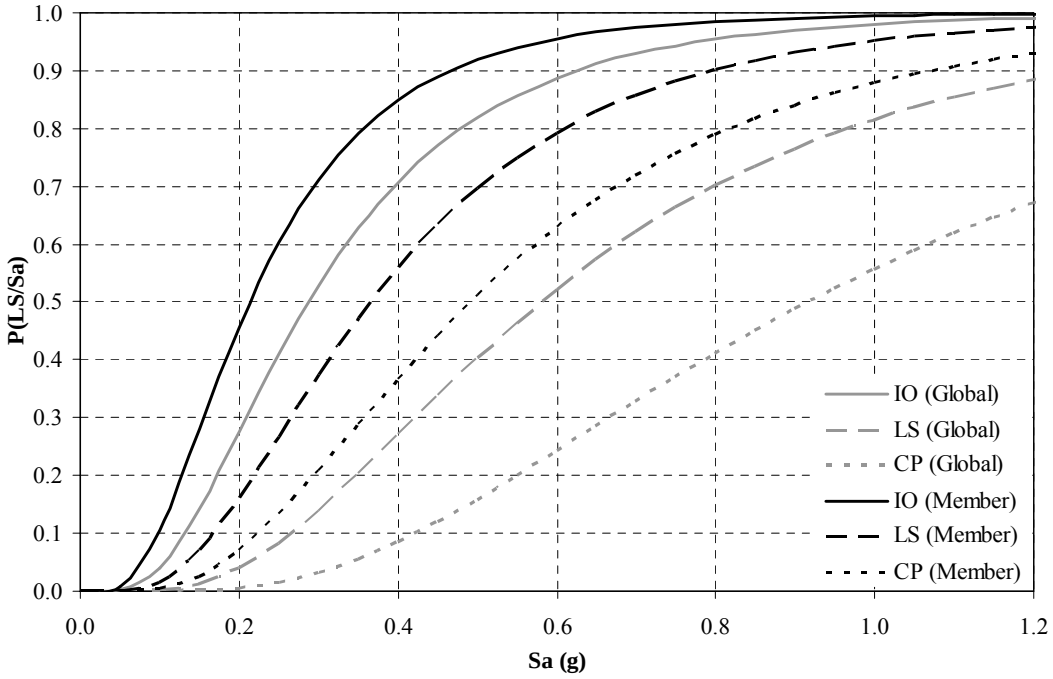

(b) Critical response push-over analysis

Fig. 6.20. Fragility curves for Retrofit 1 based on FEMA 356 member-level limits

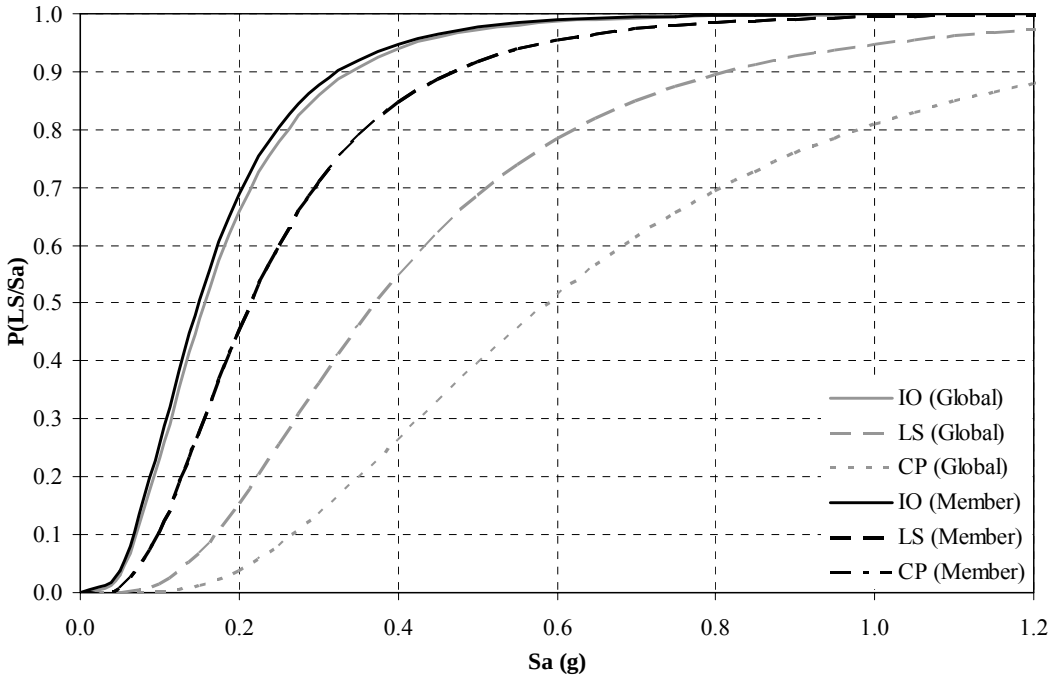

(a) Regular push-over analysis

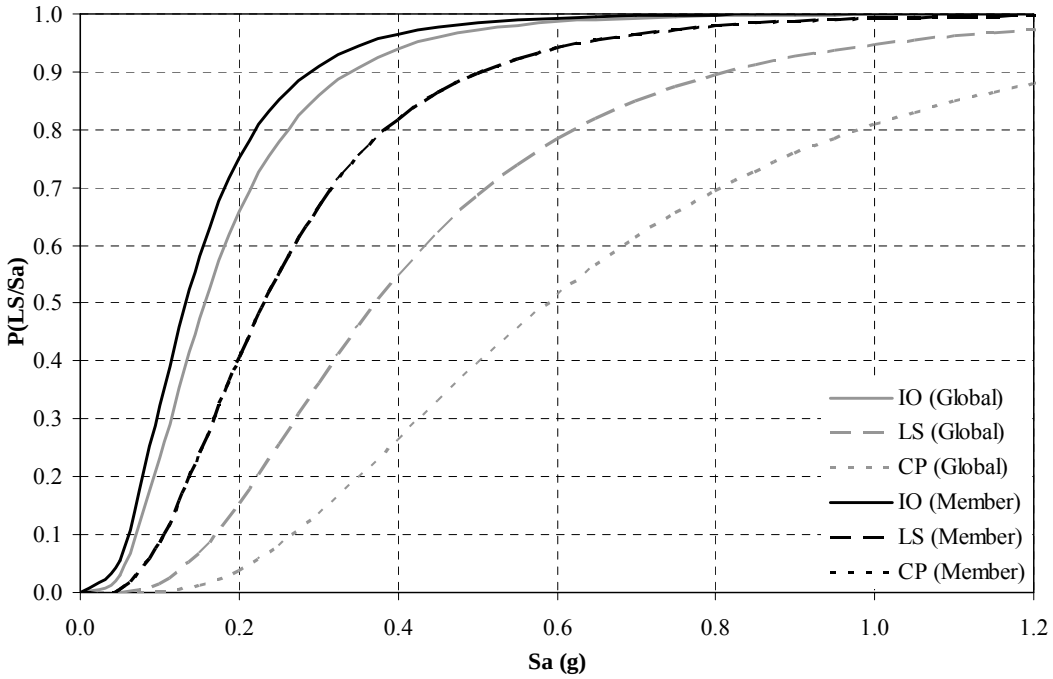

(b) Critical response push-over analysis

Fig. 6.21. Fragility curves for Retrofit 2 based on FEMA 356 member-level limits

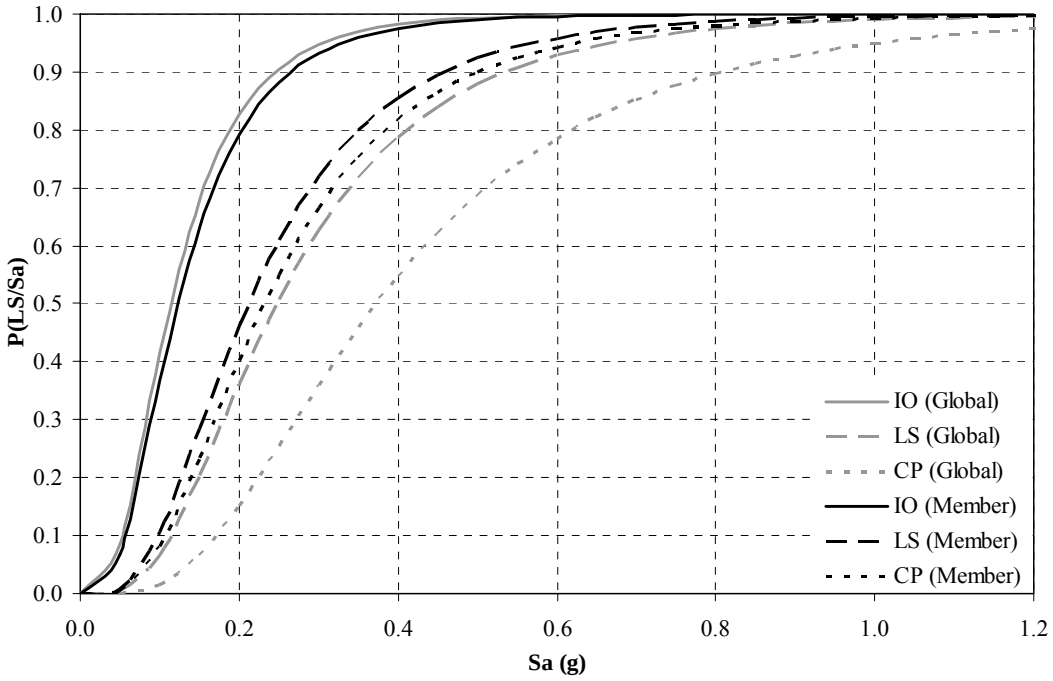

(a) Regular push-over analysis

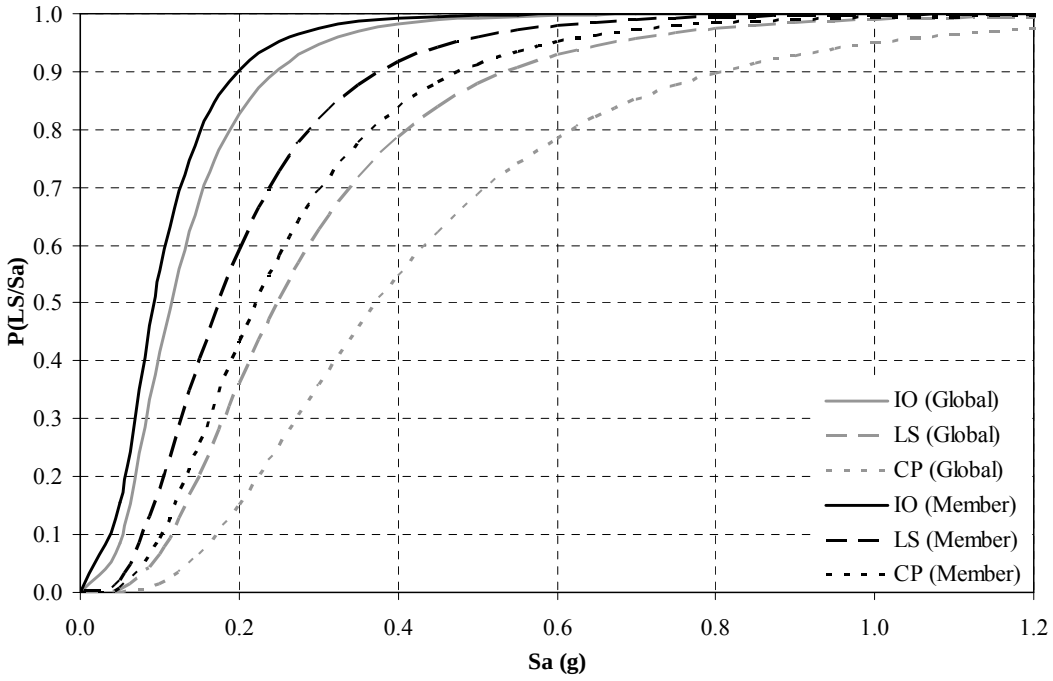

(b) Critical response push-over analysis

Fig. 6.22. Fragility curves for Retrofit 3 based on FEMA 356 member-level limits

Table 6.16 summarizes the probabilities of exceeding the CP limit state corresponding to a range of PGA values for the FEMA 356 member-level criteria developed using critical response push-over analysis. As shown, the probabilities of exceeding the CP limit state were significantly reduced by each of the retrofits for the lower PGA values. This reduction is less pronounced for PGA values above 0.5g for all retrofits. In particular, for the PGA's up to 0.2g, Retrofit 3 has the greatest impact in reducing the probability of exceeding the CP limit state, and the shear wall retrofit (Retrofit 1) has the greatest impact for PGA's above 0.3g.

Table 6.16. Probability of exceeding CP limit state based on limits from a critical response push-over analysis

Structure	Peak Ground Acceleration (PGA), g								
	0.0	0.1	0.2	0.3	0.4	0.5	0.6	0.7	0.8
Unretrofitted	0.0	0.163	0.843	0.985	0.999	1.0	1.0	1.0	1.0
Retrofit 1	0.0	0.038	0.338	0.647	0.826	0.915	0.958	0.979	0.989
Retrofit 2	0.0	0.019	0.292	0.634	0.835	0.928	0.969	0.986	0.994
Retrofit 3	0.0	0.003	0.218	0.647	0.885	0.967	0.991	0.997	0.999

Fig. 6.23 shows the fragility curves based on peak ground acceleration for each limit state for the FEMA 356 member-level criteria developed using critical response push-over analysis. As shown in Fig. 6.23, the probabilities of exceeding the IO limit state for Retrofit 1 are slightly greater than those for the unretrofitted structure for a PGA up to 0.15g. This is because the fundamental period of the structure retrofitted by shear walls is much smaller than that of unretrofitted structure so that the corresponding spectral acceleration values become large. For other retrofit cases, the probabilities of exceeding each limit state were reduced to varying degrees depending on the retrofit techniques, limit state and magnitude of the PGA.

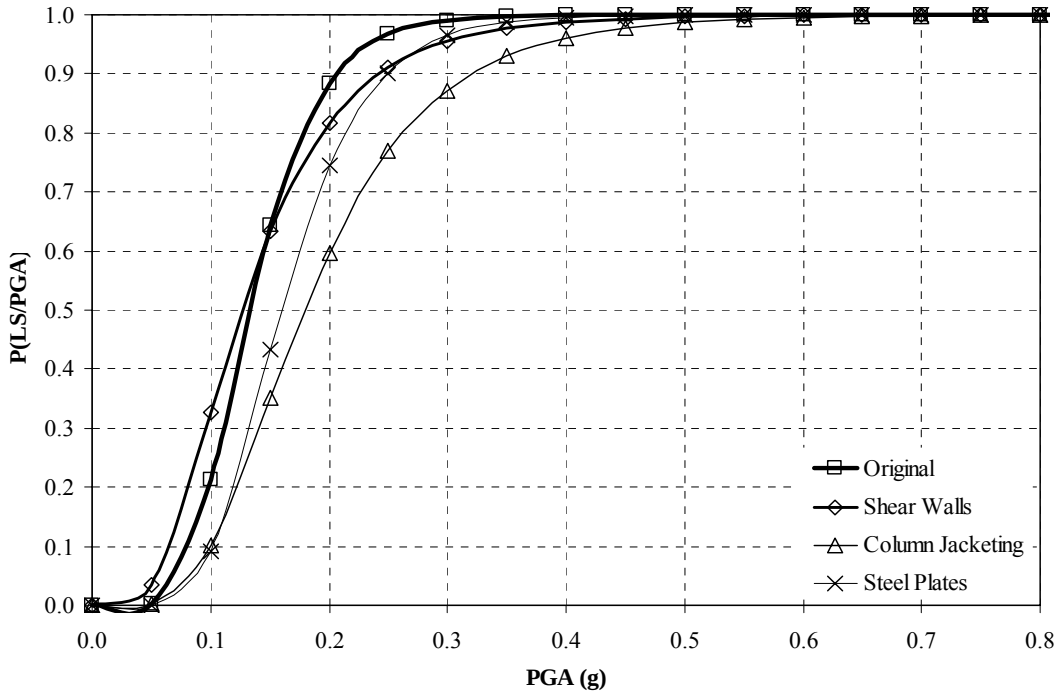

(a) IO Limit State

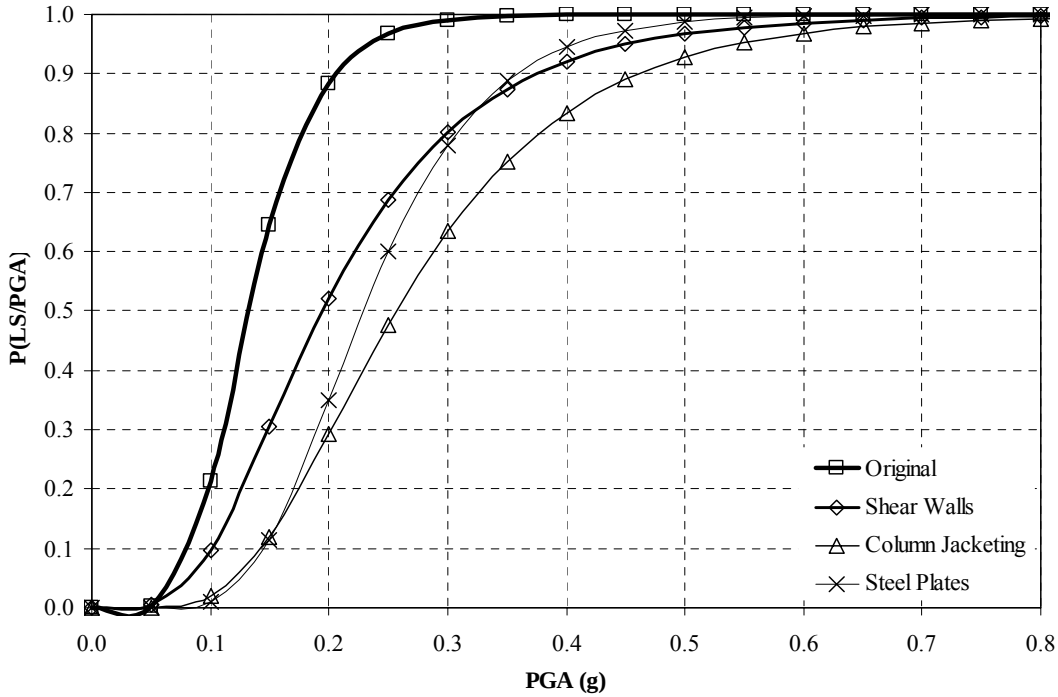

(b) LS Limit State

Fig. 6.23. Comparisons of FEMA 356 member-level fragility curves

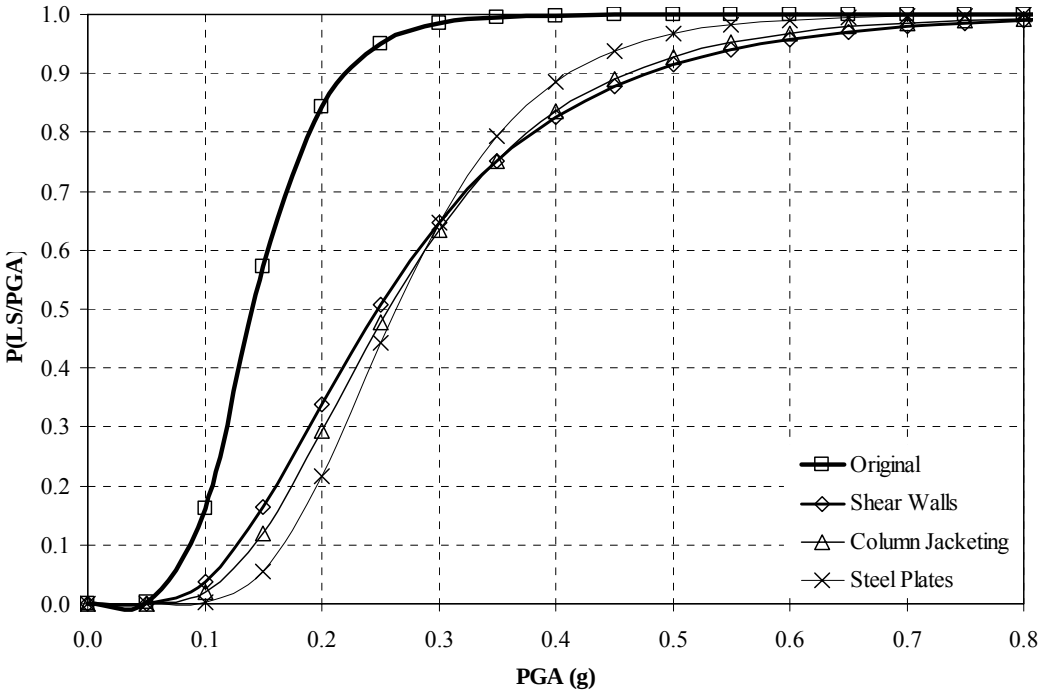

(c) CP Limit State

Fig. 6.23. Continued

6.6.3 Additional Quantitative Limits

The drift limits based on the quantitative limits described in Section 5.5.4 are provided in Table 6.17 for each retrofitted structure. For the case of the addition of shear walls, the PMI drift limit was limited to the value corresponding to shear wall failure in shear.

Table 6.17. Interstory drift (%) limits based on additional quantitative limits

Structure	Regular push-over			Critical response push-over		
	FY	PMI	SD	FY	PMI	SD
Unretrofitted	0.66	0.81	–	0.36	0.66	2.81
Retrofit 1	0.91	1.2*	–	0.74	1.2*	–
Retrofit 2	0.53	1.58	–	0.53	1.23	–
Retrofit 3	0.78	1.01	–	0.55	0.79	–

* PMI limited to 1.2% based on shear wall failure in shear.

Because the first and second story of the unretrofitted structure were most vulnerable, drift limits were determined for those stories. For the retrofitted structure, the seismic capacity of the lower stories was increased. Therefore, the drift limits for a critical story mechanism were increased due to the applied retrofit techniques. In this case, SD limit state was not detected because strength did not fall to 20% of the maximum strength. Figs. 6.24 to 6.26 show the push-over curves of the weak story and the corresponding drift limits based on the member-level criteria and additional quantitative limits for each retrofitted structure. For the shear wall retrofitted structure, the push-over curves after shear failure are shown with dotted lines.

Figs. 6.27 to 6.29 show the fragility curves for the FY and PMI limit states determined from both the regular and critical response push-over analyses. For comparison, the fragility curves using the global drift limits for each case are also shown with gray lines.

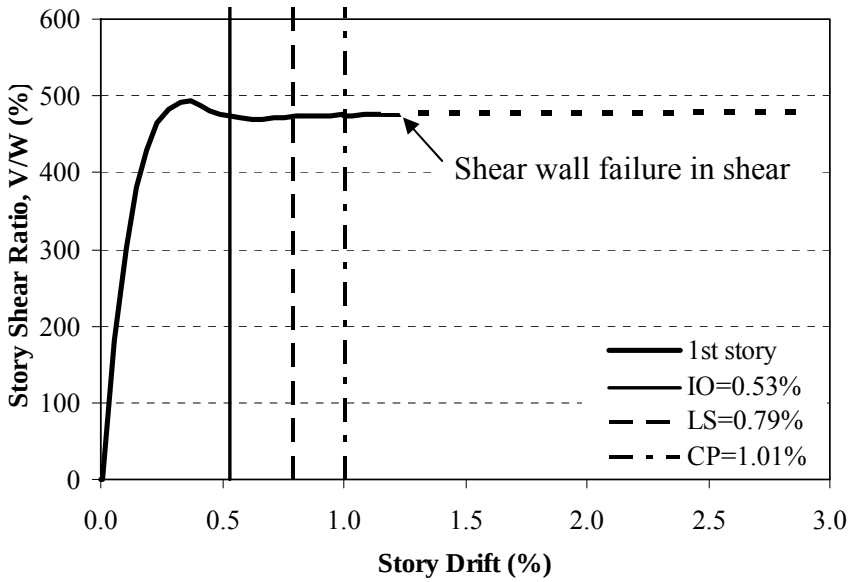

(a) FEMA 356 limits based on member-level criteria (1st story)

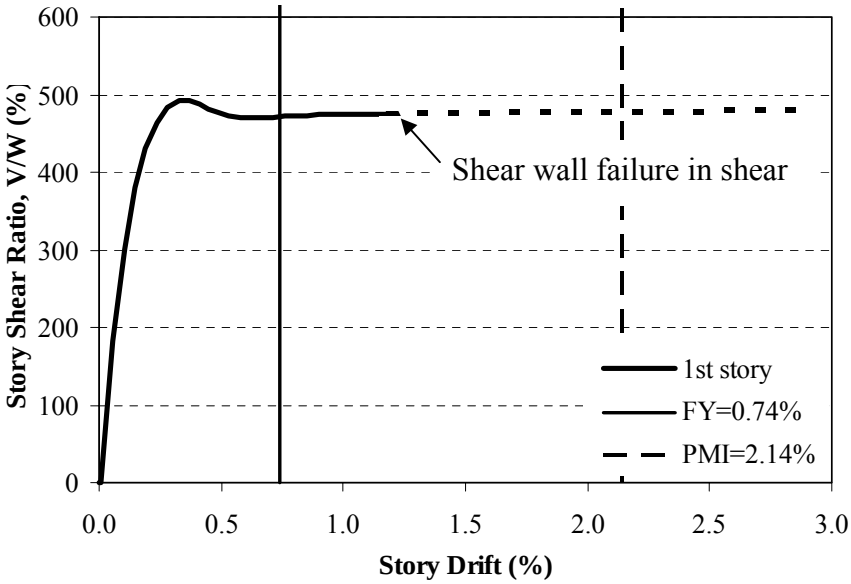

(b) Drift limits for quantitative limit states (1st story)

Fig. 6.24. Push-over curve for Retrofit 1 with critical response push-over analysis

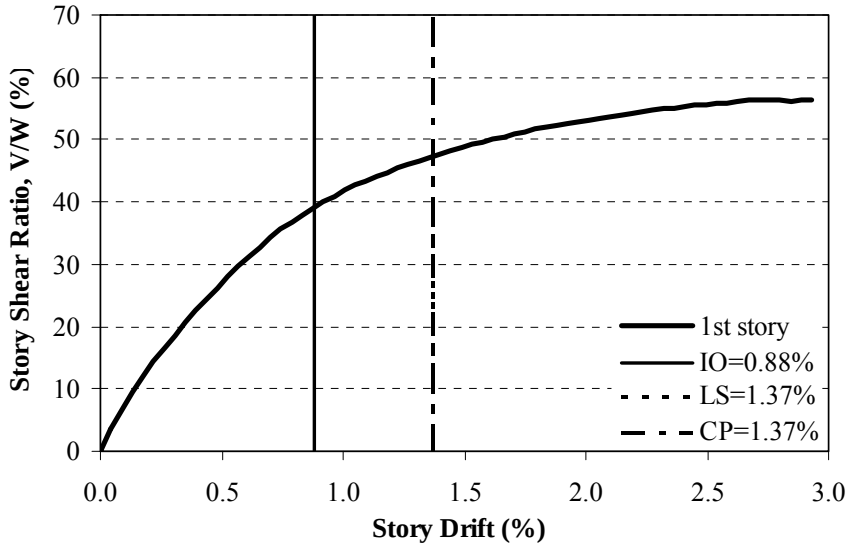

(a) FEMA 356 limits based on member-level criteria (1st story)

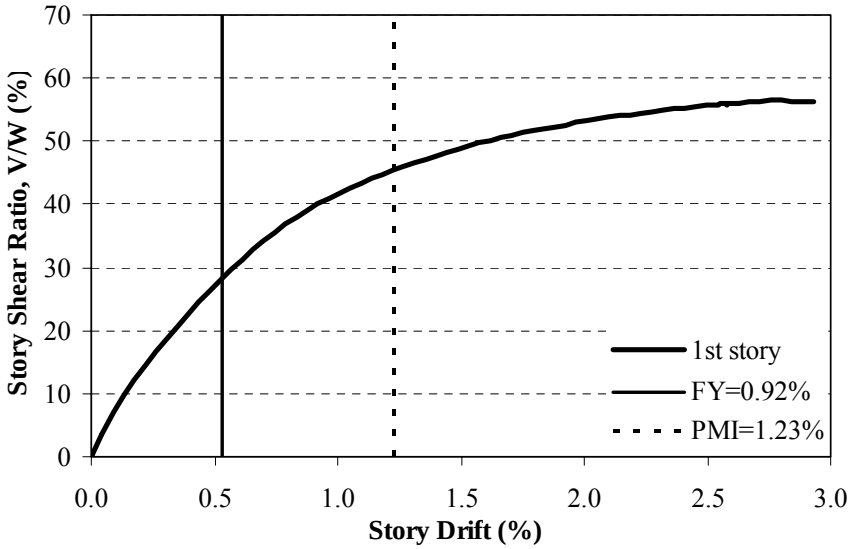

(b) Drift limits for quantitative limit states (1st story)

Fig. 6.25. Push-over curve for Retrofit 2 with critical response push-over analysis

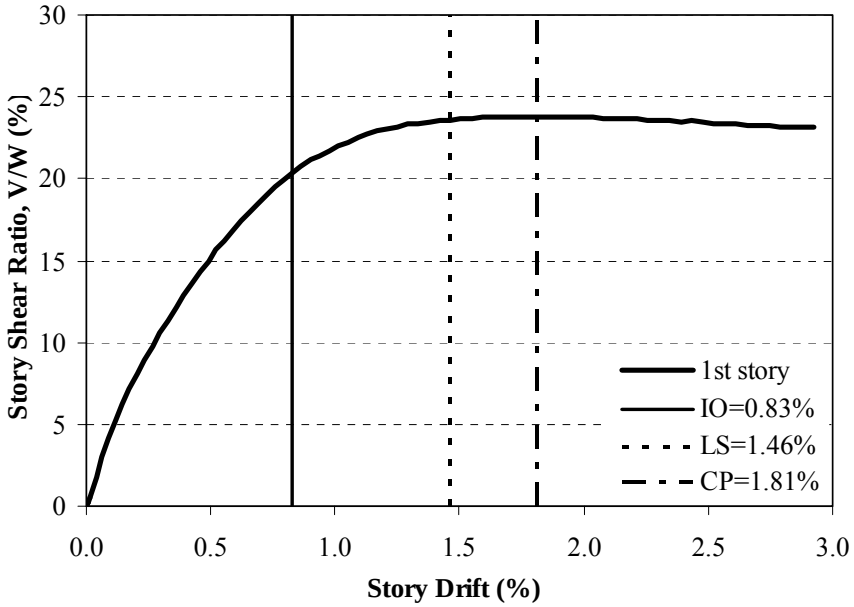

(a) FEMA 356 limits based on member-level criteria (1st story)

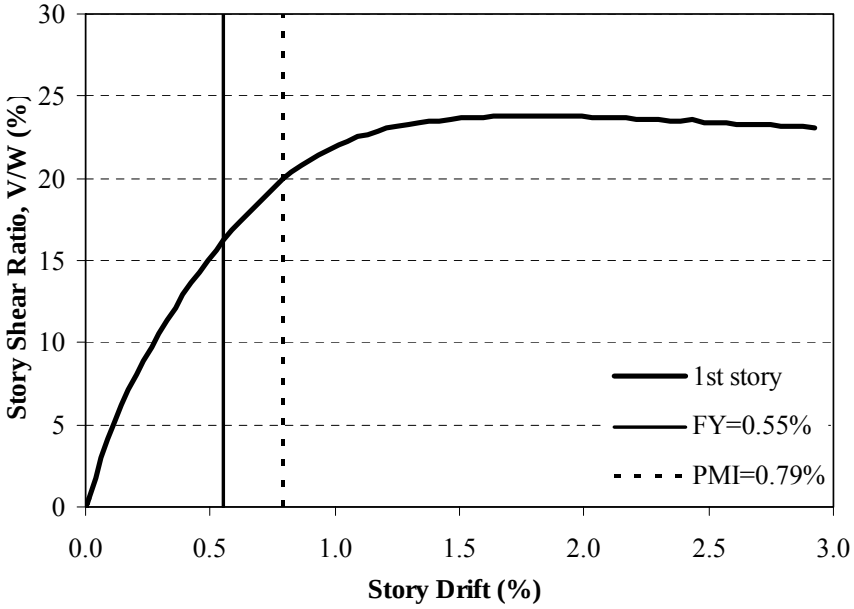

(b) Drift limits for quantitative limit states (1st story)

Fig. 6.26. Push-over curve for Retrofit 3 with critical response push-over analysis

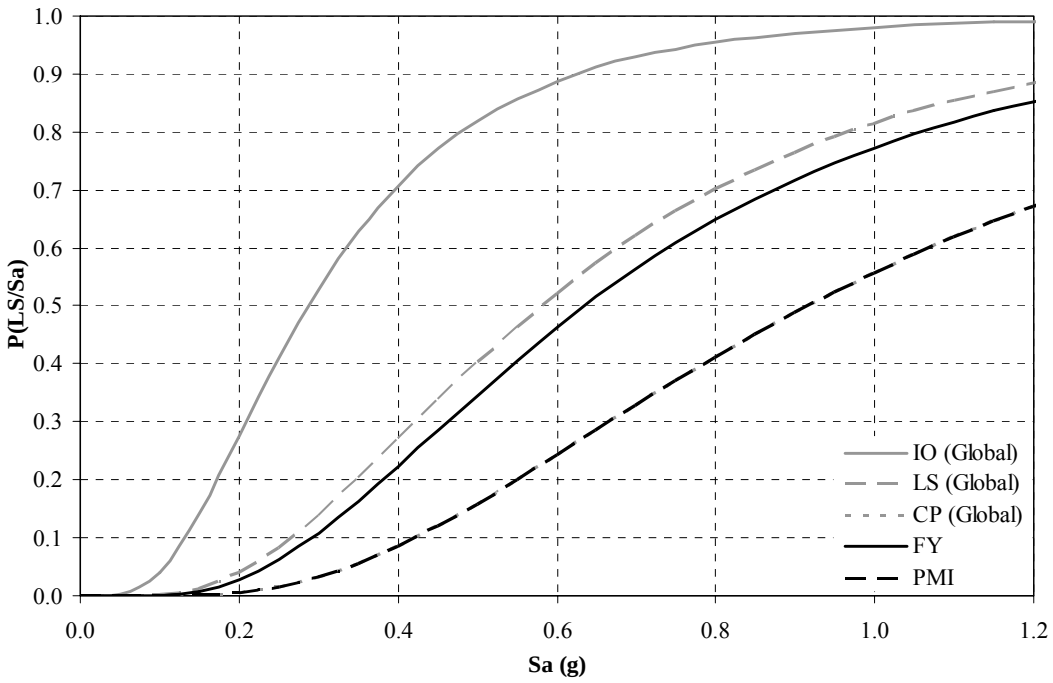

(a) Regular push-over analysis

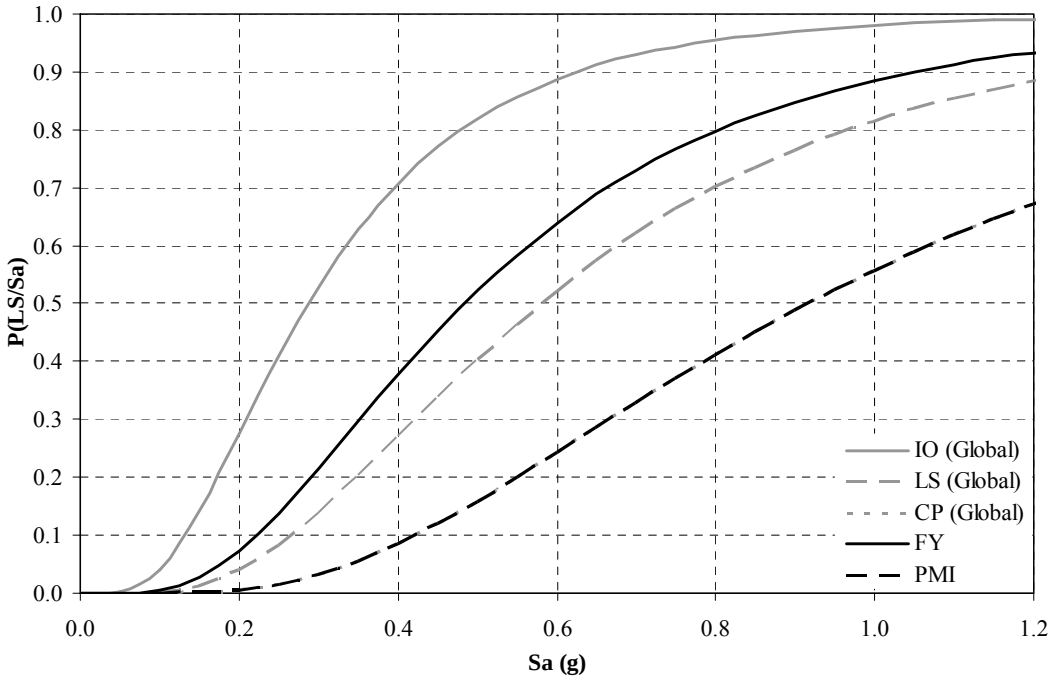

(b) Critical response push-over analysis

Fig. 6.27. Fragility curves for Retrofit 1 based on additional quantitative limits

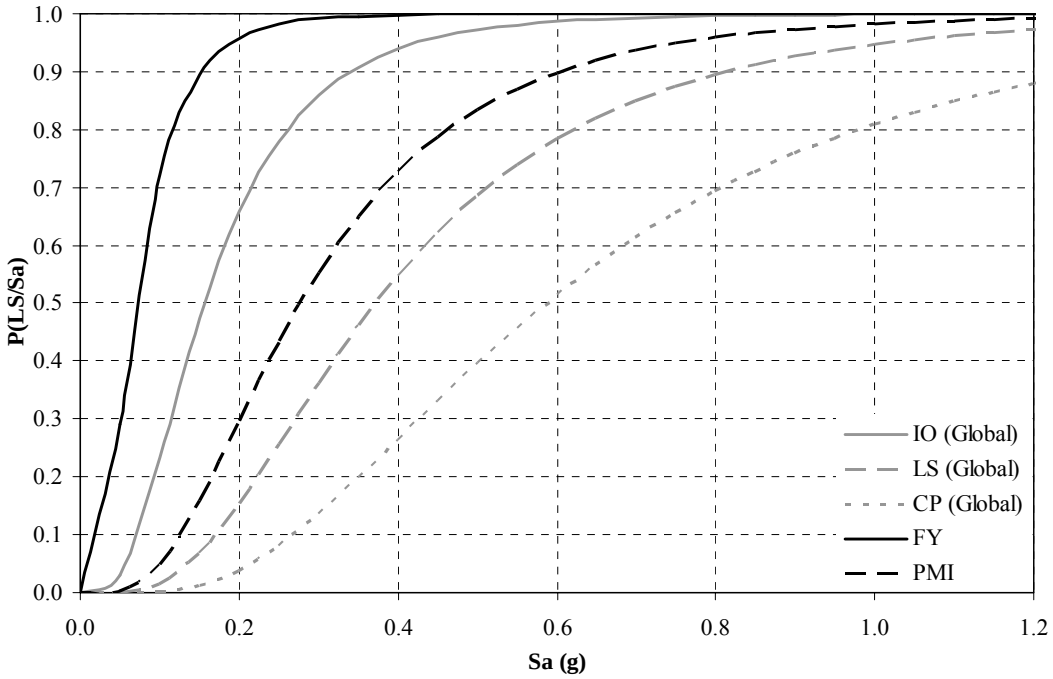

(a) Regular push-over analysis

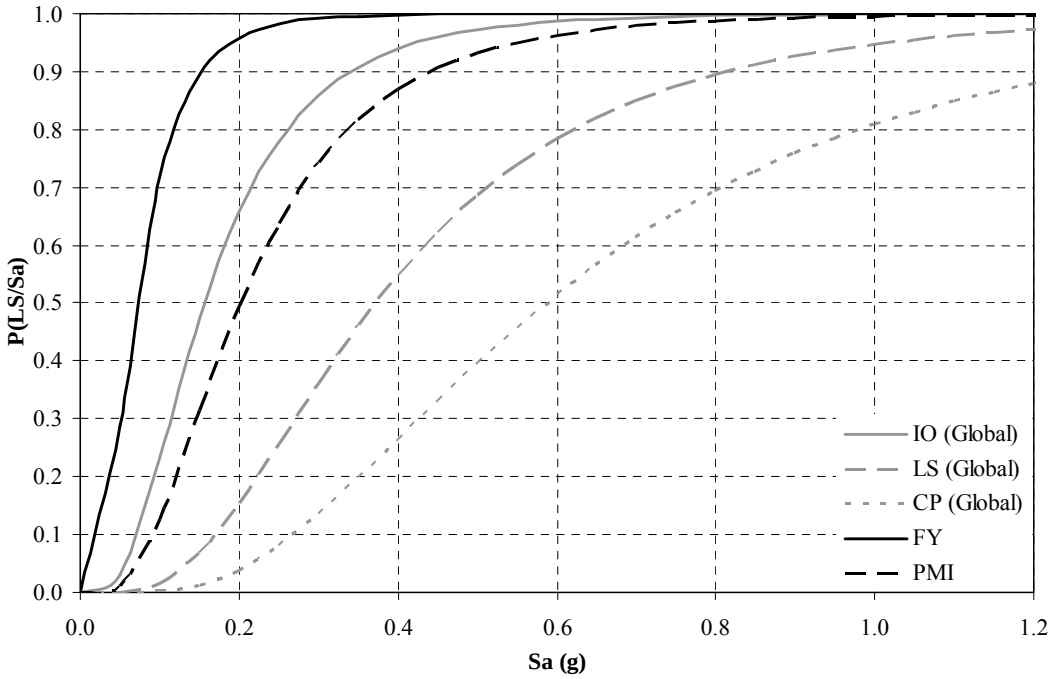

(b) Critical response push-over analysis

Fig. 6.28. Fragility curves for Retrofit 2 based on additional quantitative limits

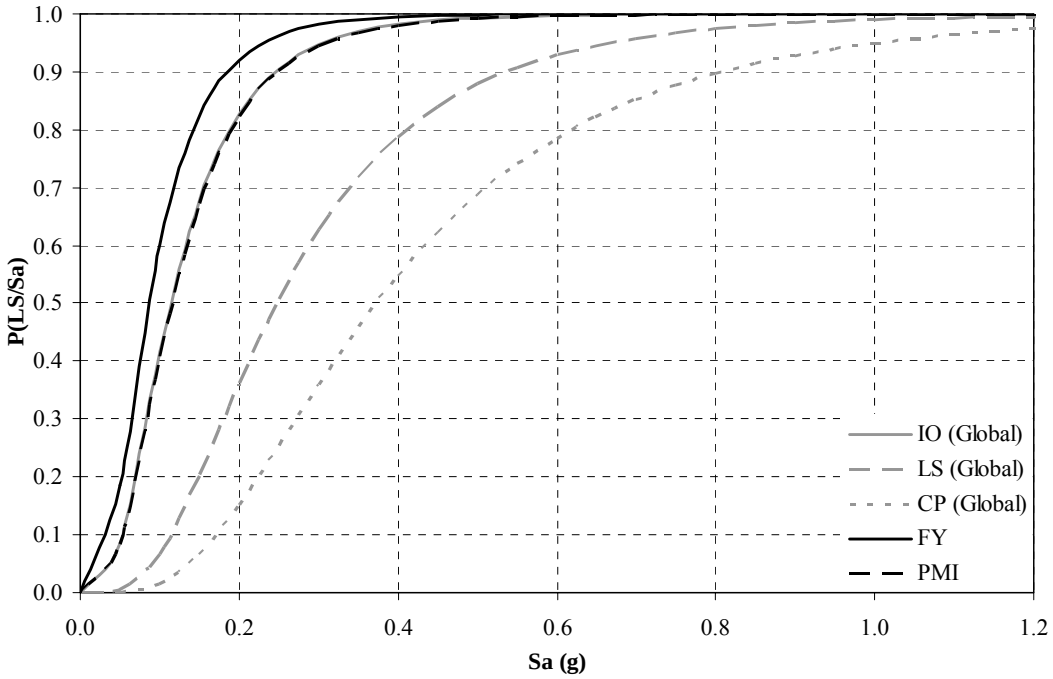

(a) Regular push-over analysis

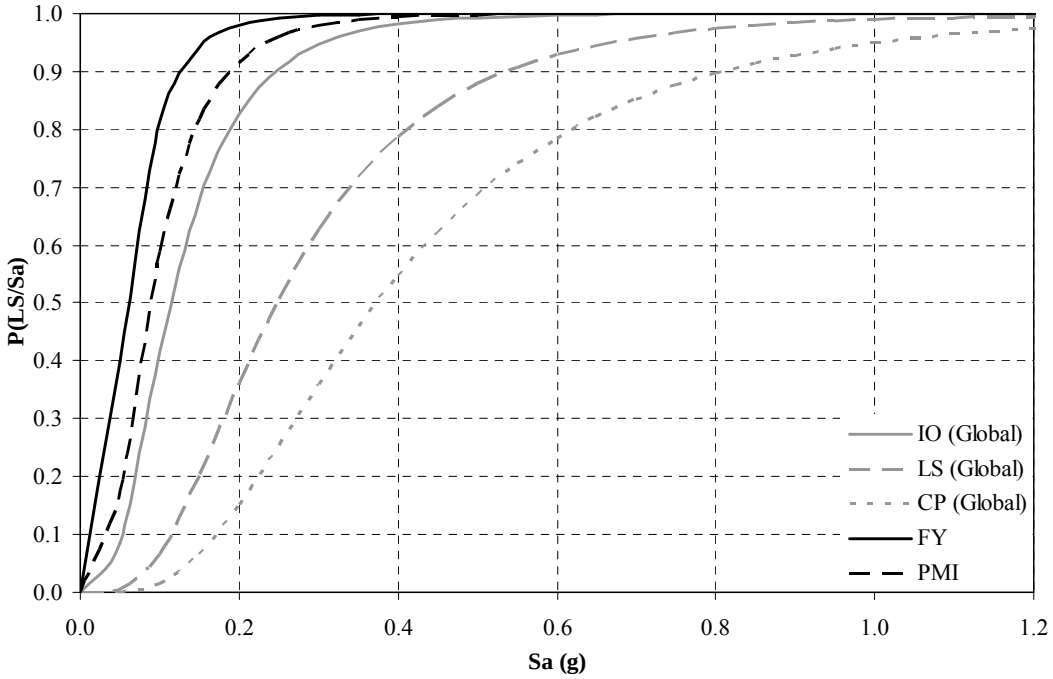

(b) Critical response push-over analysis

Fig. 6.29. Fragility curves for Retrofit 3 based on additional quantitative limits

Table 6.18 summarizes the probabilities of exceeding the PMI limit state corresponding to a range of PGA values based on drift limits determined from a critical response push-over analysis. As shown, the probabilities of exceeding the PMI limit state were reduced by each of the retrofits for the lower PGA values. In particular, Retrofit 1 has the greatest impact in reducing the probability of exceeding the PMI limit state for PGA's up to 0.8g.

Table 6.18. Probability of exceeding PMI limit state with a critical response push-over analysis

Structure	Peak Ground Acceleration (PGA), g								
	0.0	0.1	0.2	0.3	0.4	0.5	0.6	0.7	0.8
Unretrofitted	0.0	0.186	0.864	0.988	0.999	1.0	1.0	1.0	1.0
Retrofit 1	0.0	0.003	0.080	0.270	0.481	0.651	0.772	0.852	0.904
Retrofit 2	0.0	0.030	0.361	0.703	0.878	0.951	0.980	0.992	0.996
Retrofit 3	0.0	0.107	0.769	0.971	0.997	1.0	1.0	1.0	1.0

Fig. 6.30 shows the fragility curves for the FY and PMI using peak ground acceleration based on drift limits determined from a critical response push-over analysis. As shown in Fig. 6.30, the probabilities of exceeding both limit states were reduced to varying degrees depending on the retrofit technique, limit state and magnitude of the PGA.

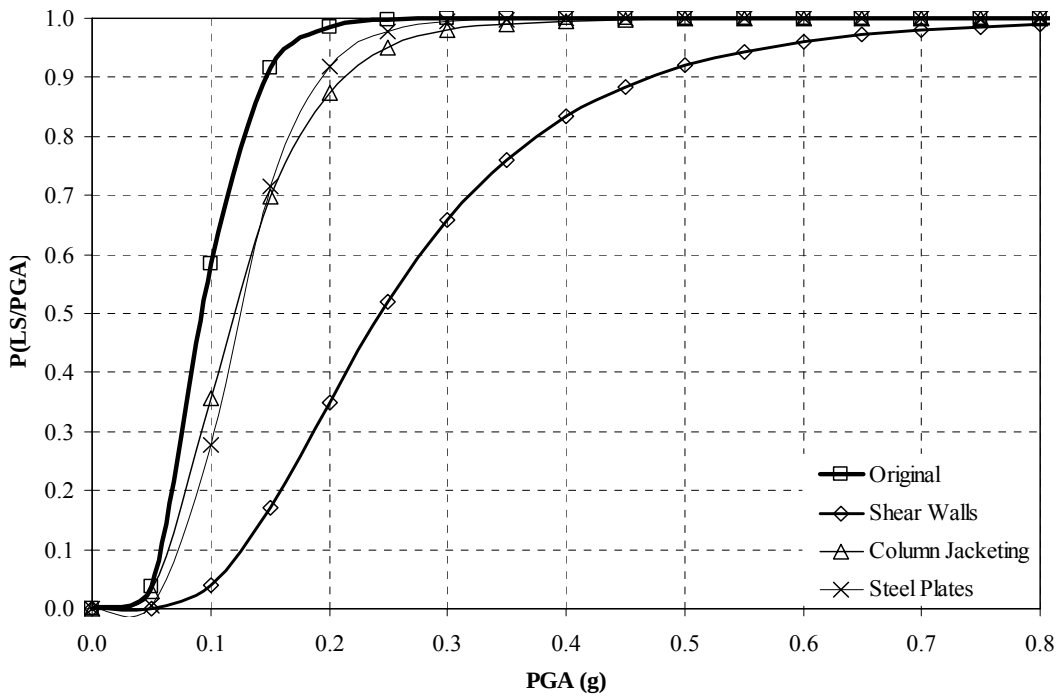

(a) FY Limit State

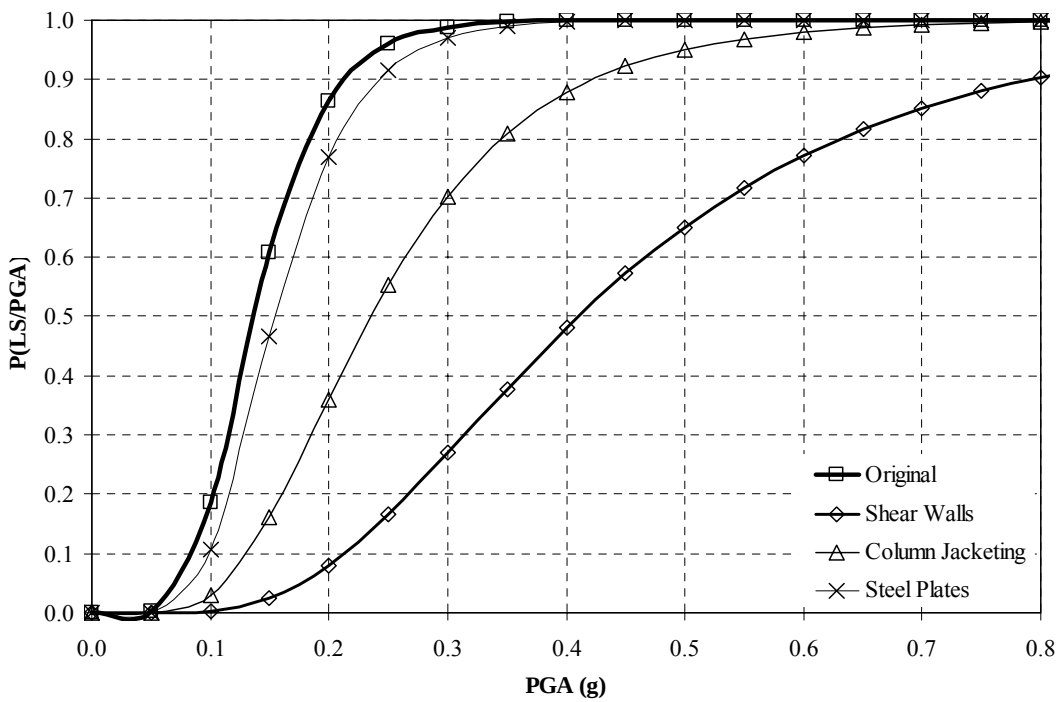

(b) PMI Limit State

Fig. 6.30. Impact of retrofit on fragility curves for quantitative limit states

6.7 Summary

In this section, the structural response of the case study building was described for three different retrofit techniques and compared with that of the unretrofitted structure. Based on the FEMA 356 global-level evaluation, the shear wall retrofit and the RC column jacketing retrofit showed an improvement. However, for the retrofit involving confinement of the column plastic hinge zones, no major change occurred in the median drift profile. In addition, for all the retrofit schemes, the FEMA 356 member-level evaluation showed that the retrofits improve the seismic performance.

Based on the analytical results, fragility curves for the retrofitted structure were developed using the FEMA 356 performance criteria and additional quantitative limit states. The fragility curves developed based on FEMA global-level drift limits and member-level plastic rotation limits were compared with those for the unretrofitted structure. In addition to this, additional quantitative limit states, described by Wen et al. (2003), were determined and compared to the limits based on the FEMA 356 criteria.

Retrofitting a structure can modify the building period and lead to the use of a different spectral acceleration for evaluation as compared to the unretrofitted structure. Therefore, peak ground acceleration was used for comparisons with the unretrofitted and retrofitted structures. In general, for all the cases including the FEMA global-level, member-level and additional quantitative drift limits, the probabilities of exceeding each limit state were significantly reduced by Retrofit 1 and 2 for PGA values above 0.2g. Retrofit 3 exhibited a smaller reduction in the probabilities of exceeding the limit states for this particular structure.

7 ADDITIONAL SEISMIC FRAGILITY ANALYSIS AND MAEVIZ IMPLEMENTATION

7.1 Introduction

This section presents the additional seismic fragility analysis of the case study building and the implementation into MAEviz, the damage visualization module. For further analysis, the synthetic ground motions developed by Rix and Fernandez-Leon (2004) were used. The global-level seismic evaluation using FEMA 356 was conducted through nonlinear analyses and the probabilistic fragility curves were developed. Finally, various seismic fragility relationships for the unretrofitted and retrofitted structure were implemented into MAEviz.

7.2 Global-Level Seismic Evaluation

FEMA 356 global-level criteria described in Table 6.10 were also applied for global-level seismic evaluation using the Rix and Fernandez-Leon (2004) motions. Fig. 7.1 shows the median maximum interstory drift profiles for the unretrofitted and three retrofitted structures based on the analyses using the Rix and Fernandez-Leon motions for the Atkinson and Boore (AB) model and the Frankel et al. (FA) model. The maximum interstory drift values were unreasonably high at certain levels of the structure for the magnitude 7.5 Frankel et al. model motions for all cases except the shear wall retrofit. Therefore, as shown in Fig. 7.1, the maximum interstory drifts for several stories are not reported.

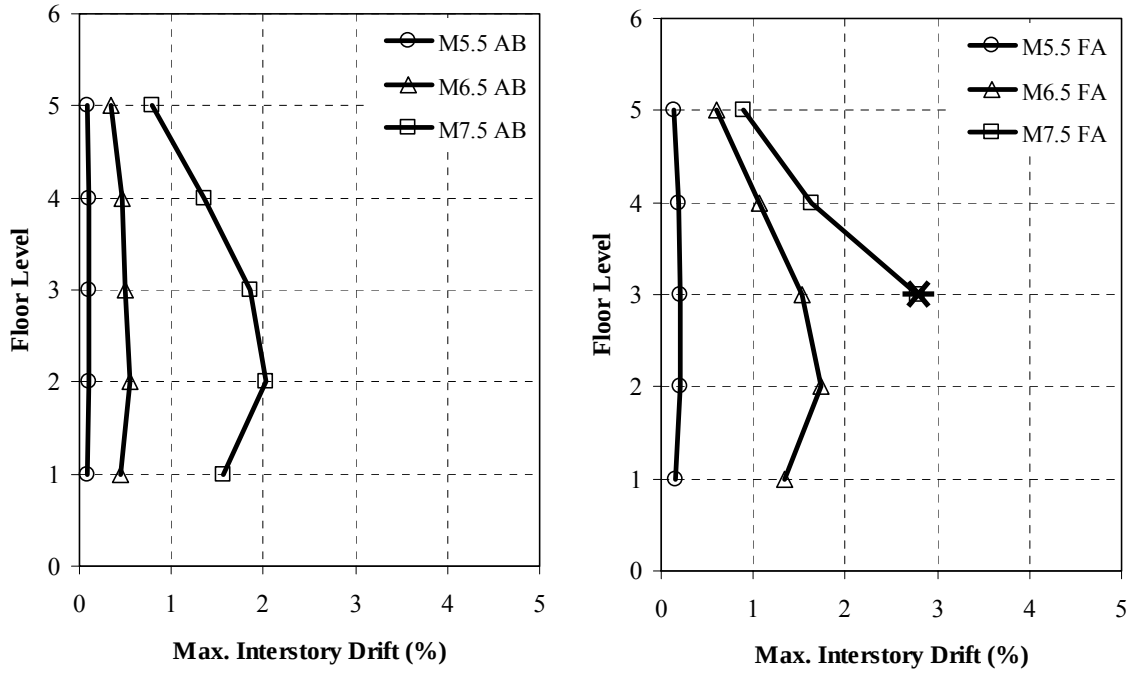

(a) Unretrofitted structure

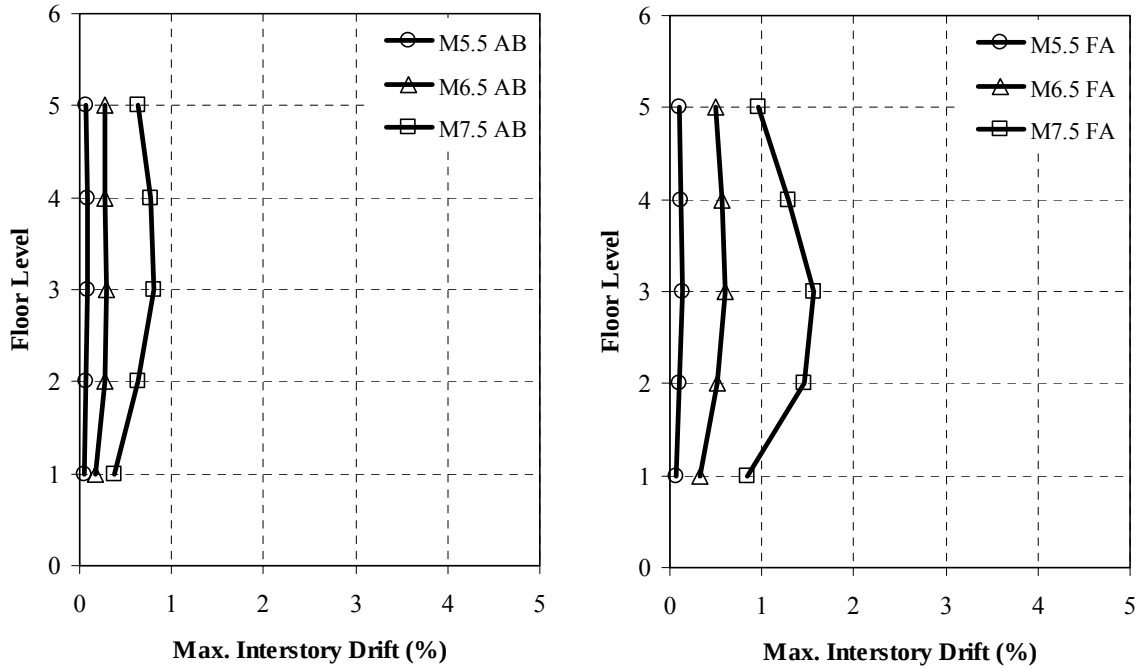

(b) Retrofit 1: Addition of shear walls

Fig. 7.1. Median maximum interstory drifts for unretrofitted and retrofitted structure (Rix and Fernandez-Leon motions)

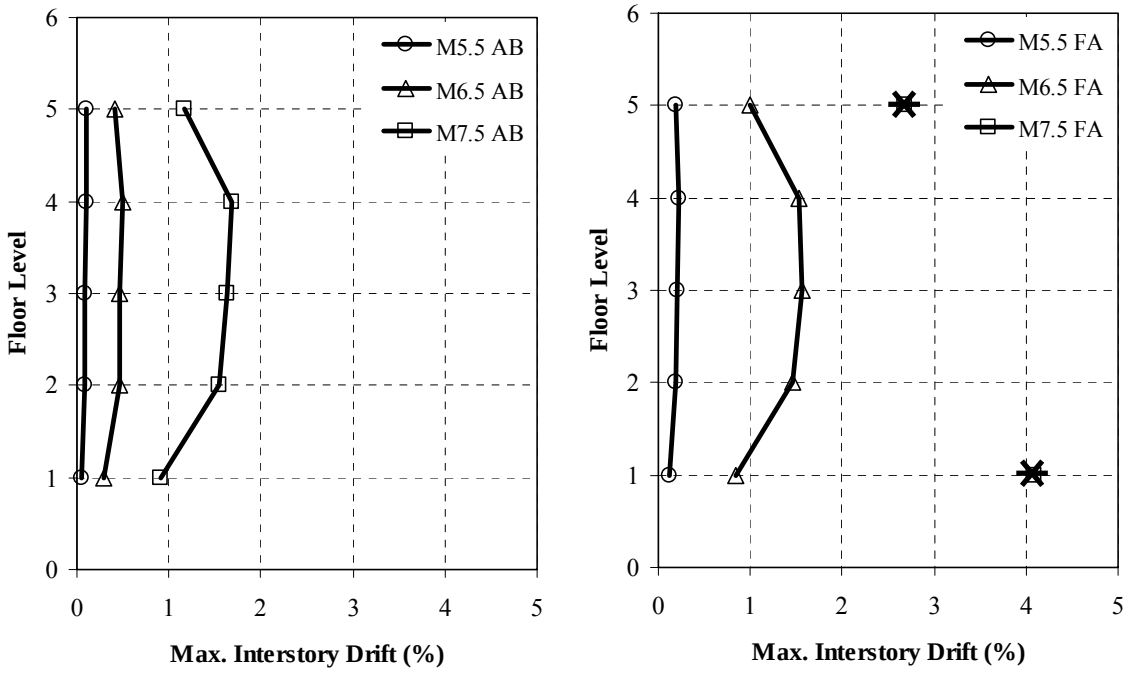

(c) Retrofit 2: Addition of RC column jackets

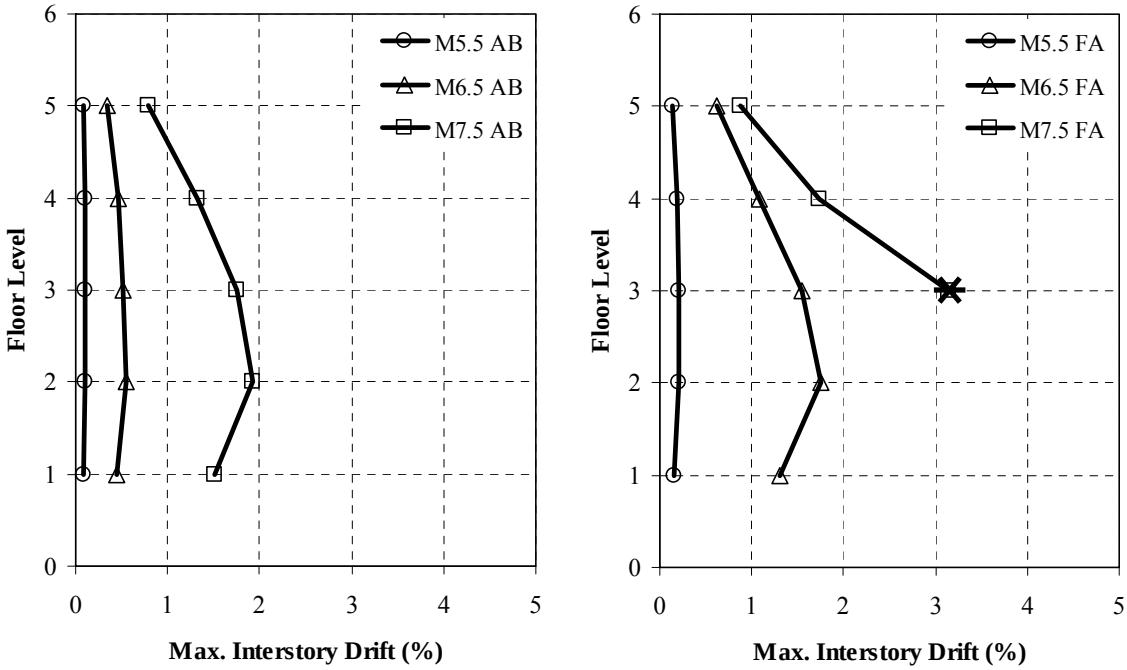

(d) Retrofit 3: Confinement of column plastic hinge zones

Fig. 7.1. Continued

As seen in Fig. 7.1, the maximum interstory drift profiles from two source models showed a significant difference for every case. In particular, the ground motions for the magnitude 7.5 Frankel et al. model provided a different profile shape than that from the analysis using the Wen and Wu motions.

7.3 Fragility Curves for Unretrofitted and Retrofitted Case Study Building

7.3.1 Global-Level Limits

To develop probabilistic fragility curves based on the Rix and Fernandez-Leon motions, spectral acceleration values from each ground motion record were used to develop the relationship between demand and structural response (drift) as discussed in Section 5. For more comparisons, fragility curves were developed for each source model used to develop the Rix and Fernandez-Leon motions separately and also for the two models combined based on global-level limits.

7.3.1.1 Atkinson and Boore Model

Fig. 7.2 shows the fitted power law equations for each unretrofitted and retrofitted structure for the Rix and Fernandez-Leon motions derived from the Atkinson and Boore source model. The spectral acceleration (S_a) for a given ground motion record is the value corresponding to the fundamental period of the structure based on cracked section properties and 5 percent damping.

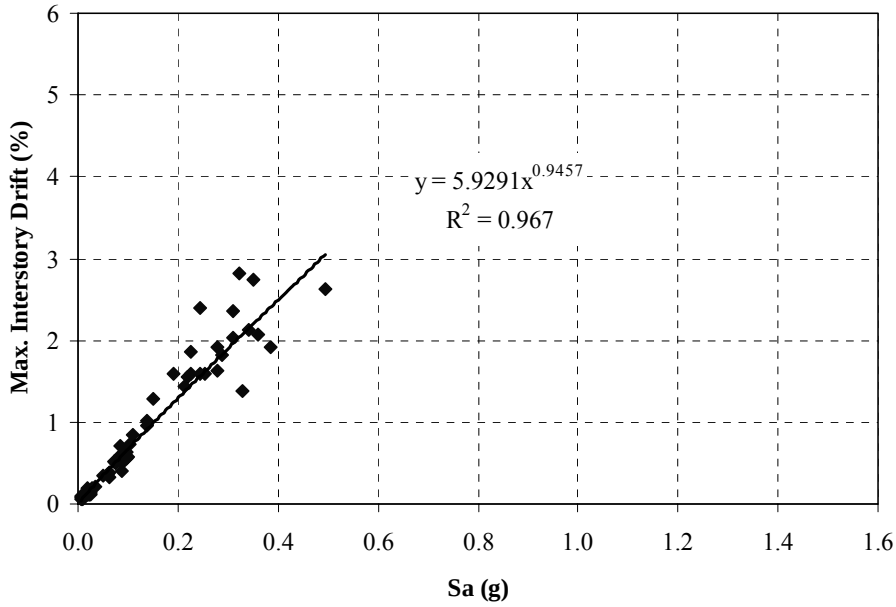

(a) Unretrofitted structure

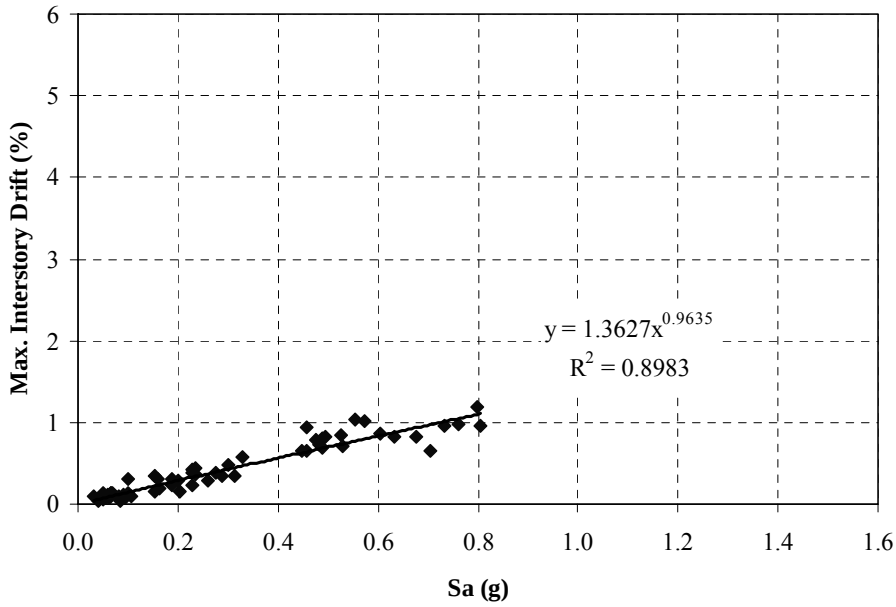

(b) Retrofit 1: Addition of shear walls

Fig. 7.2. Development of power law equations for demand drift (Rix and Fernandez-Leon motions - Atkinson and Boore model)

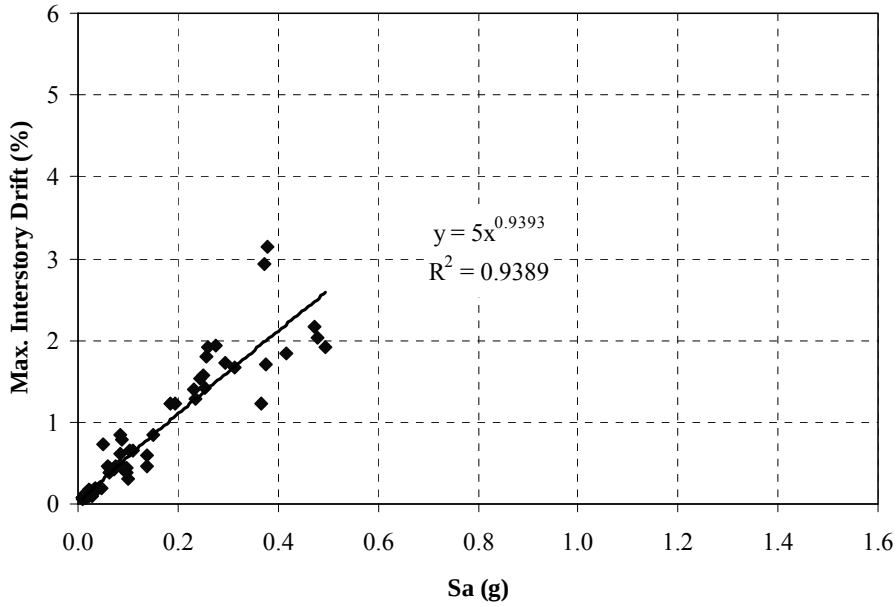

(c) Retrofit 2: Addition of RC column jackets

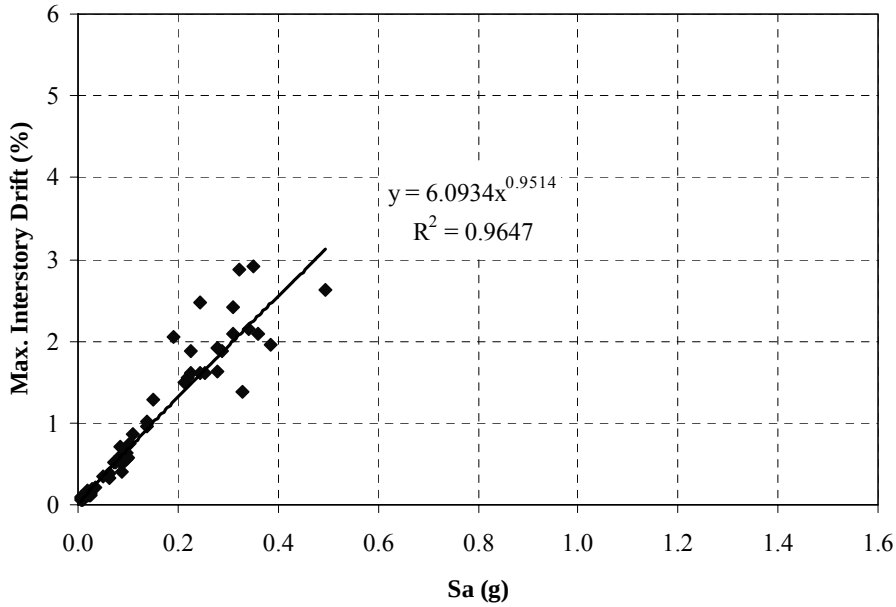

(d) Retrofit 3: Confinement of column plastic hinge zones

Fig. 7.2. Continued

The fragility curves developed for the unretrofitted and retrofitted using the three retrofit techniques are provided in Fig. 7.3. As discussed in Section 5, the punching shear failure was included as an upper bound for the CP limit state.

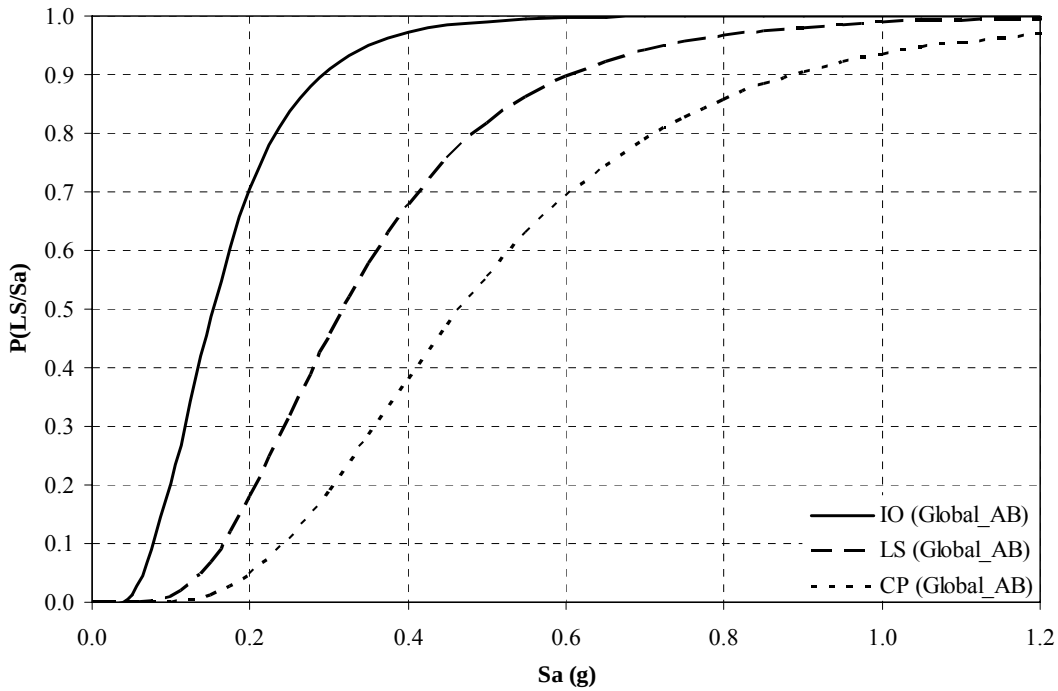

(a) Unretrofitted structure

Fig. 7.3. Global-level fragility curves (Rix and Fernandez-Leon motions - Atkinson and Boore model)

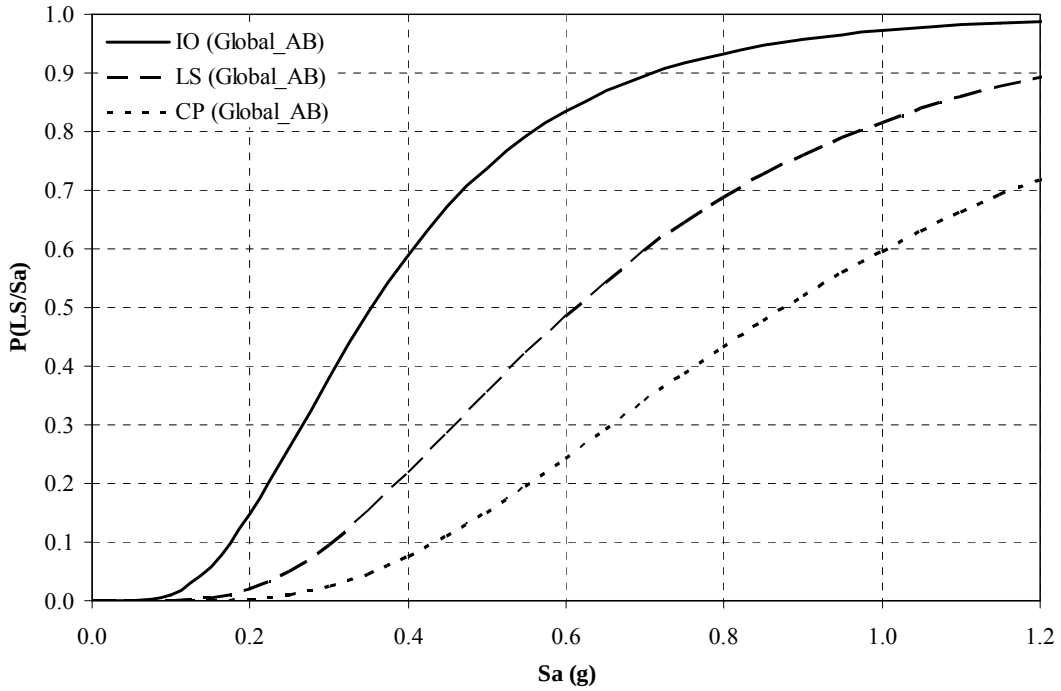

(b) Retrofit 1: Addition of shear walls

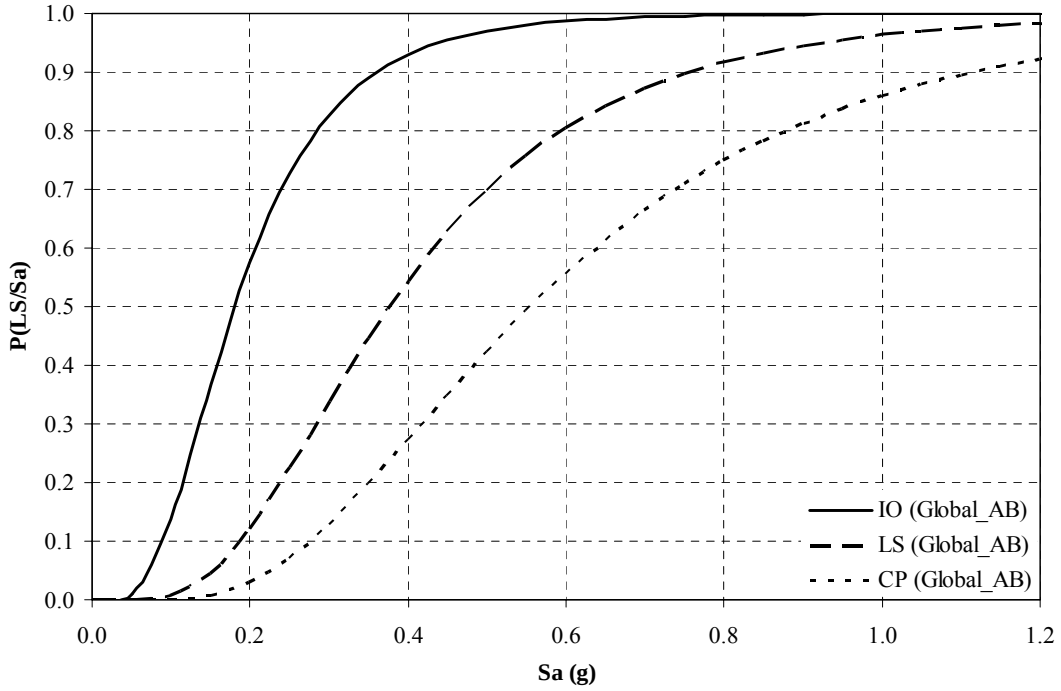

(c) Retrofit 2: Addition of RC column jackets

Fig. 7.3. Continued

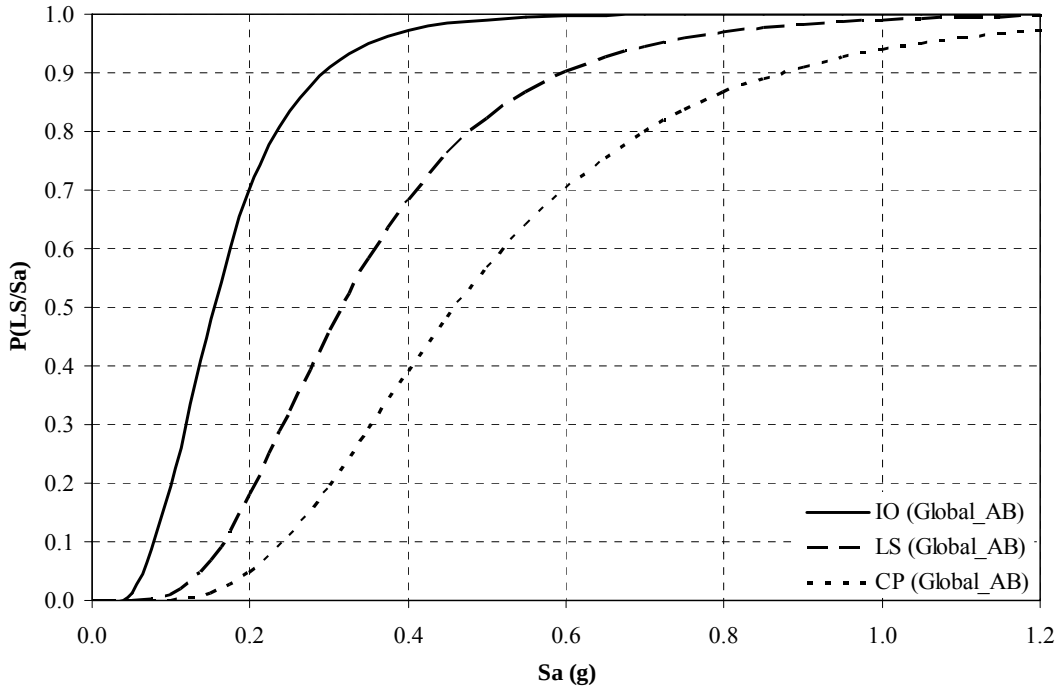

(d) Retrofit 3: Confinement of column plastic hinge zones

Fig. 7.3. Continued

As shown in Fig. 7.3, Retrofit 1 and 2 were effective based on the global-level drift limits in decreasing the probability of exceeding each limit state. However, for the case of confining the plastic hinge zones (Retrofit 3), the fragility curves for each limit state are the same as those for the unretrofitted structure, as discussed in Section 6.

7.3.1.2 Frankel et al. Model

Fig. 7.4 shows the fitted power law equations for each unretrofitted and retrofitted structure based on analysis using the Rix and Fernandez-Leon motions developed using the Frankel et al. source model. Based on the global-level seismic evaluation, the results from the magnitude 7.5 Frankel et al. motions are not included for the unretrofitted, Retrofit 2 and Retrofit 3 cases.

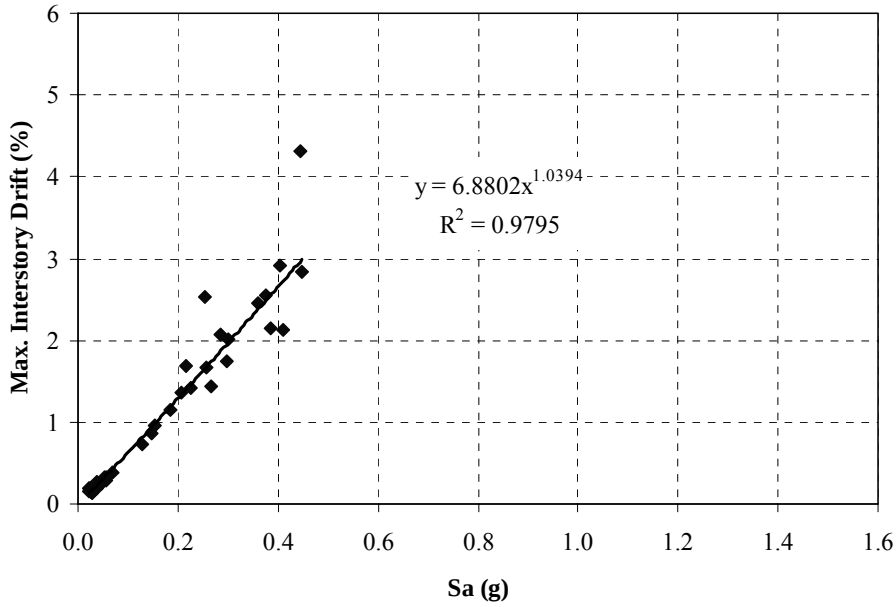

(a) Unretrofitted structure

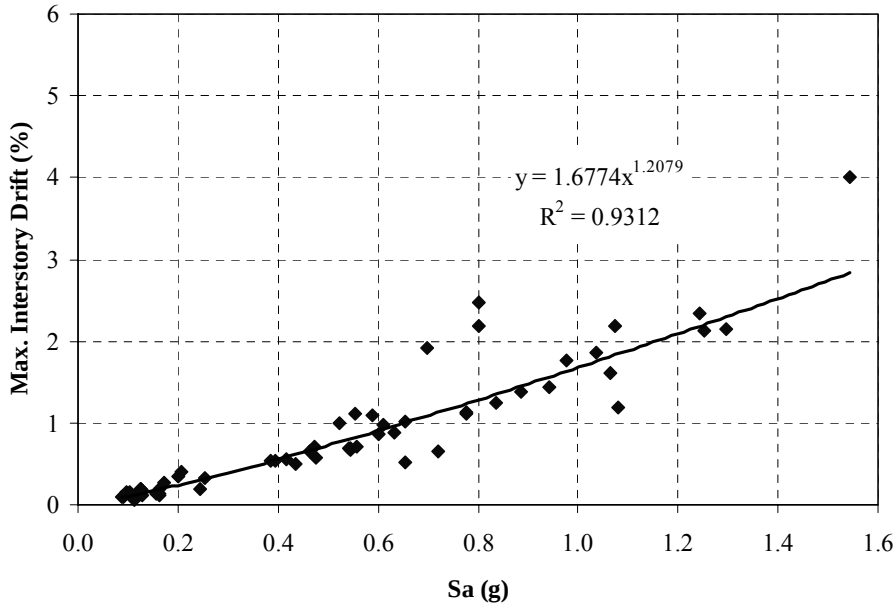

(b) Retrofit 1: Addition of shear walls

Fig. 7.4. Development of power law equations for demand drift (Rix and Fernandez-Leon motions - Frankel et al. model)

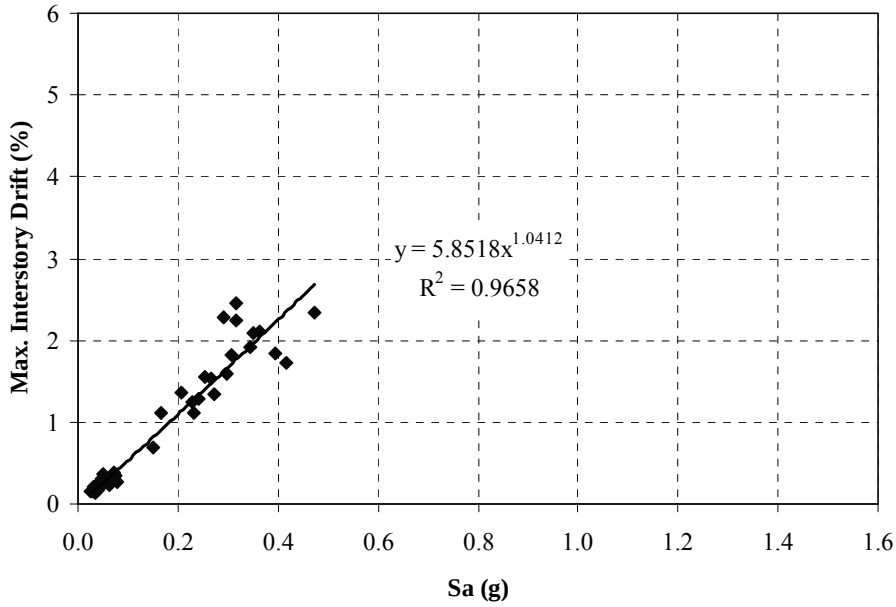

(c) Retrofit 2: Addition of RC column jackets

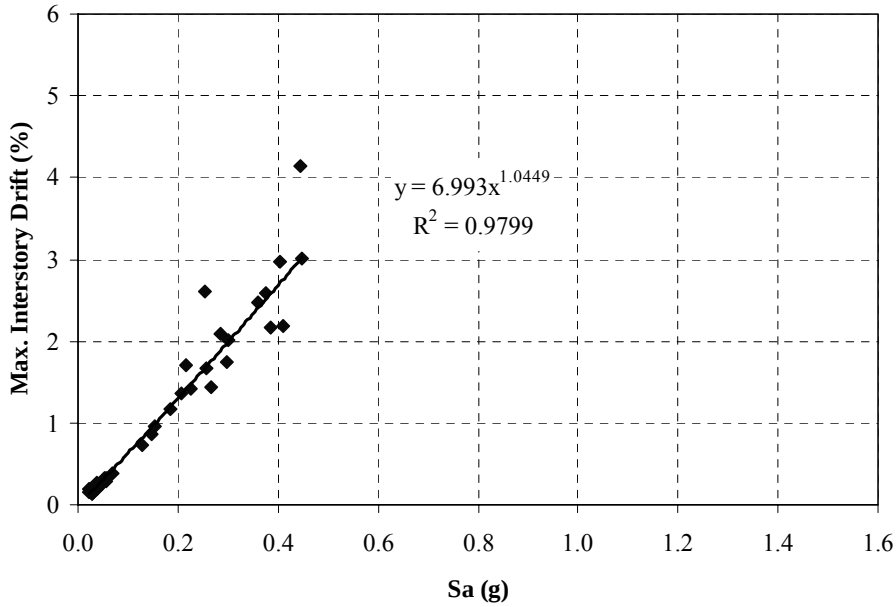

(d) Retrofit 3: Confinement of column plastic hinge zones

Fig. 7.4. Continued

The fragility curves developed for the unretrofitted and retrofitted using the three retrofit techniques are provided in Fig. 7.5. As discussed in Section 5, the punching shear failure was included as an upper bound for the CP limit state.

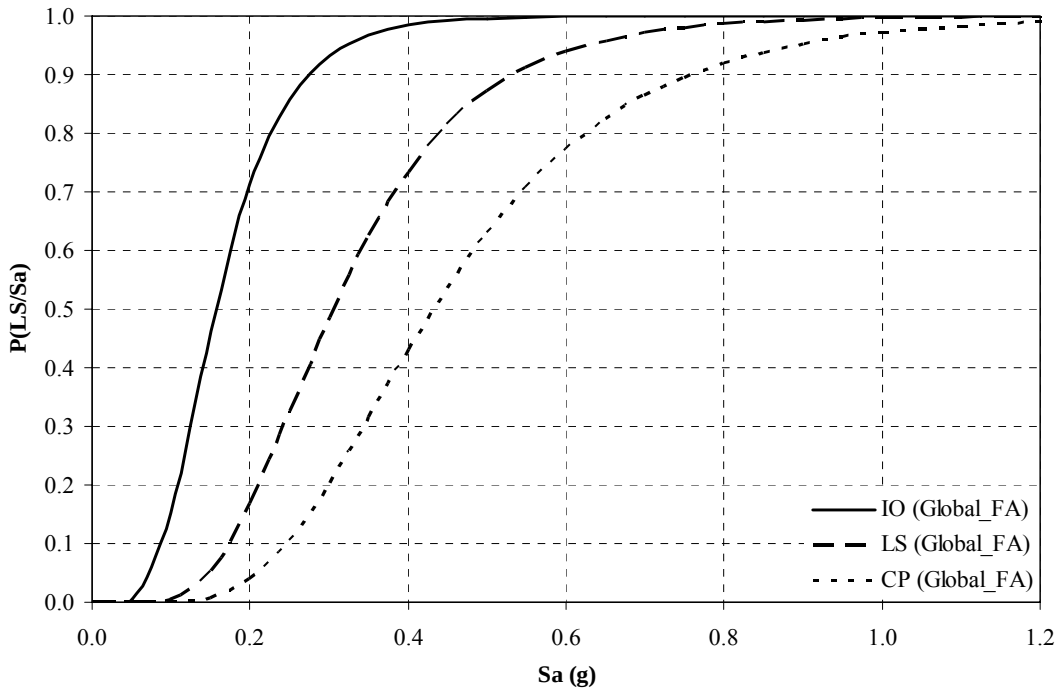

(a) Unretrofitted structure

Fig. 7.5. Global-level fragility curves (Rix and Fernandez-Leon motions - Frankel et al. model)

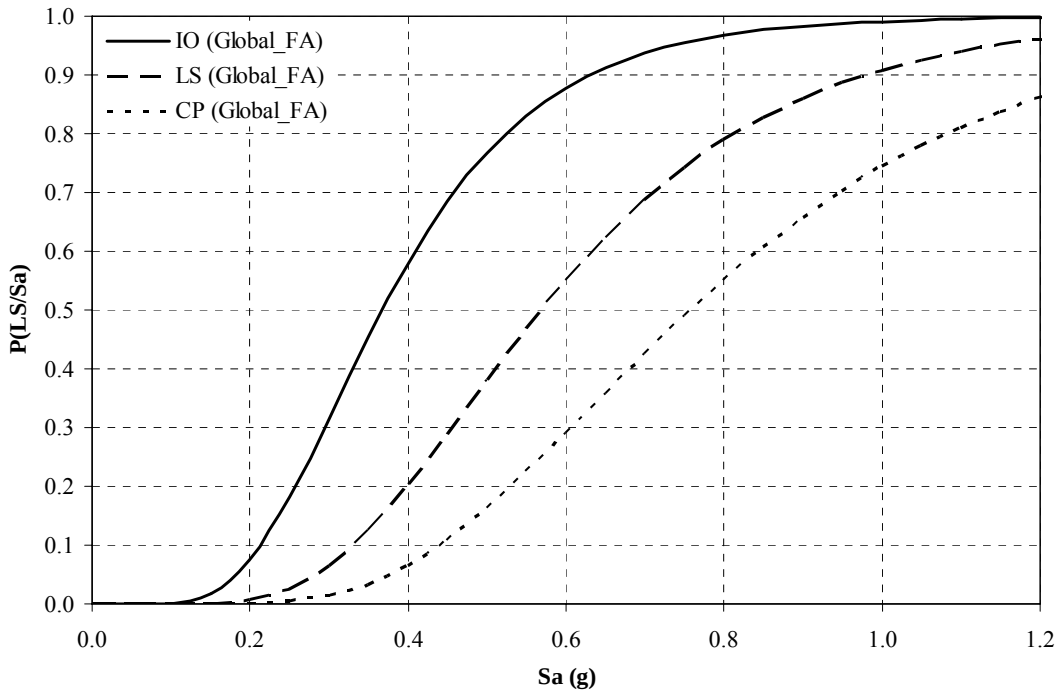

(b) Retrofit 1: Addition of shear walls

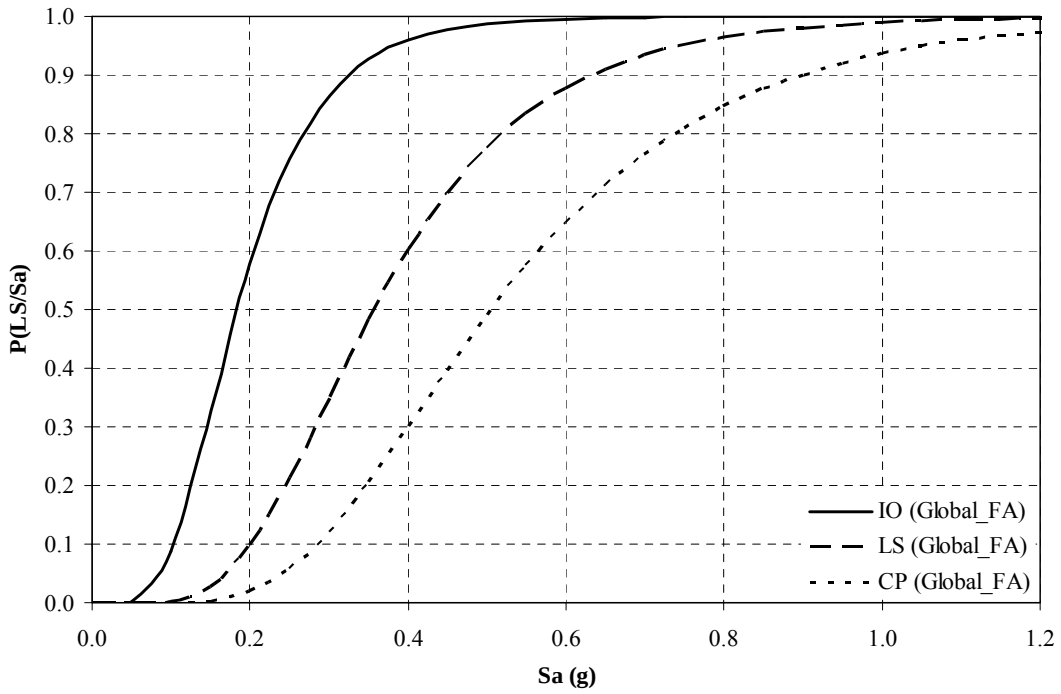

(c) Retrofit 2: Addition of RC column jackets

Fig. 7.5. Continued

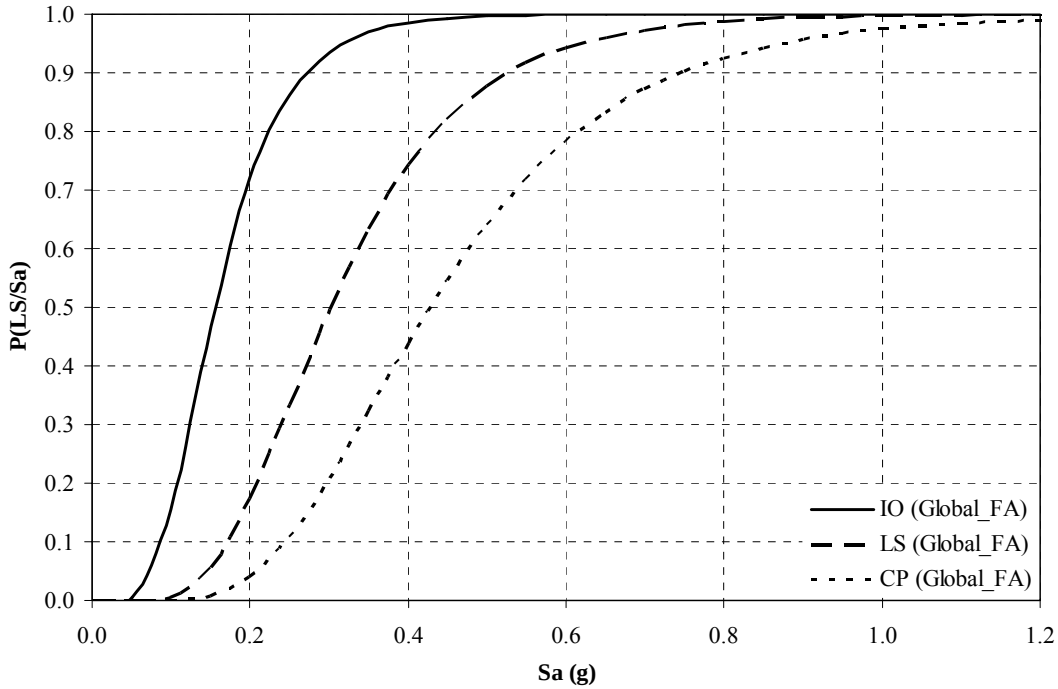

(d) Retrofit 3: Confinement of column plastic hinge zones

Fig. 7.5. Continued

The Frankel et al. motions led to fragility curves that provided the same trends as those observed in Fig. 7.3 for the Atkinson and Boore motions. Fig. 7.5 shows that based on the global-level drift limits, Retrofit 1 and 2 were effective in decreasing the probability of exceeding each limit state and Retrofit 3 had no impact.

7.3.1.3 Combination of Atkinson and Boore Model and Frankel et al. Model

Fig. 7.6 shows the fitted power law equations for each unretrofitted and retrofitted structure for the results from the Rix and Fernandez-Leon motions developed using both the Atkinson and Boore model and the Frankel et al. model. As discussed earlier, the results from the magnitude 7.5 Frankel et al. motions for the unretrofitted, Retrofit 2 and Retrofit 3 cases are not included based on the global-level seismic evaluation.

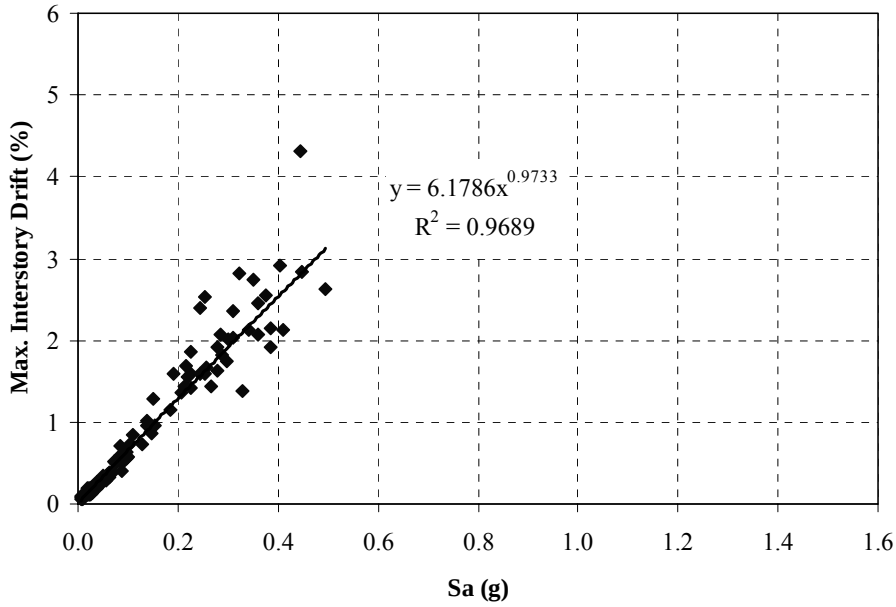

(a) Unretrofitted structure

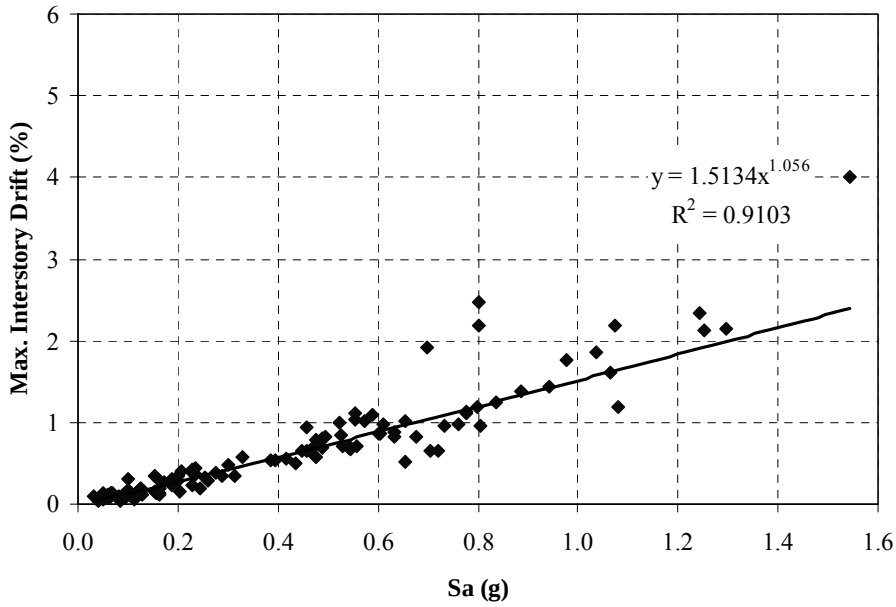

(b) Retrofit 1: Addition of shear walls

Fig. 7.6. Development of power law equations for demand drift (Rix and Fernandez-Leon motions - Atkinson and Boore model and Frankel et al. model)

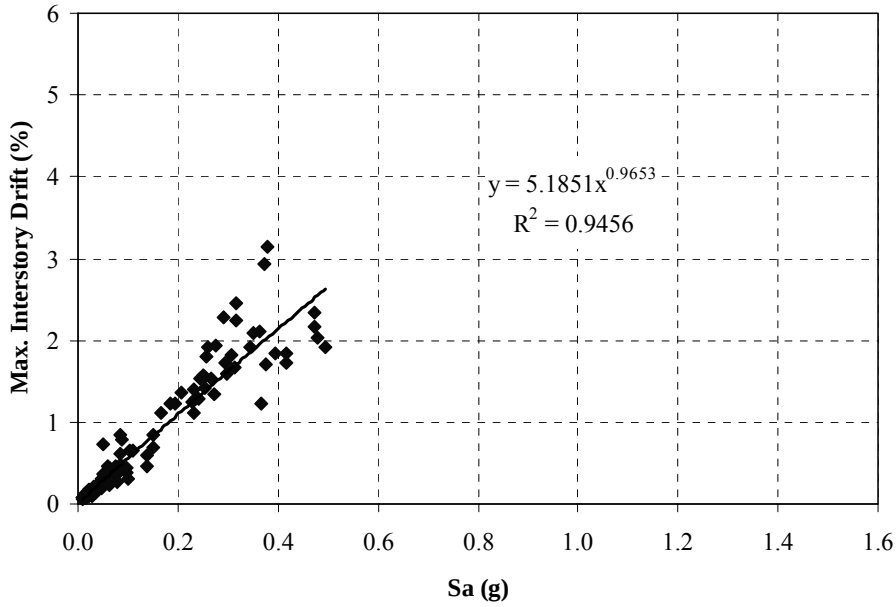

(c) Retrofit 2: Addition of RC column jackets

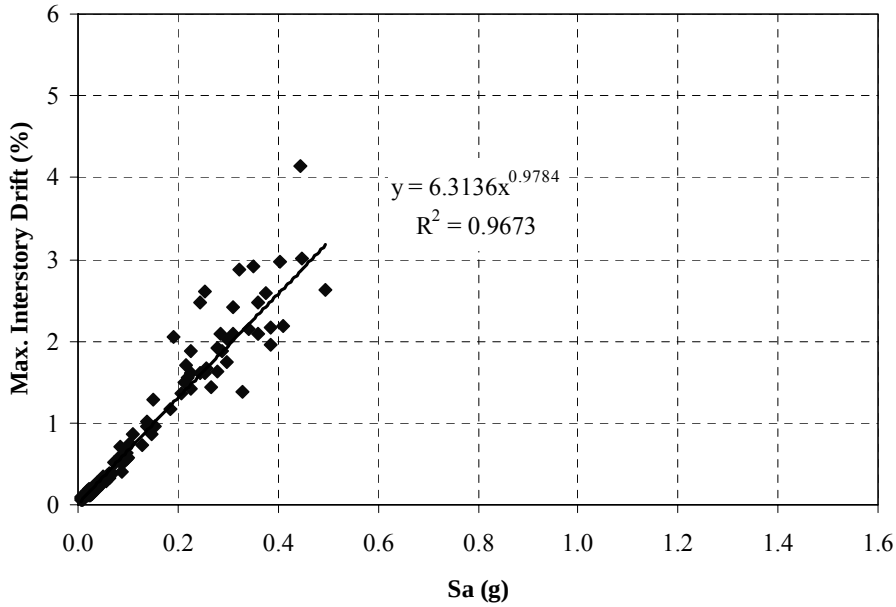

(d) Retrofit 3: Confinement of column plastic hinge zones

Fig. 7.6. Continued

Table 7.1 provides the parameters for Eq. 5.4 used in developing the global-level fragility curves for the unretrofitted and retrofitted structures

Table 7.1. Parameters for developing the global-level fragility curves for retrofit

Model	Parameter	Value
Unretrofitted	s^2	0.0427
	$\beta_{D\|S_a}$	0.204
	β_{CL}	0.3
	β_M	0.3
Retrofit 1: Addition of shear walls	s^2	0.105
	$\beta_{D\|S_a}$	0.316
	β_{CL}	0.3
	β_M	0.3
Retrofit 2: Addition of RC column jackets	s^2	0.0672
	$\beta_{D\|S_a}$	0.255
	β_{CL}	0.3
	β_M	0.3
Retrofit 3: Confinement of column plastic hinge zones	s^2	0.0454
	$\beta_{D\|S_a}$	0.211
	β_{CL}	0.3
	β_M	0.3

The global-level fragility curves developed for the unretrofitted and retrofitted structure using the three retrofit techniques are provided in Fig. 7.7. As discussed in Section 5, the punching shear failure was included as an upper bound for the CP limit state.

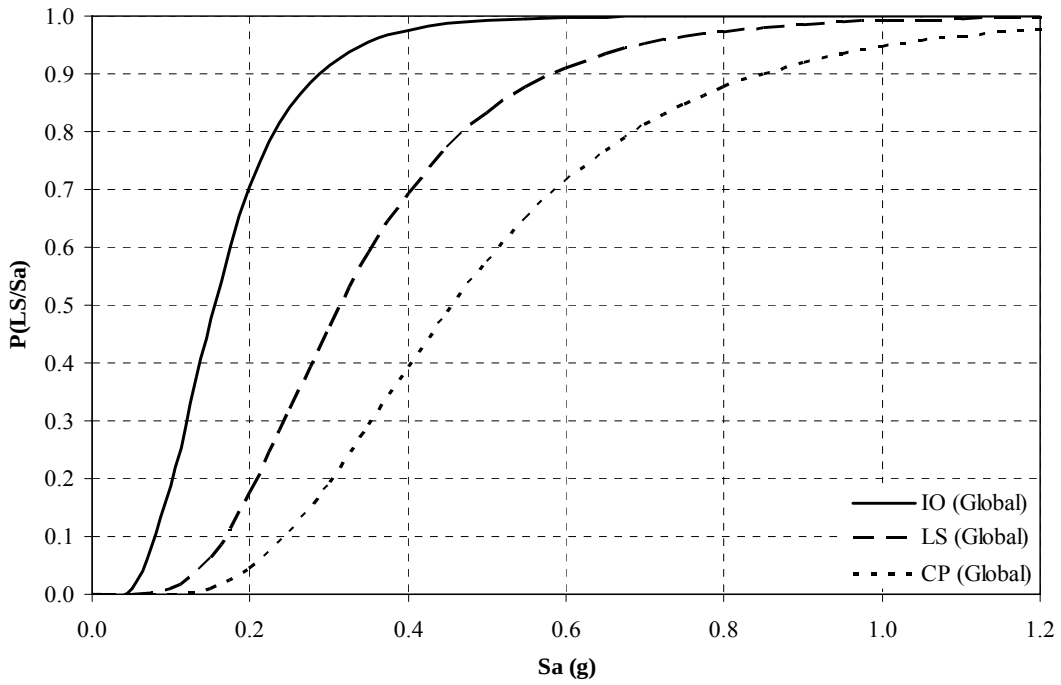

(a) Unretrofitted structure

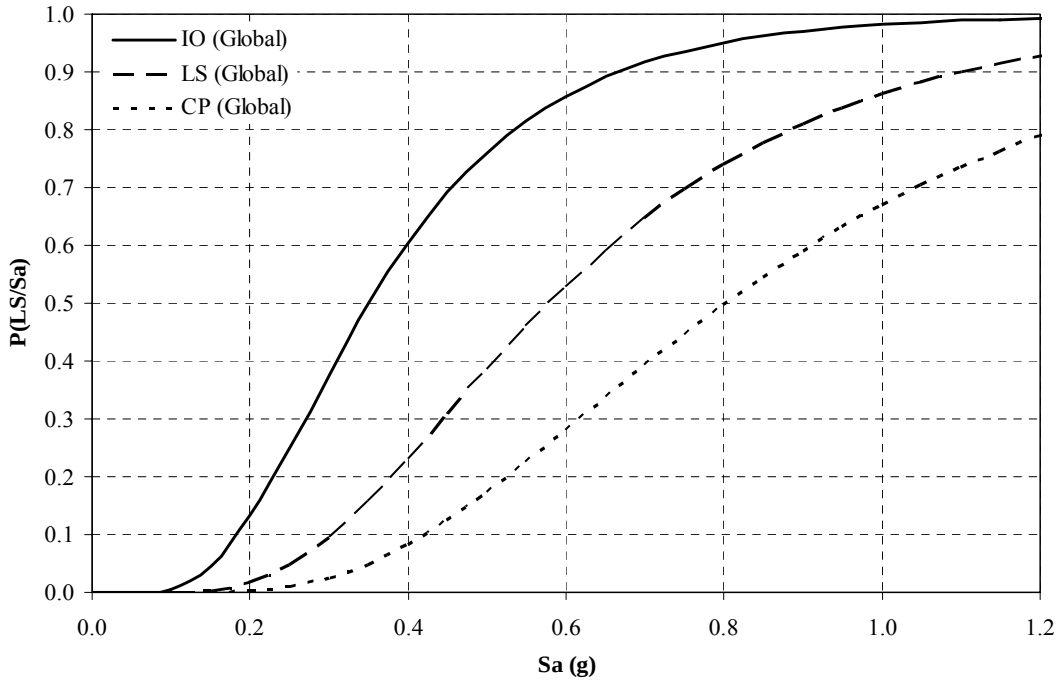

(b) Retrofit 1: Addition of shear walls

Fig. 7.7. Global-level fragility curves (Rix and Fernandez-Leon motions - Atkinson and Boore model and Frankel et al. model)

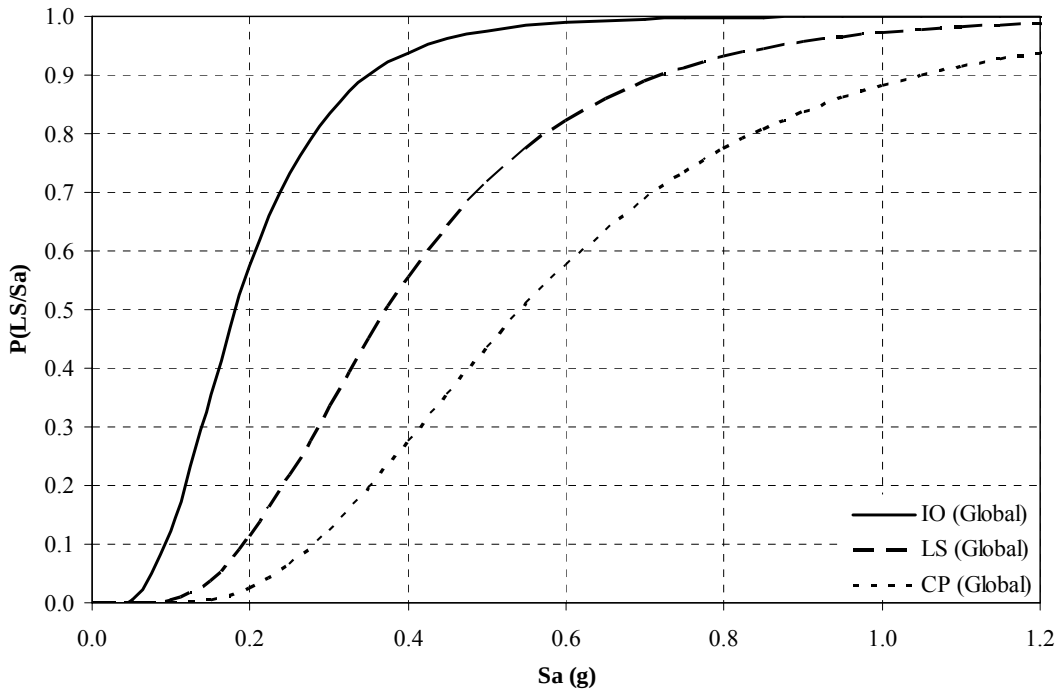

(c) Retrofit 2: Addition of RC column jackets

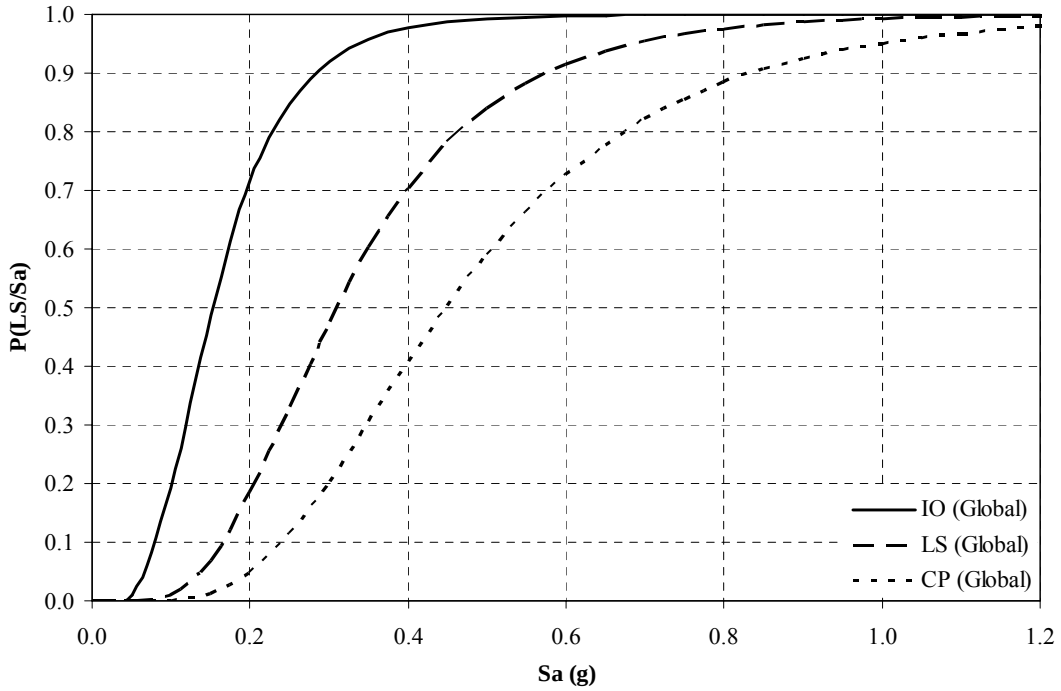

(d) Retrofit 3: Confinement of column plastic hinge zones

Fig. 7.7. Continued

As shown in Fig. 7.7, the addition of shear walls and RC column jackets were effective in decreasing the probability of exceeding each limit state. However, as noted for the fragility curves developed using the Wen and Wu motions, Retrofit 3 global-level fragility curves are the same as those for the unretrofitted structure. Fig. 7.8 shows the fragility curves using peak ground acceleration for each limit state. As shown, the probabilities of exceeding each limit state for the addition of shear walls and RC column jackets were reduced relative to the unretrofitted structure.

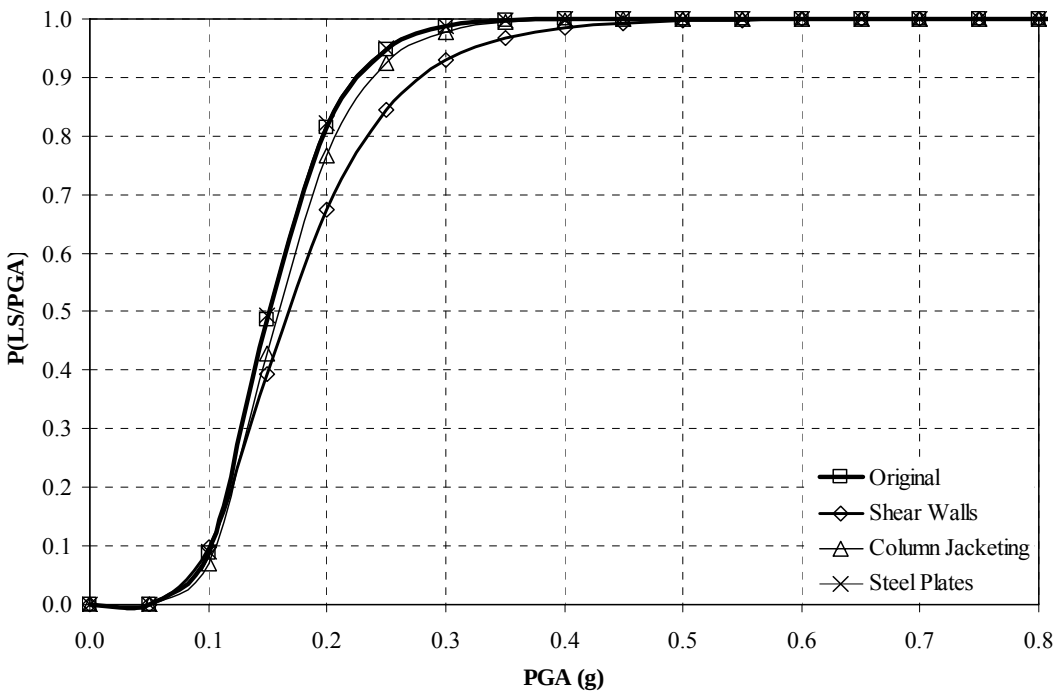

(a) IO Limit State

Fig. 7.8. Comparisons of global-level fragility curves for each limit state (Rix and Fernandez-Leon motions)

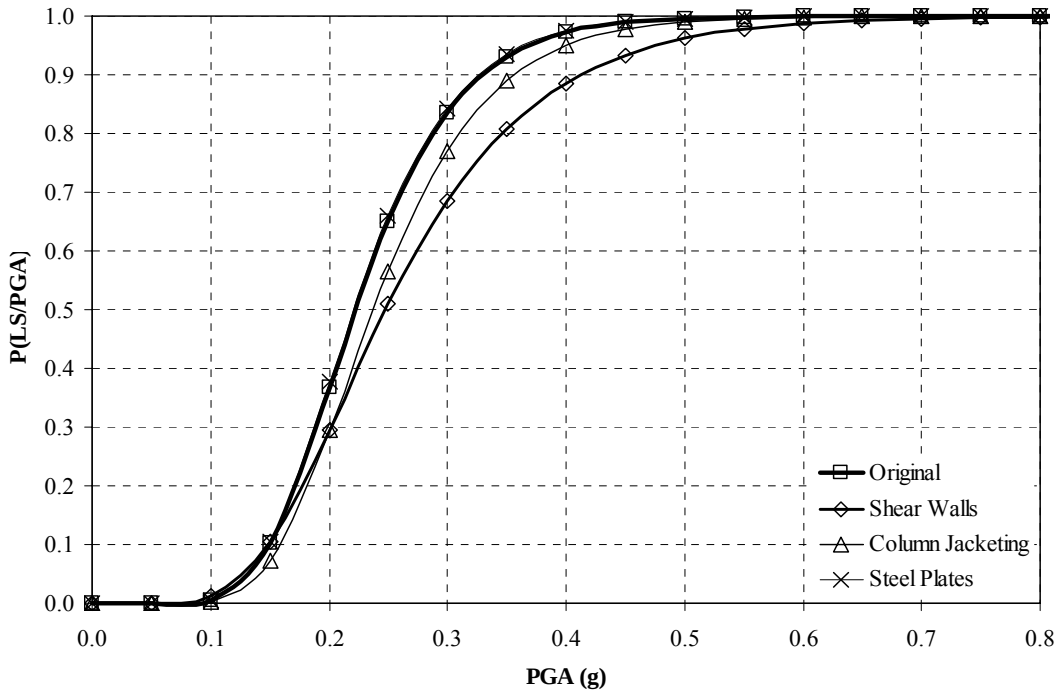

(b) LS Limit State

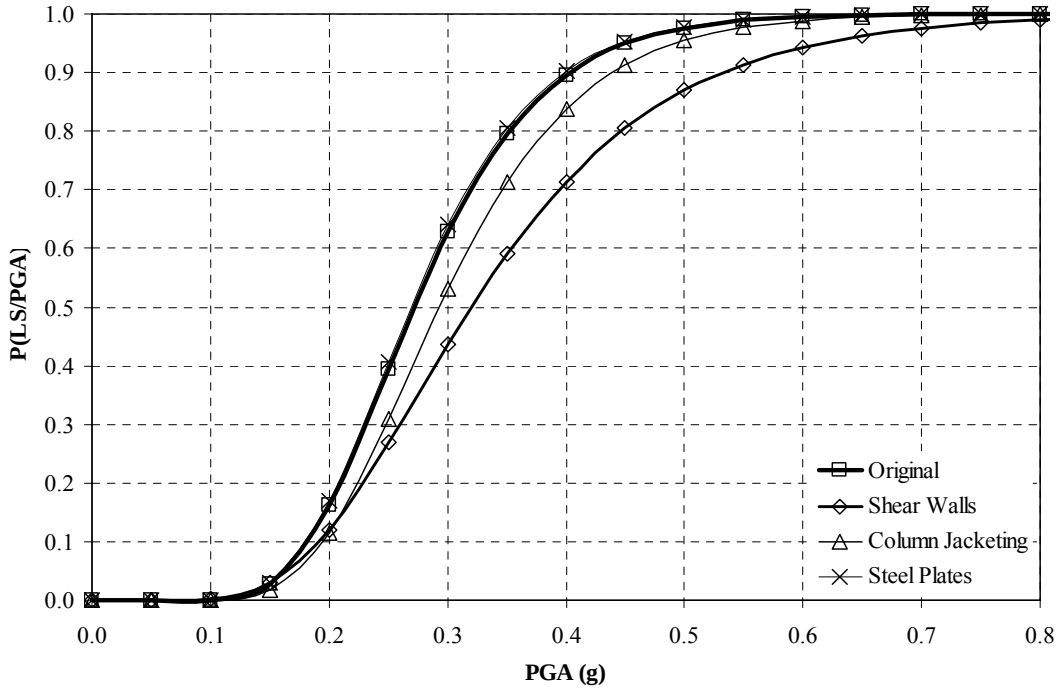

(c) CP Limit State

Fig. 7.8. Continued

7.3.2 Member-Level Limits

Member-level fragility curves for Rix and Fernandez-Leon motions were developed based on drift capacities determined from a critical response push-over summarized in Table 6.15. For comparison, fragility curves were constructed for each source model used to develop the Rix and Fernandez-Leon ground motions separately and also for the two models combined.

7.3.2.1 Atkinson and Boore Model

Fig. 7.9 shows the member-level fragility curves for each unretrofitted and retrofitted structure derived using the Rix and Fernandez-Leon motions based on the Atkinson and Boore source model.

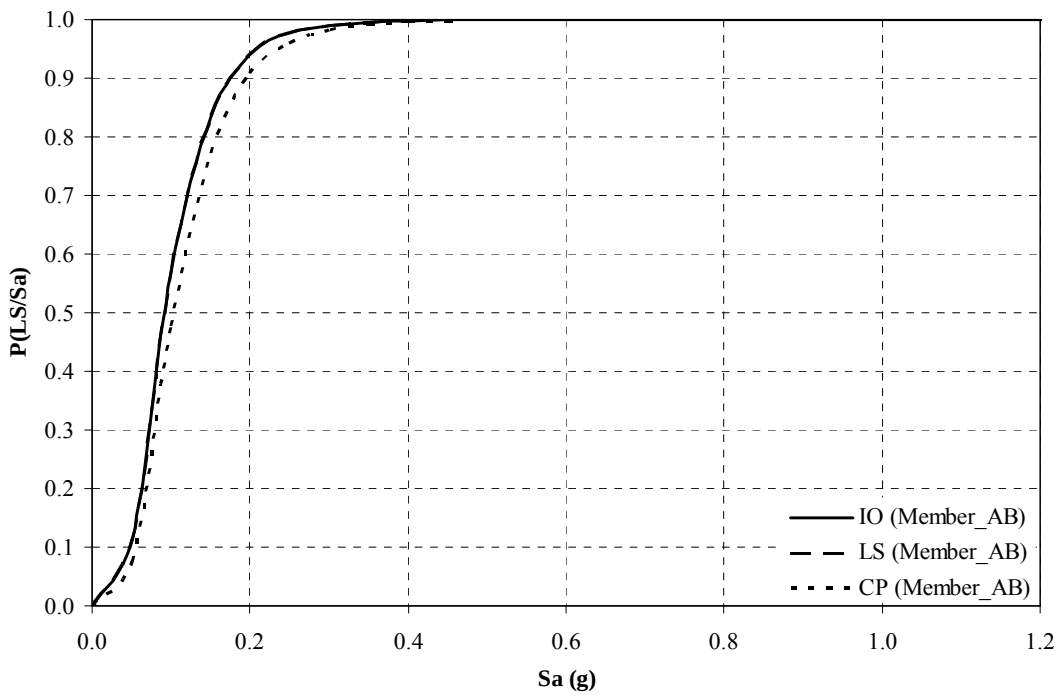

(a) Unretrofitted structure

Fig. 7.9. Member-level fragility curves (Rix and Fernandez-Leon motions - Atkinson and Boore model)

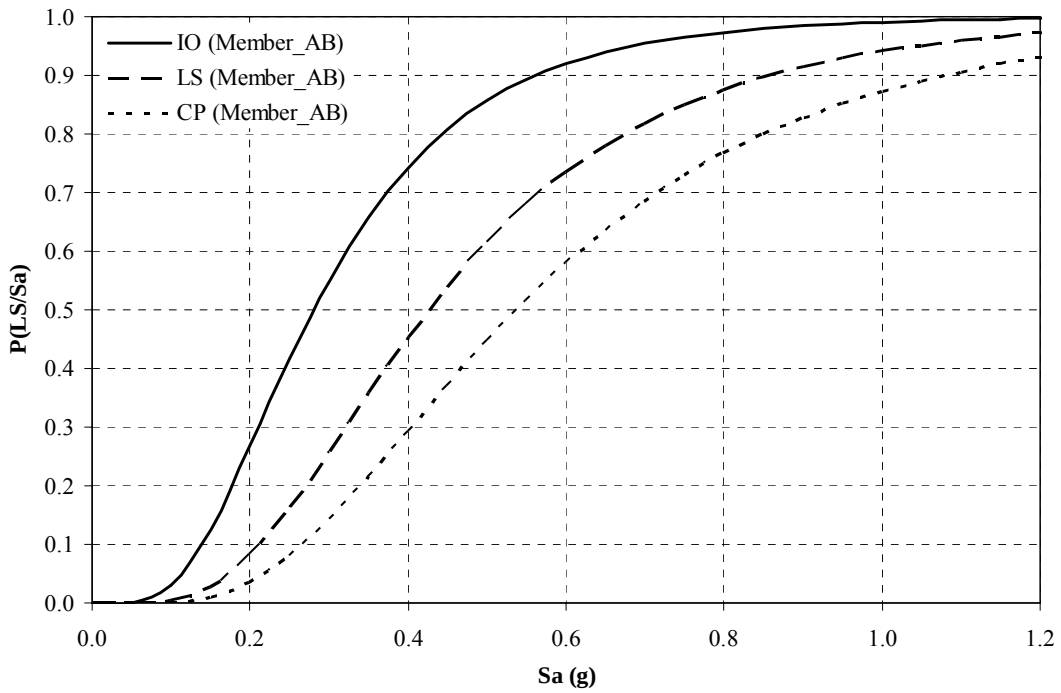

(b) Retrofit 1: Addition of shear walls

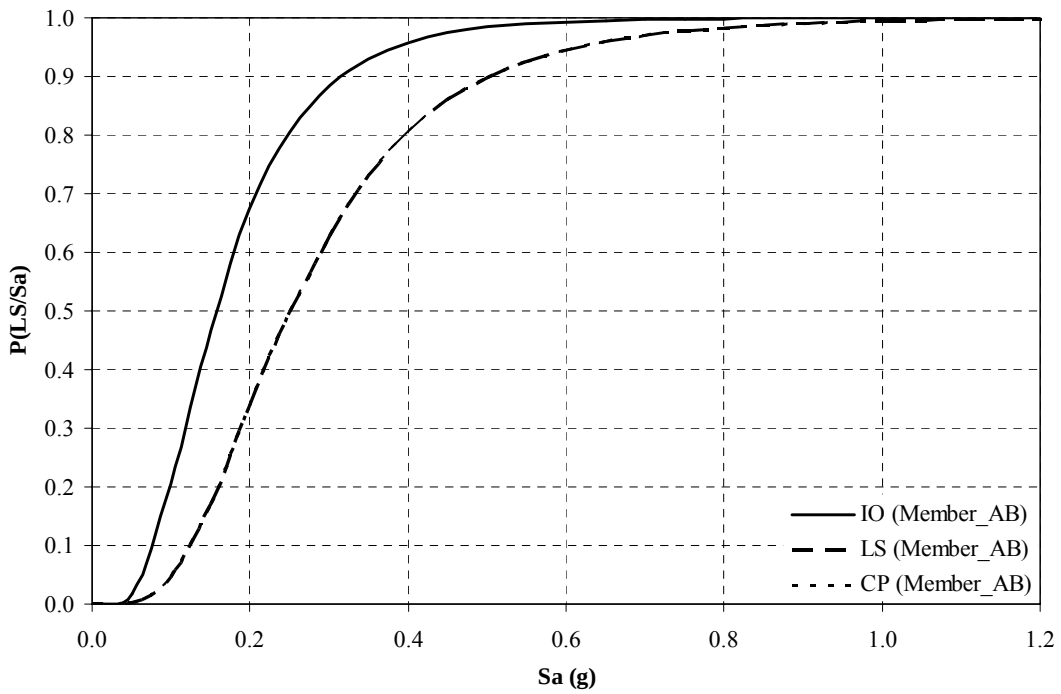

(c) Retrofit 2: Addition of RC column jackets

Fig. 7.9. Continued

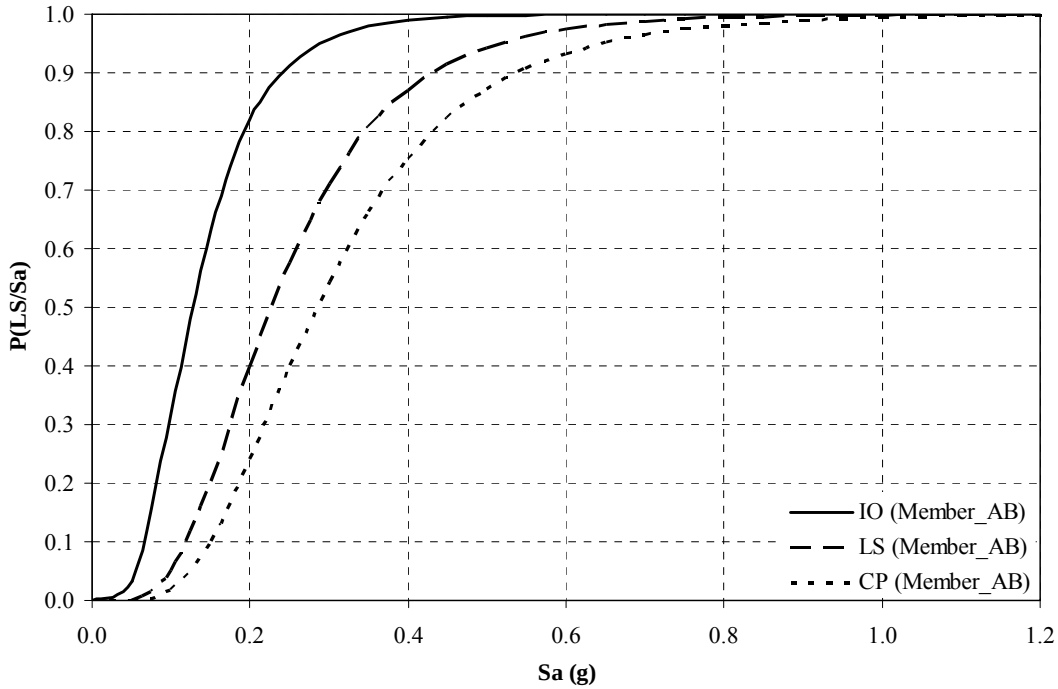

(d) Retrofit 3: Confinement of column plastic hinge zones

Fig. 7.9. Continued

As shown in Fig. 7.9, the probabilities of exceeding each limit state were reduced by all of the retrofits. In particular, the shear wall retrofit (Retrofit 1) has the greatest impact in reducing the probability of exceeding each limit state for lower values of spectral acceleration.

7.3.2.2 Frankel et al. Model

Fig. 7.10 shows the member-level fragility curves for each unretrofitted and retrofitted structure for the Rix and Fernandez-Leon motions derived using the Frankel et al. source model. Based on the global-level seismic evaluation, the results from the magnitude 7.5 Frankel et al. motions were not included for the unretrofitted, Retrofit 2 and Retrofit 3 cases.

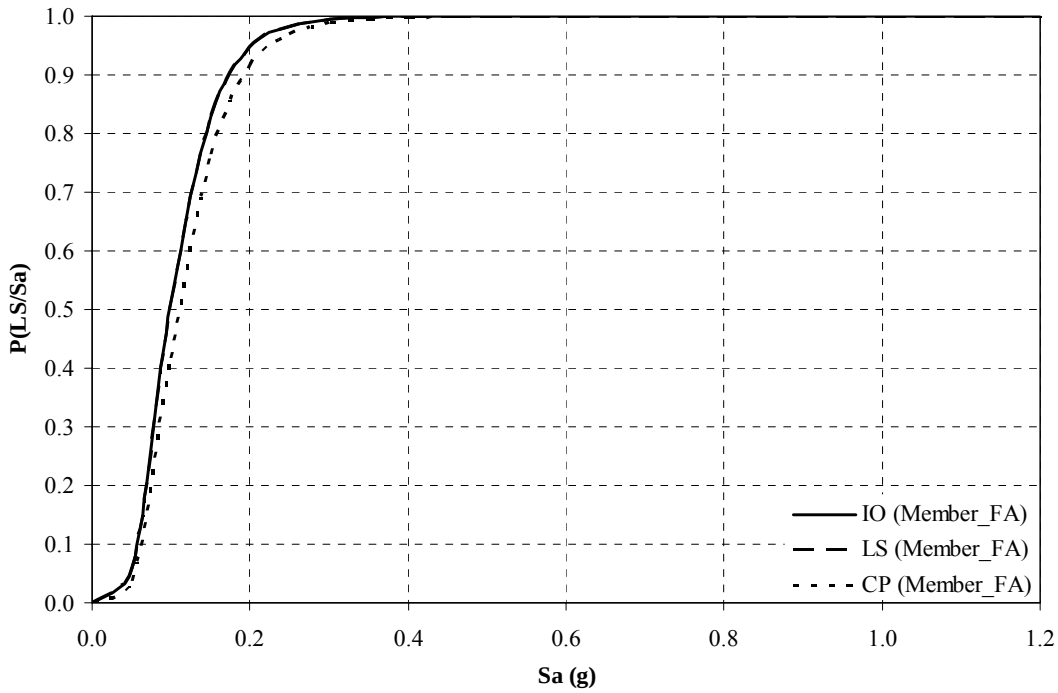

(a) Unretrofitted structure

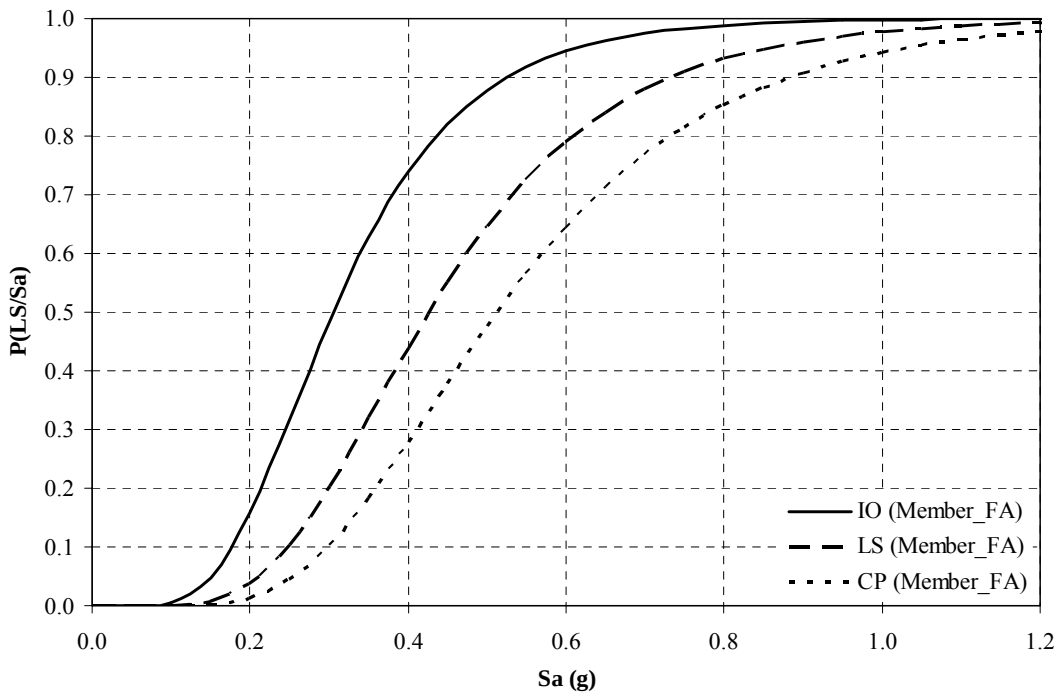

(b) Retrofit 1: Addition of shear walls

Fig. 7.10. Member-level fragility curves (Rix and Fernandez-Leon motions - Frankel et al. model)

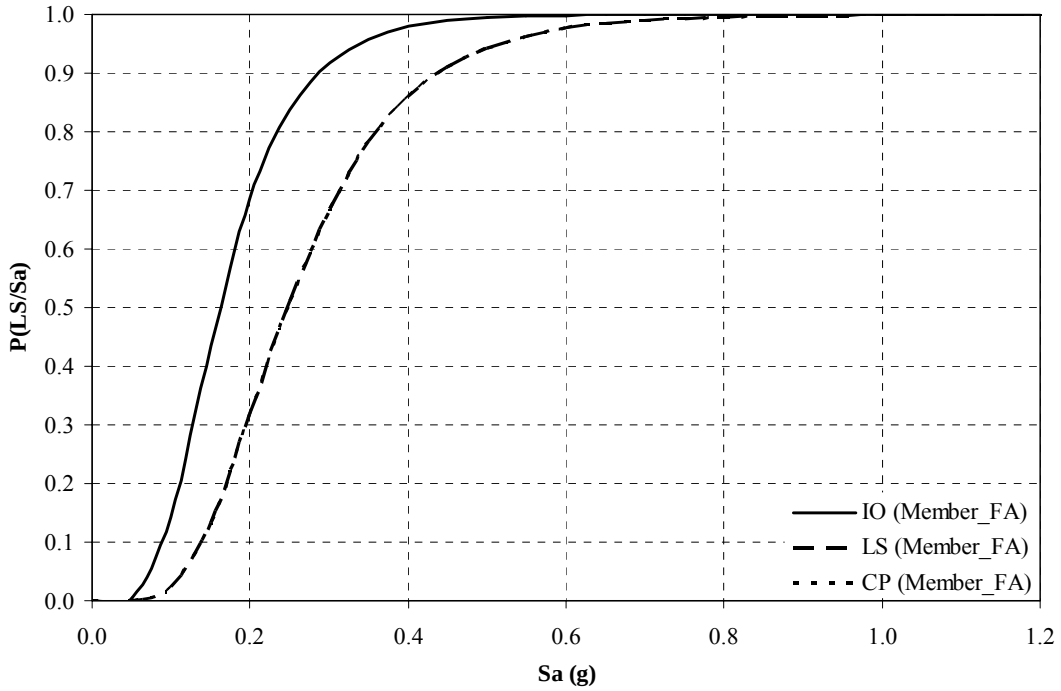

(c) Retrofit 2: Addition of RC column jackets

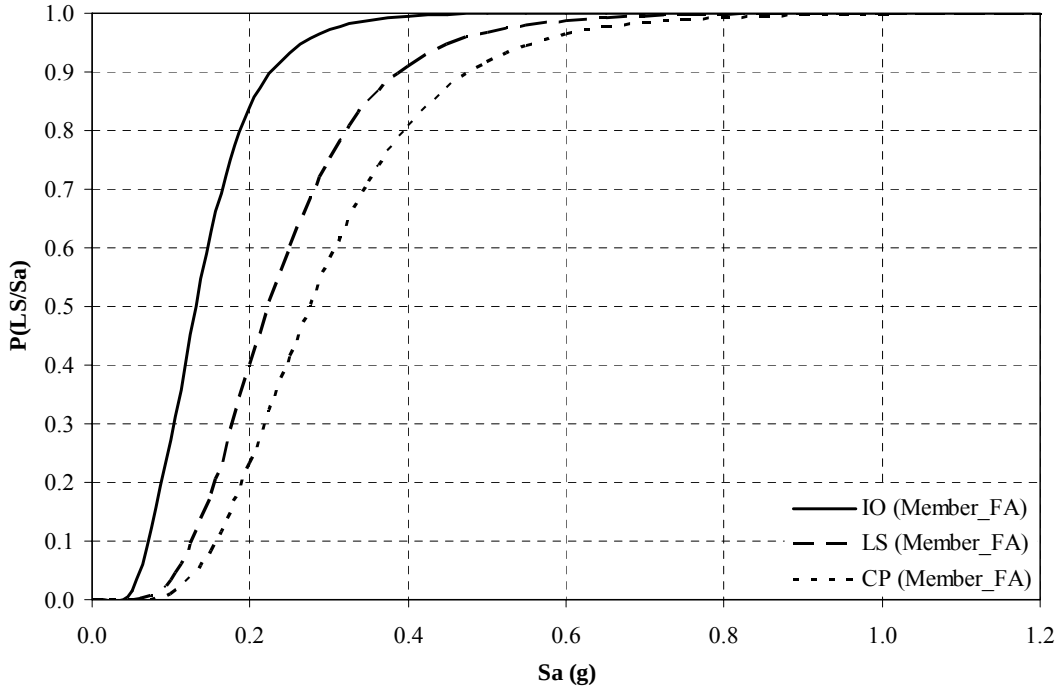

(d) Retrofit 3: Confinement of column plastic hinge zones

Fig. 7.10. Continued

As shown in Fig. 7.10, the probabilities of exceeding each limit state were reduced by all of the retrofits. In particular, the shear wall retrofit (Retrofit 1) has the greatest impact in reducing the probability of exceeding each limit state for lower values of spectral acceleration.

7.3.2.3 Combination of Atkinson and Boore Model and Frankel et al. Model

Fig. 7.11 shows the member-level fragility curves for each unretrofitted and retrofitted structure based on the Rix and Fernandez-Leon motions derived from both the Atkinson and Boore source model and the Frankel et al. source model. The results from the magnitude of 7.5 Frankel et al. motions for the unretrofitted, Retrofit 2 and Retrofit 3 cases are not included based on the global-level seismic evaluation.

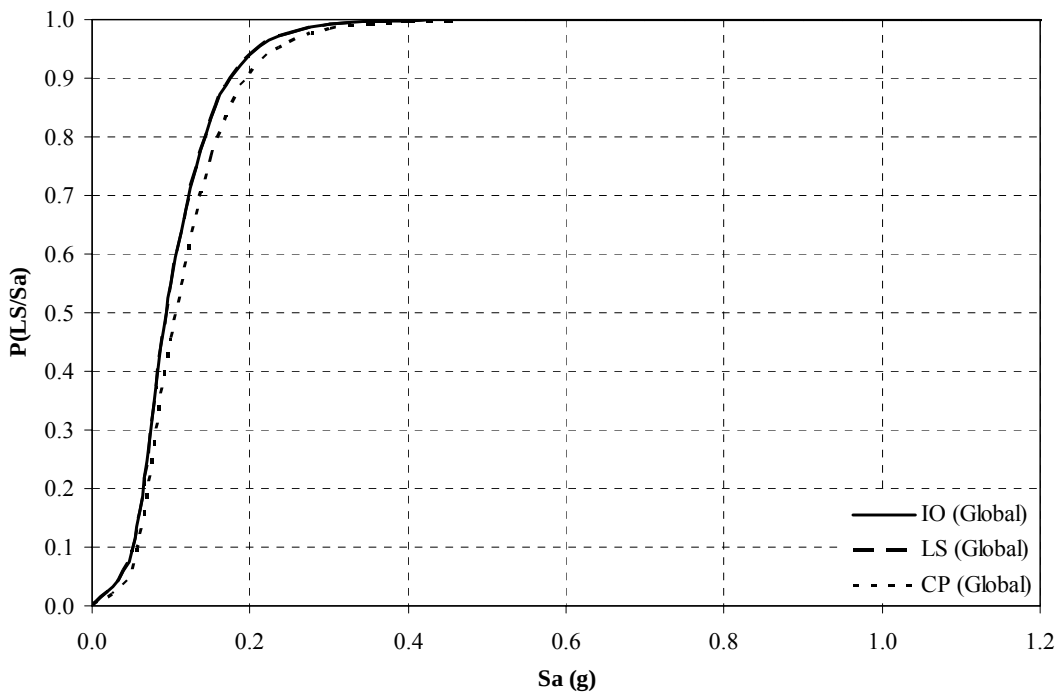

(a) Unretrofitted structure

Fig. 7.11. Member-level fragility curves (Rix and Fernandez-Leon motions - Atkinson and Boore model and Frankel et al. model)

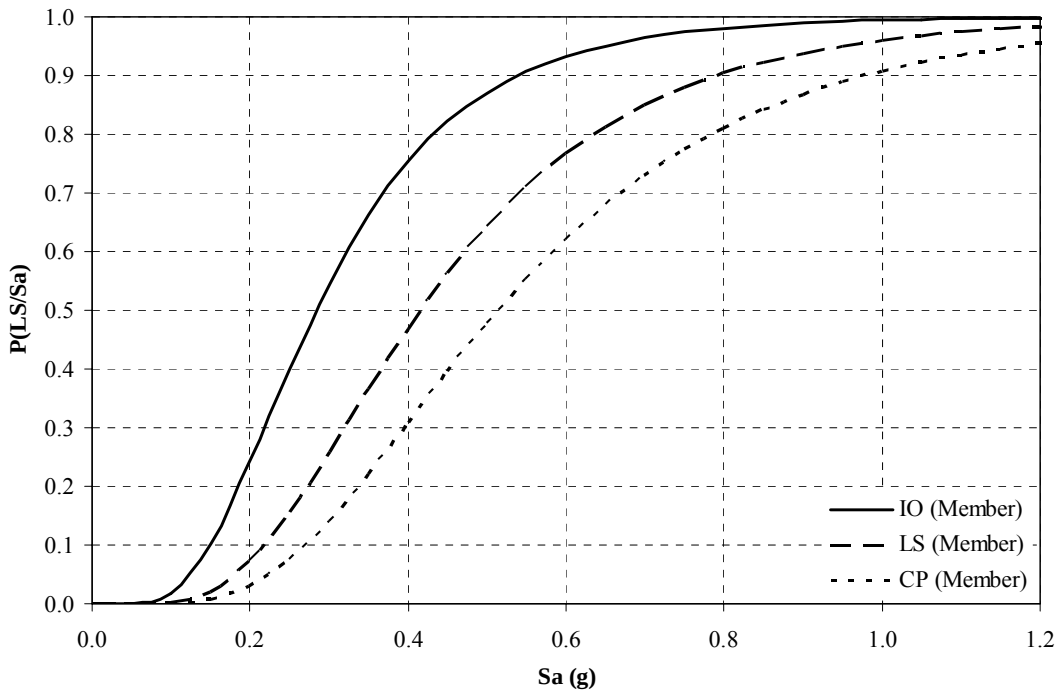

(b) Retrofit 1: Addition of shear walls

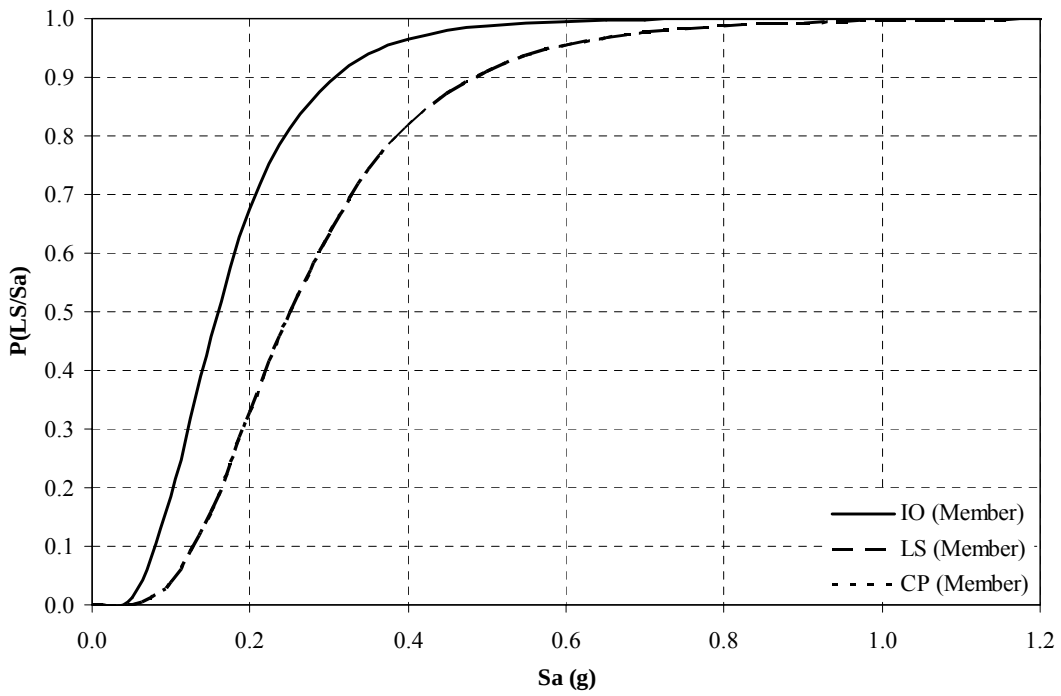

(c) Retrofit 2: Addition of RC column jackets

Fig. 7.11. Continued

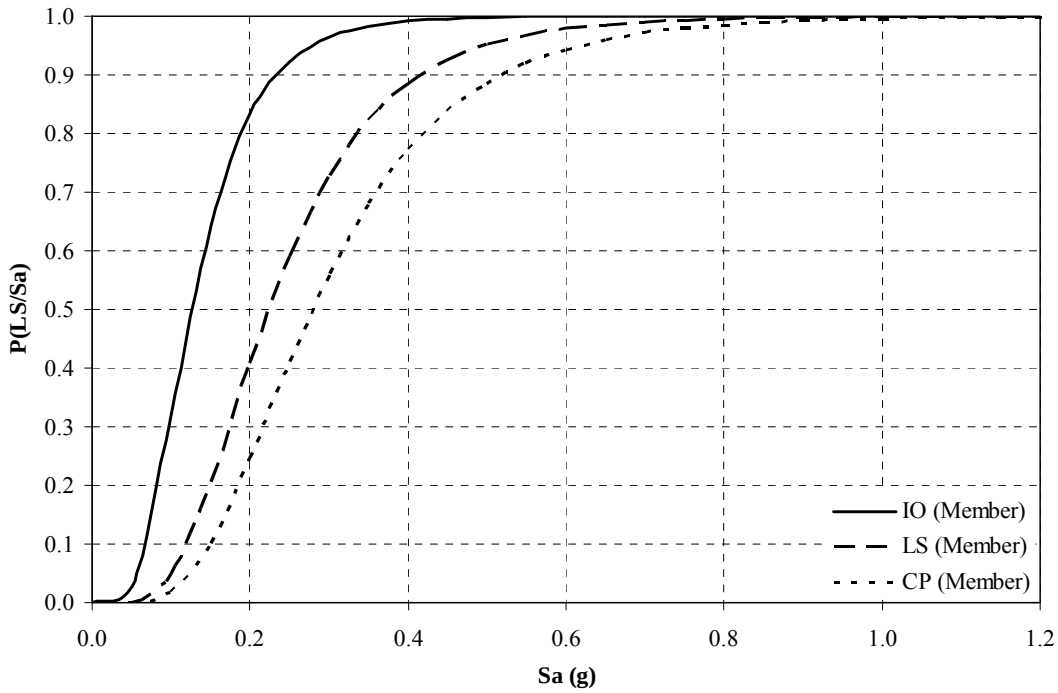

(d) Retrofit 3: Confinement of column plastic hinge zones

Fig. 7.11. Continued

Fig. 7.12 shows a comparison of the fragility curves using peak ground acceleration for each limit state based on FEMA 356 member-level criteria with a critical response push-over analysis. As shown in Fig. 7.12, the probabilities of exceeding each limit state for each retrofitted structure were reduced. The greatest reduction for the CP limit state was observed for the shear wall retrofit, followed by the RC column jacketing retrofit and the retrofit involving confinement of column plastic hinge zones.

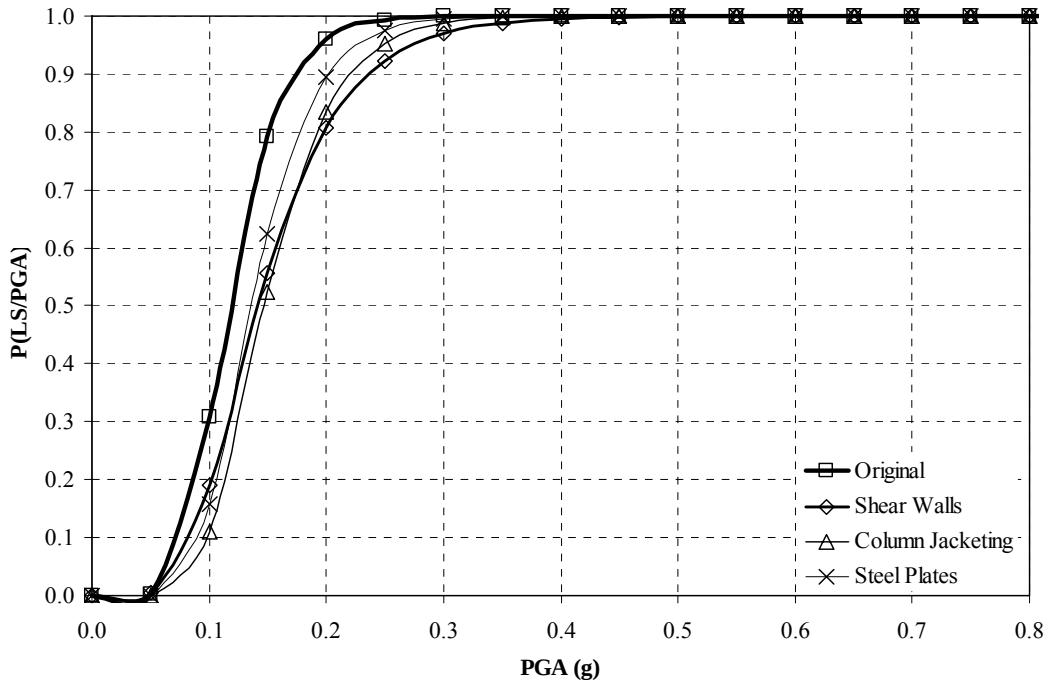

(a) IO Limit State

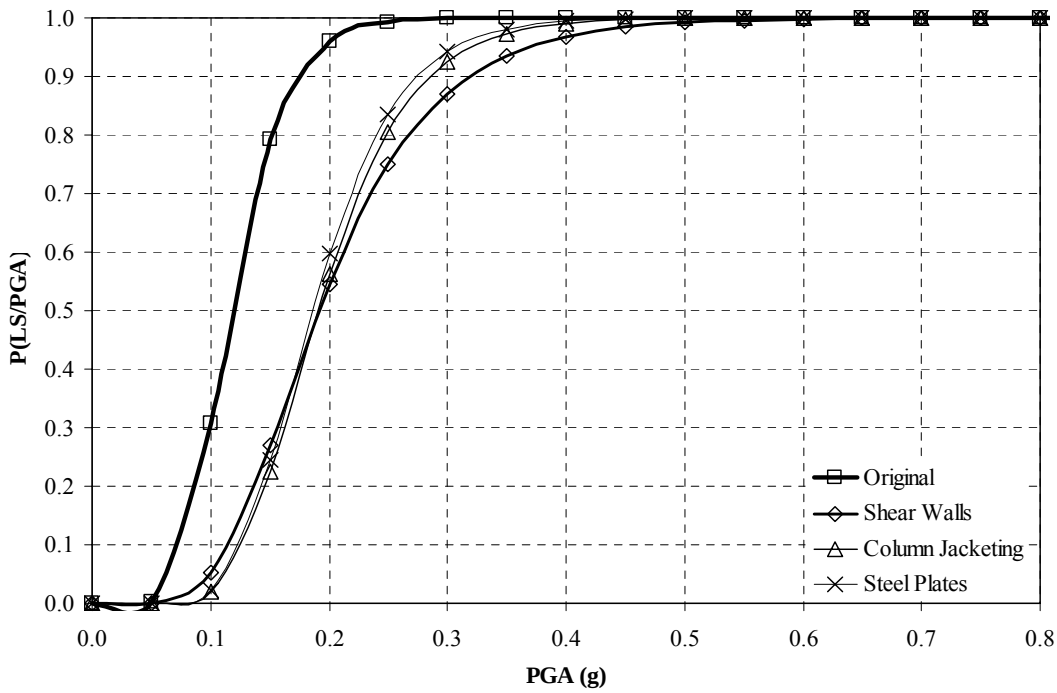

(b) LS Limit State

Fig. 7.12. Comparisons of FEMA member-level fragility curves (Rix and Fernandez-Leon motions - Atkinson and Boore model and Frankel et al. model)

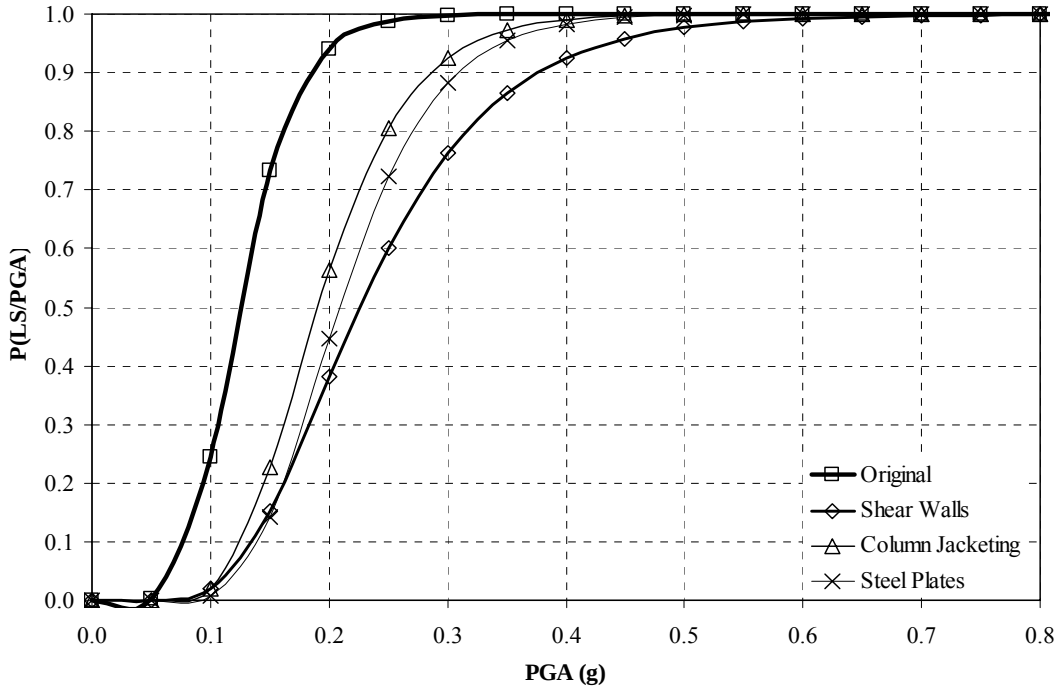

(c) CP Limit State

Fig. 7.12. Continued

7.3.3 Additional Quantitative Limits

The fragility curves based on the quantitative limits for the Rix and Fernandez-Leon motions were developed based on the drift capacities summarized in Table 6.17. For more comparisons, fragility curves were developed for each source model used to develop the Rix and Fernandez-Leon motions separately and also for the two combined.

7.3.3.1 Atkinson and Boore Model

Fig. 7.13 shows the fragility curves derived for the additional quantitative limits for each unretrofitted and retrofitted structure using the Rix and Fernandez-Leon motions based on the Atkinson and Boore source model.

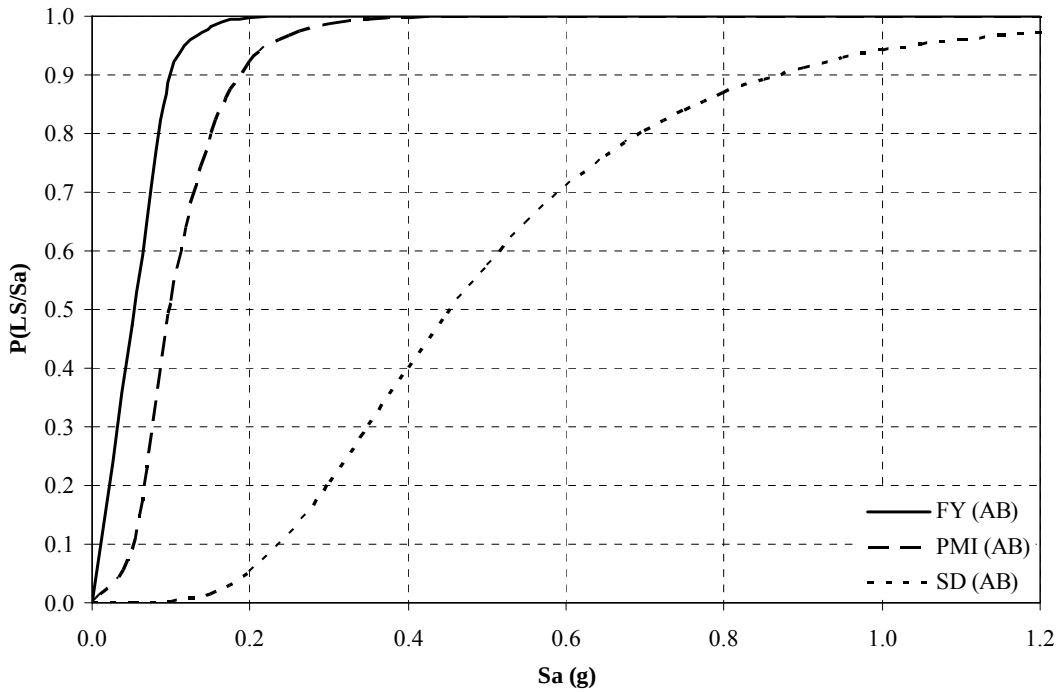

(a) Unretrofitted structure

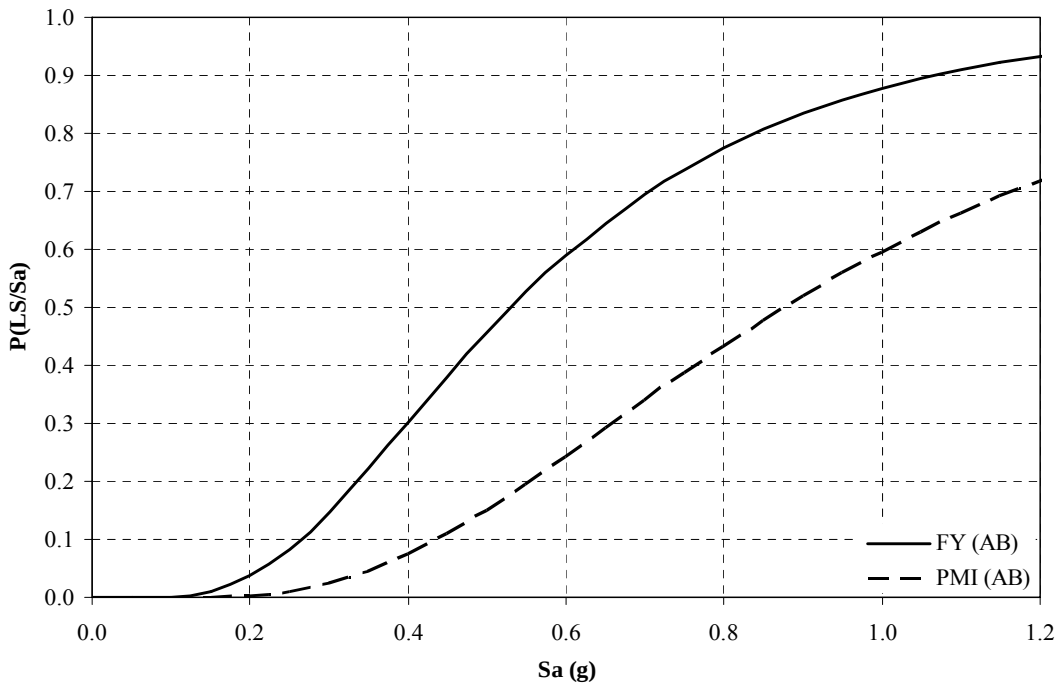

(b) Retrofit 1: Addition of shear walls

Fig. 7.13. Fragility curves based on additional quantitative limits (Rix and Fernandez-Leon motions - Atkinson and Boore model)

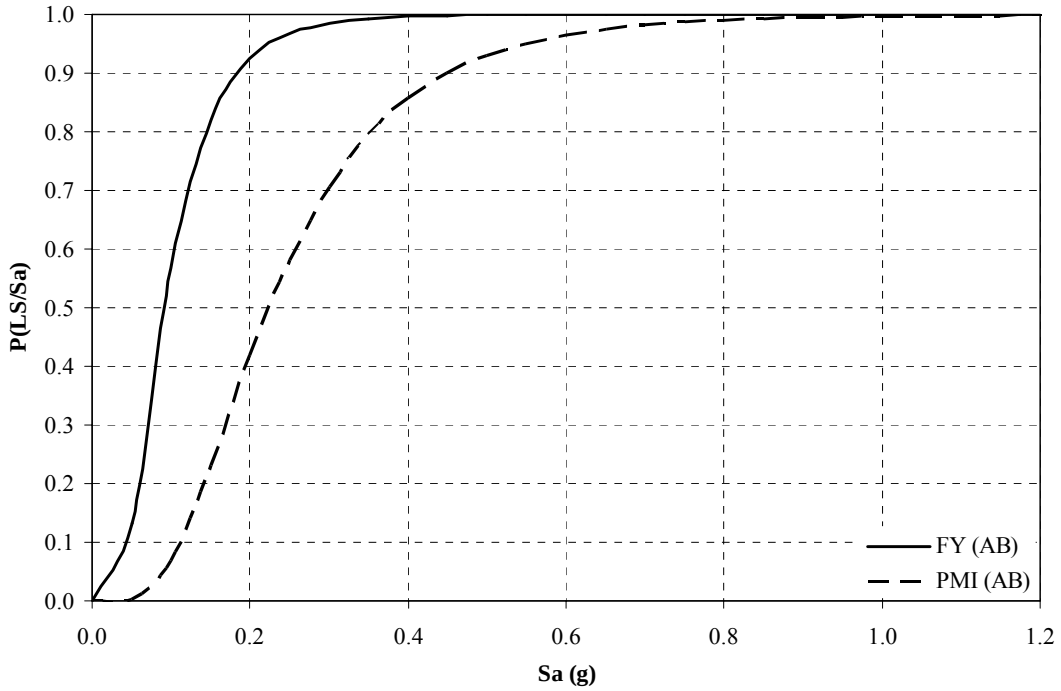

(c) Retrofit 2: Addition of RC column jackets

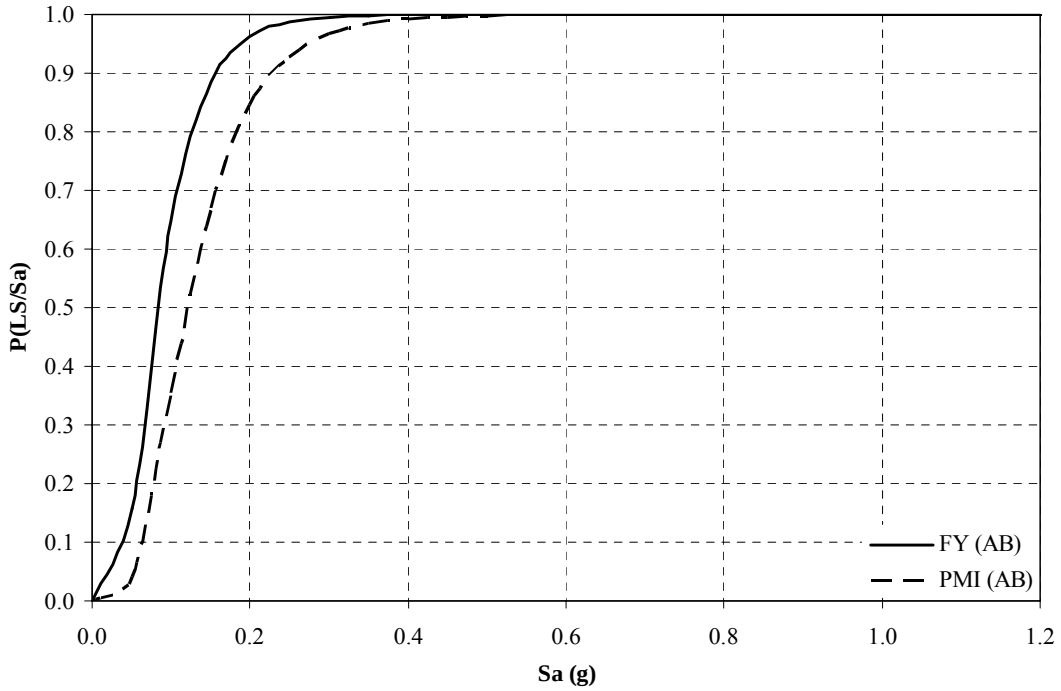

(d) Retrofit 3: Confinement of column plastic hinge zones

Fig. 7.13. Continued

As shown in Fig. 7.13, the probabilities of exceeding FY and PMI limit states for the addition of shear walls were reduced significantly up to the spectral acceleration of 1.2.

7.3.3.2 Frankel et al. Model

Fig. 7.14 shows the fragility curves derived for the additional quantitative limits for each unretrofitted and retrofitted structure using the Rix and Fernandez-Leon motions based on the Frankel et al. source model. Based on the global-level seismic evaluation, the results from the magnitude 7.5 Frankel et al. motions were excluded for the unretrofitted, Retrofit 2 and Retrofit 3 cases.

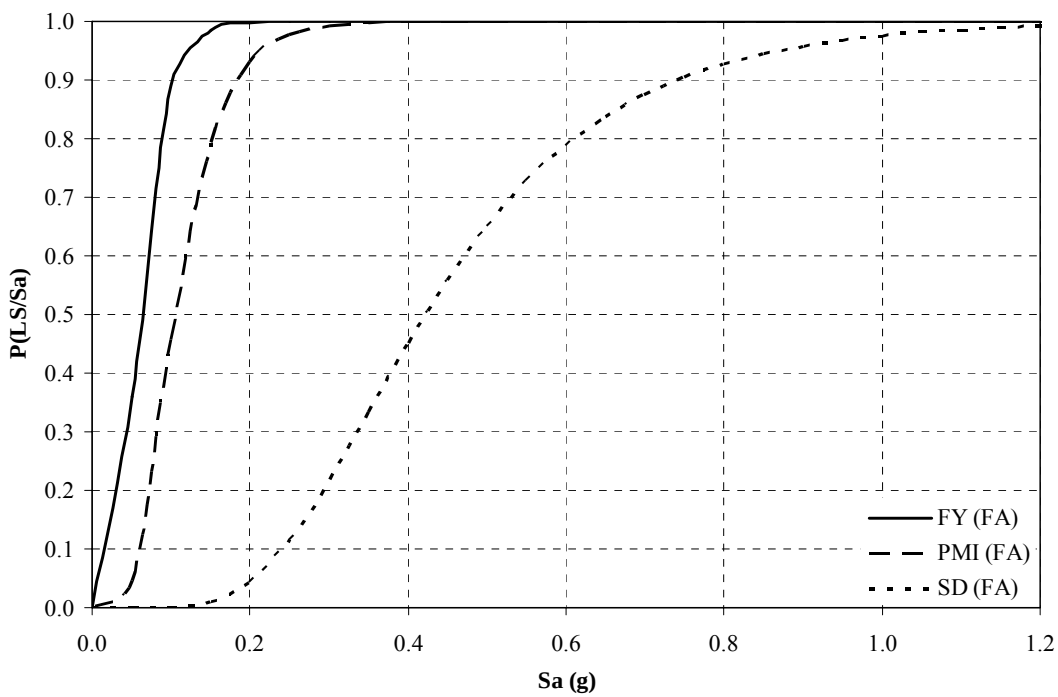

(a) Unretrofitted structure

Fig. 7.14. Fragility curves based on additional quantitative limits (Rix and Fernandez-Leon motions - Frankel et al. model)

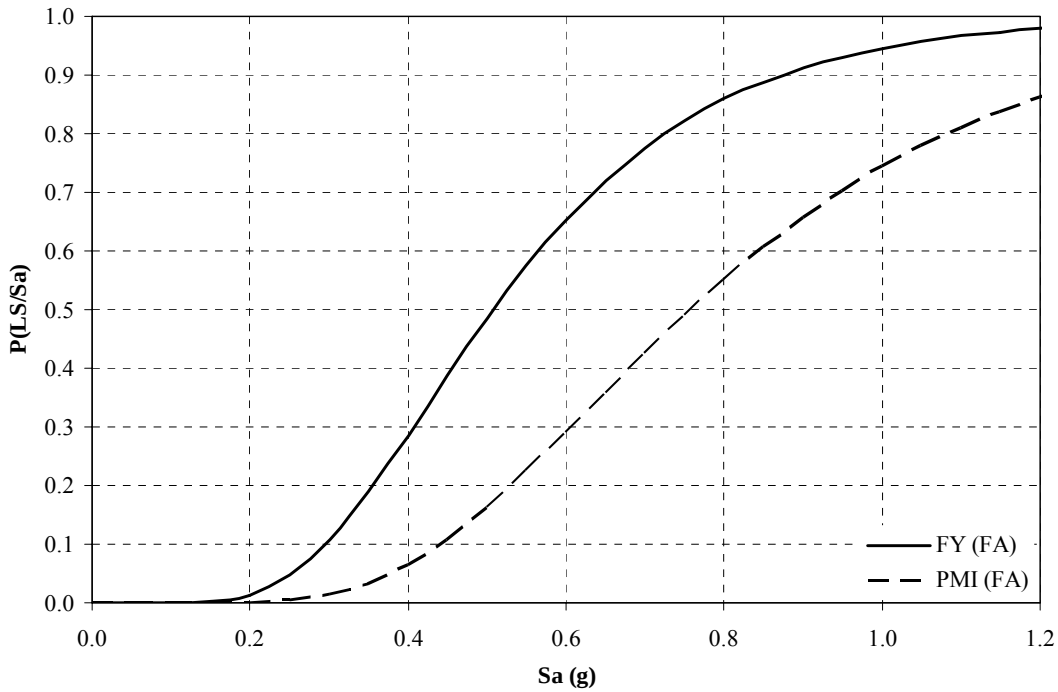

(b) Retrofit 1: Addition of shear walls

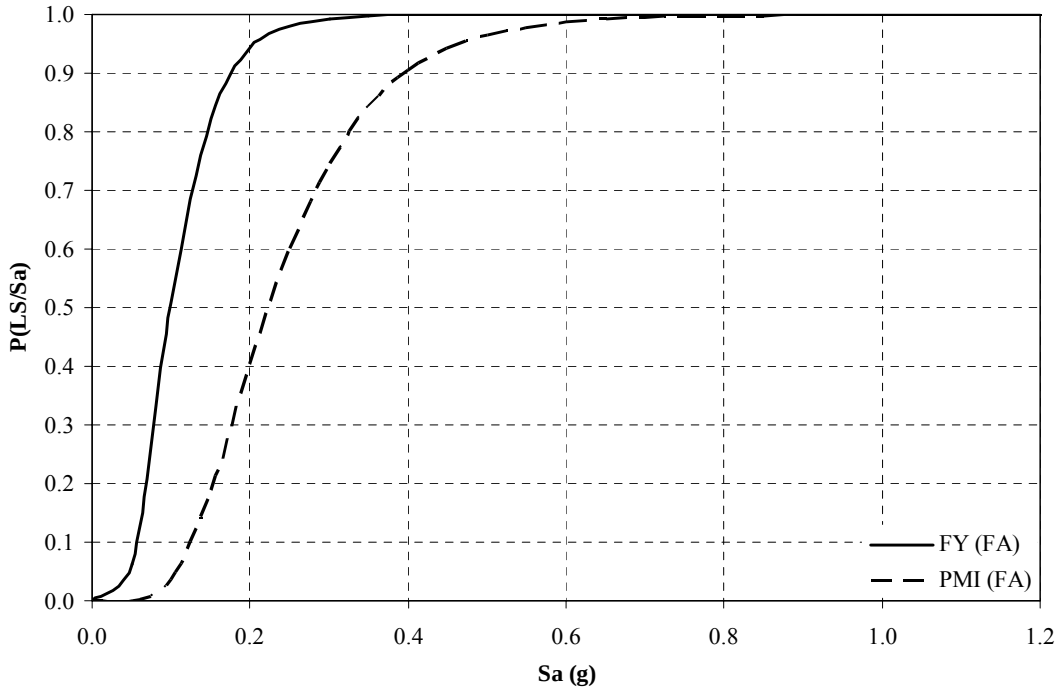

(c) Retrofit 2: Addition of RC column jackets

Fig. 7.14. Continued

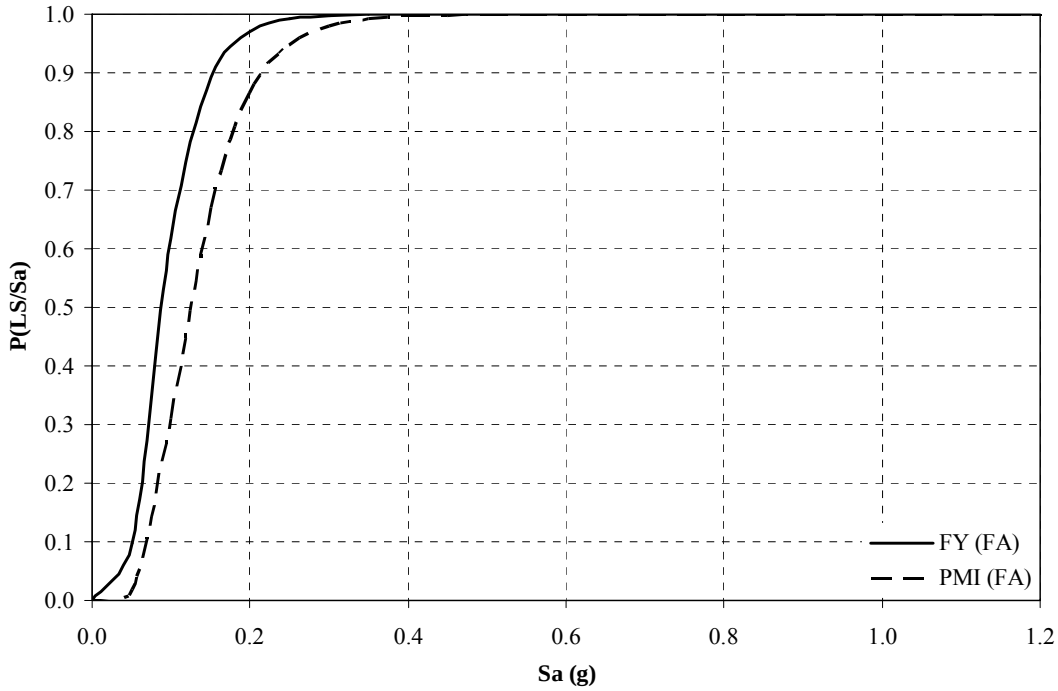

(d) Retrofit 3: Confinement of column plastic hinge zones

Fig. 7.14. Continued

As shown in Fig. 7.14, the probabilities of exceeding FY and PMI limit states for the addition of shear walls were reduced significantly for spectral acceleration up to 1.2.

7.3.3.3 Combination of Atkinson and Boore Model and Frankel et al. Model

Fig. 7.15 shows the fragility curves based on the additional quantitative limits for each unretrofitted and retrofitted structure for the Rix and Fernandez-Leon motions developed using both the Atkinson and Boore source model and Frankel et al. source model. The results from the magnitude 7.5 Frankel et al. motions for the unretrofitted, Retrofit 2 and Retrofit 3 cases were not included based on the global-level seismic evaluation. As shown in Fig. 7.15, the probabilities of exceeding FY and PMI limit states for the addition of shear walls were reduced significantly for spectral acceleration up to 1.2.

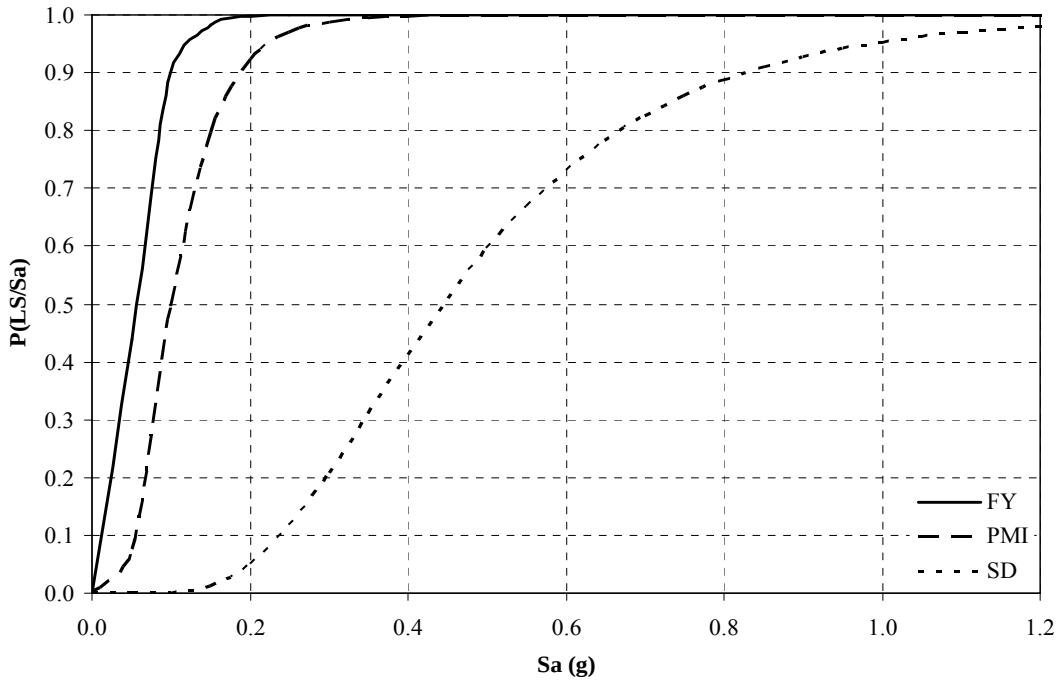

(a) Unretrofitted structure

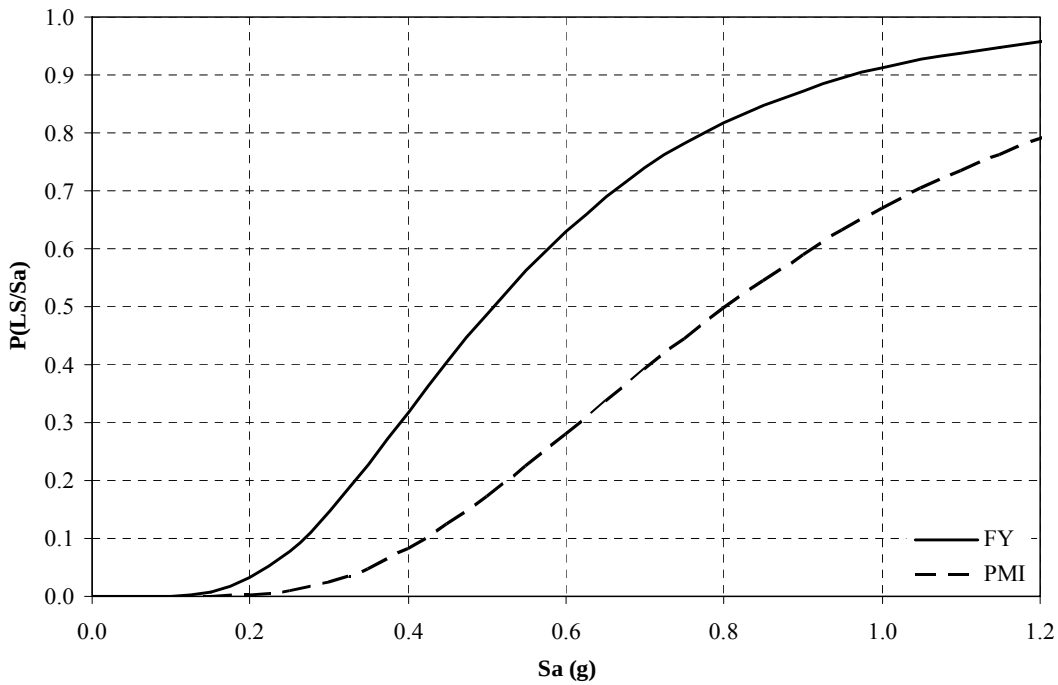

(b) Retrofit 1: Addition of shear walls

Fig. 7.15. Fragility curves based on additional quantitative limits (Rix and Fernandez-Leon motions - Atkinson and Boore model and Frankel et al. model)

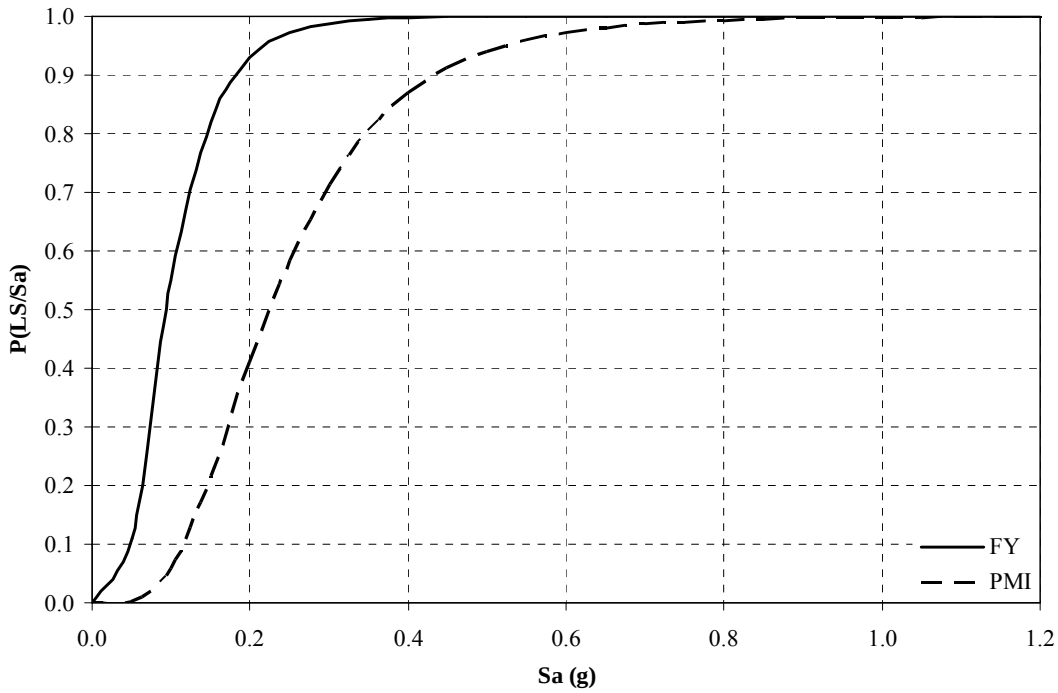

(c) Retrofit 2: Addition of RC column jackets

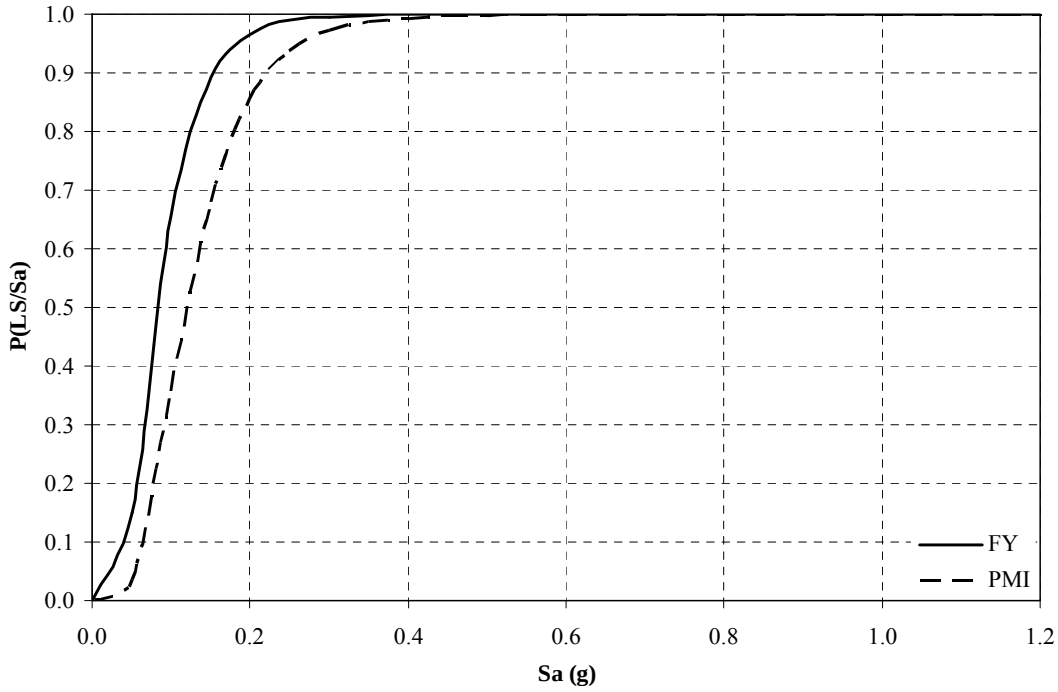

(d) Retrofit 3: Confinement of column plastic hinge zones

Fig. 7.15. Continued

Fig. 7.16 shows the fragility curves for each limit state based on the additional quantitative limits with a critical response push-over analysis. As shown in Fig. 7.16, the probabilities of exceeding each limit state for each retrofitted structure were reduced.

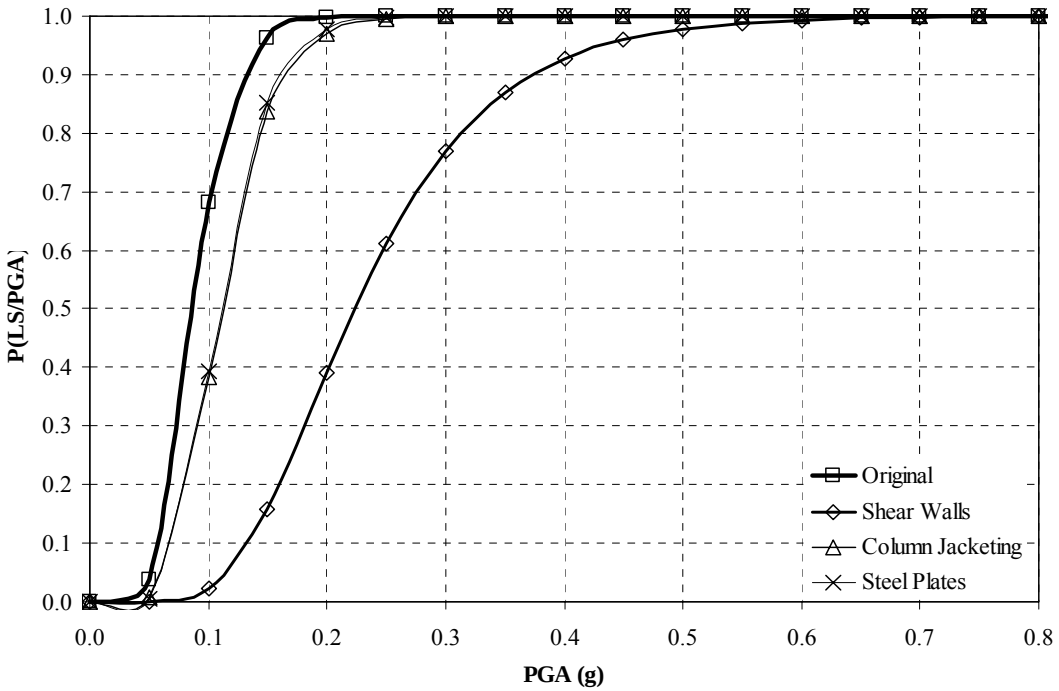

(a) FY Limit State

Fig. 7.16. Comparisons of fragility curves based on additional quantitative limits (Rix and Fernandez-Leon motions - Atkinson and Boore model and Frankel et al. model)

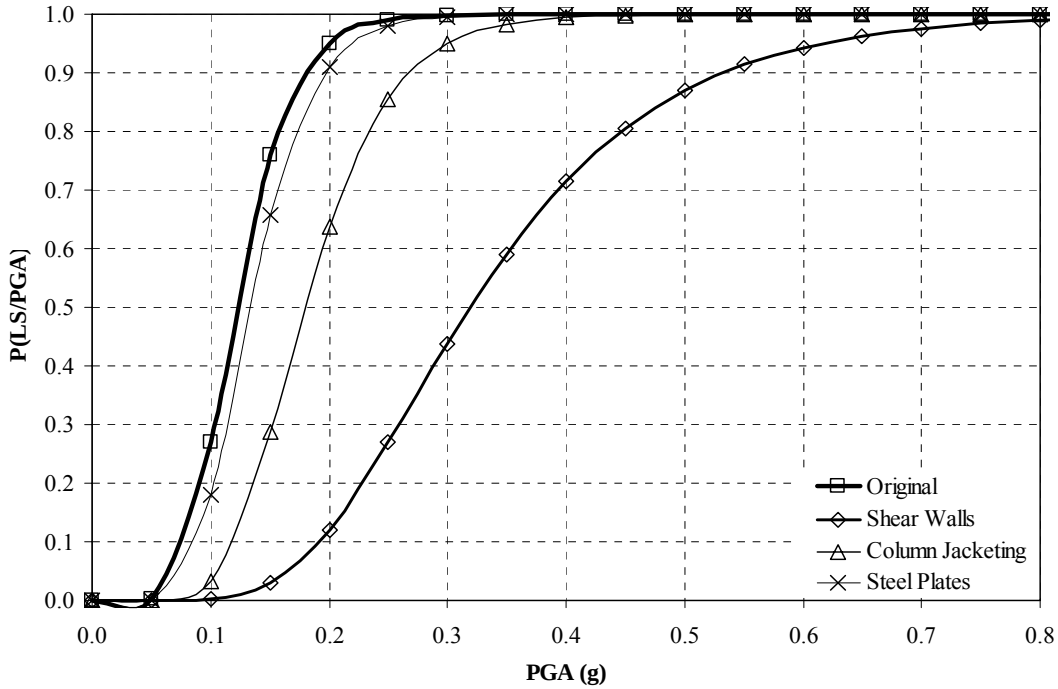

(b) PMI Limit State

Fig. 7.16. Continued

As shown in Fig. 7.16, for both cases of FY and PMI limit states, the probabilities of exceeding each limit state for retrofitted structures were reduced significantly for peak ground accelerations up to 0.8. In particular, the shear wall retrofit (Retrofit 1) has the greatest impact in reducing the probability of exceeding all the limit states.

For the comparison between the Wen and Wu motions and the Rix and Fernandez-Leon motions, the Rix and Fernandez-Leon motions provide lower probabilities of exceeding each limit state. For the two different source models used to develop the Rix and Fernandez-Leon motions, there are significant differences in seismic fragility. Therefore, for further analysis, fragility curves were determined using the ground motions from both source models to minimize uncertainties from the ground motion data.

7.4 MAEviz Implementation

7.4.1 General

MAEviz (ALG 2004) is a risk assessment tool developed by the MAE Center that provides useful information for decision makers. The objective of this program is to provide damage synthesis for use in earthquake risk assessment through interactive visualization technology. To present a damage estimation for a specific region, this program integrates tools and results from MAE Center research projects including GIS data, ground motion data, inventory data of structures and fragility relationships for unretrofitted and retrofitted structures. MAEviz follows the CBE methodology to estimate structural damage and seismic losses including impacts on transportation networks, social, and economic systems.

7.4.2 Methodology

To reduce the number of parameters to define the fragility curves, the following equation was used for describing the fragility curves for input to MAEviz.

$$P\left(LS \middle| S_a\right) = \Phi\left(\frac{\ln S_a - \lambda_C}{\beta_C}\right) \tag{7.1}$$

where:

$P\left(LS \middle| S_a\right)$ = Probability of exceeding a limit state given a spectral acceleration value

Φ = Standard normal cumulative distribution function

S_a = Spectral acceleration

λ_C , β_C = Modification parameters

Because this relationship is different from the original formulation in Eq. 5.4, two modification parameters were used to match the original fragility curves. The first parameter, λ_C, is used to adjust the MAEViz curve such that it matches the original curve at the point for 50% of probability of exceedance for the limit state of concern. The second parameter, β_C, defines the slope of the fragility curve to match the original fragility curve.

7.4.3 Fragility Curve Parameters

As an example, the fragility curve for the unretrofitted structure developed using the MAEviz implementation methodology is shown in Fig. 7.17. In this figure, the corresponding fragility curves for each limit state closely match and overlap one another, as desired. The modification parameters derived for Eq. 7.1 are provided in Tables 7.2 to 7.5 for all the fragility curves with spectral acceleration and PGA based on the Wen and Wu motions and the Rix and Fernandez-Leon motions using both source models, respectively. Figs. 7.18 to 7.19 show the fragility curves using spectral acceleration for MAEviz implementation based on the analysis using the Wen and Wu motions and the Rix and Fernandez-Leon motions. In addition, Figs. 7.20 to 7.25 show the fragility curves using PGA for MAEviz implementation based on the analysis using the Wen and Wu motions and the Rix and Fernandez-Leon motions.

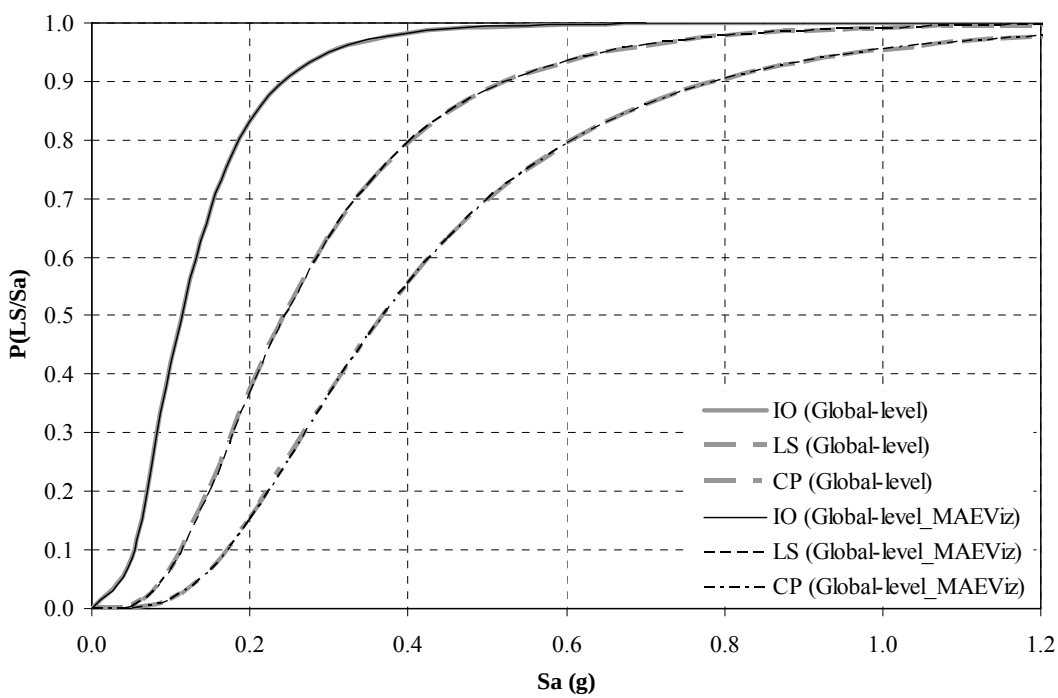

Fig. 7.17. Comparisons of original fragility curves with fragility curves expressions used in MAEviz

Table 7.2. Fragility curve parameters using spectral acceleration for MAEviz implementation (Wen and Wu motions)

Structure	Limit State	λ_C	β_C
Unretrofitted structure	IO (Global-Level)	-2.18	0.593
	LS (Global-Level)	-1.41	
	CP (Global-Level)	-0.998	
	IO (Member-Level, Critical)	-2.73	
	LS (Member-Level, Critical)	-2.73	
	CP (Member-Level, Critical)	-2.60	
	FY (Quantitative, Critical)	-3.33	
	PMI (Quantitative, Critical)	-2.66	
	SD (Quantitative, Critical)	-1.03	
Retrofit 1: Addition of shear walls	IO (Global-Level)	-1.25	0.600
	LS (Global-Level)	-0.540	
	CP (Global-Level)	-0.0900	
	IO (Member-Level, Critical)	-1.54	
	LS (Member-Level, Critical)	-1.00	
	CP (Member-Level, Critical)	-0.700	
	FY (Quantitative, Critical)	-0.730	
	PMI (Quantitative, Critical)	-0.0900	
Retrofit 2: Addition of RC column jackets	IO (Global-Level)	-1.86	0.605
	LS (Global-Level)	-0.980	
	CP (Global-Level)	-0.530	
	IO (Member-Level, Critical)	-2.03	
	LS (Member-Level, Critical)	-1.47	
	CP (Member-Level, Critical)	-1.47	
	FY (Quantitative, Critical)	-2.65	
	PMI (Quantitative, Critical)	-1.61	
Retrofit 3: Confinement of column plastic hinge zones	IO (Global-Level)	-2.19	0.598
	LS (Global-Level)	-1.39	
	CP (Global-Level)	-0.990	
	IO (Member-Level, Critical)	-2.40	
	LS (Member-Level, Critical)	-1.75	
	CP (Member-Level, Critical)	-1.51	
	FY (Quantitative, Critical)	-2.84	
	PMI (Quantitative, Critical)	-2.44	

Table 7.3. Fragility curve parameters using PGA for MAEviz implementation (Wen and Wu motions)

Structure	Limit State	λ_C	β_C
Unretrofitted structure	IO (Global-Level)	-1.73	0.350
	LS (Global-Level)	-1.28	
	CP (Global-Level)	-1.05	
	IO (Member-Level, Critical)	-2.03	
	LS (Member-Level, Critical)	-2.03	
	CP (Member-Level, Critical)	-1.96	
	FY (Quantitative, Critical)	-2.38	
	PMI (Quantitative, Critical)	-1.99	
	SD (Quantitative, Critical)	-1.06	
Retrofit 1: Addition of shear walls	IO (Global-Level)	-1.84	0.510
	LS (Global-Level)	-1.26	
	CP (Global-Level)	-0.900	
	IO (Member-Level, Critical)	-2.08	
	LS (Member-Level, Critical)	-1.63	
	CP (Member-Level, Critical)	-1.40	
	FY (Quantitative, Critical)	-1.41	
	PMI (Quantitative, Critical)	-0.890	
Retrofit 2: Addition of RC column jackets	IO (Global-Level)	-1.61	0.460
	LS (Global-Level)	-1.05	
	CP (Global-Level)	-0.750	
	IO (Member-Level, Critical)	-1.73	
	LS (Member-Level, Critical)	-1.36	
	CP (Member-Level, Critical)	-1.36	
	FY (Quantitative, Critical)	-2.14	
	PMI (Quantitative, Critical)	-1.45	
Retrofit 3: Confinement of column plastic hinge zones	IO (Global-Level)	-1.72	0.350
	LS (Global-Level)	-1.27	
	CP (Global-Level)	-1.03	
	IO (Member-Level, Critical)	-1.84	
	LS (Member-Level, Critical)	-1.48	
	CP (Member-Level, Critical)	-1.34	
	FY (Quantitative, Critical)	-2.09	
	PMI (Quantitative, Critical)	-1.87	

Table 7.4. Fragility curve parameters using spectral acceleration for MAEviz implementation (Rix and Fernandez-Leon motions using both source models)

Structure	Limit State	λ_C	β_C
Unretrofitted structure	IO (Global-Level)	-1.88	0.485
	LS (Global-Level)	-1.16	
	CP (Global-Level)	-0.78	
	IO (Member-Level, Critical)	-2.36	
	LS (Member-Level, Critical)	-2.36	
	CP (Member-Level, Critical)	-2.25	
	FY (Quantitative, Critical)	-2.92	
	PMI (Quantitative, Critical)	-2.3	
	SD (Quantitative, Critical)	-0.81	
Retrofit 1: Addition of shear walls	IO (Global-Level)	-1.05	0.505
	LS (Global-Level)	-0.550	
	CP (Global-Level)	-0.220	
	IO (Member-Level, Critical)	-1.26	
	LS (Member-Level, Critical)	-0.875	
	CP (Member-Level, Critical)	-0.665	
	FY (Quantitative, Critical)	-0.680	
	PMI (Quantitative, Critical)	-0.220	
Retrofit 2: Addition of RC column jackets	IO (Global-Level)	-1.7	0.513
	LS (Global-Level)	-0.985	
	CP (Global-Level)	-0.608	
	IO (Member-Level, Critical)	-1.84	
	LS (Member-Level, Critical)	-1.38	
	CP (Member-Level, Critical)	-1.38	
	FY (Quantitative, Critical)	-2.37	
	PMI (Quantitative, Critical)	-1.49	
Retrofit 3: Confinement of column plastic hinge zones	IO (Global-Level)	-1.88	0.480
	LS (Global-Level)	-1.17	
	CP (Global-Level)	-0.802	
	IO (Member-Level, Critical)	-2.07	
	LS (Member-Level, Critical)	-1.49	
	CP (Member-Level, Critical)	-1.28	
	FY (Quantitative, Critical)	-2.49	
	PMI (Quantitative, Critical)	-2.12	

Table 7.5. Fragility curve parameters using PGA for MAEviz implementation (Rix and Fernandez-Leon motions using both source models)

Structure	Limit State	λ_C	β_C
Unretrofitted structure	IO (Global-Level)	-1.89	0.310
	LS (Global-Level)	-1.50	
	CP (Global-Level)	-1.30	
	IO (Member-Level, Critical)	-2.15	
	LS (Member-Level, Critical)	-2.15	
	CP (Member-Level, Critical)	-2.09	
	FY (Quantitative, Critical)	-2.45	
	PMI (Quantitative, Critical)	-2.12	
	SD (Quantitative, Critical)	-1.32	
Retrofit 1: Addition of shear walls	IO (Global-Level)	-1.79	0.400
	LS (Global-Level)	-1.39	
	CP (Global-Level)	-1.14	
	IO (Member-Level, Critical)	-1.95	
	LS (Member-Level, Critical)	-1.65	
	CP (Member-Level, Critical)	-1.49	
	FY (Quantitative, Critical)	-1.50	
	PMI (Quantitative, Critical)	-1.14	
Retrofit 2: Addition of RC column jackets	IO (Global-Level)	-1.84	0.320
	LS (Global-Level)	-1.44	
	CP (Global-Level)	-1.23	
	IO (Member-Level, Critical)	-1.92	
	LS (Member-Level, Critical)	-1.66	
	CP (Member-Level, Critical)	-1.66	
	FY (Quantitative, Critical)	-2.21	
	PMI (Quantitative, Critical)	-1.72	
Retrofit 3: Confinement of column plastic hinge zones	IO (Global-Level)	-1.89	0.320
	LS (Global-Level)	-1.52	
	CP (Global-Level)	-1.31	
	IO (Member-Level, Critical)	-2.00	
	LS (Member-Level, Critical)	-1.69	
	CP (Member-Level, Critical)	-1.57	
	FY (Quantitative, Critical)	-2.23	
	PMI (Quantitative, Critical)	-2.02	

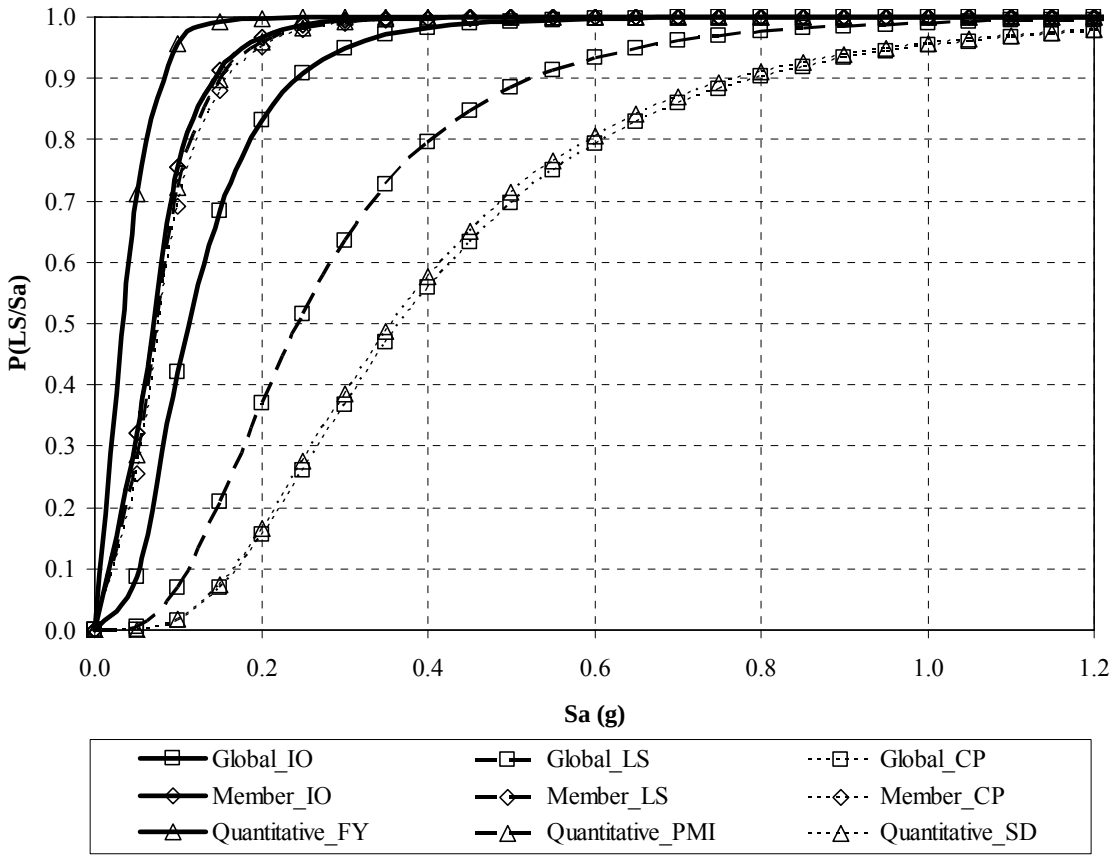

(a) Unretrofitted structure

Fig. 7.18. Fragility curves using spectral acceleration for MAEviz implementation based on Wen and Wu motions

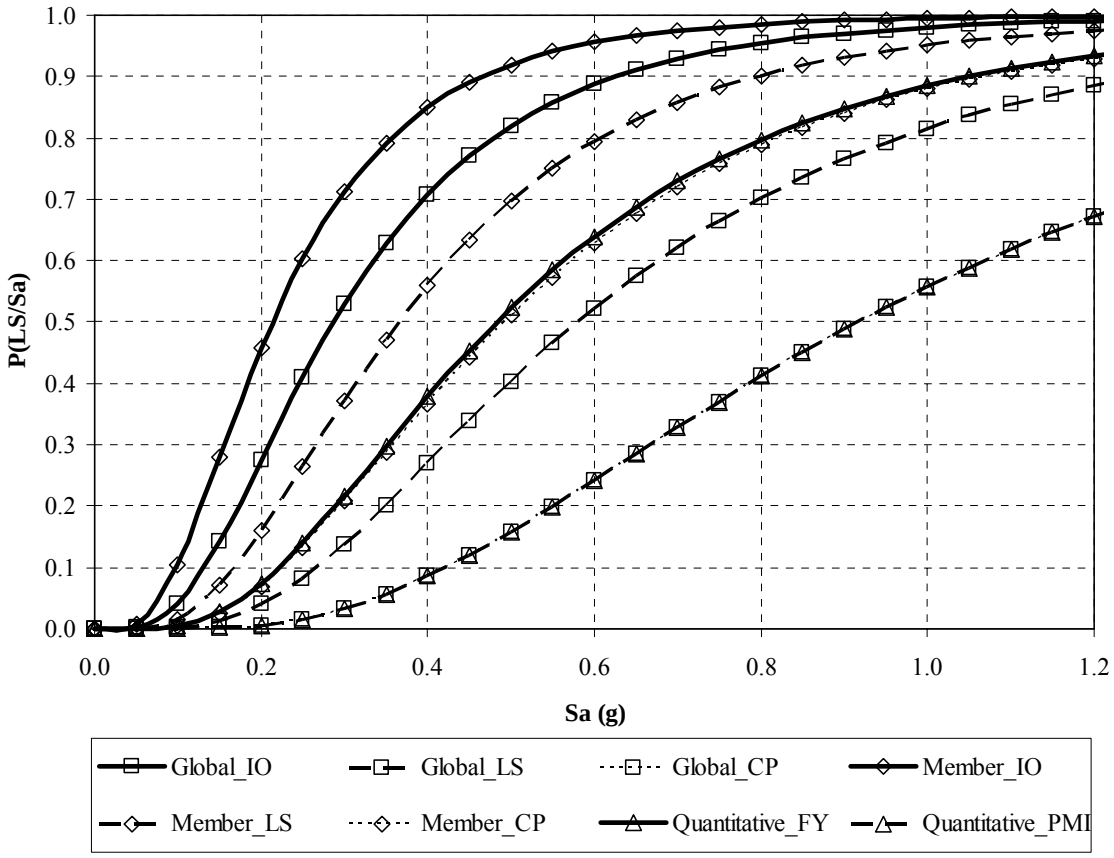

(b) Retrofit 1: Addition of shear walls

Fig. 7.18. Continued

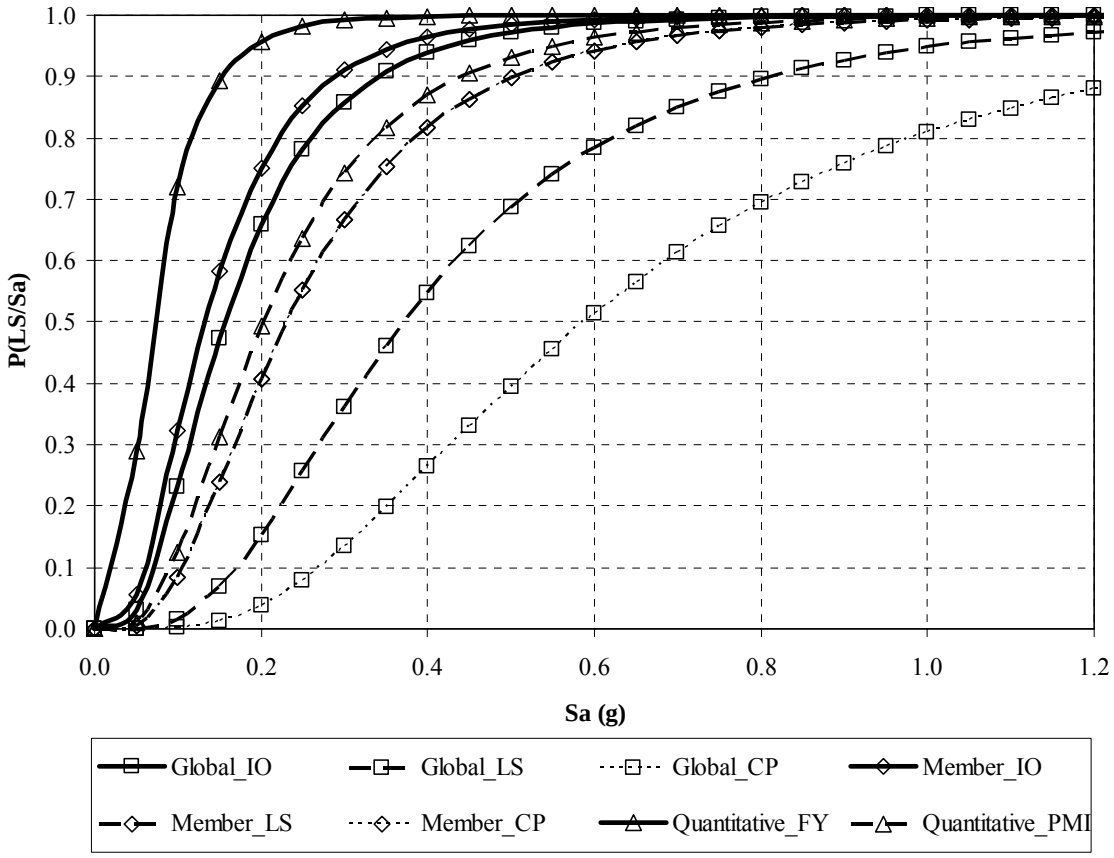

(c) Retrofit 2: Addition of RC column jackets

Fig. 7.18. Continued

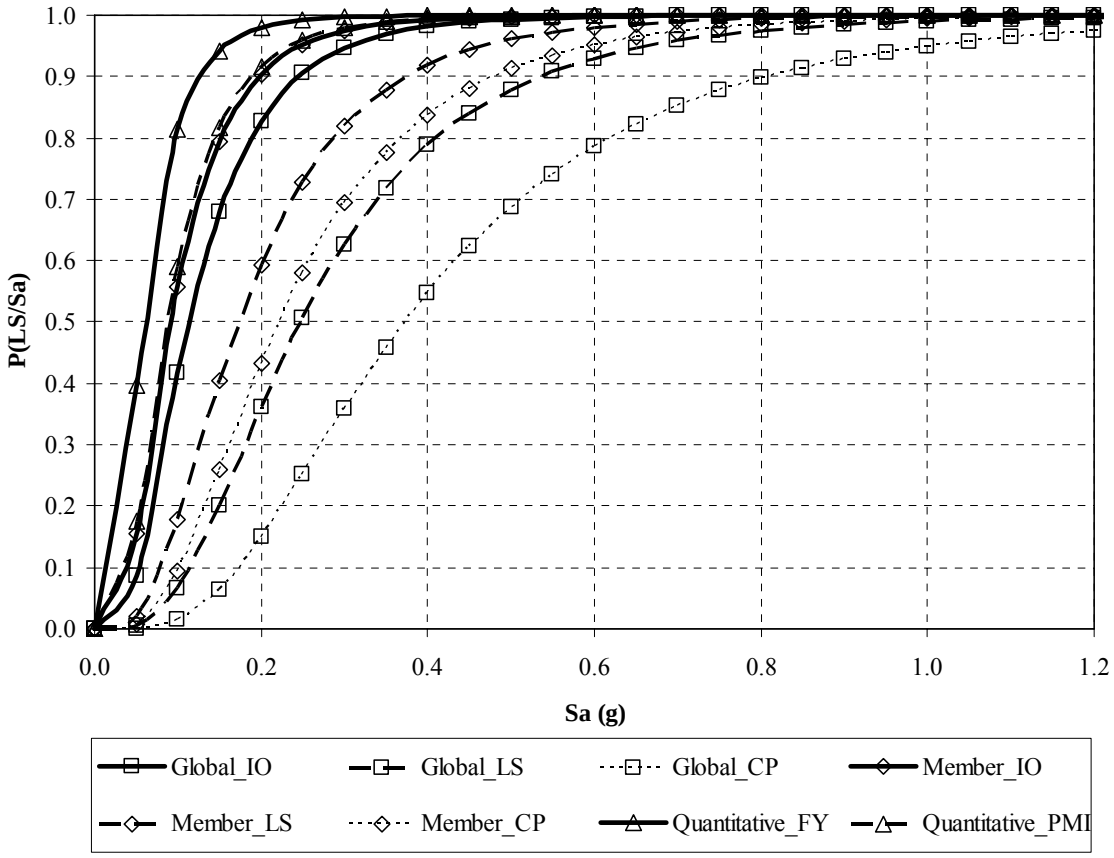

(d) Retrofit 3: Confinement of column plastic hinge zones

Fig. 7.18. Continued

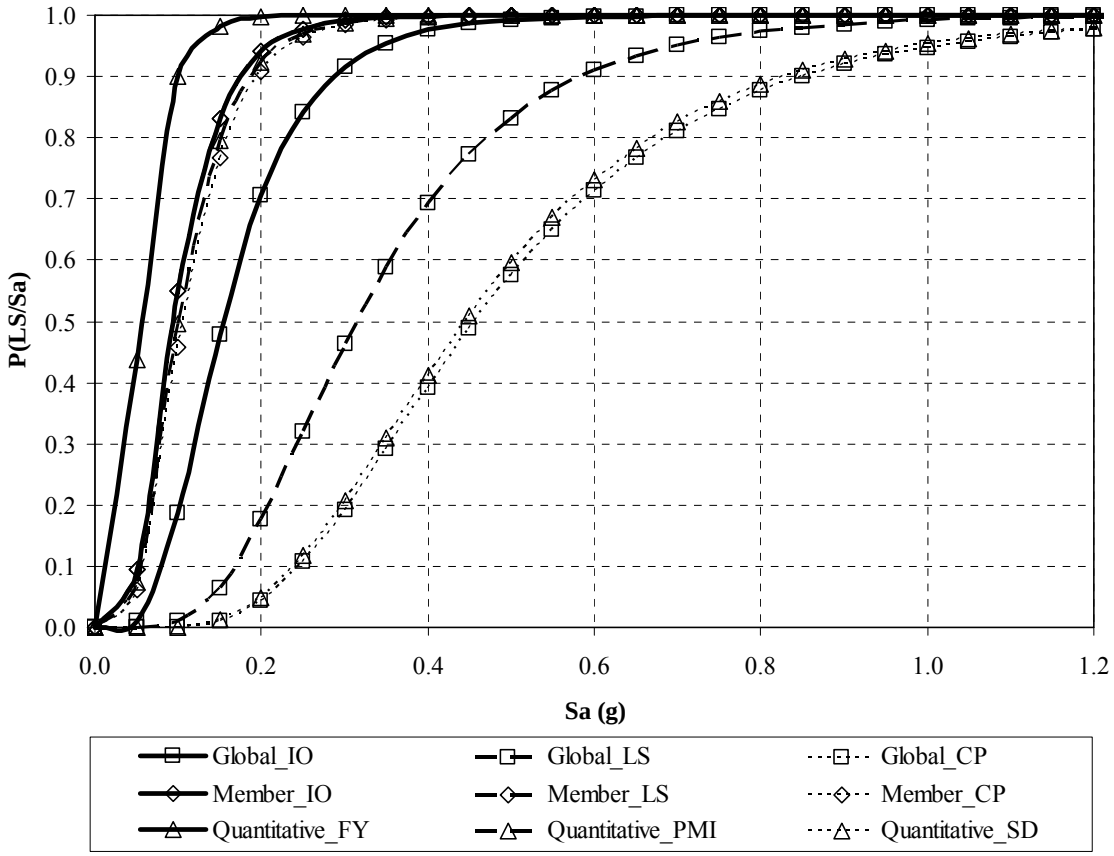

(a) Unretrofitted structure

Fig. 7.19. Fragility curves using spectral acceleration for MAEviz implementation based on Rix and Fernandez-Leon motions

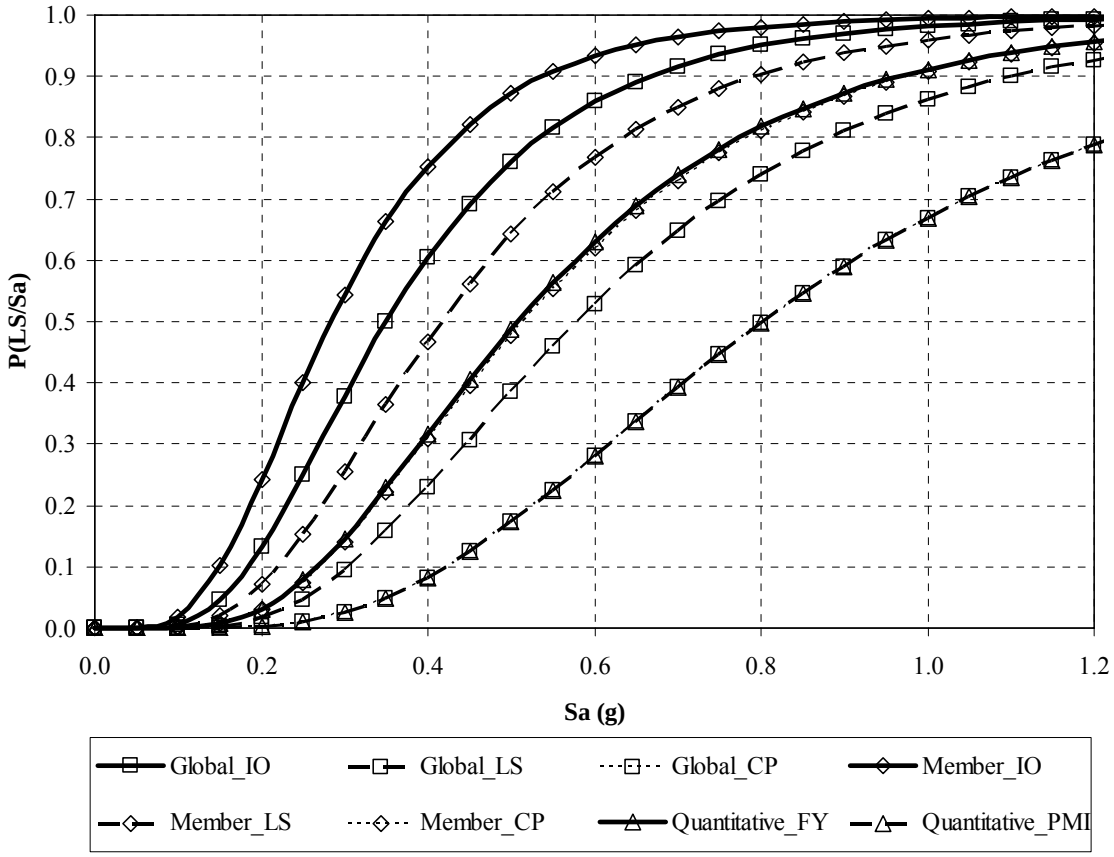

(b) Retrofit 1: Addition of shear walls

Fig. 7.19. Continued

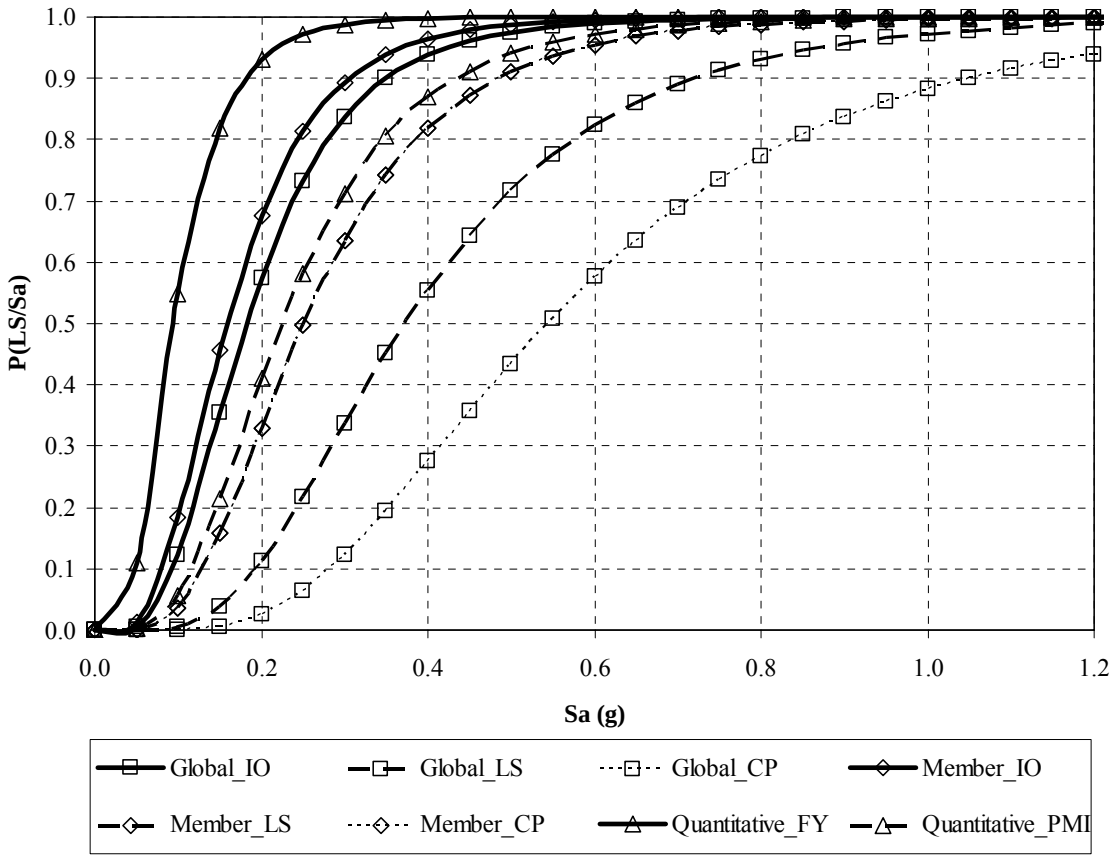

(c) Retrofit 2: Addition of RC column jackets

Fig. 7.19. Continued

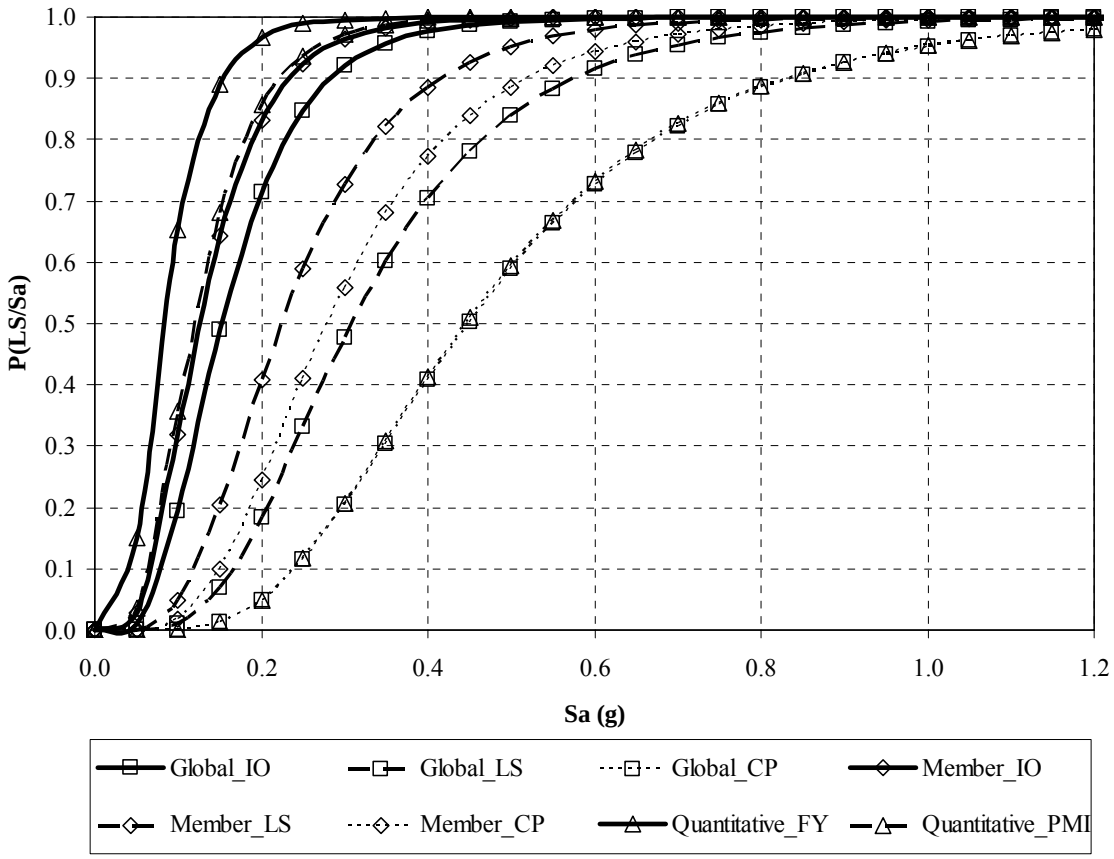

(d) Retrofit 3: Confinement of column plastic hinge zones

Fig. 7.19. Continued

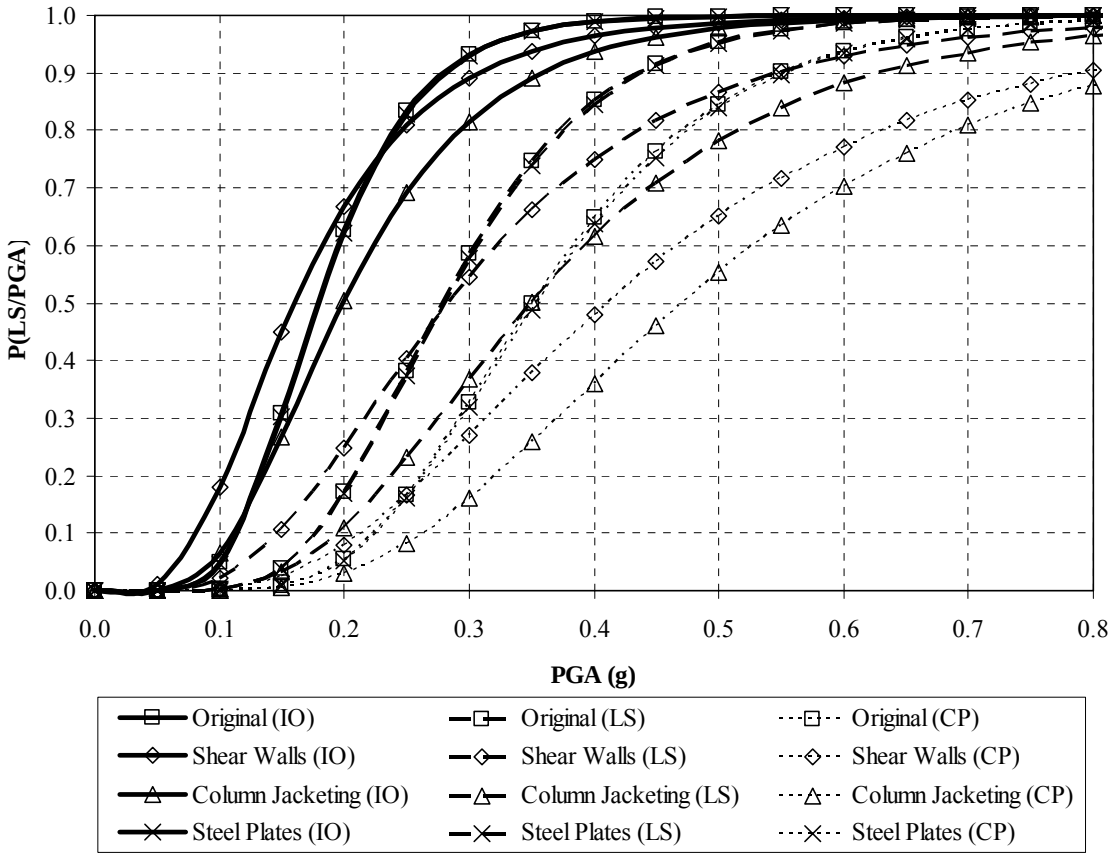

Fig. 7.20. Fragility curves using PGA for MAEviz implementation based on FEMA 356 global-level drift limits (Wen and Wu motions)

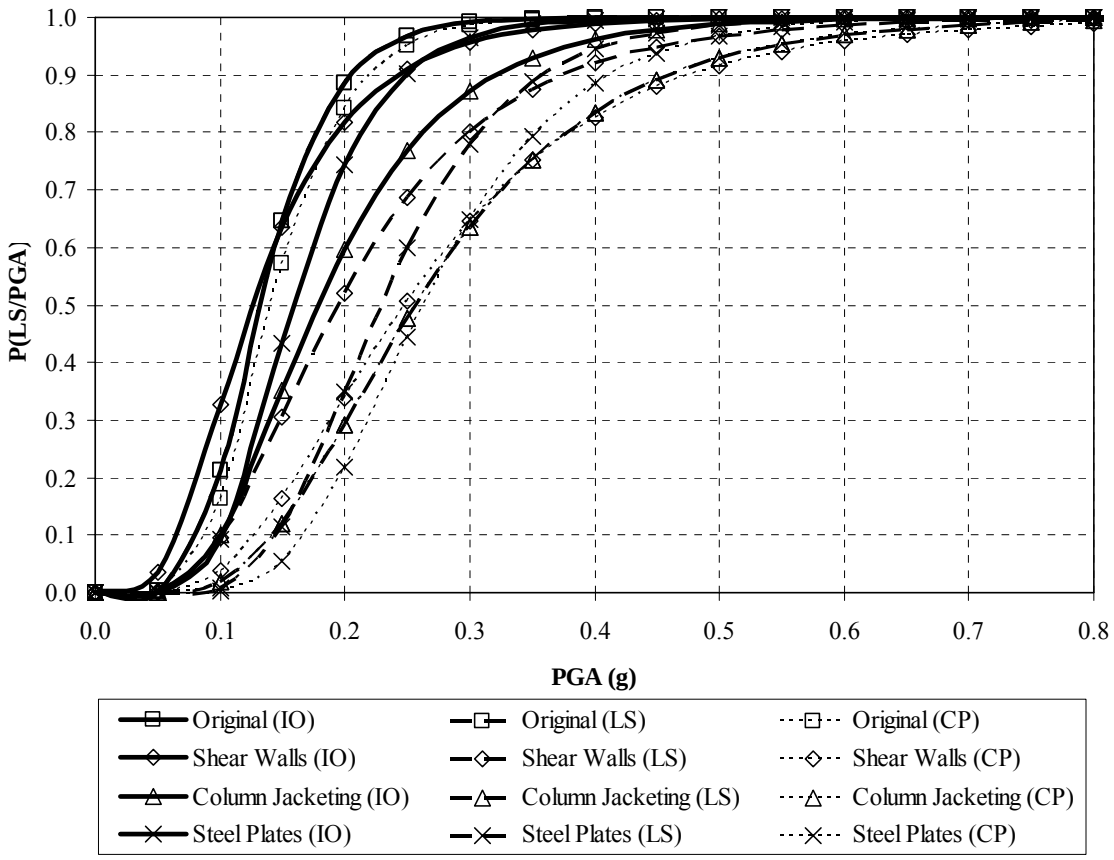

Fig. 7.21. Fragility curves using PGA for MAEviz implementation based on FEMA 356 member-level drift limits (Wen and Wu motions)

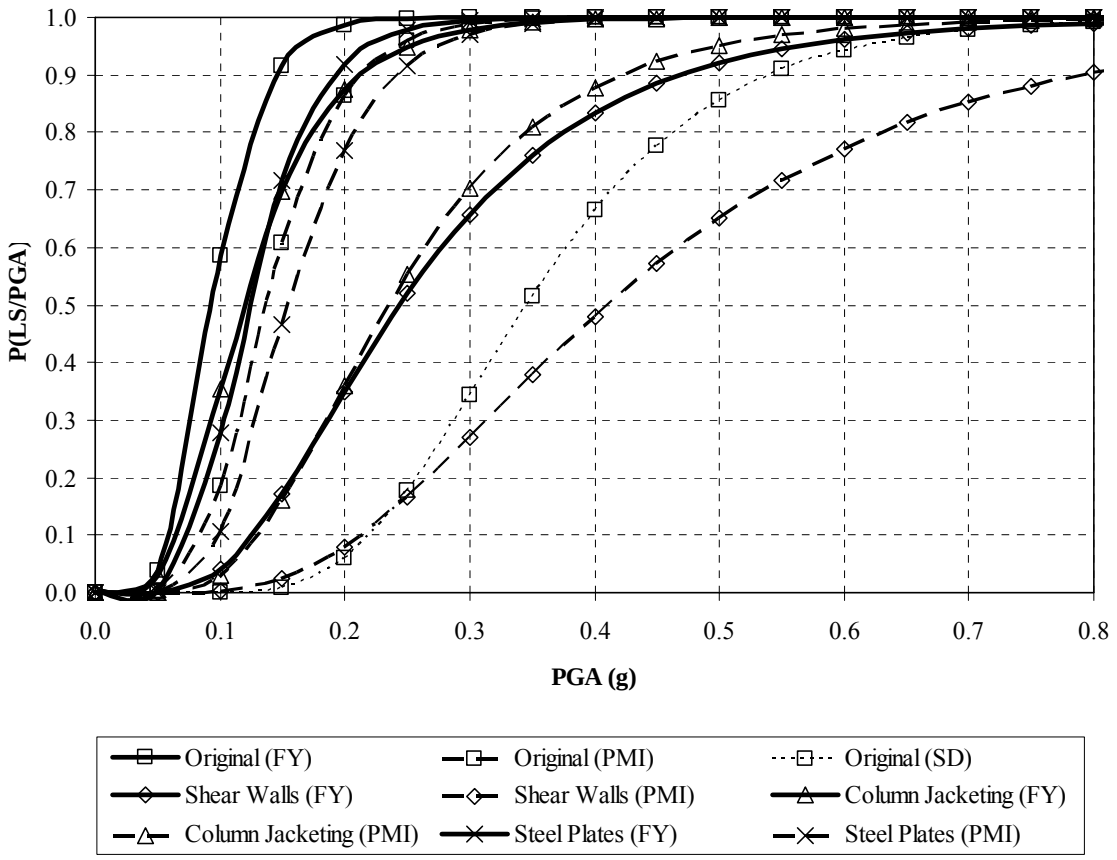

Fig. 7.22. Fragility curves using PGA for MAEviz implementation based on additional quantitative drift limits (Wen and Wu motions)

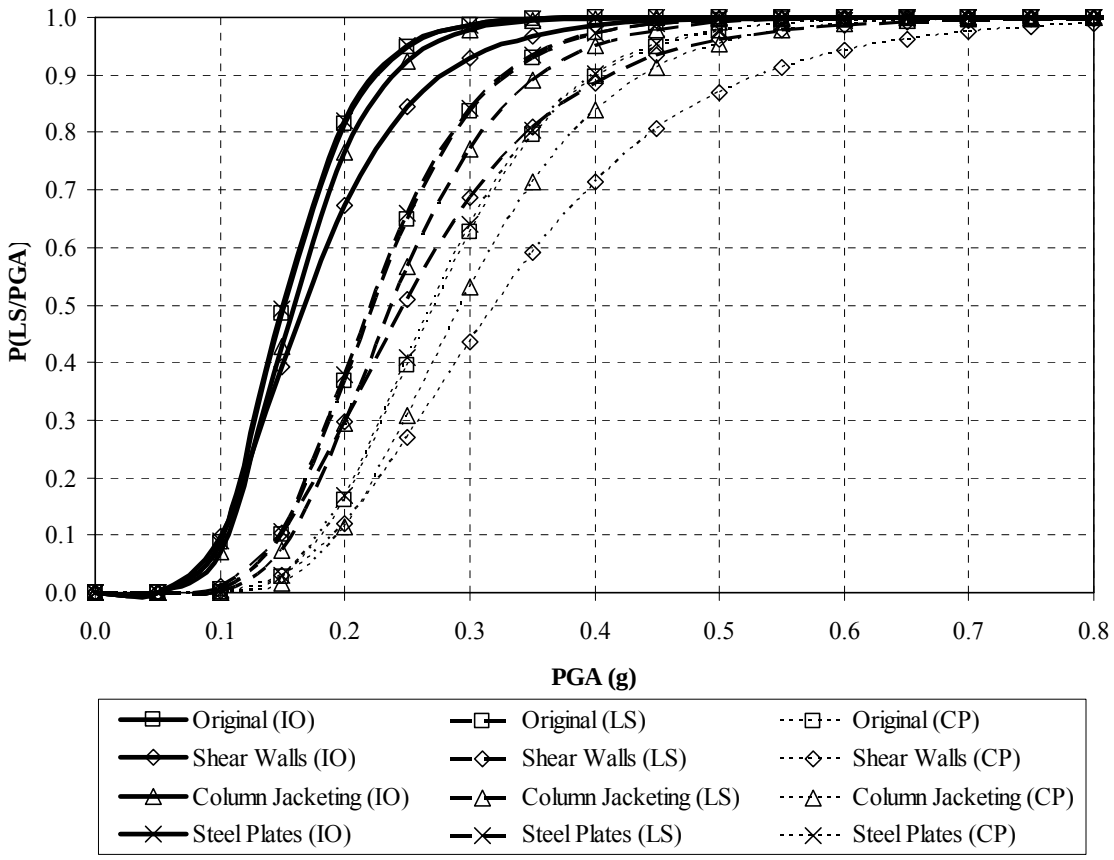

Fig. 7.23. Fragility curves using PGA for MAEviz implementation based on FEMA 356 global-level drift limits (Rix and Fernandez-Leon motions)

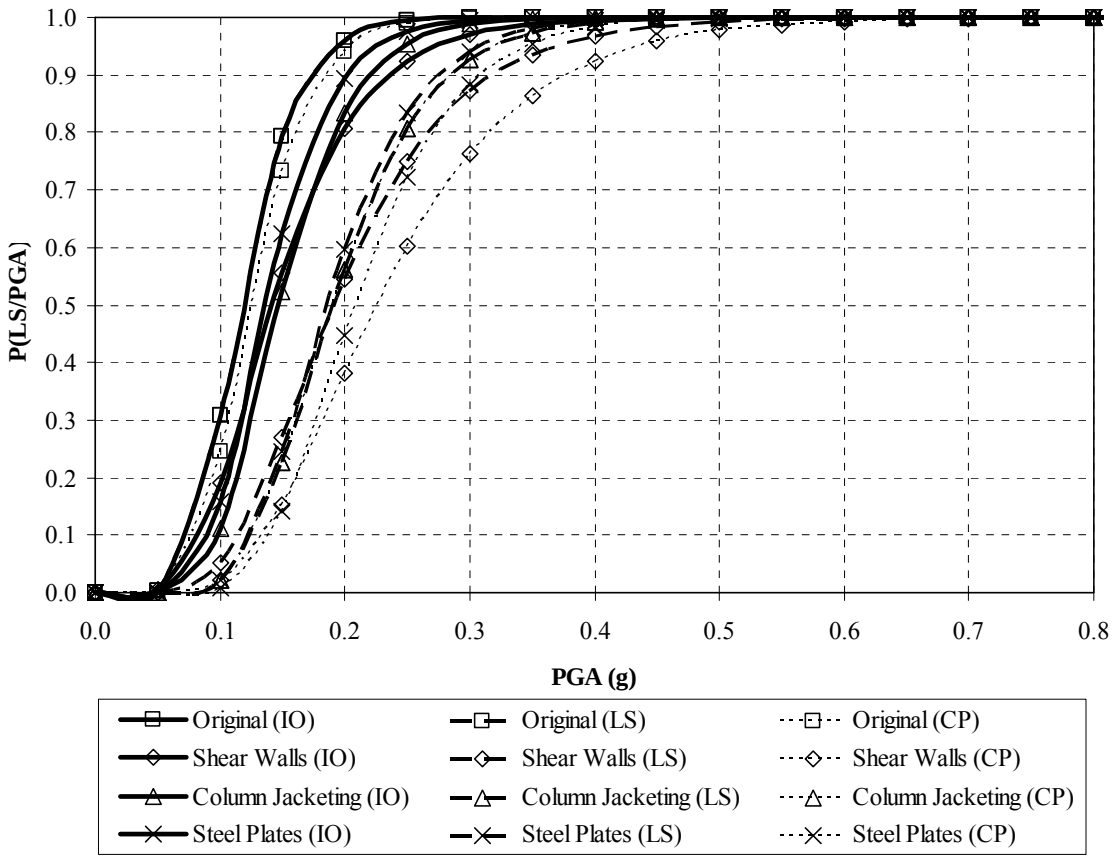

Fig. 7.24. Fragility curves using PGA for MAEviz implementation based on FEMA 356 member-level drift limits (Rix and Fernandez-Leon motions)

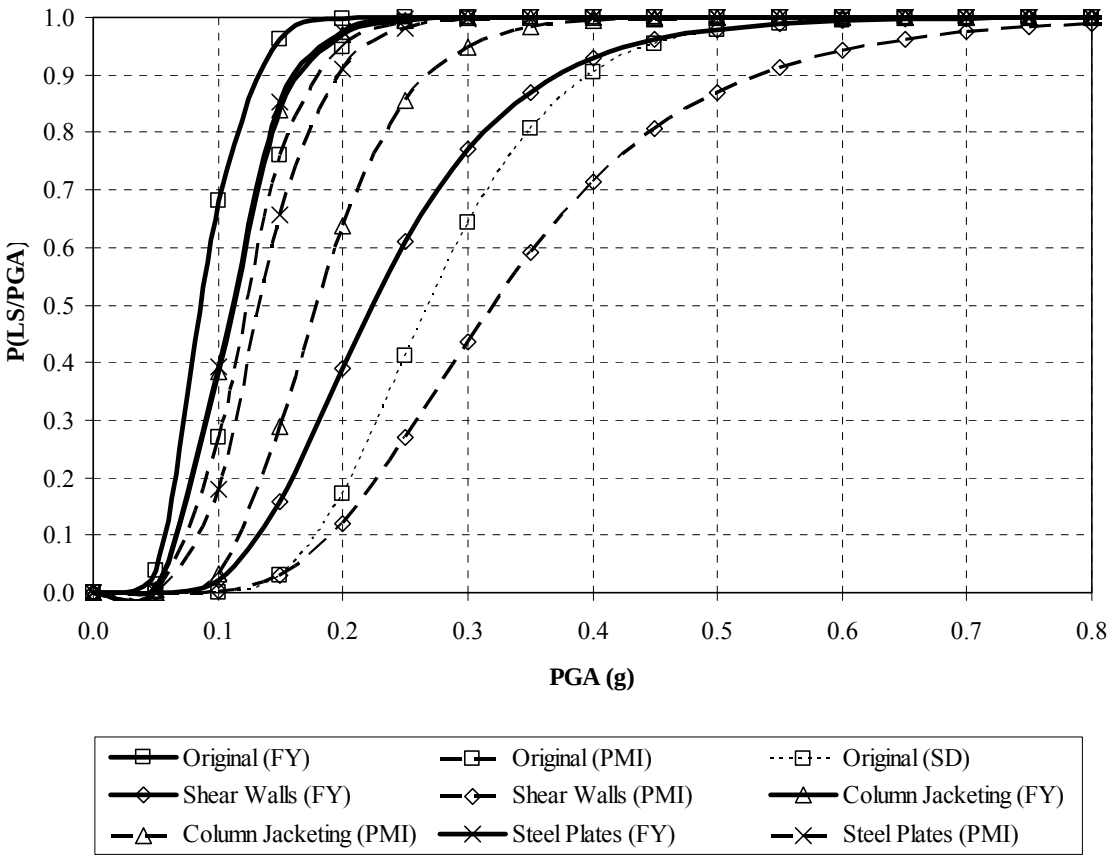

Fig. 7.25. Fragility curves using PGA for MAEviz implementation based on additional quantitative drift limits (Rix and Fernandez-Leon motions)

As shown in Figs 7.18 to 7.25, in general, the probabilities of exceeding each limit state based on the FEMA 356 member-level drift limits gives higher values than those for the global-level drift limits. For the additional quantitative drift limit case, the probability of exceeding FY and PMI limit states is reduced the most when Retrofit 1 is applied.

7.4.4 Default Sets of Fragility Curves

In the earlier section, various fragility curves for the case-study structures were developed based on different parameters including ground motions, earthquake intensity measure, and limit states. It is convenient that the default sets of fragility curves for

each type of structure are defined. For determining the default sets of fragility curves, three performance levels (PL1, PL2, and PL3) were used and each performance level was matched with the developed fragility curves based on the structural behavior. The ground motion sets developed by Rix and Fernandez-Leon were determined as a default ground motion because recent research allowed the inclusion of soil nonlinearity in the site response parameters. For the default earthquake intensity measure, spectral acceleration was selected. Table 7.6 shows the suggested performance level and corresponding interstory drift limits of the default fragility curves for each type of structure.

Table 7.6. Suggested performance level and corresponding interstory drift (%) limits for default fragility curves

Structure	PL1	PL2	PL3
Unretrofitted structure	FY=0.358	PMI=0.66	SD=2.81
Retrofit 1	IO(M^1)=0.4	LS(M^1)=0.6	CP(G^2)=1.2
Retrofit 2	FY=0.53	PMI=1.23	CP(G^2)=2.9
Retrofit 3	FY=0.55	PMI=0.79	CP(G^2)=2.9

Notes:
1. FEMA 356 member-level limits
2. Global-level limits provided as guidance in FEMA 356

7.5 Summary

In this section, the additional seismic fragility analysis for the case study structure using the Rix and Fernandez-Leon (2004) motions was presented. In addition, the implementation of the fragility curves into MAEviz, the damage visualization module, was discussed. The fragility curves were developed based on three different drift limits (FEMA 356 global-level, member-level, and additional quantitative limits) using the Rix and Fernandez-Leon synthetic motions (2004) and compared with those developed using Wen and Wu motions (2000). For the MAEviz implementation, the suggested default sets of fragility curves were selected for each type of structure.

For the comparison between the Wen and Wu motions and the Rix and Fernandez-Leon motions, the Rix and Fernandez-Leon motions provide lower probabilities of exceeding each limit state. For the two different source models used to develop the Rix and Fernandez-Leon motions, there are significant differences in seismic fragility. Therefore, for further analysis, fragility curves using both source models were used to reduce the uncertainty due to the ground motions.

In general, the probabilities of exceeding each limit state were reduced for the retrofitted structures. In particular, Retrofit 1 has the greatest impact in reducing the probability of exceeding each limit state.

8 SUMMARY, CONCLUSIONS AND RECOMMENDATIONS

8.1 Summary

Through nonlinear structural analysis, the seismic performance of a reinforced concrete (RC) flat-slab building structure was evaluated and three retrofit techniques were selected and applied to the structure. In addition, the effectiveness of the applied retrofit techniques was assessed through the development of probabilistic fragility curves. The case study building was designed to be representative of those constructed in St. Louis, Missouri and Memphis, Tennessee in the mid-1980s. This building was designed according to the load requirements in the ninth edition of the *Building Officials and Code Administrators (BOCA) Basic/National Code* (BOCA 1984). The design of structural components was carried out according to the provisions of the *American Concrete Institute (ACI) Building Code Requirements for Reinforced Concrete, ACI 318-83* (ACI Comm. 318 1983). The case study building is a five-story RC flat-slab building with a perimeter moment resisting frame and an overall height of 20.4 m (67 ft.).

Because there is not adequate recorded strong motion to characterize the seismicity for specific locations in the Mid-America region, synthetic ground motion data developed by Wen and Wu (2000) for St. Louis, Missouri and Memphis, Tennessee were used for the dynamic analysis and fragility curve development. In addition, new synthetic ground motion data developed by Rix and Fernandez-Leon (2004) for Memphis, Tennessee were used for the dynamic analysis and development of additional fragility curves. Two different approaches for modeling and analyzing the case study building were evaluated: a fiber model using the ZEUS-NL program and a macro-model using the DRAIN-2DM program. In addition, two structural analysis methods, nonlinear static analysis and nonlinear dynamic analysis, were used to predict the seismic behavior of the building under lateral demands. Based on a comparison of results from two structural nonlinear analysis programs (ZEUS-NL and DRAIN-2DM), the ZEUS-NL

program was selected for additional analytical studies to evaluate the expected seismic performance of the structure for the St. Louis and Memphis synthetic ground motions.

Based on the analytical results, seismic evaluations were conducted using FEMA 356 performance criteria using both global-level and member-level approaches. FEMA 356 suggests member-level acceptance criteria for three performance levels (Immediate Occupancy, Life Safety and Collapse Prevention). Global-level drift limits are also provided, but are intended only for guidance. For the global-level evaluation, the maximum interstory drifts for each story were determined based on the results of nonlinear dynamic analysis and the median maximum response was determined for a suite of motions. According to FEMA 356, the Basic Safety Objective (BSO) is defined as LS performance for the Basic Safety Earthquake 1 (BSE-1) earthquake hazard level and CP performance for the BSE-2 earthquake hazard level. BSE-1 is defined as the smaller of an event corresponding to 10% probability of exceedance in 50 years (10% in 50 years) and 2/3 of BSE-2, which is the 2% probability of exceedance in 50 years (2% in 50 years) event.

For the global-level (drift-based) evaluation, the structure met the BSO recommended by FEMA 356 for both the 10% and 2% probabilities of exceedance in 50 years Wen and Wu (2000) ground motions for St. Louis and Memphis. However, for the member-level evaluation that uses plastic rotation limits for each member, a number of structural components including beams, columns and slabs did not satisfy the FEMA 356 BSO of Collapse Prevention (CP) for the 2% probability of exceedance in 50 years Memphis motions developed by Wen and Wu (2000).

Based on the seismic evaluation, three retrofit techniques were applied to enhance the seismic performance of the structure: addition of shear walls, addition of RC column jackets, and confinement of the column plastic hinge regions using externally bonded steel plates. The retrofits were selected to impact the major structural

response parameters: stiffness, strength and ductility. The shear walls were added to the two central bays of the exterior frame, leading to an increase in the global stiffness and strength of the structure. Column jacketing was applied to the columns that did not satisfy with FEMA 356 member-level (plastic hinge) limits and increased the strength and stiffness of the structure. The addition of external steel plates confined the plastic hinge zones at the ends of vulnerable columns to increase ductility. Nonlinear static and dynamic analyses were performed to predict the seismic behavior of the retrofitted structure. Based on the analytical results, a seismic evaluation was conducted.

Fragility curves were developed for the both retrofitted and unretrofitted structures. The fragility curves developed based on FEMA global-level drift limits and member-level plastic rotation limits were compared. In addition to this, additional quantitative limit states, suggested by Wen et al. (2003), were determined and compared to the limits based on the FEMA 356 criteria. These included first yield (FY), plastic mechanism initiation (PMI) and strength degradation (SD). The drift limits corresponding to the FEMA 356 member-level criteria and additional quantitative limits were determined from traditional push-over analysis and a critical response (story-by-story) push-over analysis suggested by Dooley and Bracci (2001). Finally, recommendations were made for implementing the seismic fragility analysis results into MAEviz (ALG 2004), the earthquake risk assessment tool developed by the Mid-America Earthquake Center.

8.2 Conclusions

The following conclusions were made based on the results of this study:

1. The comparison of analytical results from nonlinear analysis using ZEUS-NL (fiber model) and DRAIN-2DM (macro model) showed good agreement, especially at lower load magnitudes. However, for the nonlinear static analysis,

ZEUS-NL provided a more reasonable prediction of the inelastic behavior of the structure including P-delta effects. For the nonlinear dynamic analysis, the maximum building drift and maximum base shear were similar for the two analysis programs. The ZEUS-NL program was selected for additional analytical studies to evaluate the expected seismic performance of the structure using synthetic ground motions.

2. A comparison between nonlinear static (push-over) and nonlinear dynamic analysis gave good agreement of global response. In particular, for lower amplitudes of motion, the global responses were relatively similar.

3. For seismic evaluation using the FEMA 356 criteria, it was found that the predicted response of the case study building for the St. Louis motions was within the BSO limits. For the 10% in 50 years events, the BSO was satisfied based on both the global-level and member-level criteria. However, for the 2% in 50 years Memphis motions, the BSO was not satisfied based on the global-level and member-level criteria.

4. Three retrofit techniques were applied to the case study building to impact the major structural response parameters. For all retrofits, the seismic performance of the structure was enhanced based on the analytical results from both the nonlinear static and nonlinear dynamic analyses.

5. Fragility curves using the FEMA 356 global-level criteria were developed for both the unretrofitted and retrofitted case study buildings. Addition of shear walls and RC column jackets reduced the probability of exceeding each limit state. However, seismic retrofitting with steel plates for ductility enhancement did not impact the fragility curves based on the selected global-level criteria.

6. The drift limits based on member-level criteria were determined with two different definitions of limit states using push-over analysis. As a result, drift limits based on FEMA 356 member-level (plastic rotation) criteria did not match well and tended to be lower than the FEMA 356 global-level (drift) limits. This is because drift limits for member-level criteria are affected by many characteristics specific to the structure, such as details of reinforcement and level of confinement (ductility). In addition, the global-level (drift) limits provided as guidance in FEMA 356 are intended for well-detailed buildings, while the case study structure has relatively poor details with respect to ductility.

7. Fragility curves using the FEMA 356 member-level criteria were developed for both the unretrofitted and retrofitted case study buildings. All three retrofit techniques reduced the probability of exceeding each limit state considered.

8. For the additional analyses based on the Rix and Fernandez-Leon synthetic ground motions, analytical results from two source models gave a significant difference in building response. In particular, the analysis using the magnitude 7.5 Frankel et al. source model gave extremely high building drifts.

9. In general, the probabilities of exceeding each limit state based on the FEMA 356 member-level drift limits are higher than those for the global-level drift limits. In addition to this, for all limit states including the FEMA 356 global-level, member-level and the additional quantitative drift limits, the probability of exceeding FY and PMI limit states is reduced the most by Retrofit 1.

10. To compare the unretrofitted and retrofitted structures, the fragility curves developed using peak ground acceleration, are recommended. This is because the spectral acceleration of concern can vary when the structure is retrofitted and so a direct comparison for a specified spectral acceleration may not be

appropriate. However, for the comparison of limit states for a particular structure, the fragility curves developed by using spectral acceleration are suggested.

11. For comparing the seismic fragility of the case study structure with other types of structures such as a steel frame, masonry and wood frame structure, the global-level drift limits may provide a more general standard. However, for a more refined evaluation, the FEMA 356 member-level or additional quantitative limits are recommended. This is because these drift limits were developed using a detailed structure-specific analysis, and therefore, these better reflect the characteristics and susceptibility to damage of the case study structure.

12. For MAEviz implementation, seismic fragility curves based on the Rix and Fernandez-Leon motions are recommended because these motions were developed based on site amplification factors that reflect the soil nonlinearity and uncertainties from the effect of the deep soil column of the Upper Mississippi Embayment. However, the Wen and Wu motions are useful when the seismic demand is required in terms of probabilistic events (i.e. 10% and 2% probabilities of exceedance in 50 years).

8.3 Recommendations for Future Research

The work in this report has been limited to a five-story reinforced concrete flat-slab structural frame system. Hence, the structural fragility curves are not generic to this type of structural system because many structural configurations are possible. Further research is being conducted under MAE Center project EE-1 and will be published at a later date. Some of the future research needs related to seismic fragility and retrofitting are listed below:

1. This study could be extended to other types of structures, including steel, masonry, composite and other concrete structures to develop fragility curves. In

addition to this, further research to verify performance criteria for limit states would be beneficial. For instance, additional experimental and analytical studies to match the limit states with actual damage data for developing more general fragility curves are encouraged.

2. It would be useful to consider the performance of nonstructural members when the limit states are defined.

3. An assessment model that evaluates not only the structural performance but also economic or social impacts of damage would be useful. Then vulnerability functions associated with a specified economic or social impact should be developed. Based on this information, the mitigation option with the best cost-to-benefit ratio can be determined considering additional important factors.

REFERENCES

Abrams, D.P., Elnashai, A.S. and Beavers, J.E. (2002), "A New Engineering Paradigm: Consequence-Based Engineering," Linbeck Lecture Series in Earthquake Engineering: Challenges of the New Millennium, University of Notre Dame's Linbeck Distinguished Lecture Series, Notre Dame, IN.

Automated Learning Group (ALG) (2004), "MAEviz Introduction and Tutorial," National Center for Supercomputing Applications (NCSA), Sep., 2004.

Aycardi, L.E., Mander, J.B. and Reinhorn, A.M. (1994), "Seismic Resistance of Reinforced Concrete Frame Subasseblages," *ACI Structural Journal*, 91, (5), 559-560.

ACI Committee 318 (1983), *Building Code Requirements for Reinforced Concrete* (ACI 318-83), American Concrete Institute, Detroit, MI.

ACI Committee 318 (2002), *Building Code Requirements for Reinforced Concrete* (ACI 318-02), American Concrete Institute, Farmington, MI.

AISC (2001), *Manual of Steel Construction: Load and Resistance Factor Design* (3rd edition), American Institute of Steel Construction, Chicago, IL.

Al-Haddad, M.S. and J.K. Wight (1986). "Feasibility and consequences of moving beam plastic hinging zones for earthquake resistant design of R/C buildings," *Report No. UMCE 86-1*, Department of Civil Engineering, University of Michigan, Ann Arbor, MI.

Altin, S., Ersoy, U. and Tankut, T. (1992), "Hysteretic Response of Reinforced-Concrete Infilled Frames," *Journal of Structural Engineering*, 118, (8), 2133-2150.

ASCE (2000), *Prestandard and Commentary for the Seismic Rehabilitation of Buildings (FEMA 356)*, prepared by American Society of Civil Engineers for the Federal Emergency Management Agency, Washington, D.C.

ATC (1996), *Seismic Evaluation and Retrofit of Concrete Buildings (ATC-40)*, prepared by Applied Technology Council, Redwood City, CA.

Atkinson, G. and Boore, D. (1995), "New Ground Motions Relations for Eastern North America," *Bulletin of the Seismological Society of America*, 85, 17-30.

Badoux, M. and Jirsa, J.O. (1990), "Steel Bracing of RC Frame for Seismic Retrofitting," *Journal of Structural Engineering*, 116, (1), 55-74.

BOCA (1984), *Building Officials and Code Administrators (BOCA) Basic/National Code/1984*, Building Officials and Code Administrators International, Inc., Country Club Hills, IL.

Bracci, J.M., Reinhorn, A.M. and Mander, J.B. (1995), "Seismic Retrofit of RC Frame Buildings Designed for Gravity Loads: Performance of Structural Model," *ACI Structural Journal*, 92, (6), 771-723.

Bush, T.D., Jones, E.A. and Jirsa, J.O. (1991), "Behavior of RC Frame Strengthened Using Structural Steel Bracing," *Journal of Structural Engineering*, 117, (4), 1115-1126.

Constantinou, M.C., Kartoum, A. and Kelly, J.M. (1992), "Analysis of Compression of Hollow Circular Elastomeric Bearings," *Engineering Structures*, 14, (2), 103-111.

Cornell, C.A., Jalayer, F., Hamburger, R.O., and Foutch, D.A. (2002), "Probabilistic Basis for 2000 SAC Federal Emergency Management Agency Steel Moment Frame Guidelines," *Journal of Structural Engineering*, 128, (4), 526-533.

Dooley, K.L. and Bracci, J.M. (2001), "Seismic Evaluation of Column-to-Beam Strength Ratios in Reinforced Concrete Frames," *ACI Structural Journal*, 98, (6), 843-851.

Drosos, V. (2003), "Synthesis of Earthquake Ground Motions for the New Madrid Seismic Zone," M.S. Thesis, Georgia Institute of Technology, Atlanta, GA.

Dumova-Jovanoska, E. (2000), "Fragility Curves for Reinforced Concrete Structures in Skopje (Macedonia) Region," *Soil Dynamics and Earthquake Engineering*, 19, 455-466.

Elnashai, A.S., Papanikolaou, V. and Lee, D.H. (2002), "ZEUS-NL User Manual," University of Illinois at Urbana-Champaign / Mid-America Earthquake Center.

Elnashai, A.S. and Pinho, R. (1998), "Repair and Retrofitting of RC Walls Using Selective Techniques," *Journal of Earthquake Engineering*, 2, (4), 525-568.

Elnashai, A.S., Pinho, R. and Antoniou (2000), "INDYAS – A Program for Inelastic Dynamic Analysis of Structures," *Research Report ESEE/00-2,* Engineering Seismology and Earthquake Engineering Section, Imperial College, London.

Elnashai, A.S. and Salama, A.I. (1992), "Selective Repair and Retrofitting Techniques for RC Structures in Seismic Regions," *Research Report ESEE/92-2,* Engineering Seismology and Earthquake Engineering Section, Imperial College, London.

Farhey, D.N., Adin, M.A. and Yankelevsky, D.Z. (1993), "Repair of RC Column-Flat Slab Joints," *Proc., 17th Regional European Seminar on Earthquake Engineering,* Haifa, Israel, 459-469.

FEMA (1997a), *NEHRP Guidelines for the Seismic Rehabilitation of Buildings (FEMA 273)*, prepared by the Building Seismic Safety Council for the Federal Emergency Management Agency, Washington, D.C.

FEMA (1997b), *NEHRP Commentary on the Guidelines for Seismic Rehabilitation of Buildings (FEMA 274)*, prepared by the Building Seismic Safety Council for the Federal Emergency Management Agency, Washington, D.C.

Frankel, A., Mueller, C., Barnhard, T., Perkins, D., Leyendecker, E., Dickman, N., Hanson, S., and Hopper, M. (1996), "National Seismic Hazard Maps: Documentation," *USGS Open-File Report 96-532*.

Fu, Y. (1996), "Frame Retrofit by Using Viscous and Viscoelastic Dampers," *Proc., 11th World Conference on Earthquake Engineering*, Acapulco, Mexico (CD-Rom).

Gardoni, P., Kiureghian, A.D., and Mosalam, K.M. (2002), "Probabilistic Capacity Models and Fragility Estimates for Reinforced Concrete Columns based on Experimental Observations," *Journal of Structural Engineering*, 128, (10), 1024-1038.

Gates, W.E., Hart, G.C., and Crouse, C.B. (1990), "Vibration Studies of an Existing Building for Base Isolation Retrofit," *Proc., 4th U.S. National Conference on Earthquake Engineering,* Palm Springs, CA, 3, 559-568.

Goel, S.C. and Masri, A.C. (1996), "Seismic Strengthening of an RC Slab-Column Frames with Ductile Steel Bracing," *Proc., 11th World Conference on Earthquake Engineering*, Acapulco, Mexico (CD-Rom).

Gulkan, P. and Sozen, M.A. (1999), "Procedure for Determining Seismic Vulnerability of Building Structures," *ACI Structural Journal*, 96, (3), 336-342.

Harries, K., Ricles, J., Sause, R., Pessiki, S. and Walkup, L. (1998), "Seismic Retrofit of Non-Ductile Reinforced Concrete Building Columns Using FRPC Jackets," *Proc., 6th U.S. National Conference on Earthquake Engineering,* Seattle, WA (CD-Rom).

Hart, J.F. (2000), "Analysis of a Typical Midwestern Structure Subjected to Seismic Loads," University Undergraduate Research Fellow Program Senior Honor Thesis, Department of Civil Engineering, Texas A&M University, College Station, TX.

Hassan, A.F. and Sozen, M.A. (1997), "Seismic Vulnerability Assessment of Low-Rise Buildings in Regions with Infrequent Earthquakes," *ACI Structural Journal*, 94, (1), 31-39.

Hueste, M.B.D. and Wight, J.K. (1997a), "Evaluation of a Four-Story Reinforced Concrete Building Damaged During the Northridge Earthquake," *Earthquake Spectra*, 13, (3), 387-414.

Hueste, M.B.D. and Wight, J.K. (1997b), "Evaluation of a Reinforced Concrete Building Damaged during the Northridge Earthquake and Development of a Punching Shear Failure Model for Nonlinear Analysis," *Rep. UMCEE 97-17*, Dept. of Civ. And Envir. Engrg., Uninversity of Michigan, Ann Arbor, Mich.

Hueste, M.B.D. and Wight, J.K. (1999), "Nonlinear Punching Shear Failure Model for Interior Slab-column Connections," *Journal of Structural Engineering*, 125, (9), 997-1008.

Hwang, H.M. and Huo, J.-R. (1994), "Generation of Hazard-Consistent Fragility Curves for Seismic Loss Estimation Studies," *Technical Report NCEER-94-0015*, National Center for Earthquake Engineering Research, State University of New York at Buffalo, Buffalo, NY.

Hwang, H.M. and Huo, J.-R. (1996), "Simulation of Earthquake Acceleration Time Histories," *Technical Report*, Center for Earthquake Research and Information, University of Memphis, Memphis, TN.

IES (1998), Visual Analysis V3.5, Integrated Engineering Software, Inc., Bozeman, MT.

Inukai, M. and Kaminosono, T. (2000), "Seismic Performance of an existing RC frame retrofitted by Precast Prestressed Concrete Shear Walls," *Proc., 12th World Conference on Earthquake Engineering*, Auckland, New Zealand (CD-Rom) .

International Code Council (ICC) (2003), *International Building Code* (IBC 2003), Falls Church, VA.

Jirsa, J.O. and Kreger, M. (1989), "Recent Research on Repair and Strengthening of Reinforced Concrete Structures," *Proceedings, ASCE Structures Congress*, San Francisco, CA, 1, 679-688.

Johnston, A.C. (1996), "Seismic Moment Assessment of Earthquakes in Stable Continental Regions; III, New Madrid 1811-1812, Charleston, 1886 and Lisbon 1755," *Geophysical Journal International*, 126 (2), 314-344.

Kannan, A.E. and Powell, G.H. (1973), "A General Purpose Computer Program for Dynamic Analysis of Inelastic Plane Structures," *Report No. EERC 73-6*, Earthquake Engineering Research Center, University of California, Berkeley, CA.

Kawamura, S., Sugisaki, R., Ogura, K., Maezawa, S., Tanaka, S., and Yajima, A. (2000), "Seismic Isolation Retrofit in Japan," *Proc., 12th World Conference on Earthquake Engineering*, Auckland, New Zealand (CD-Rom).

Krawinkler, H. (1999), "Challenges and Progress in Performance-Based Earthquake Engineering*," International Seminar on Seismic Engineering for Tomorrow – In Honor of Professor Hiroshi Akiyama*, Tokyo, Japan.

Kunisue, A., Koshika, N., Kurokawa Y., Sakamoto M., Suzuki N., and Tagami J. (2000), "Retrofitting Method of Existing Reinforced Concrete Buildings Using Elasto-Plastic Steel Dampers," *Proc., 12th World Conference on Earthquake Engineering*, Auckland, New Zealand (CD-Rom).

Lew, H.S. and Kunnath, S.K. (2002), "Assessment of Structural Systems Evaluation Methods Based on Local Seismic Demands," Innovations in Design with Emphasis on Seismic, Wind, and Environmental Loading; Quality Control and Innovations in Materials/Hot-Weather Concreting (SP-209), *ACI 5th International Conference*, Cancun, Mexico.

Lombard, J., Humar, J.L. and Cheung, M.S. (2000), "Seismic Strengthening and Repair of Reinforced Concrete Shear Walls," *Proc., 12th World Conference on Earthquake Engineering*, Auckland, New Zealand (CD-Rom).

Luo, Y. and Durrani, A.J. (1994), "Seismic Retrofit Strategy for Non-Ductile Flat-Plate Connections," *Proc., 5th U.S. National Conference on Earthquake Engineering,* Chicago, IL, 3, 627-636.

Mander, J.B., Priestley, M.J. and Park, R. (1988), "Theoretical Stress-Strain Model for Confined Concrete," *Journal of Structural Engineering*, 114, (8), 1804-1826.

Martinez-Cruzado, J.A., Qaisrani, A.-N., and Moehle, J.P. (1994), "Post-tensioned Flat-Plate Slab-Column Connections Subjected to Earthquake Loading," *Proc., 5th U.S. National Conference on Earthquake Engineering,* Chicago, IL, 2, 139-148.

McKeown, F.E. (1982), "Overview and discussion," Investigations of the New Madrid, Missouri, Earthquake Region, *USGS Professional Paper 1236*, 1-14, Washington, D.C.

Miranda, E. and Bertero, V.V. (1990), "Post-tensioning Techniques for Seismic Upgrading of Existing Low-Rise Buildings," *Proc., 4th U.S. National Conference on Earthquake Engineering,* Palm Springs, CA, 3, 393-402.

Moehle, J.P. (2000), "State of Research on Seismic Retrofit of Concrete Building Structures in the US," *US-Japan Symposium and Workshop on Seismic Retrofit of Concrete Structures,* Tokyo, Japan.

Munshi, J.A. (1998), "Energy Dissipation of Viscoelastically Damped Reinforced Concrete Systems," *Proc., 6th U.S. National Conference on Earthquake Engineering,* Seattle, WA (CD-Rom).

National Center for Supercomputing Applications (NCSA) (2004), "Mid-America Earthquake (MAE) Center Damage Visualization Module," 2004. http://alg.ncsa.uiuc.edu/do/projects/visualization/mae;jsessionid=E8EAB161FAEFB129BDB12D964D510B0A

Park, Y.J., Ang, A.H.-S. and Wen, Y.K. (1985), "Seismic Damage Analysis of Reinforced Concrete Buildings," *Journal of Structural Engineering*, 111, (4), 740-757.

Paulay, T. and Priestley, M.J.N. (1992), *Seismic Design of Reinforced Concrete and Masonry Buildings*, Wiley, NY.

Pekcan, G., Mander, J.B., and Chen, S.S. (1995), "The Seismic Response of a 1:3 Scale Model R.C. Structure with Elastomeric Spring Dampers," *Earthquake Spectra*, 11, (2), 249-267.

Pincheira, J.A. (1992), "Seismic Strengthening of Reinforced Concrete Frames Using Post-Tensioned Bracing Systems," Ph.D. Dissertation, Department of Civil Engineering, University of Texas at Austin, Austin, TX.

Pincheira, J.A. and Jirsa, J.O. (1995), "Seismic Response of RC Frames Retrofitted with Steel Braces or Walls," *Journal of Structural Engineering*, 121, (8), 1225-1235.

Powell, G.H. (1973), "DRAIN-2D, User's Guide," *Report No. EERC 73-22*, Earthquake Engineering Research Center, University of California, Berkeley, CA.

Priestley, M.J.N., Seible, F., Xiao, Y., and Verma, R. (1994), "Steel Jacket Retrofitting of Reinforced Concrete Bridge Columns for Enhanced Shear Strength – Par 1: Theoretical Considerations and Test Design," *ACI Structural Journal*, 91, (4), 394-405.

Raffaelle, G.S. and J.K. Wight (1992), "R/C Eccentric Beam-Column Connections Subjected to Earthquake-Type Loading," *Report No. UMCEE 92-18*, Department of Civil Engineering, University of Michigan, Ann Arbor, MI.

Reinhorn, A.M., Barron-Corverra, R. and Ayala, A.G. (2002), "Global Spectral Evaluation of Seismic Fragility of Structures," *Proc., 7th U.S. National Conference on Earthquake Engineering,* Boston, MA (CD-Rom).

Rix, G.J. and Fernandez-Leon, A. (2004), "Earthquake Ground Motion Simulation," Sep. 2004. http://www.ce.gatech.edu/research/mae_ground_motion/

SEAOC (1995), *Vision 2000 a Framework for Performance-Based Engineering*, Structural Engineers Association of California, Sacramento, CA.

Shama, A.A., Mander, J.B. and Chen, S.S. (2002), "Seismic Investigation of Steel Pile Bents: II. Retrofit and Vulnerability Analysis," *Earthquake Spectra*, 18, (1), 143-160.

Shedlock, K.M. and Johnston, A.C. (1994), "Introduction – Investigation of the New Madrid Seismic Zone," Investigations of the New Madrid, Missouri, Earthquake Region, *USGS Professional Paper 1538*, pp. A1-A5, Washington, D.C.

Shinozuka, M., Feng, M.Q., Lee, J. and Naganuma, T. (2000a), "Statistical Analysis of Fragility Curves," *Journal of Engineering Mechanics*, 126, (12), 1224-1231.

Shinozuka, M., Feng, M.Q., Kim, H.-K. and Kim, S.-H. (2000b), "Nonlinear Static Procedure for Fragility Curve Development," *Journal of Engineering Mechanics*, 126, (12), 1287-1295.

Soubra, K.S., J.K. Wight and A.E. Naaman (1992), "Fiber reinforced concrete joints for precast construction in seismic areas," *Report No. UMCEE 92-2*, Department of Civil Engineering, University of Michigan, Ann Arbor, MI.

Tang, X. and Goel, S.C. (1988), "DRAIN-2DM technical notes and user's guide," *Research Report UMCE 88-1*, Department of Civil Engineering, University of Michigan, Ann Arbor, MI.

Tena-Colunga, A., Gomez-Soberon, C., and Munoz-Loustaunau, A. (1997), "Seismic Isolation of Buildings Subjected to Typical Subduction Earthquake Motions for the Mexican Pacific Coast," *Earthquake Spectra*, 13, (3), 505-532.

Teran-Gilmore, A., Bertero, V.V., and Youssef, N. (1995), "Seismic Rehabilitation of Framed Buildings Infilled with Unreinforced Masonry Walls Using Post-tensioned Steel Braces," *UCB/EERC-95/06*, Berkeley, Earthquake Engineering Research Center (EERC), University of California, Berkeley.

Thermou, G. and Elnashai, A.S. (2002), "Performance Parameters and Criteria for Assessment and Rehabilitation," Seismic Performance Evaluation and Retrofit of

Structures (SPEAR), *European Earthquake Engineering Research Network Report*, Imperial College, UK.

Trifunac, M.D. and Brady, A.G. (1975), "A Study on the Duration of Strong Earthquake Ground Motion," *Bulletin of the Seismological Society of America*, 65, (3), 581-626.

Wen, Y.K., Ellingwood, B.R., Veneziano, D. and Bracci, J.M. (2003), "Uncertainty Modeling in Earthquake Engineering," *Mid-America Earthquake (MAE) Center Project FD-2 Report*, 12 Feb. 2003, Urbana, IL.

Wen, Y.K., Ellingwood, B.R. and Bracci, J.M. (2004), "Vulnerability Functions," *Mid-America Earthquake (MAE) Center Project DS-4 Report*, submitted for review, Feb. 2004, Urbana, IL.

Wen, Y.K. and Wu, C.L. (2000), "Generation of Ground Motions for Mid-America Cities," Mid-America Earthquake (MAE) Center, 27 Jan. 2000. http://mae.ce.uiuc.edu/newsite/research/rr-1/gmotions/index.html

Wen, Y.K. and Wu, C.L. (2001), "Uniform Hazard Ground Motions for Mid-America's Cities," *Earthquake Spectra*, 17, (2), 359-384.

Yang, G., Spencer Jr., B.F., Carlson, J.D. and Sain, M.K. (2002), "Large-Scale MR Fluid Dampers: Modeling and Dynamic Performance Considerations," *Engineering Structures*, 24, 309-323.

APPENDIX A - GROUND MOTION DATA

As mentioned in Section 4.4, details of all ground motion records used in the analysis are provided in this Appendix.

Table A.1. 10% probability of exceedance in 50 years ground motions for St. Louis, Missouri (Wen and Wu 2000)

Ground motion record ID	Peak ground acceleration (g)	Duration (s)	Duration of 95% energy (s)	Body-wave magnitude	Focal depth (km)	Epicentral distance from St. Louis (km)
l10_01s	0.127	41.0	18.9	6.0	2.7	76.4
l10_02s	0.097	81.9	27.0	6.9	9.3	202
l10_03s	0.091	81.9	34.4	7.2	4.4	238
l10_04s	0.111	41.0	23.6	6.3	9.8	252
l10_05s	0.129	41.0	16.0	5.5	2.9	123
l10_06s	0.113	41.0	22.0	6.2	7.7	208
l10_07s	0.097	81.9	27.2	6.9	1.7	194
l10_08s	0.118	41.0	20.6	6.2	27.6	175
l10_09s	0.106	41.0	21.6	6.2	6.5	221
l10_10s	0.085	81.9	28.8	6.9	2.7	237

Table A.2. 2% probability of exceedance in 50 years ground motions for St. Louis, Missouri (Wen and Wu 2000)

Ground motion record ID	Peak ground acceleration (g)	Duration (s)	Duration of 95% energy (s)	Body-wave magnitude	Focal depth (km)	Epicentral distance from St. Louis (km)
l02_01s	0.230	150	48.9	8.0	17.4	267
l02_02s	0.246	150	49.9	8.0	9.1	230
l02_03s	0.830	20.5	9.8	5.4	2.1	28.7
l02_04s	0.249	81.9	31.9	7.1	5.5	253
l02_05s	0.190	150	40.2	8.0	17.4	254
l02_06s	0.243	81.9	26.7	6.8	5.8	225
l02_07s	0.244	150	56.9	8.0	33.9	196
l02_08s	0.239	150	28.2	8.0	9.1	261
l02_09s	0.245	150	30.4	8.0	9.1	281
l02_10s	0.544	41.0	14.9	5.9	4.4	47.7

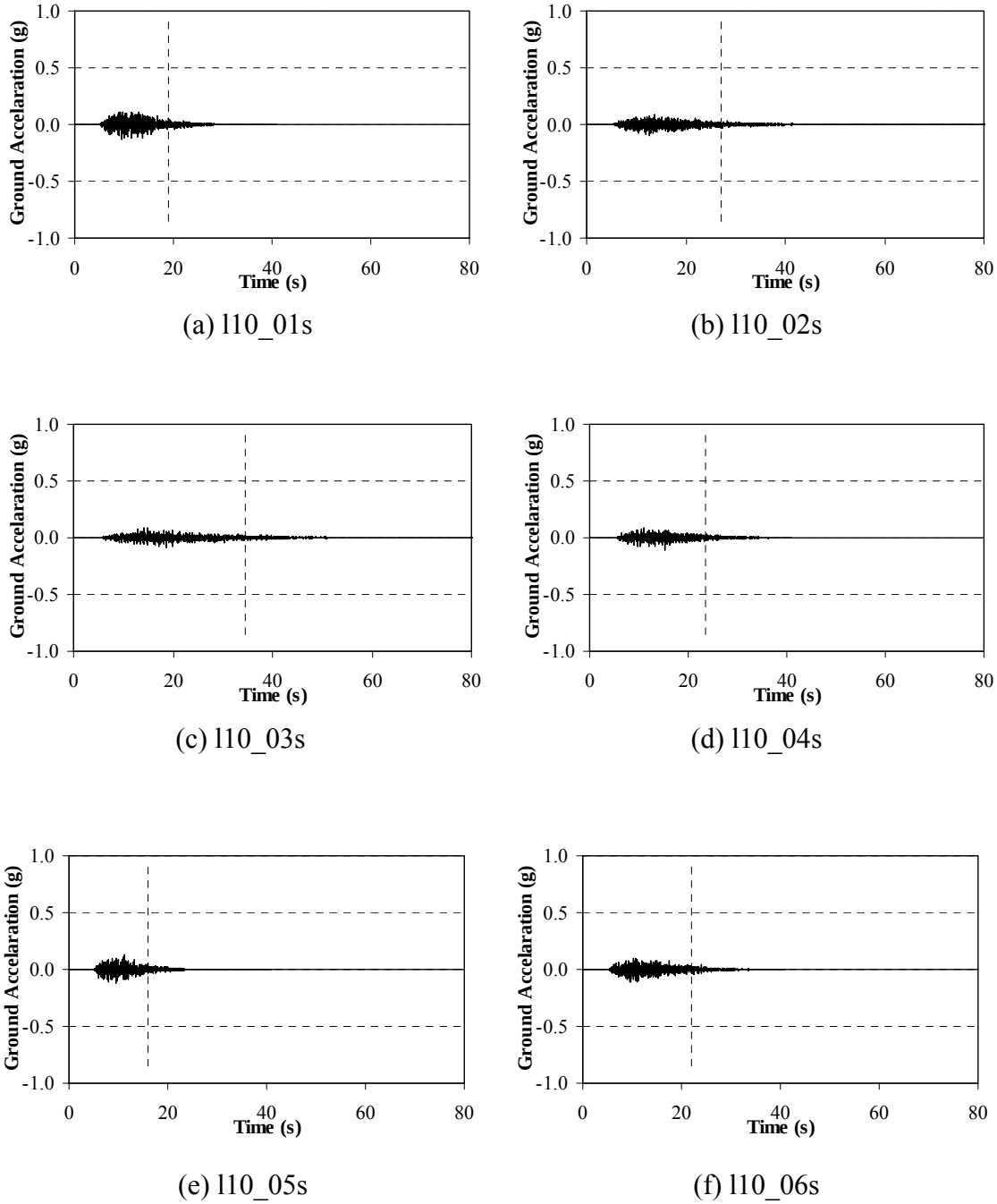

Fig. A.1. Acceleration time histories for 10% in 50 years St. Louis Motions (Wen and Wu 2000)

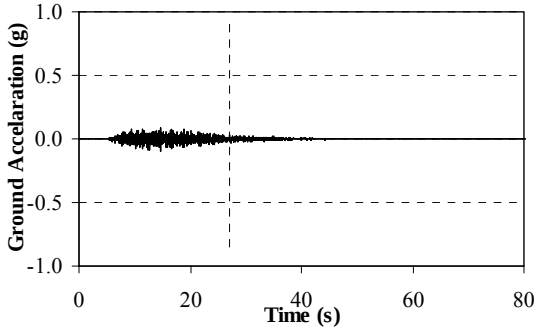

(g) l10_07s

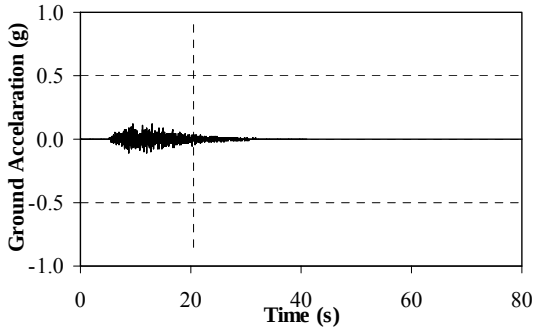

(h) l10_08s

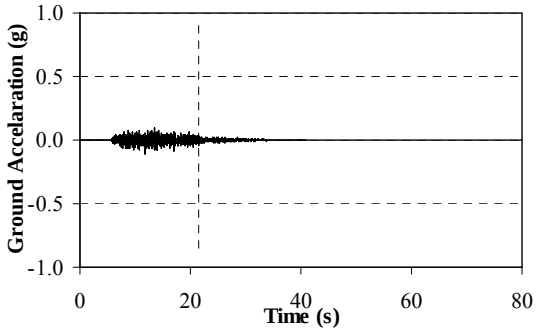

(i) l10_09s

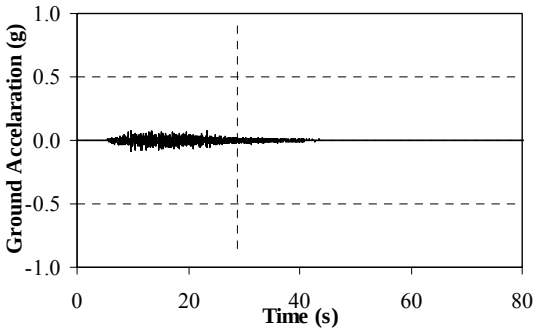

(j) l10_10s

Fig. A.1. Continued

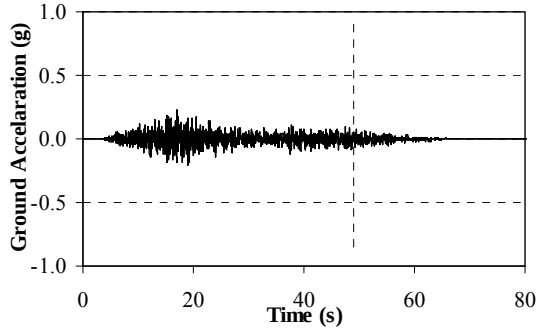

(a) l02_01s

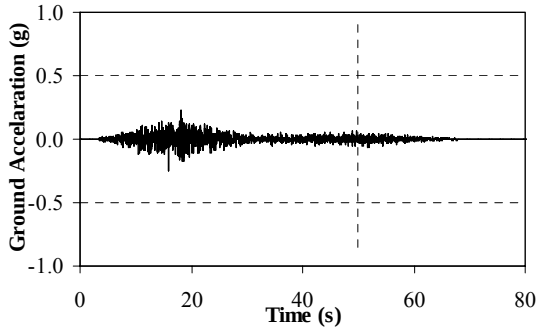

(b) l02_02s

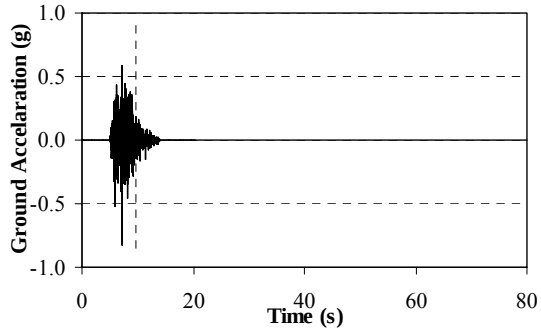

(c) l02_03s

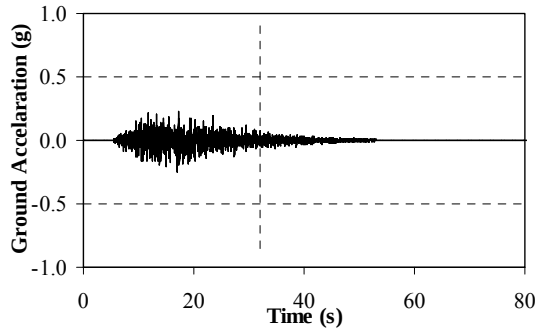

(d) l02_04s

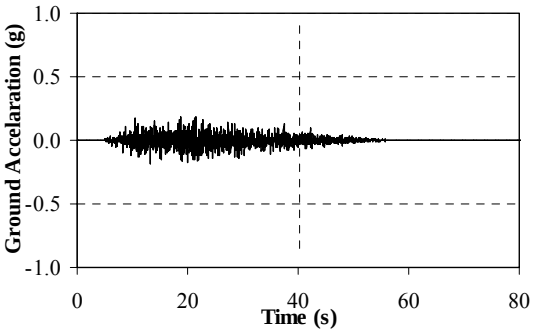

(e) l02_05s

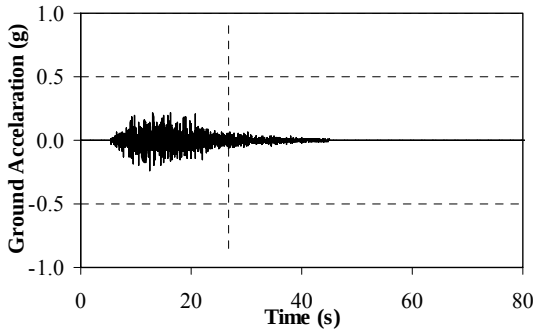

(f) l02_06s

Fig. A.2. Acceleration time histories for 2% in 50 years St. Louis motions (Wen and Wu 2000)

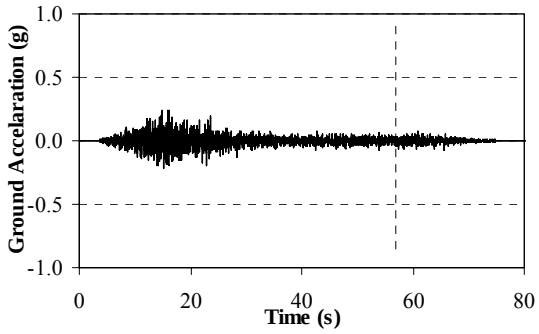

(g) l02_07s

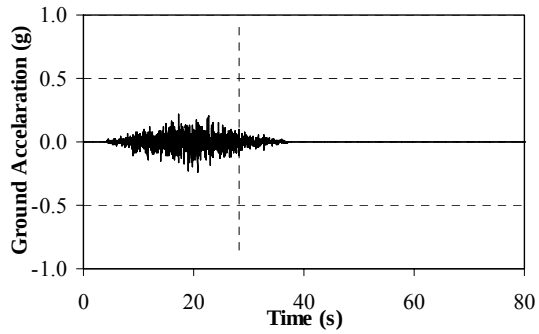

(h) l02_08s

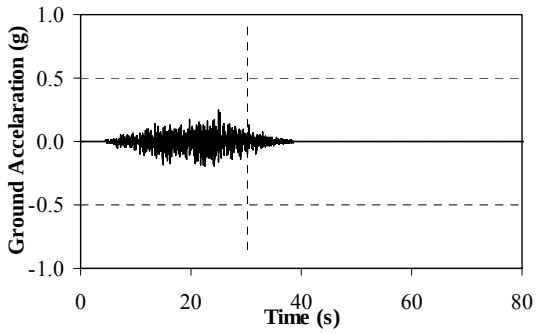

(i) l02_09s

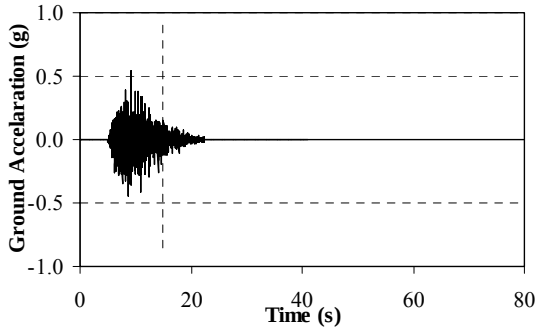

(j) l02_10s

Fig. A.2. Continued

Table A.3. 10% probability of exceedance in 50 years ground motions for Memphis, Tennessee (Wen and Wu 2000)

Ground motion record ID	Peak ground acceleration (g)	Duration (s)	Duration of 95% energy (s)	Body-wave magnitude	Focal depth (km)	Epicentral distance from Memphis (km)
m10_01s	0.059	41.0	22.2	6.3	5.2	121
m10_02s	0.075	41.0	19.7	6.4	6.7	57.5
m10_03s	0.070	41.0	17.5	6.8	18.1	125
m10_04s	0.068	41.0	23.4	6.8	2.1	92.4
m10_05s	0.108	41.0	14.9	6.2	27.0	107
m10_06s	0.054	150	48.9	6.2	3.2	41.2
m10_07s	0.070	41.0	20.3	6.5	11.5	58.8
m10_08s	0.088	20.5	12.4	6.5	23.9	129
m10_09s	0.093	20.5	10.2	6.3	9.5	166
m10_10s	0.064	41.0	18.5	6.8	8.7	35.6

Table A.4. 2% probability of exceedance in 50 years ground motions for Memphis, Tennessee (Wen and Wu 2000)

Ground motion record ID	Peak ground acceleration (g)	Duration (s)	Duration of 95% energy (s)	Body-wave magnitude	Focal depth (km)	Epicentral distance from Memphis (km)
m02_01s	0.439	150	29.2	8.0	25.6	148
m02_02s	0.333	150	23.5	8.0	33.9	186
m02_03s	0.360	150	23.7	8.0	25.6	163
m02_04s	0.323	150	52.8	8.0	9.10	170
m02_05s	0.476	150	36.2	8.0	9.10	97.6
m02_06s	0.416	150	37.1	8.0	17.4	118
m02_07s	0.365	150	24.8	8.0	17.4	119
m02_08s	0.292	150	20.9	8.0	9.10	146
m02_09s	0.335	150	26.0	8.0	9.10	171
m02_10s	0.412	150	22.2	8.0	17.4	188

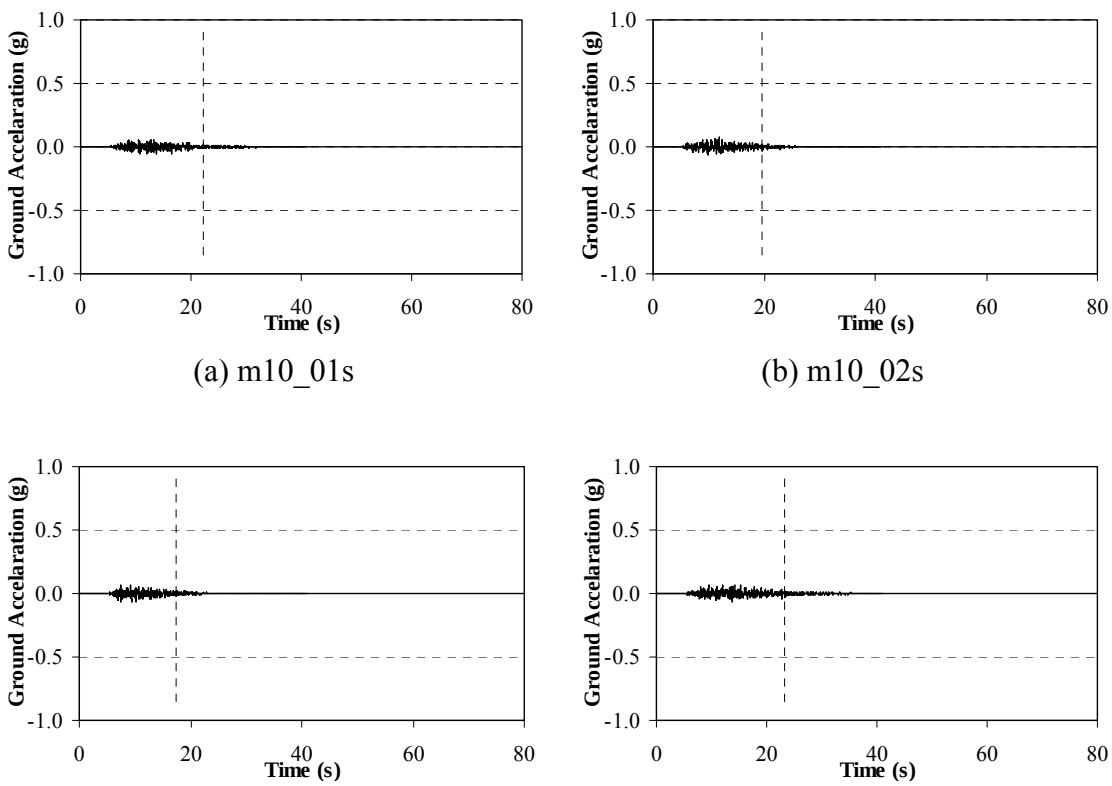

(a) m10_01s (b) m10_02s

(c) m10_03s (d) m10_04s

Fig. A.3. Acceleration time histories for 10% in 50 years Memphis motions (Wen and Wu 2000)

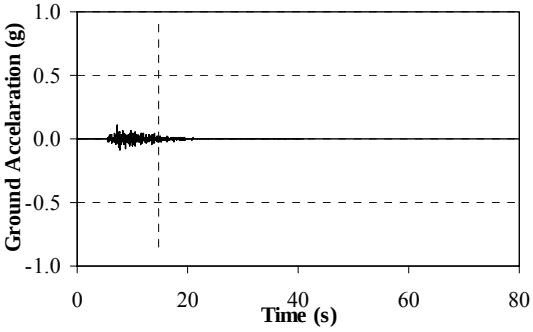

(e) m10_05s

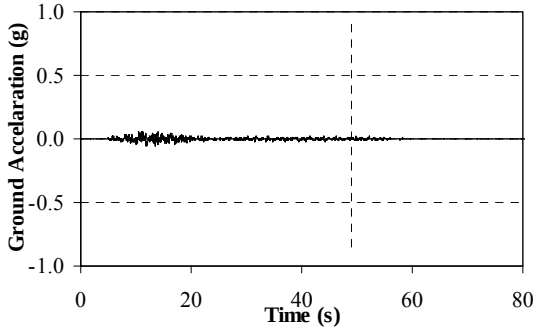

(f) m10_06s

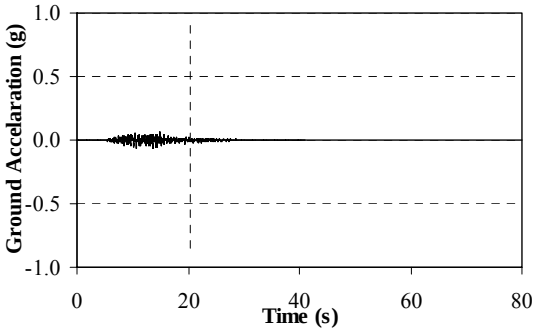

(g) m10_07s

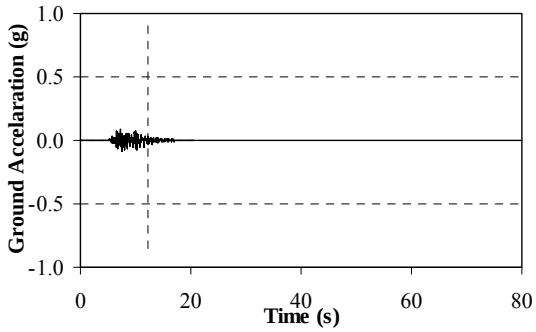

(h) m10_08s

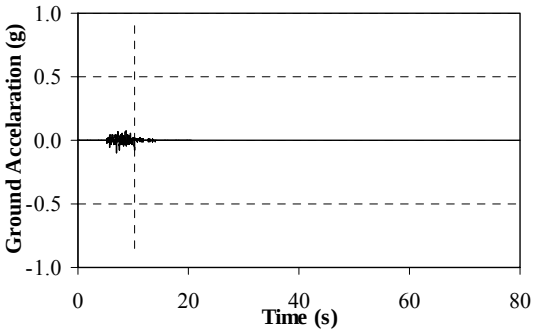

(i) m10_09s

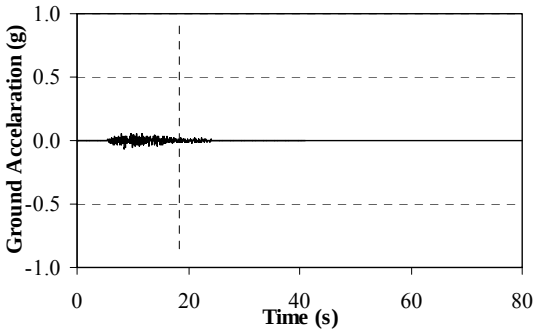

(j) m10_10s

Fig. A.3. Continued

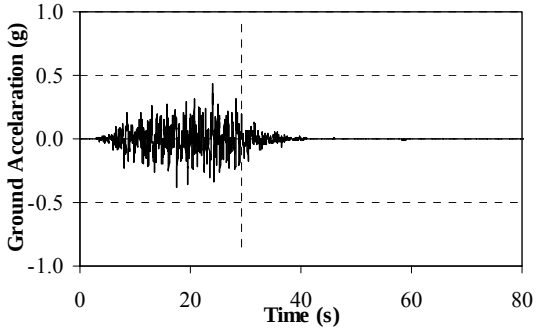

(a) m02_01s

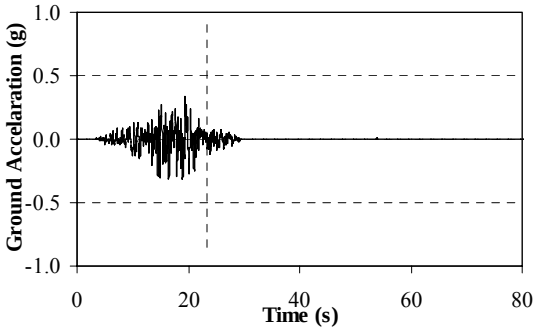

(b) m02_02s

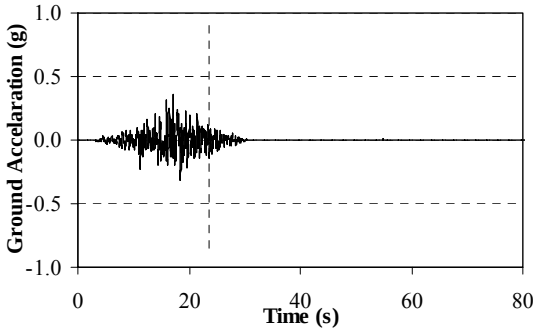

(c) m02_03s

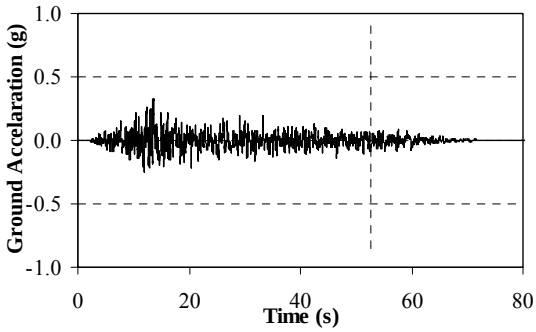

(d) m02_04s

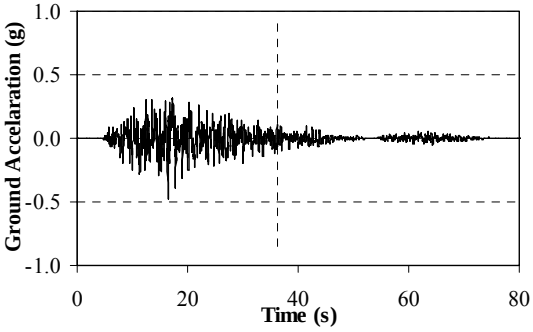

(e) m02_05s

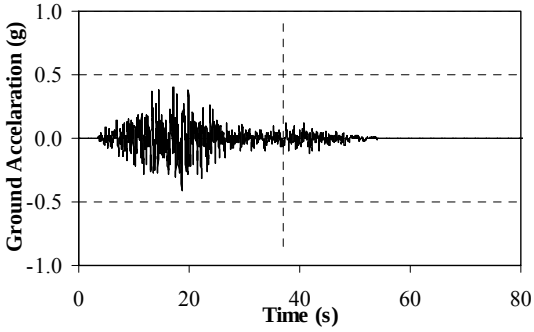

(f) m02_06s

Fig. A.4. Acceleration time histories for 2% in 50 years Memphis motions (Wen and Wu 2000)

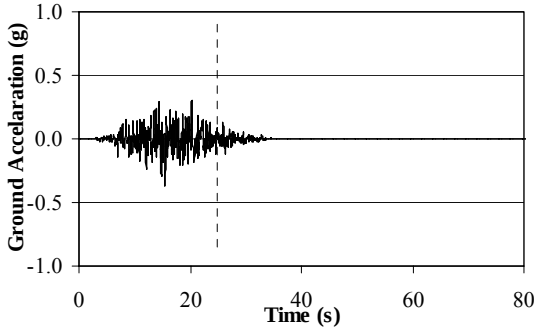

(g) m02_07s

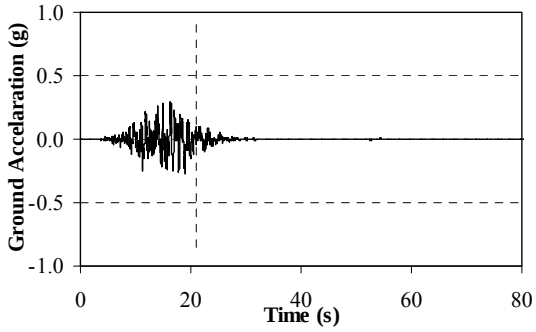

(h) m02_08s

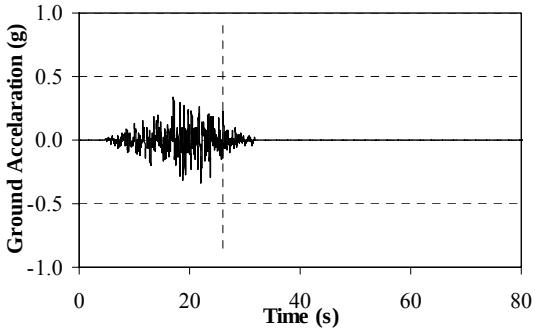

(i) m02_09s

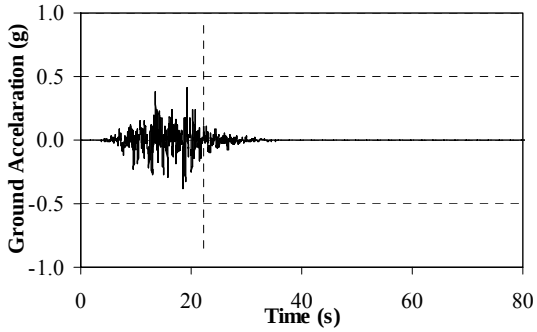

(j) m02_10s

Fig. A.4. Continued

Table A.5. Magnitude 5.5, 20 km hypocentral distance Memphis ground motions - Atkinson and Boore model (Rix and Fernandez-Leon 2004)

Ground motion record ID	Peak ground acceleration (g)	Duration (s)	Duration of 95% energy (s)
m55d020ab01	0.0497	9.02	5.65
m55d020ab02	0.0398	8.95	5.81
m55d020ab03	0.0630	8.49	4.56
m55d020ab04	0.0519	9.24	5.40
m55d020ab05	0.0479	9.26	5.64
m55d020ab06	0.0388	9.06	6.06
m55d020ab07	0.0397	9.46	5.84
m55d020ab08	0.0376	9.22	5.35
m55d020ab09	0.0625	9.40	5.04
m55d020ab10	0.0497	9.26	5.44
m55d020ab11	0.0485	9.14	5.22
m55d020ab12	0.0657	8.95	5.05
m55d020ab13	0.0428	9.22	5.47
m55d020ab14	0.0481	9.17	5.48
m55d020ab15	0.0436	9.05	5.50
m55d020ab16	0.0586	9.33	5.43
m55d020ab17	0.0389	9.08	5.39
m55d020ab18	0.0390	9.38	5.92
m55d020ab19	0.0566	9.08	4.91
m55d020ab20	0.0540	8.83	5.26

Table A.6. Magnitude 6.5, 20 km hypocentral distance Memphis ground motions - Atkinson and Boore model (Rix and Fernandez-Leon 2004)

Ground motion record ID	Peak ground acceleration (g)	Duration (s)	Duration of 95% energy (s)
m65d020ab01	0.0905	15.2	9.12
m65d020ab02	0.0899	15.3	9.89
m65d020ab03	0.114	14.6	9.63
m65d020ab04	0.134	14.8	8.74
m65d020ab05	0.107	15.0	9.23
m65d020ab06	0.0834	15.2	9.69
m65d020ab07	0.0944	15.0	9.92
m65d020ab08	0.121	15.2	8.85
m65d020ab09	0.103	15.3	9.51
m65d020ab10	0.128	14.9	9.94
m65d020ab11	0.121	15.1	9.47
m65d020ab12	0.102	14.2	8.97
m65d020ab13	0.100	15.0	8.60
m65d020ab14	0.0971	15.4	9.68
m65d020ab15	0.0960	15.1	10.1
m65d020ab16	0.103	16.1	9.44
m65d020ab17	0.101	15.3	10.1
m65d020ab18	0.101	14.7	9.07
m65d020ab19	0.0886	15.0	9.04
m65d020ab20	0.112	15.3	9.88

Table A.7. Magnitude 7.5, 20 km hypocentral distance Memphis ground motions - Atkinson and Boore model (Rix and Fernandez-Leon 2004)

Ground motion record ID	Peak ground acceleration (g)	Duration (s)	Duration of 95% energy (s)
m75d020ab01	0.205	37.4	23.3
m75d020ab02	0.269	33.9	22.2
m75d020ab03	0.195	36.2	23.8
m75d020ab04	0.232	37.0	24.1
m75d020ab05	0.244	37.3	25.5
m75d020ab06	0.178	36.4	23.6
m75d020ab07	0.177	37.0	23.1
m75d020ab08	0.181	34.7	22.7
m75d020ab09	0.231	35.2	23.8
m75d020ab10	0.242	35.8	21.7
m75d020ab11	0.236	35.4	23.8
m75d020ab12	0.264	33.9	23.6
m75d020ab13	0.206	37.5	25.1
m75d020ab14	0.182	36.0	22.0
m75d020ab15	0.221	34.9	22.0
m75d020ab16	0.204	35.5	24.4
m75d020ab17	0.248	35.5	23.2
m75d020ab18	0.213	35.0	23.7
m75d020ab19	0.215	33.7	22.6
m75d020ab20	0.187	36.5	24.5

Table A.8. Magnitude 5.5, 20 km hypocentral distance Memphis ground motions - Frankel et al. model (Rix and Fernandez-Leon 2004)

Ground motion record ID	Peak ground acceleration (g)	Duration (s)	Duration of 95% energy (s)
m55d020fa01	0.0800	8.55	5.23
m55d020fa02	0.0821	9.18	5.93
m55d020fa03	0.0599	8.72	5.39
m55d020fa04	0.0691	8.68	5.80
m55d020fa05	0.0599	8.72	5.45
m55d020fa06	0.0693	8.90	5.52
m55d020fa07	0.0779	8.93	5.46
m55d020fa08	0.0727	8.92	5.75
m55d020fa09	0.0728	8.71	5.33
m55d020fa10	0.0538	8.92	5.44
m55d020fa11	0.0687	8.32	5.39
m55d020fa12	0.0681	8.89	5.33
m55d020fa13	0.0938	8.87	5.96
m55d020fa14	0.0545	9.10	5.63
m55d020fa15	0.0865	8.67	5.38
m55d020fa16	0.0834	8.62	5.27
m55d020fa17	0.0695	8.62	5.79
m55d020fa18	0.0954	8.68	5.86
m55d020fa19	0.0543	8.87	5.40
m55d020fa20	0.0822	8.93	5.53

Table A.9. Magnitude 6.5, 20 km hypocentral distance Memphis ground motions - Frankel et al. model (Rix and Fernandez-Leon 2004)

Ground motion record ID	Peak ground acceleration (g)	Duration (s)	Duration of 95% energy (s)
m65d020fa01	0.157	14.1	9.80
m65d020fa02	0.150	13.8	8.91
m65d020fa03	0.210	13.2	8.73
m65d020fa04	0.214	12.9	8.12
m65d020fa05	0.187	12.6	8.92
m65d020fa06	0.224	13.4	9.22
m65d020fa07	0.230	13.8	8.90
m65d020fa08	0.151	14.4	9.64
m65d020fa09	0.286	13.8	8.82
m65d020fa10	0.149	14.2	9.31
m65d020fa11	0.258	12.9	8.33
m65d020fa12	0.190	12.5	8.89
m65d020fa13	0.242	13.2	9.37
m65d020fa14	0.170	14.2	8.94
m65d020fa15	0.174	15.1	9.63
m65d020fa16	0.207	14.5	9.52
m65d020fa17	0.184	13.6	8.08
m65d020fa18	0.224	13.3	8.44
m65d020fa19	0.242	13.4	8.24
m65d020fa20	0.268	13.0	7.28

Table A.10. Magnitude 7.5, 20 km hypocentral distance Memphis ground motions - Frankel et al. model (Rix and Fernandez-Leon 2004)

Ground motion record ID	Peak ground acceleration (g)	Duration (s)	Duration of 95% energy (s)
m75d020fa01	0.357	27.4	19.8
m75d020fa02	0.447	29.0	17.7
m75d020fa03	0.436	29.3	18.5
m75d020fa04	0.405	26.9	18.3
m75d020fa05	0.376	25.6	19.4
m75d020fa06	0.452	25.6	17.5
m75d020fa07	0.277	27.6	18.8
m75d020fa08	0.320	29.7	19.0
m75d020fa09	0.374	28.9	19.7
m75d020fa10	0.486	27.3	18.3
m75d020fa11	0.390	27.9	18.0
m75d020fa12	0.464	27.9	17.4
m75d020fa13	0.426	27.8	19.4
m75d020fa14	0.387	26.6	18.8
m75d020fa15	0.392	27.6	18.4
m75d020fa16	0.586	27.0	17.1
m75d020fa17	0.465	28.2	19.2
m75d020fa18	0.548	27.1	18.2
m75d020fa19	0.418	29.6	19.6
m75d020fa20	0.645	25.1	16.6

APPENDIX B - ADDITIONAL DYNAMIC ANALYSIS RESULTS FOR THE UNRETROFITTED BUILDING

As mentioned in Chapter 5, dynamic analysis results using ZEUS-NL with the Wen and Wu motions for St. Louis, Missouri and Memphis, Tennessee are provided.

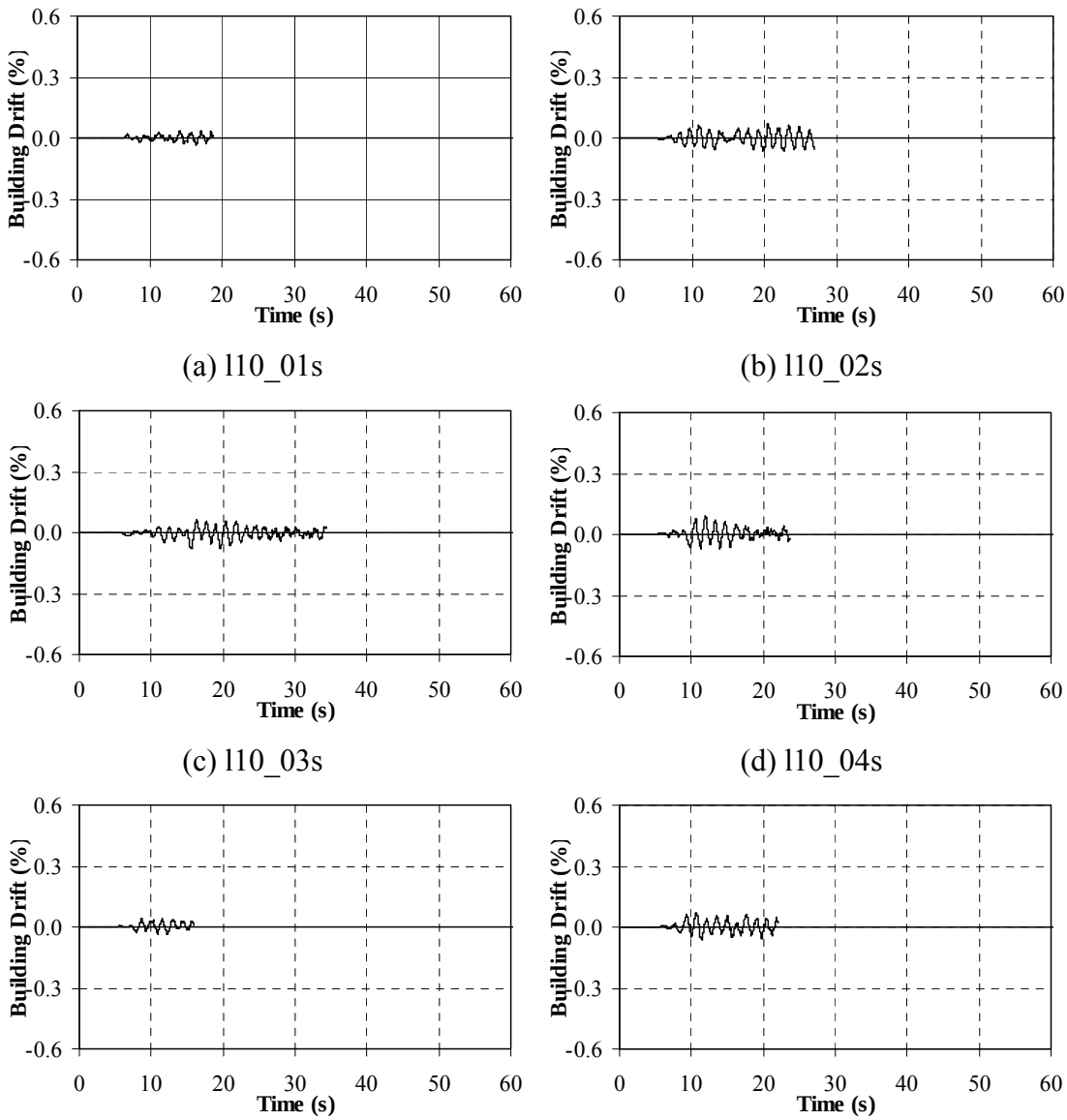

(a) l10_01s (b) l10_02s (c) l10_03s (d) l10_04s (e) l10_05s (f) l10_06s

Fig. B.1. Building drift time histories for 10% in 50 years St. Louis Motions

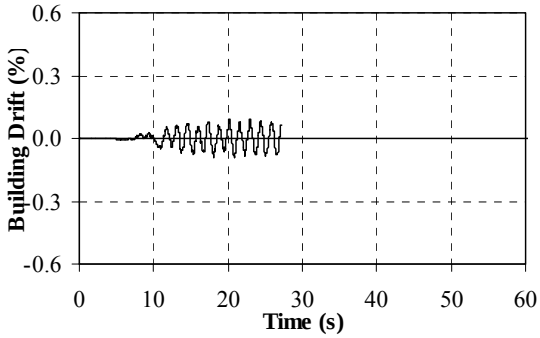

(g) l10_07s

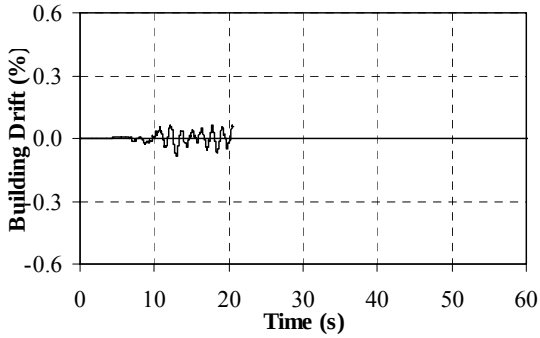

(h) l10_08s

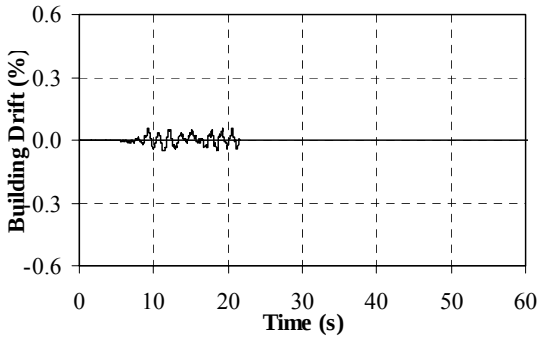

(i) l10_09s

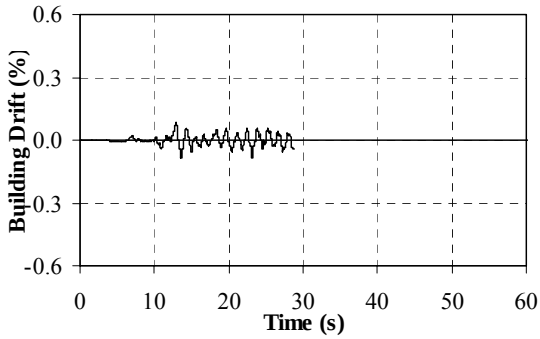

(j) l10_10s

Fig. B.1. Continued

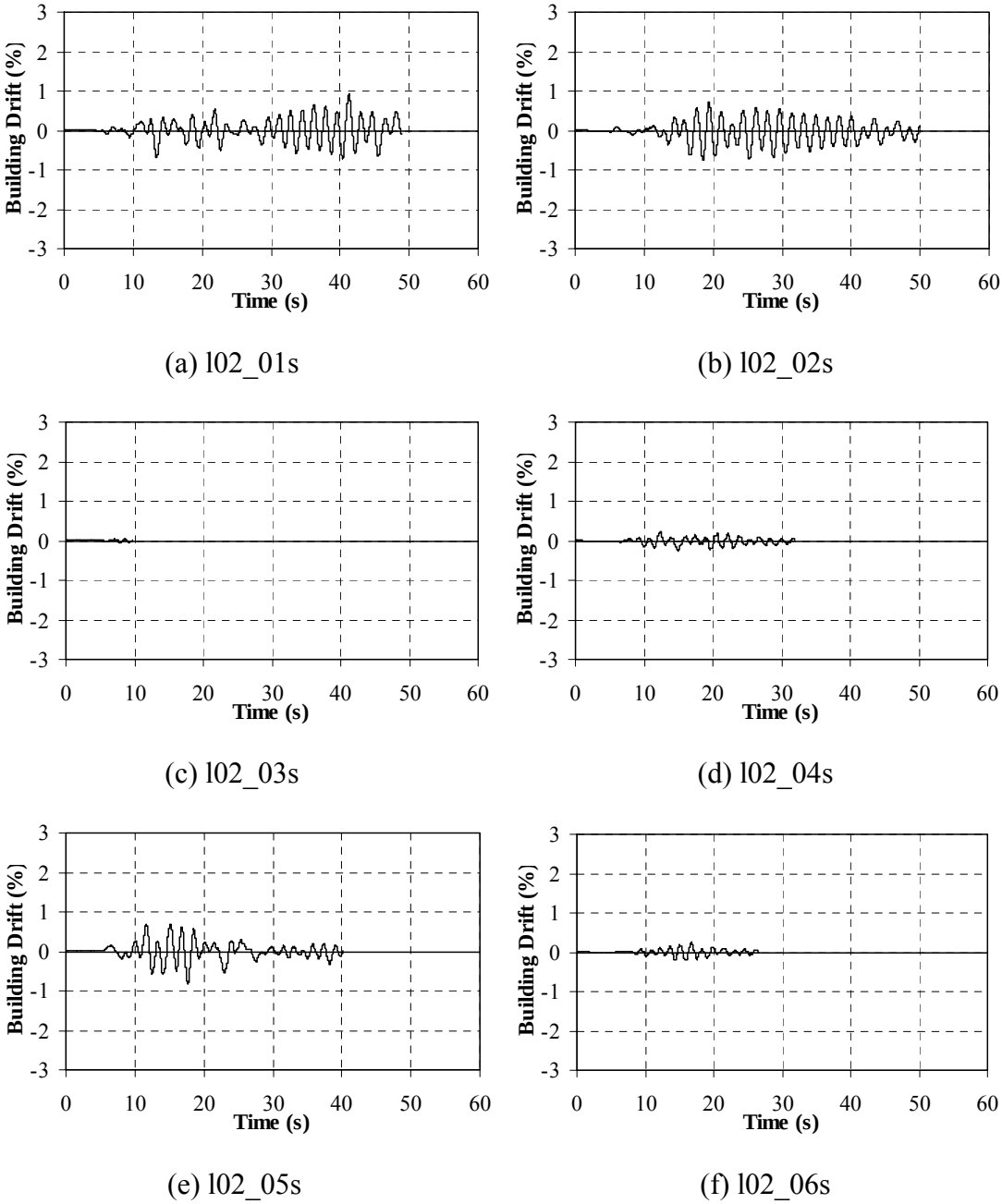

Fig. B.2. Building drift time histories for 2% in 50 years St. Louis Motions

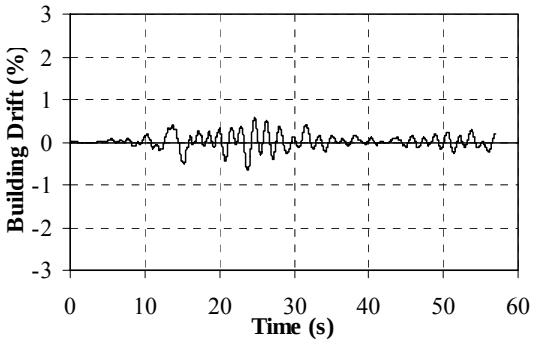

(g) l02_07s

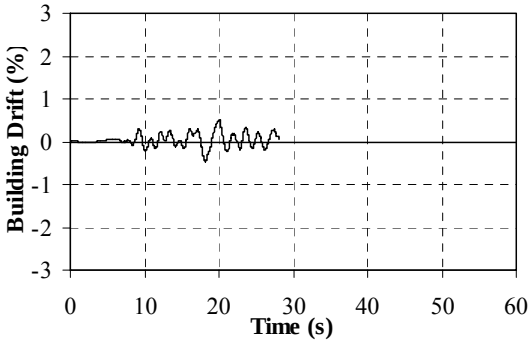

(h) l02_08s

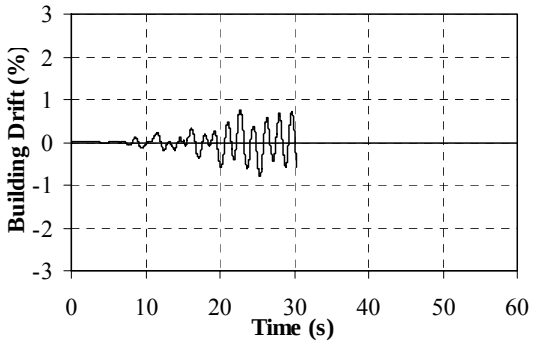

(i) l02_09s

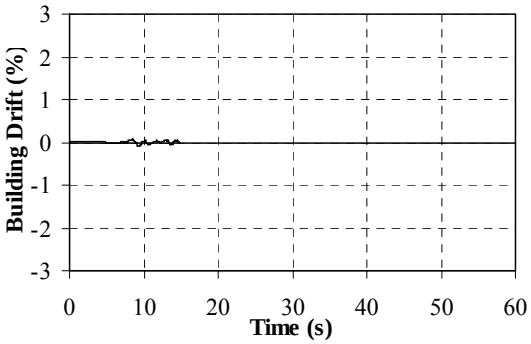

(j) l02_10s

Fig. B.2. Continued

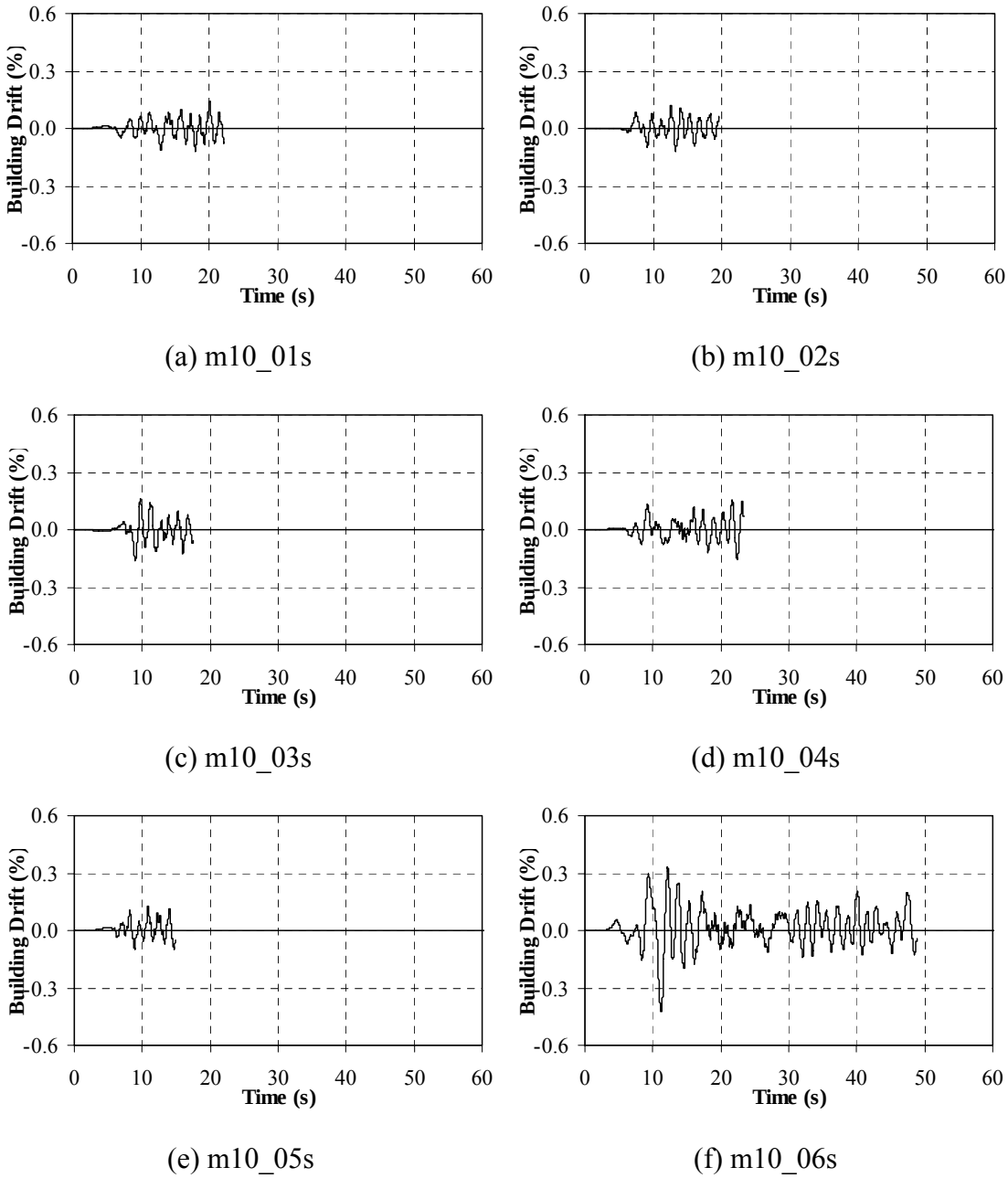

Fig. B.3. Building drift time histories for 10% in 50 years Memphis Motions

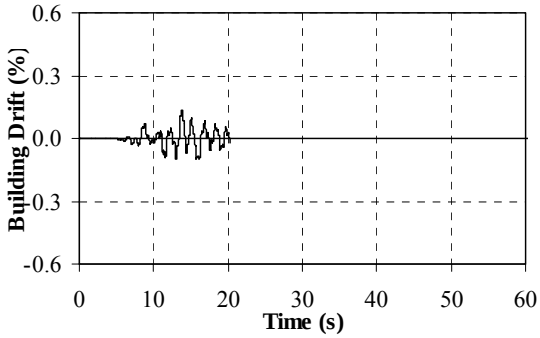

(g) m10_07s

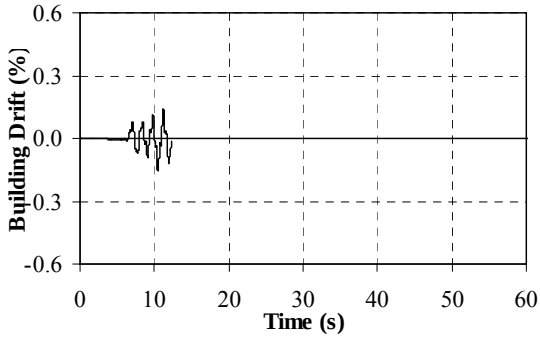

(h) m10_08s

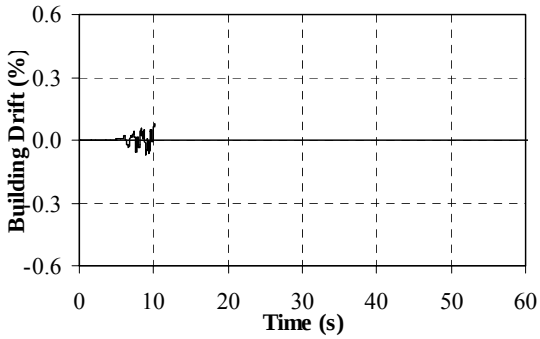

(i) m10_09s

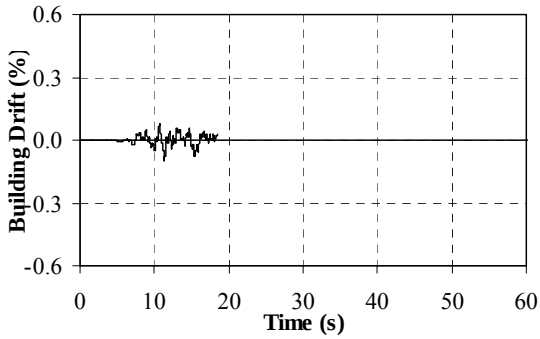

(j) m10_10s

Fig. B.3. Continued

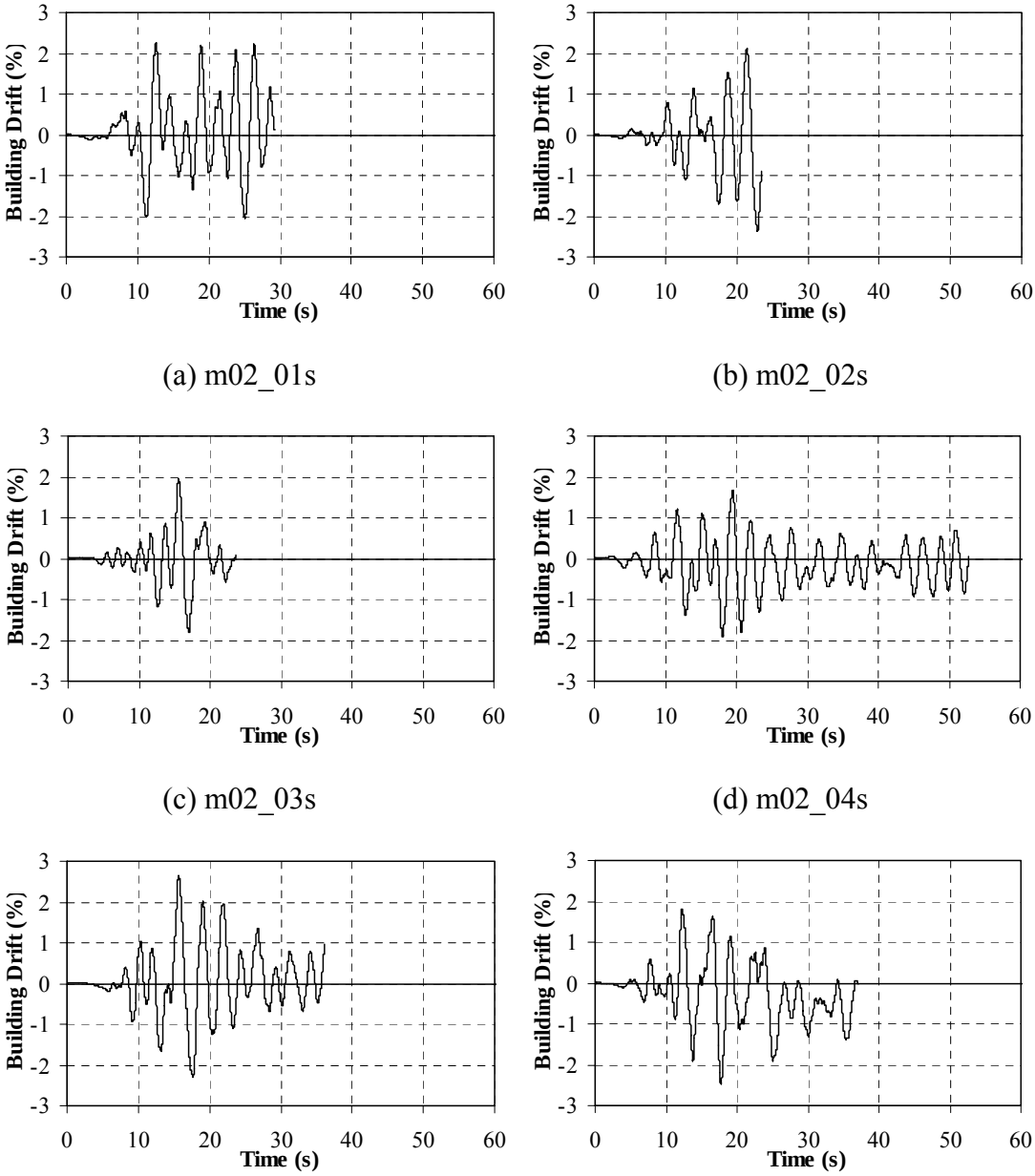

(a) m02_01s (b) m02_02s

(c) m02_03s (d) m02_04s

(e) m02_05s (f) m02_06s

Fig. B.4. Building drift time histories for 2% in 50 years Memphis Motions

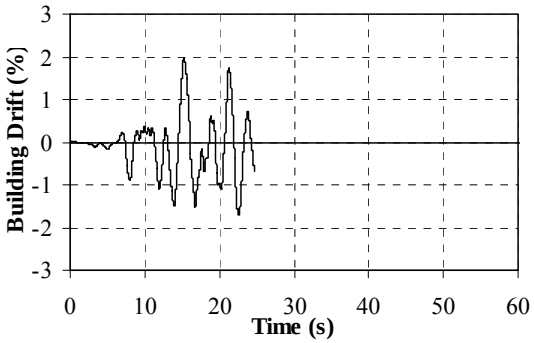

(g) m02_07s

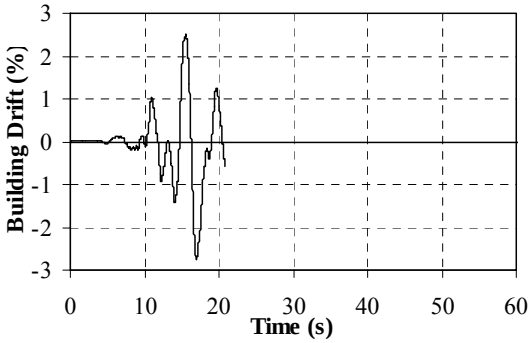

(h) m02_08s

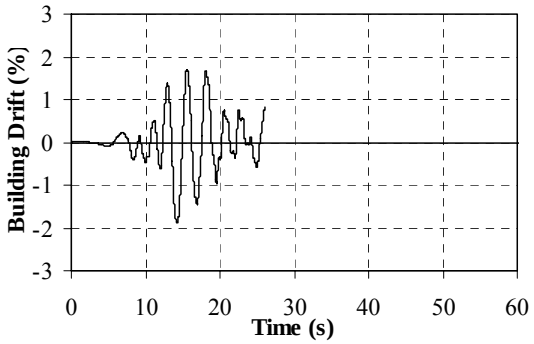

(i) m02_09s

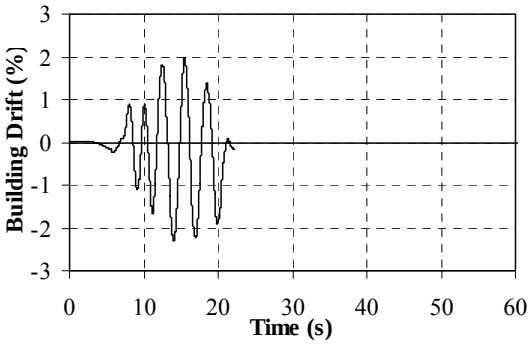

(j) m02_10s

Fig. B.4. Continued